Assessment and Modelling of Quaternary and Quinary HPGR Performance for Iron Ore Applications

by

Tulio Junqueira Marques

B. Mining Engineering, Federal University of Ouro Preto, 2016

A THESIS SUBMITTED IN PARTIAL FULFILLMENT OF THE REQUIREMENTS FOR THE DEGREE OF
MASTER OF APPLIED SCIENCE

in

THE FACULTY OF GRADUATE AND POSTDOCTORAL STUDIES
(Mining Engineering)

THE UNIVERSITY OF BRITISH COLUMBIA
(Vancouver)

December 2020

©Tulio Junqueira Marques, 2020

The following individuals certify that they have read, and recommend to the Faculty of Graduate and Postdoctoral Studies for acceptance, the thesis entitled:

Assessment and Modelling of Quaternary and Quinary HPGR Performance for Iron Ore Applications

submitted by Tulio Junqueira Marques in partial fulfilment of the requirements for

the degree of Master of Applied Science

in Mining Engineering

Examining Committee:

Dr. Bern Klein, Professor, Mining Engineering, UBC
Supervisor

Dr. Davide Elmo, Associate Professor, Mining Engineering, UBC
Supervisory Committee Member

Dr. Persio Rosario, Hatch
Supervisory Committee Member

Additional Supervisory Committee Member:

Dr. Armando Correa de Araujo, ArcelorMittal S.A.
Supervisory Committee Member

Abstract

The complexity degree of a mining plant's comminution circuit is critical for allowing the processing of low-grade iron ore deposits. Considering that the comminution stage is responsible for most of the energy consumption in a mineral processing plant, the pursuit of energy-efficient technologies is a major challenge of the mining industry. The High Pressure Grinding Rolls (HPGR) have been applied for over 20 years and is widely recognized in terms of energy savings. However, the limited access to industry and academic studies about the HPGR performance and the lack of a widely industry accepted bench-scale laboratory test for sizing and modelling HPGRs are major hindrances that must be addressed in order to promote the machine acceptance and implementation.

The research's main objectives were to evaluate the HPGR amenability to comminute iron ore in a two-stage HPGR circuit and extend the applicability of Davaanyam's (2015) Direct Calibration and Database-Calibrated methodologies for predicting the energy consumption and size reduction of HPGRs through laboratory-scale piston-press tests. The HPGR performance and modelling evaluation for quaternary and quinary applications were supported by a combination of laboratory-scale testing, pilot-scale testing and modelling work.

Results obtained from the research showed that the HPGR is suitable for comminuting iron ore in open circuit quaternary and closed circuit quinary applications. The performance evaluation revealed a strong linear relationship between the machine's specific pressing force and net specific energy consumption. The size reduction also increased linearly with the increase of the pressing force. The ore moisture content revealed to be detrimental to the HPGR's throughput at high concentrations but did not impact the performance in terms of size reduction. The Direct Calibration methodology was successfully applied to iron ore for quaternary applications, but the current Database-Calibrated regression models resulted in poor energy-size reduction predictions. because the variable levels for the quaternary application extended beyond the ones used for developing the current regression

models. The results indicate that the database needs to be extended to finer sizes, higher moisture levels and possibly ore types.

Lay Summary

The High Pressure Grinding Rolls (HPGR) have been applied for over 20 years in the mining industry and is widely recognized in terms of energy savings. However, the limited access to industry and academic studies about the HPGR performance and the lack of a widely industry accepted bench-scale laboratory test for sizing and modelling HPGRs are major hindrances that must be addressed in order to promote the machine acceptance and implementation. Considering this, the purpose of this research was to evaluate the HPGR amenability to comminute iron ore in a two-stage HPGR circuit, and to extend the applicability of Davaanyam's (2015) Direct Calibration and Database-Calibrated methodologies for predicting the energy consumption and size reduction of HPGRs through laboratory-scale piston-press tests.

Preface

This project work is a part of the UBC HPGR research program that took place at the University of British Columbia and was supported by Mitacs and ArcelorMittal. The objective was to evaluate the HPGR amenability to comminute iron ore in a two-stage HPGR circuit, and to extend and validate the applicability of Davaanyam's Direct Calibration and Database-Calibrated methodologies for predicting the energy consumption and size reduction of HPGRs through piston-press tests.

Under the supervision of Dr. Bern Klein, Professor at the Norman B. Keevil Institute of Mining Engineering at the University of British Columbia, I was responsible for developing the test program, conducting the test work and interpreting the results. Chengtie Wang assisted in developing the pilot HPGR and piston-press test work plan. Amit Kumar, Giovanni Pamparana and Cherezade Soto Saud assisted with the pilot HPGR and piston-press testing.

Table of Contents

List of Tables

List of Figures

List of Symbols

Symbol:	Description:
D	Roll diameter [mm]
E_{SP}	Net specific energy consumption of HPGR test [kWh/t]
F_{80}	80% passing aperture size of feed by weight [mm]
F_{50}	50% passing aperture size of feed by weight [mm]
F_{SP}	Specific pressing force of HPGR test [N/mm^2]
L	Roll width [mm]
$\dot{m}$	M-dot or Specific throughput constant [ts/m^{3}h]
P_{80}	80% passing aperture size of product by weight [mm]
P_{idle}	Idle motor power draw of HPGR [kW]
P_{total}	Total motor power draw during HPGR test [kW]
Q	HPGR test throughput [t/h]
v	Roll peripheral speed [m/s]
w	Moisture content [%]

Acknowledgements

I am profoundly thankful to my supervisory committee, especially my supervisor Professor Bern Klein, for his guidance throughout this research project. I would like to express my gratitude for the support of all sponsors involved in providing the materials and funds necessary for conducting this study.

I would like to convey my sincere gratitude and thanks to ArcelorMittal for sponsoring this research project and for welcoming me at Serra Azul Mine and Maizières Research Center. I would like to thank Diego Arenare for providing me assistance during sample collection and for providing background information about Serra Azul's project.

I would like to express my sincere thanks to Dr. Armando Correa and Dr Persio Rosario, as both mentors and friends, for their support and guidance throughout my research, and for introducing me to the field of mineral processing.

The assistance of Chengtie Wang, Amit Kumar, Sijia Liu, Pils Li, Giovanni Pamparana, Santiago Seiler, and Cherezade Soto in performing the HPGR tests, and their constant support and guidance are also deeply acknowledged.

I thank Maren Klein for welcoming me to Vancouver and for making my adaptation to the new environment a very pleasant one.

I thank my wife, Karla, for her love and support throughout this journey, which was certainly challenging, but highly rewarding.

Last but not least, I would like to express sincere appreciation to my parents for their love and constant support.

Chapter 1

INTRODUCTION

1.1 Background

Iron ore is vital for the global economy since it is the primary raw material from which metallic iron is extracted to manufacture steel. Between 2000 to 2015, the world's crude steel production almost doubled. For example, China showed an increase of 540% in its crude steel production over the last decade. However, it has also been observed that the high-grade iron ores, also categorized as direct shipping ore (DSO), are facing depletion on their reserves, and as an expected side effect, low-grade hematite and magnetite deposits are now under increasing development (Jankovic, 2015). All these factors combined have been increasing the need for iron ore processing and the comminution complexity with regards to achieving particle size reduction requirements.

This scenario calls attention to a well-known public issue regarding the comminution stage, which is its massive energy consumption. According to Wang (2013), about 50 to 80% of the total energy consumption in a mineral processing plant is addressed to the comminution stage. Nowadays, concerning the processing of hard-rock, low-grade deposits, the most common comminution circuits make use of some form of tumbling mill such as Ball Mills, Autogenous Grinding (AG) Mills or Semi-Autogenous Grinding (SAG) Mills to break the rocks to a targeted particle size (Drozdiak, 2011). However, despite the SAG-based comminution circuit's popularity, Morley and Staples (2010) highlight their high energy consumption and throughput sensitivity when treating hard ores.

As stated by the U.S Department of Energy (DOE, 2007), the grinding sector offers many opportunities for energy savings, where the largest of them, accounting for 70% of the possible savings, depends on implementing more energy-efficient technologies. For iron ore operations, especially for magnetite deposits, the challenge has been to minimize the operating costs, which by no coincidence, is dominated by the cost of power required to grind the ore to achieve acceptable liberation and concentrate iron grades together with low impurity content. The implementation of efficient comminution circuits is continually growing in importance since a carbon tax is expected to become a significant addition to the operating costs of iron ore deposits (Jankovic and Valery, 2010).

The High Pressure Grinding Rolls (HPGR) is considered as one of the most significant recent developments in the comminution area for processing hard rocks. According to Barrios and Tavares (2016), the HPGR success is associated with improved energy efficiency, grinding capacity, lower sensitivity to grindability variations and higher metal recovery in downstream processes compared to conventional crushing and grinding technologies. However, despite being recognized as a viable crushing and grinding technology, the HPGR acceptance and implementation in the mining industry has been slow, especially for hard-rock applications.

One of the major drawbacks that remains is the limited access to industry and academic studies about the HPGR performance. Currently, most of the studies and publications about the HPGR technology focus on circuit trade-offs such as HPGR versus SAG Mill-based circuits, where the goal is to discuss subjects of broad interest such as energy savings, or mechanical improvements that have been implemented by manufacturers. In contrast, detailed analysis of the HPGR performance and operating parameters such as the specific pressing force, net specific throughput and operating gap, which are essential during the machine selection and sizing, are scarce or, at times, unavailable for certain ores.

Another critical hindrance is the uncertainty regarding the reliability of modelling and scale-up from laboratory or pilot operations to industrial installations. As stated by McClintock (2018), there is currently no industry-accepted bench-scale test for sizing or modelling HPGRs for hard-rock applications, and the majority of the methodologies that have been published so far are proprietary. With an initiative to solve this limitation, for more than ten years, the University of British Columbia (UBC) has been developing a set of HPGR models using data obtained from more than 200 pilot-scale HPGR tests and piston-die based laboratory tests (Wang et al., 2019; McClintock, 2018; Davaanyam, 2015; Kumar, 2014, Nadolski, 2012). In 2015, Davaanyam proposed three bench-scale test methodologies for predicting the specific energy consumption and size reduction of HPGRs through piston-press tests: the Direct Calibration; the Database-Calibrated and the Simulation-Based methodologies. The energy and size reduction predictions proved to be reasonably accurate, ranging from ±10% to ±25% depending on the methodology.

Since their publication, Davaanyam's methodologies have been used in several UBC projects, thus accomplishing their primary objective of simplifying pilot HPGR test programs by reducing the required number of tests and sample requirements. Pilot-scale HPGR tests are widely known to be expensive and to require large quantities of samples. Nevertheless, there is still plenty of room for investigations and studies that must done to refine these methodologies. For instance, the methodologies have not been validated for iron ore applications and detailed analysis of how the feed properties such as moisture content affect the energy and size reduction predictions have not yet been researched.

1.2 Thesis Objectives

This thesis focused on the study of fine crushing of iron ores with High Pressure Grinding Rolls and the ability to predict the energy and size reduction of HPGRs through piston-press tests. The main objectives were to evaluate the HPGR amenability to comminute iron ore in a two-stage HPGR circuit, and to extend and validate the applicability of Davaanyam's Direct Calibration and Database-Calibrated methodologies for predicting the energy-size reduction relationship with low sample requirements.

To date, Davaanyam's Database-Calibrated and Direct Calibration Methodologies both proved to be effective solutions for predicting the energy-size reduction of HPGRs with low sample requirements. However, the Direct-Calibration methodology has not yet been applied and validated to iron ore. In addition, the proposed regression models from the Database-Calibrated methodology has not been applied to iron ore.

A list of primary and secondary objectives is presented below:

I. Assessment of the HPGR amenability to comminute iron ore when applied in a two-stage HPGR circuit.

- Evaluate the HPGR performance for open circuit quaternary applications,
- Evaluate the HPGR performance for closed circuit quinary applications,
- Analyze the effects of the applied specific pressing force and ore moisture content in the HPGR performance.

II. Demonstrate and evaluate modelling methodologies for sizing HPGRs.

- Create a suitable iron ore database for applying the Direct Calibration and Database-Calibrated methodology.

- Demonstrate a step-by-step on how to apply both methodologies and validate their application for iron ore.
- Assess how moisture affects the energy and size reduction predictions when utilizing the Direct Calibration methodology.
- Evaluate if the Database-Calibrated models proposed by Davaanyam (2015) provides reasonable energy-size predictions for iron ore applications.

The thesis includes the following chapters to address these objectives:

Chapter 2 provides a literature review on the HPGR technology, focusing on its operating parameters, performance assessment and modelling.

Chapter 3 describes the experimental procedure followed for the pilot HPGR tests and laboratory-scale piston-press tests. This chapter also includes descriptions about the iron ore samples from Serra Azul case study and the UBC's pilot HPGR and piston-press machines.

Chapter 4 presents results and discussions regarding the pilot testing program. This section covers the HPGR performance analysis for quaternary open circuit and quinary closed circuit applications to iron ore.

Chapter 5 presents results and discussions of a step-by-step analysis of the Direct-Calibration methodology applications to iron ore.

Chapter 6 presents results and discussions regarding the applicability of the Database-Calibrated methodology to iron ore.

This thesis is concluded in Chapter 7 with the presentation of the study's main conclusions and recommendations for future work.

Chapter 2

LITERATURE REVIEW

Researches concerning comminution technology are under continuous review, and increasing emphasis is being given to the study of the High-Pressure Grinding Rolls (HPGRs), which often proves to be one of the most energy-efficient methods of crushing even when applied to hard ores (Saramak & Kleiv, 2013).

2.1 High Pressure Grinding Roll Technology

2.1.1 Concept of the HPGR Machine

The High Pressure Grinding Rolls (HPGR) is currently seen as a relatively new comminution technology that relies on compression breakage mechanisms to break particles within a particle bed between two counter-rotating rolls. The technology has proven to be more energy-efficient than conventional tumbling mills (AG/SAG mills), and its particle breakage mechanism, which is preferential along the grain boundaries, is believed to enhance liberation at coarser particle sizes, thus leading to benefits in downstream processes such as leaching or flotation. Figure 2-1 illustrates the main components of a typical HPGR unit.

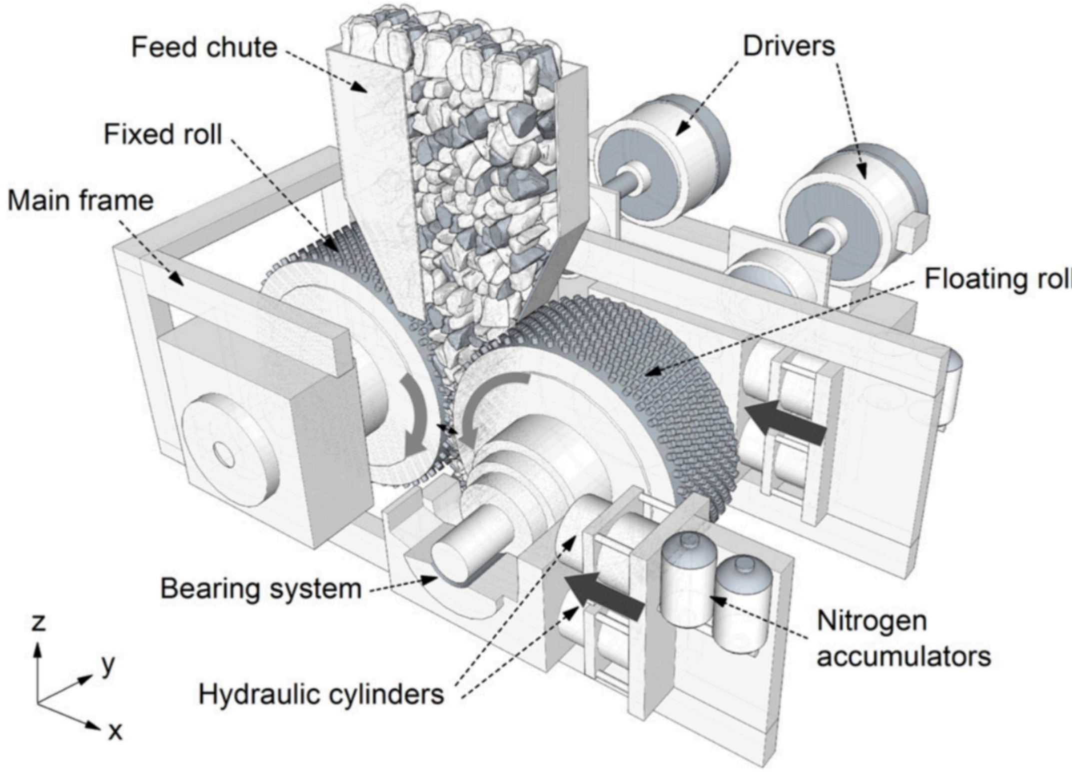

Figure 2-1: Schematics of the HPGR

(Source: Barrios & Tavares, 2016)

In contrast to conventional crushers or tumbling mills where the dominant breakage mechanisms are the impact and abrasion, the HPGR comminution principle makes use of the compression breakage mechanism. The HPGR also differs from the traditional crushing rolls since the particles are broken by compression in a packed particle bed instead of direct nipping of the particles between the two rolls. Between the HPGR's counter-rotating rolls, a particle bed is pressed to densities of up to 75 to 85% of the actual material density (Aydoğan et al., 2006; Schneider, et al., 2009; Schönert, 1988). According to Fuerstenau, Shukla and Kapur (1991), the confined-bed comminution that occurs in the HPGR is more energy-efficient than the standard single-particle breakage as the energy is transmitted directly to the material, and also from one particle to another, hence leading to the breakage of particles under a very high-stresses.

The HPGR working principle is summarized as follow:

I. The feed chute is used to create a choke feed before the material reaches the rolls. As reiterated by Morley (2006), 'the HPGR must be choke-fed to maintain comminution efficiency.

II. The choke feed reaches two counter-rotating cylindrical rolls, one of which is fixed in the main frame (Fixed roll), while the other (Floating roll) is attached to a movable bearing system that allows it to move horizontally, expanding and contracting the gap, as the comminution takes place.

III. As the feed material is compressed by the counter-rotating rolls, a back-pressure to push the rolls apart is generated. To counterbalance the back-pressure, the floating roll is forced against the material by Hydraulic cylinders, which are commonly equipped with Nitrogen accumulators that allow control and monitoring over a pre-defined pressure.

IV. Finally, the product is discharged in the form of a compressed cake or flake that may have to be de-agglomerated before being sent to downstream processes.

Conforming to Bearman (2006), HPGR roll diameters typically range from 0.5m to 2.8m, and the roll width can vary from 0.2 m to 1.8 m. Both roll diameters and width configurations, including its aspect ratio, differs from one manufacturer to the other. As for the machine throughput, from pilot to industrial scale, the rates can vary from 20 to 3,000 tph, and each roll can support a motor power up to 3,000 kW.

2.1.1.1 Pressure distribution within the HPGR rolls

According to Rashidi et al. (2017), once a material reaches the HPGR counter-rotating rolls, three distinct zones can be identified during the operation. The first zone was identified as the acceleration zone, followed by the grinding zone and relaxation zone. Figure 2-2 presents a description of each zone. Once the material passes through the HPGR rolls, it is exposed to a gradient of pressure intensity along the gap between the rolls, as illustrated by Figure 2-3.

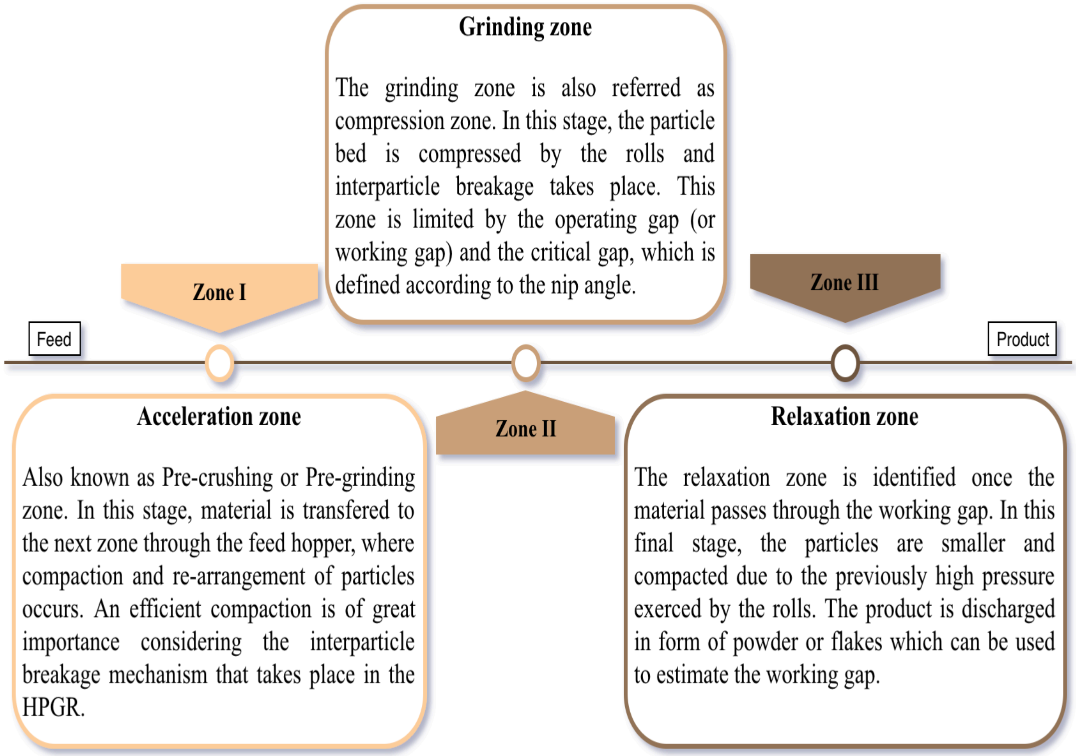

Figure 2-2: HPGR grinding zones

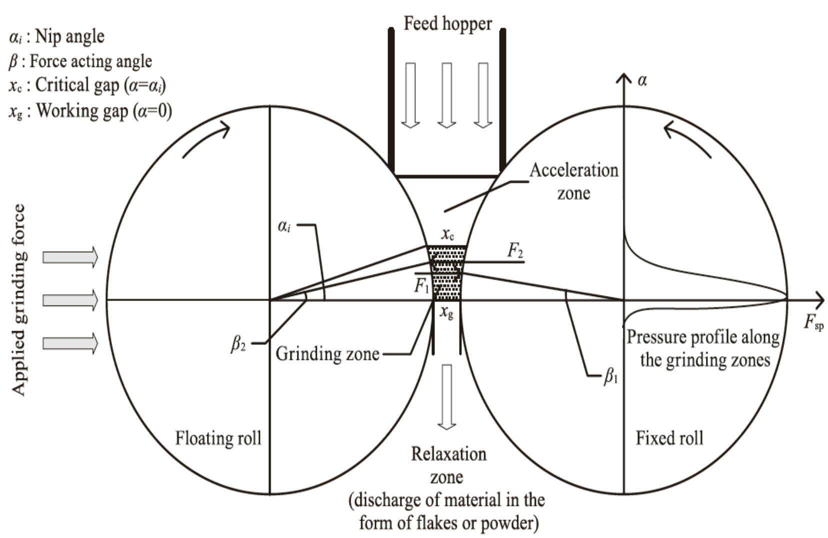

Figure 2-3: Grinding zones within the HPGR

(Source: Rashidi et al., 2017)

The pressure profile along the grinding zones shows that maximum pressure values are achieved when the material is about to reach the working gap, where the distance between the rolls is lowest.

Depending on the design of the rolls, HPGRs can experience what is called the "edge effect". Similarly to the gradient pressure observed from the critical gap to the working gap, there is also a gradient pressure across the width of the rolls. In this case, higher pressures are observed at the center of the rolls and decrease towards the edges. Consequently, product from the center of the rolls usually present a higher size reduction and superior portion of fines compared to products from the edges. Nadolski (2012) was able to model the stress field across the roll width of an HPGR for copper ore, as shown in Figure 2-4.

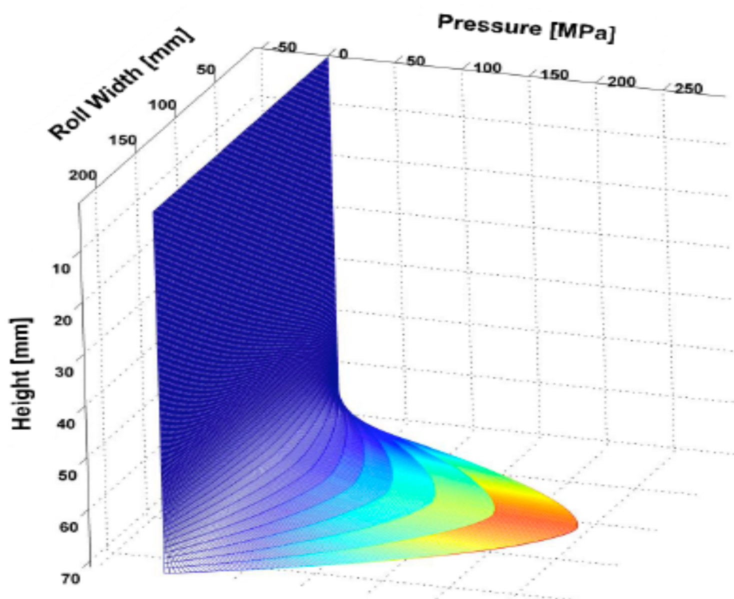

Figure 2-4: Modelled stress field across the HPGR roll

(Source: Nadolski, 2012)

Recent studies such as the ones of van der Ende (2019) and Knapp (2019) have shown that the edge effect can be minimized by adding cheek plates to the HPGR rolls and also by allowing the rolls to skew relatively to each other. The cheek plates prevent the material from flowing over the roller edges while the skewing between the rolls allows the machine to compensate for the uneven pressure caused by feed segregation.

2.1.1.2 HPGR Wear Protection Systems

The wear protection is one of the critical factors that must be considered when it comes to determining the operating costs and availability of an HPGR. Since its first appearance in the cement industry, different kinds of wear protection systems have been designed to improve machine efficiency so that it can meet the cement and mineral applications requirements. It is essential to mention that a wear protection system is not only defined by the kind of wear protection surface applied, but also the roll design. The following section presents the different types of roll surface profiles that have been used by the leading HPGR manufacturers and their characteristics.

The roll design can be divided into three configurations, as illustrated in Figure 2-5.

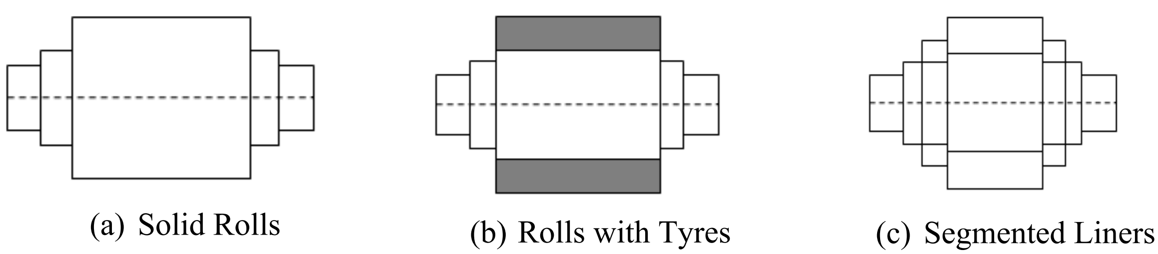

Figure 2-5: HPGR roll designs

Klymowsky et al. (2002) reviewed the differences between each of the three roll designs (Table 2-1) and also between the wear protection surfaces (Table 2-2). It is important to note that different designs can also be combined with various surface protections.

Table 2-1: Varieties of HPGRs rolls designs

Roll design	Construction	Applications	Advantages	Disadvantages
Solid Rolls	Compound castings or forging	Cement industry (grinding of hot clinker)	Low cost and low wear rates in cement applications	Not applied in the Mining Industry due to high wear rates
Rolls with Tyres	Compound, Bainite and Ni-hard castings	Cement Industry and Mining Industry	Low maintenance costs, longer life-times and no pressure restriction	Higher downtimes when compared to Segments
Rolls with segmented liners	Steel and Ni-hard castings	Mining Industry	Shorter downtimes and excellent performance on iron and diamond applications	Higher capital cost and only applied at low pressing forces

According to Nadolski (2012), during the 1990s, experiments showed that rolls with segmented liners were not appropriate for hard rock applications. After that, the manufacturers focused their lining upgrades on tire-based wear surfaces for this application.

Table 2-2: HPGR wear protection surfaces

Base material	Surface material	Surface type
Forging	Hard facing, hard metal studs or hard metal tiles	Smooth or welded-on profiles
Hard or Compound castings (Bainite or Ni-hard IV)	Not required	Smooth, welded-on profiles or grooved

Köppern developed the Hexadur surface protection, which is composed of hexagonal tiles of an abrasion-resistant material set into a softer matrix. The studded rolls are characterized by cylinder-shaped metal carbide pieces (studs) inserted into the roll surface. Both options have the advantage of promoting the formation of a protective layer of feed material on the surface of the rolls. As a result, they are well suited for hard rock applications since lower wear rates of the roll surface are achieved (Morley, 2010). Figure 2-6 shows the different types of wear protection surfaces, including the Hexadur technology.

(a) Welded-on profile (b) Studded profile (c) Hexadur profile

Figure 2-6: HPGR wear protection surfaces

For iron ore applications, Weir (2018) reported that their HPGRs roll surfaces were achieving a minimum lifetime of 14,000 hours and a maximum of 36,000 hours, depending on the operating conditions (refer to Table 2-3).

Table 2-3: Achieved lifetime of the HPGR roll surfaces

(Source: Weir, 2018)

Achieved Lifetime of HPGR Roll Surfaces (Operating Hours)	
Iron ore (pellet feed)	14,000 – 36,000
Iron ore (coarse)	6,000 – 17,000
Gold ore (coarse)	6,000 – 10,000
Kimberlite (coarse)	4,000 – 10,000
Phosphate ore (coarse)	6,000 – 12,000

2.1.2 HPGR History

In the late 1970s, the concept behind the HPGR working principle was first introduced by Professor Klaus Schönert. Initially, from his studies on single-particle breakage, Schönert (1988) concluded that slow compression loading of single particles was the most energy-efficient way of causing particle breakage. Next, he continued his research through fundamental studies over the interparticle breakage phenomena, where the breakage of beds of particles in a piston-die press was analyzed. The results revealed that confined particle-bed breakage was less energy efficient than single-particle breakage, but still considerably more efficient than tumbling mill grinding.

After acquiring his patent in 1977, Schönert started to negotiate its license with two German manufacturers, ThyssenKrupp Polysius and Weir, to produce the first HPGR units for industrial applications. The HPGR manufacturing process showed to be challenging, and issues such as the wear rate on the rolls were of great concern. Following its way to commercialization, Köppern, which is also a German manufacturer, further contributed to promoting the HPGR by making use of their previous experiences with developing roller presses for the briquetting process.

The HPGR was initially introduced as a cement industry product in the mid-1980s, where the objective was to treat comparatively easily crushed materials (Morley, 2006). The former units were applied for pre-grinding in front of Ball Mill circuits. Initial results not only revealed that the HPGRs could handle higher throughputs than the currently applied comminution technologies, but also gains of 10 to 30% on energy savings were reported (Gunter et al., 1996; Wüstner, 1986). About ten years later, to achieve the standard size requirements of the cement industry, HPGRs started to be applied in a closed circuit configuration, followed by Ball Mills (Schönert, 1995).

Despite its success in the cement industry, the HPGR acceptance in the mineral processing field was considerably slow from its first commercial application in 1985 through the 1990s. The first advance happened in 1987-88 when the diamond company De Beers installed an HPGR unit at their Premier diamond mine in South Africa. The results revealed that fine crushing with precise micro-cracking of kimberlite minerals in the HPGR liberated diamonds undamaged, while still reducing the circuit energy consumption. Next, continuous developments in the HPGR technology such as the use of studded rolls and improvements in the wear rates led companies like Argyle Diamonds in Australia to install units that were capable of crushing lamproite, which is even harder than kimberlite. By 2006, more than 20 HPGRs were already working at diamond operations around the world, including De Beers and Debswana mines in Africa and the Diavik and Ekati mines in Canada (Casteel, 2006).

After its recognition in the diamond processing, by the 1990s, the HPGR commenced its applications in the iron ore industry, where the technology immediately became a reference for pellet feed preparation (Casteel, 2005). In 2000, 450 HPGR units had been installed worldwide. As expected, the majority of the installations (400 units) were aimed at the cement and slag grinding industries, while the remaining 50 had been implemented in the diamond and iron ore industries (Knecht, 2004).

Despite its acceptance in the cement industry, Lim & Weller (1997) reported that one of the main reasons that fewer units had been applied to other segments of the minerals industry were the uncertainties and challenges in scaling up from laboratory and pilot-scale tests to full-scale comminutions circuits.

Following the HPGRs adaptation in the mineral processing industry, considerable interest in their application to hard rock ore processing such as harder copper and gold ores arose in the middle 1990s. According to von Michaelis (2009), the main attractions of the HPGRs to the hard rock ore processing are their high throughput rate and their ability to generate a product that reduces energy consumption and increases grinding capacity in downstream processes such as Ball Milling.

In 1995, Cyprus Amax commissioned a full-scale HPGR unit to mill ores at the Sierrita copper mine in Arizona, USA. Although the metallurgical results showed to be outstanding, the wear costs slowed down further investments in the technology. By taking the wear rate problem into account, the HPGR manufacturers focused their work on the machine roll and wear designs. After ten years of development for hard rock ore processing, the HPGR finally got its first commercial unit at the Cerro Verde mine in 2006. The constant search for an optimal wear design led to innovations such as the Hexadur wear protection, developed by Köppern around 1997, which allowed the HPGR to achieve up to 95% availability (Casteel, 2006).

Based on van der Meer and Maphosa (2012) analysis of the uptake of the HPGR technology in the mineral industry, by 2012, more than 100 HPGRs were already in operation or being installed, as illustrated in Figure 2-7, and new installations for various ore types and different applications quickly emerged after its first implementation in the hard rock ore processing, as described in Figure 2-8.

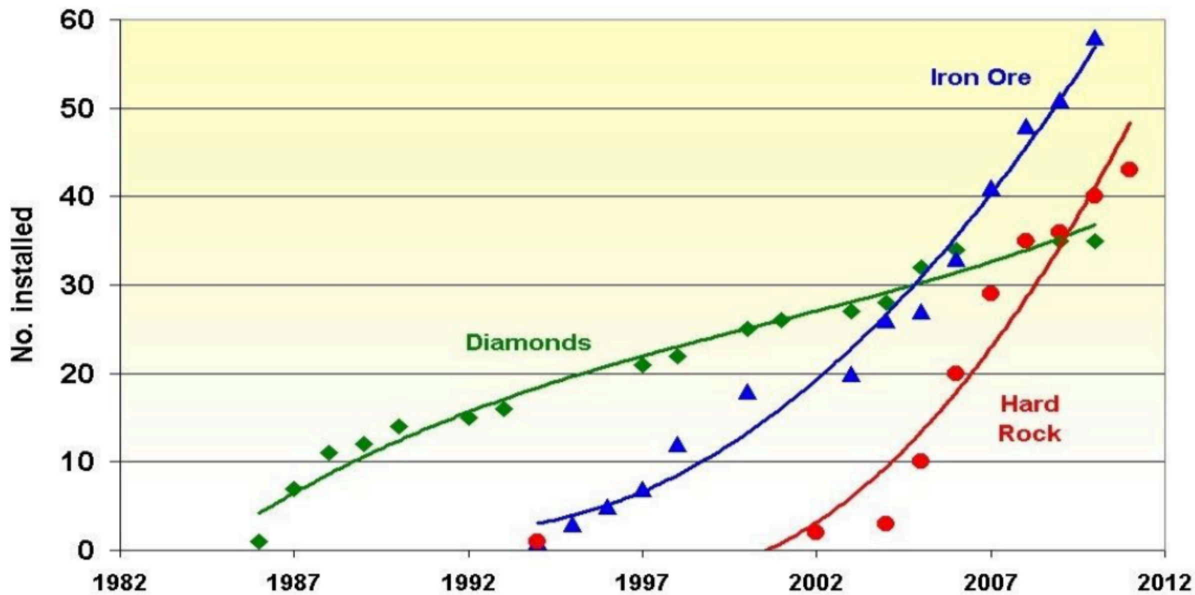

Figure 2-7: HPGR applications in the mining industry

(Source: Burchardt et al., 2011)

Project	Company	Location	No. of HPGRs	Throughput, kt/d	Ore Type	Year	Reference
Toquepala	Southern Peru Copper Corporation	Peru	2	~60	Copper porphyry	2017	—
Cerro Verde 2	Freeport-McMoRan	Peru	8	~240	Copper porphyry	2016	Vanderbeek and Gunson 2015
Sierra Gorda	KGHM/Sumitomo	Chile	4	~110	Copper-molybdenum	2014	López 2011
Morenci	Freeport-McMoRan	USA	1	> 115	Copper porphyry	2014	Herman et al. 2015; Knorr et al. 2015; Mular et al. 2015
Tropicana	AngloGold Ashanti	Australia	1	~15	Gold	2013	Gardula et al. 2015; Kock et al. 2015
Cuajone	Southern Peru Copper Corporation	Peru	1	~90 (quaternary)	Copper porphyry	2013	—
Salobo	Vale	Brazil	2	~33	Copper, gold	2012	—
Cadia Hill	Newcrest	Australia	1	~55 (HPGR-semiautogenous grinding hybrid)	Copper, gold	2012	Engelhardt et al. 2015
Peñasquito	Goldcorp	Mexico	1	~+100 (pebble crusher circuit)	Polymetallic	2010	—
Boddington	Newmont	Australia	4	~100	Gold, copper	2009	Hart et al. 2011; Tavani et al. 2015
Mogalakwena	Anglo Platinum	South Africa	1	~25	Platinum	2008	Rule et al. 2008, 2015
Grasberg	Freeport-McMoRan	Indonesia	2	~70 (quaternary)	Copper, gold	2007	—
Cerro Verde 1	Freeport-McMoRan	Peru	4	~108	Copper porphyry	2006	Koski et al. 2011; Vanderbeek et al. 2006

Figure 2-8: List of HPGR in base and precious metal installations

(Source: Daniel et al., 2019)

2.1.3 HPGR: Pros and Cons

It has been demonstrated that the HPGR has plenty of advantages to offer when compared to conventional comminution machines, but it does have disadvantages and hindrances to be considered. The following sections list the main pros and cons that have been identified and proven by researchers and manufacturers.

2.1.3.1 Advantages

Weir (2018) listed the following benefits of HPGR technology to the minerals industry:

- Low energy consumption (0.8-3kWh/t),
- Ability to process moist ores,
    - Fe, pellet feed (6-12%),
    - Fe, Cu, Au ores (2-6%),
    - Diamond Ore (2-8%),
    - Phosphate Ore (3-8%),
- Enhanced downstream process recovery and grindability,
- Improved grade of downstream products,
- Low maintenance requirements,
- Low space requirements,
- Low vibration and noise,
- High availability (>95%),
- High wear surface life (4,000-36,000 hrs).

According to Anguelov et al. (2008), selecting an HPGR circuit instead of conventional SAG circuits can result in energy savings of up to 20%, reduced grinding media consumption and overall operating costs. In additional, HPGR circuits also have smaller footprint compared to other crushers and ball mills of equivalent capacity.

Regarding the energy consumption subject, Wang et al. (2013) conducted a comparison between a novel HPGR-stirred mill circuit, an HPGR-Ball Mill circuit and the conventional SAG mill-based circuits. The HPGR-Ball Mill circuit achieved a 21% reduction in energy consumption when compared with a SAG-Ball Mill circuit at a P80 grind size of 160 µm, and the HPGR-stirred mill circuit revealed even more positive results, with a 34% reduction in energy consumption over the SAG-Ball mill circuit at a P80 grind size of 75 µm.

Von Michaelis (2009) also reported that energy savings ranging from 10-20% are expected when comparing HPGR vs. SAG mill-based circuits. However, the energy savings are ore-specific, thus the performance of the machine can be influenced by the ore characteristics. For example, the author mentioned a case study at Vista Gold's Mt. Todd, Western Australia, where an HPGR was able to reduce the total energy consumption of a conventional semi-autogenous/Ball Mill/crushing circuit (SABC) by almost 35%, while Vanderbeek et al. (2006) compared the specific energy consumption of Cerro Verde's conventional SABC circuit with an HPGR-Ball Mill circuit and concluded that total savings of more than 20% could be achieved.

It is also worth mentioning that HPGR grinding can enhance an overall circuit throughput. For example, Dunne et al. (2004) conducted a comparison between the comminution performance of the HPGR and conventional cone crushing at the Argyle diamond mine. The results revealed that the cone crusher utilized 0.5 kWh/t and produced 8-10% material below 2.3mm, while the HPGR operated at energy levels up to three times higher and produced 32-48% material below 2.3mm. The throughput enhancement is of high importance since it allows a reduction in the required number of crushing or grinding units.

Considering that currently the majority of the ore bodies contain lower grade ore that is harder or require more processing stages than the ones from decades ago, the increase in the throughput and lower energy consumption are significant factors to take into consideration for high productivity processing plants that need minimization of operating cost in order to reach viability (Burchardt and Kessler, 2015).

A further significant advantage of the HPGR originates from its compression mechanism, which is known to cause micro-cracks in the obtained product. The presence of micro-cracks in the HPGR product can reduce the product work index and consequently increase the grinding capacity of subsequent milling stages. For instance, in cyanide leaching processes for gold ores, these micro-cracks have shown to improve the extraction rate by 5-25% (Senchenko et al., 2016). Figure 2-9 illustrates a comparison between gold ore particles that were crushed by an HPGR (a) and a cone crusher (b).

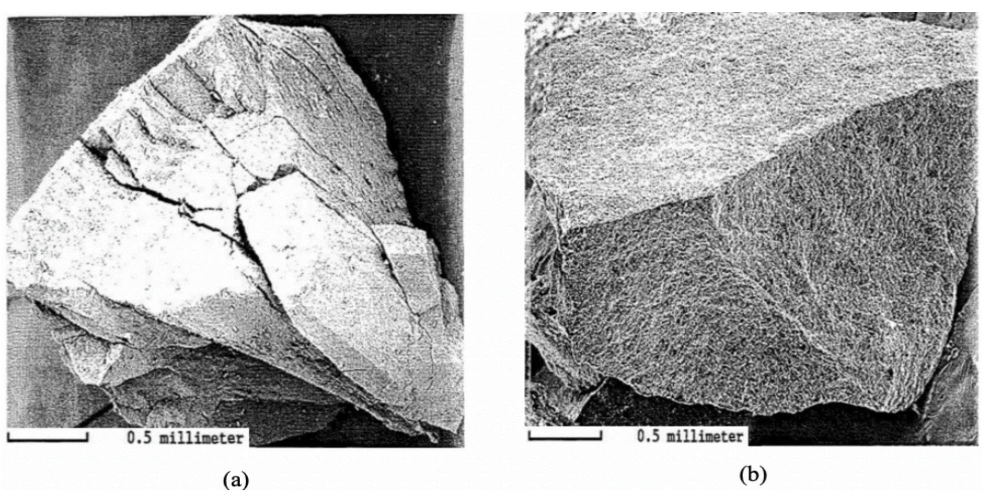

Figure 2-9: (a) HPGR crushing vs (b) conventional crushing

(Source: Adams, 2016)

Barani and Balochi (2016) conducted a comparative study on the effect of using conventional and HPGR crushing on the Ball Mill grinding kinetics of iron ore and reported that the HPGR not only increased the breakage rate of iron ore but also produced a softer feed for the

Ball Mill grinding stage. Besides its substantial savings in energy and grinding media when compared to tumbling mills, the HPGR may also be regarded as a metallurgical tool since it can improve downstream processes performances such as grinding, cyanide leaching and flotation.

2.1.3.2 Disadvantages

HPGRs usually have higher capital costs than conventional comminution equipment such as SAG mills. The higher capital costs are mainly due to the need for auxiliary equipment like screens or crushers, which are often required in multi-stage HPGR crushing circuits. As stated by Anguelov (2008), the capital cost needed for installing HPGRs is generally 6% to 10% higher than equivalent SAG Mills. As a case in point, Vanderbeek et al. (2006) conducted a capital cost comparison at Cerro Verde operation and showed that the HPGR capital cost exceeded the SABC's direct costs by approximately 23.5%.

Morley (2006) reiterated that the main disadvantages to the adoption of HPGRs in hard-rock processing are:

I. The generally conservative nature of the mining industry.

II. Perception of high cost, especially with regards to the replacement of wear parts in abrasive applications.

III. A scarcity of the definition of the requirements for robust flowsheet design of an HPGR-based comminution circuit.

IV. Uncertainties regarding the reliability of modelling and scale-up from laboratory or pilot operations to industrial installations.

Another downside of HPGRs is that they are not generally suitable for the treatment of highly weathered ores or feeds containing a large proportion of fines/clays. Although this disadvantage does not apply for applications where the treated material is already mainly composed by fine particles (e.g. fine grinding of concentrates), Bearman (2006) reported that fine and weathered material diminishes the action of the rolls and thereby reduces the efficiency of comminution of the larger feed particles.

HPGRs are also sensitive to feed top size, especially on hard-rock applications. As stated by Morley (2003), while the rolls surface wear rate is a function primarily of the abrasion index of the ore, stud breakage is mainly a function of top-size. Therefore, it is recommended that the feed top size does not exceed the roll operating gap.

Lastly, the HPGR performance can be lowered when treating feeds with high moisture content. Although the impacts may vary depending on the HPGR application and ore type, it has been reported that excessive moisture can cause washout of the autogenous layer on studded rolls and increases slippage on smooth rolls, thus affecting the machine performance and increasing the wear rate. On the other hand, feeding the machine with dry material may also be problematic since it generates a considerable amount of dust. Therefore, dry operations that have limited access to water may see this as a critical disadvantage (Anguelov, 2008).

2.1.4 HPGRs in the Iron Ore Industry

The HPGR technology made its first appearance in the iron ore industry in the 1990s and was initially used for grinding iron ore concentrates for pelletizing. According to Köppern (2018), which is one of the principal HPGR manufacturers, the machine rapidly proved to be of high efficiency, increasing the throughput of pellet plants by up to 30%. Whether as an individual grinding device or in combination with Ball Mills, the HPGR has been demonstrating to not only increase the circuit throughput but also to enhance the pellet quality.

Table 2-4 summarizes Casteel's (2006) review about some of the industrial HPGR applications in the iron ore industry up to 2004. Although most of the early HPGR applications were aimed for pellet feed preparation, technological innovations have been expanding its applicability range. After 2001, with improved wear protection designs, the HPGR quickly gained recognition as a feasible option over conventional tertiary and quaternary crushing machines such as cone crushers and SAG Mills. Nowadays, as exemplified in this research's case study, mining companies have started to implement the HPGR in fine crushing and grinding applications.

Recent studies such as the one of van der Meer et al. (2015) have been exploring the HPGR applications in dry grinding operations. According to the authors, dry processing of iron ores is becoming more popular due to increased operating costs and the scarcity of process water in arid regions of the world.

Table 2-4: Examples of industrial HPGR applications in the iron ore industry

Project:	Year:	Application:	Findings:
LKAB, Malmberget mine, Sweden	1994	Pellet feed preparation	Fine grinding filter cake process allowed high throughput at reduced energy consumption and improved grain characteristics
LKAB, Kiruna mine, Lapland	1995		
Vale, Tubarão pellet plant, Brazil	1996		
Cleveland Cliffs, Empire mine, USA	1997	Pebble Crushing	High throughput was achieved, and studded tires reported over 14,600 operating hours
SNIM, Mauritania	1998	Pebble grinding	
Kudremukh Iron Ore Co. India	1998	Pellet feed preparation	Filter cake grinding applicability
Vale, Vitória pellet plant, Brazil	2003		The HPGR proved to be a viable alternative for replacing Ball Mill grinding circuits at pellet plants, without the need for thickeners and filters
Samarco, Ponta Ubu processing plant, Brazil	2003		
WISCO Minerals, Chengchao operation, China	2002		HPGRs were initially applied to improve the strength of the pellets and increase the porosity of the final product. At the Shagang plant, the machine was applied to comminute filter cake with around 8% residual moisture
WISCO Minerals, E-Zhou pelletizing plant, China	2004		
Zhangjiang Hongchang Pellet Co, Shagang plant, China			
CMP, Romeral plant, Chile	2004	Tertiary/Quaternary crushing	Achieved high throughputs and resulted in 15-25% energy savings in the pelletizing plant

2.1.5 Pellet Feed Grinding by HPGR

A standard pellet feed preparation circuit consists of using Ball Mills to re-grind the concentrate to a size that is suitable for agglomeration, followed by dewatering processes to adjust the moisture content to below 8-9%. This circuit is known to be costly and problematic since the dewatering and filtering stages lose efficiency when dealing with very small particle sizes. Since its introduction in the iron ore industry, the HPGR became an alternative for the standard Ball Mill circuits. As mentioned by Burchardt et al. (2011), the HPGR can replace, entirely or partly, Ball Milling stages, and it can also be applied after filtering stages. Abazarpoor et al. (2018) reiterated the importance of the re-grinding stage since flotation, magnetic and gravity separation circuits usually reduce the fines fraction of the pellet feed, and hence its specific surface area (SSA).

When applied ahead or after Ball Milling, the HPGR can provide the following benefits to the circuit (Shu and Yongqing, 2008):

I. Reduces the ore residence time in Ball Mill stages, thus increasing the milling capacity and reducing the media consumption.

II. Reduces the operating cost associated with dewatering and filtering stages.

III. Reduces overall energy consumption since the energy consumed by the HPGR and filters is lower than the Ball Mill.

Table 2-5 exemplifies two large-scale operations in Brazil where the HPGR was successfully applied in pellet feed preparation.

Table 2-5: HPGR applications in pellet plants

(Source: Kessler and Burchardt, 2015)

Project:	Circuit description:
Vale, Vitória pellet plant, Brazil	Their circuit had three Ball Mills (Thyssen Krupp, diameter 5.5 m, length 12 m) with 5.35 MW drives and one HPGR (Polycom-20/15). The Ball Mill product has a specific surface area of 2000 cm^2/g and a single pass HPGR grinding yields a pelletizing product with specific a surface area of 2000 cm^2/g at an overall capacity of 1000 t/h.
Vale, São Luis pellet plant, Brazil	Three HPGRs (Polycom 17/12) were applied to produce a grinding product with a specific surface area of 2000 cm^2/g at a capacity of 650 t/h. The previous Ball Milling stage was removed as the HPGR product achieved products with an almost double specific surface area.

It can be noted that both circuit descriptions presented in Table 2-5 emphasize the effect on the specific surface area of the HPGR product. As mentioned by van der Meer (2015), when applied in pre-pelletizing stages, HPGR comminution involves a combination of fines generation and creation of a product with a high specific surface area. Therefore, the formation of high-quality pellets depends on its proportion of fines, which is defined by both size distribution and specific surface area. For example, Abazarpoor and Halali (2017) studied the particle size and shape of iron ore pellet feed using Ball Mill and HPGR grinding methods and observed that the HPGR product generated a higher surface area when compared with the Ball Mill product. For samples having the same Blaine specific surface area, the amount of fines particles produced by the HPGR was higher than in a Ball Mill.

2.1.6 HPGR Applications in Crushing and Pre-concentration Plants

In general, current HPGR applications focus around either open circuit tertiary crushing or pre-grinding stages, being a viable option over the conventional third and fourth stage crushers such as Rod Mills, Pebble Crushers in (S)AG circuits, or closed circuit operations with classification (van der Meer and Gruendken, 2010). Considering the potential flowsheets that have been proposed for HPGR applications, those applying the machine as a tertiary crusher in closed circuit with fine screens are expected to provide maximum energy efficiency (Rosario et al., 2011). As stated by Kessler and Burchardt (2015), when applied as a quaternary crusher to produce finer feed for Ball Milling, the HPGR can enhance the productivity of a processing plant by up to 30%.

According to von Michaelis (2009), the advantage of commissioning a single HPGR unit was first seen in the Los Colorados mine. The HPGR replaced multiple third and fourth stage crushing units and was installed in closed circuit to produce more than 1,000 tph of -6 mm product from a 65 mm feed material. Several benefits were observed, including high wear protection lifetimes (over 8,000 hours) and low power consumption (1.3 kWh/t).

Figure 2-10 shows a simplified flowsheet of the HPGR-based circuit at the Los Colorados mine:

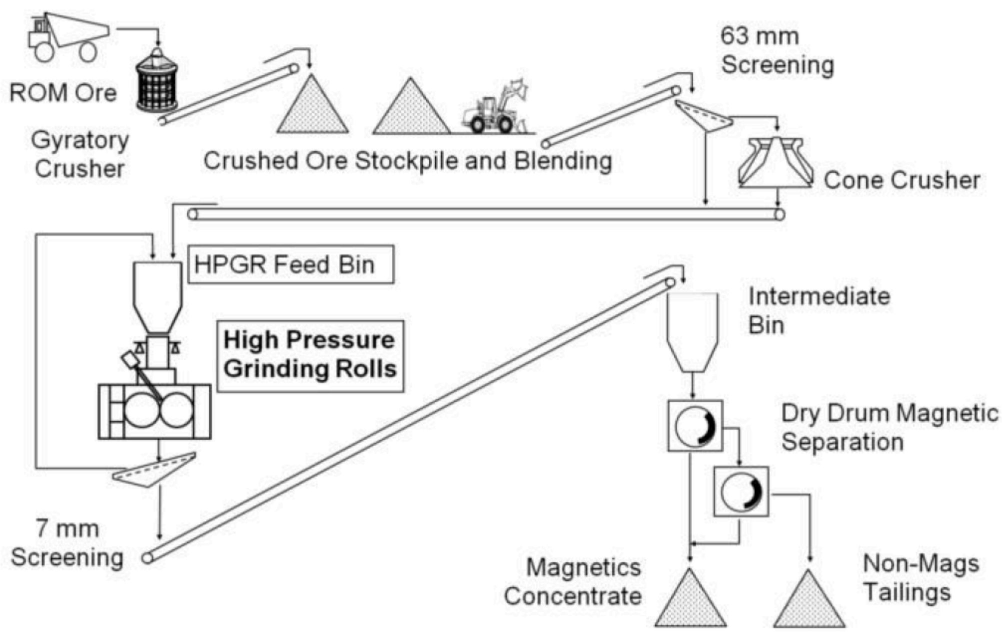

Figure 2-10: Simplified flowsheet of Los Colorados comminution circuit

(Source: van der Meer and Maphosa, 2012)

HPGR pilot testing conducted at the Los Colorados plant revealed that the machine could not only replace the existing tertiary and quaternary crushers but also considerably improve downstream processes in the pellet plant. After its implementation in the industrial plant, the pellet plant increased the Ball Milling capacity by 30% and reduced the overall energy consumption by almost 20%. In addition, the rolls wear life was considerably higher, reaching 12,000 hours, and the machine availability was above 97%.

Jankovic (2015) compared four circuit options for a 10 Mtpa ore processing plant to treat a hard, fine-grained silica-rich magnetite ore. The best results were obtained in a circuit where the application of the HPGR and stirred mill technologies reduced the energy consumption by up to 25% compared to conventional flowsheets with wet tumbling mills. The author also accounted for savings with grinding media and observed a significant reduction of up to 26% of the operating costs.

2.2 HPGR Sizing and Operating Parameters

The HPGR is well known for its particularities when it comes to operating parameters. Apart from standard parameters such as roll speed in conventional roll crushers or feed properties, the HPGR also has specific parameters that are used to describe its performance and are applied to machine sizing and selection stages, as presented below:

2.2.1 Specific Throughput Constant

The HPGR specific throughput, also known as m-dot or ṁ, is expressed as the machine throughput [tph], divided by the roll width [m], roll diameter [m] and the peripheral roll speed [m/s], as shown in Equation. 2.1.

$$m - dot = \frac{M}{D \times L \times v} \tag{2.1}$$

where:

M = throughput rate [tph],

D = roll diameter [m],

L = roll width [m],

v = roll peripheral speed [m/s],

m-dot = specific throughput constant [ts/m^{3}h].

It is important to mention that the m-dot is independent of the machine size and therefore allows up- or downscaling for a given feed material and roll surface (Neumann, 2006). This feature allows the m-dot parameter to be used to compare HPGR results from different suppliers for scale-ups.

Table 2-6 presents the m-dot values reported from 177 pilot-scale HPGR tests that were conducted at the University of British Columbia. Studies such as the one of Herman et al. (2015) and Banani et al. (2011) have shown that depending on the dimensions of the rolls, industrial-scale HPGR units can present up to 30% higher m-dot than determined from pilot-scale testing.

Table 2-6: m-dot values from UBC pilot-scale HPGR database

(Source: McClintock & Klein, 2016)

Ore Type	Specific Throughput Constant [ts/m^{3}h]	Standard Deviation
Ag	234	2.8
Au	226	16.8
Cu-Au	215	16.5
Cu-Au-Ag	228	14.2
Cu-Mo	210	35.2
Dolomite	261	5.4
Granodiorite	187	14.9
Hematite	**233**	**13.9**
Kimberlite	172	37.0
Limestone	231	28.1
Ni	207	10.0
Pd	276	32.5
Taconite	269	8.6
Tungsten	242	14.4

2.2.2 Net Specific Energy Consumption

The specific energy consumption (E_{SP}) of an HPGR refers to its power input [kW] divided by the throughput rate [tph]. When it comes to HPGR scale-up and performance evaluations, the net specific energy consumption parameter is more appropriate than the total energy consumption since it does not account for the idle power draw (Rosario, 2010). The E_{SP} can be expressed as follow:

$$E_{SP} = \frac{(Pt - Pi)}{M} \tag{2.2}$$

where:

E_{SP} = net specific energy consumption [kWh/t],

Pt = total main motor power [kW],

Pi = idle power draw [kW],

M = throughput rate [tph].

According to Bearman (2006), the E_{SP} is usually proportional to the applied specific pressing force (F_{SP}) and common operational values for studded rolls vary from 1 to 3.5 kWh/t. In addition, the E_{SP} can be affected by the feed size distribution and top size.

2.2.3 Operating Gap

The operating gap of an HPGR indicates the smallest distance between the fixed roll and the floating roll while the HPGR is operating. According to Morley (2006), this parameter is not adjustable by the operator and is a function primarily of the roll diameter, the ore characteristics and the roll surface texture. Knapp et al. (2019) showed through an extensive database that the operating gap can be estimated as being equal to approximately 2.5% of the roll diameter.

2.2.4 Specific Pressing Force

The specific pressing force (F_{SP}) of an HPGR corresponds to the total force applied by its hydraulic system to the rotating roll, divided by the rolls projected area (D x L) (Senchenko and Kulikov, 2016). The F_{SP} can be expressed as follow:

$$F_{SP} = \frac{Ftotal}{D \times L} \tag{2.3}$$

where:

F_{SP} = specific pressing force [N/mm^2],

Ftotal = total hydraulic pressing force [N],

D = roll diameter [mm],

L = roll width [mm].

As highlighted by Kumar (2014), the F_{SP} is a key parameter since it controls the HPGR's energy consumption, product size distribution and the operating gap. As seen in Eq. 2.3 and like the specific throughput constant parameter, the F_{SP} represents a normalized value, which means it is also independent of machine size and can be used in machine scale-up processes. For reference, standard F_{SP} operating values are in the range of 1 to 4.5 N/mm^2 for studded roll surfaces and up to 6 N/mm^2 for the Hexadur technology (Morley, 2010).

Figure 2-11 shows the relationship between the HPGR operating parameters that can be used in scale-up processes. It should be noted that different terminologies have been used in HPGR publications to represent the operating parameters. For example, in this study, the specific grinding pressure terminology shown in Figure 2-11 refers to the specific pressing force, and specific power consumption refers to net specific energy consumption (E_{SP}). It should be noted that the roll dimensions are directly related to the required specific throughput constant (m-dot), while HPGR motors are sized based on the required net specific energy consumption.

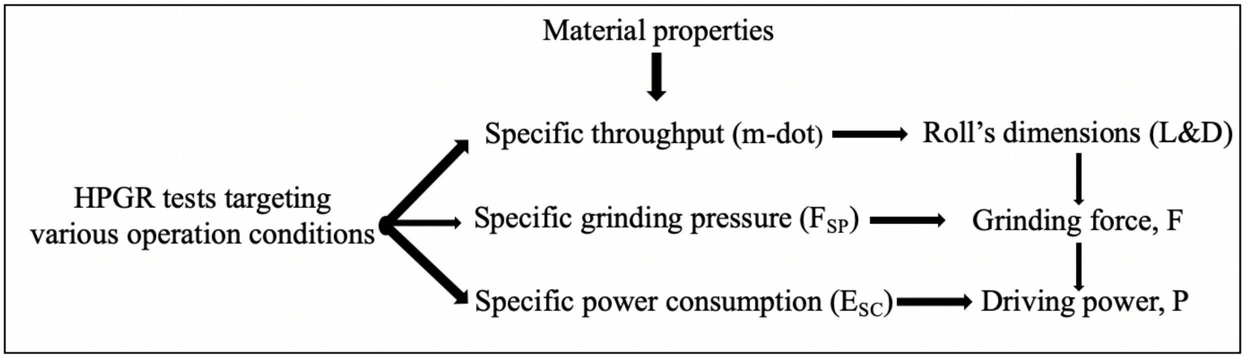

Figure 2-11: Relationship between the HPGR scale-up parameters

(Source: Rashidi et al., 2017)

Sizing of HPGRs is critical for meeting throughput requirements and achieving the desired product fineness. HPGR sizing is predominantly performed by manufacturers. The procedure is costly and involves acquiring large amounts of samples of up to 6 tons of material which is then used in pilot-scale testing to generate the necessary data for sizing the machine.

2.3 Assessing HPGR Performance

The effectiveness of the HPGR performance is determined by its operating factors as well as by the specific properties of the feed material (Schönert and Lubjhun, 1990). The particular properties of the feed material include factors such as the mineralogical composition, mineralogical texture, granulometric composition, top size, moisture content, abrasion index and grindability (Daniel et al., 2009).

A common practice for analyzing the HPGR performance through pilot testing is to acquire various data points tests conducted at different pressing forces, roll speed over a range of moistures, and then investigate how these variables affect the machine performance in terms of the net specific throughput and the net specific energy consumption. The test work performed in this study had the specific pressing force and ore moisture as the main variables for analysis.

Key questions that need to be addressed from a detailed HPGR pilot test work include:

i. How does the specific pressing force affect the net specific energy consumption?

ii. Does the E_{SP} increase linearly with the F_{SP}? If yes, up to which point?

iii. How is the operating gap affected by changes in the F_{SP} and ore moisture?

iv. How are the E_{SP} and F_{SP} being affected by changes in the ore moisture level?

v. How is the m-dot affected by changes in the feed properties such as if the feed is coarser, finer or if the size distribution is truncated?

Considering that this research focused on conducting a detailed analysis of HPGR pilot-scale testing and also to make use of methodologies that aim to predict the machine energy consumption and size reduction, it was essential to review and understand how the HPGR operating parameters interact with each other and to confirm if the findings are in line with published literature.

2.3.1 Specific Pressing Force and Reduction Ratio

Saramak and Kleiv (2013) reported that the reduction ratio is expected to increase linearly with the F_{SP} up to a certain limiting point (refer to Figure 2-12). This limiting point is referred to as the *energy saturation* point, which is a processing condition that defines the optimum conditions of the HPGR for a given ore type and application. In case the process operates at energies above the energy saturation point, higher energy consumptions are expected, and the linearity between the specific pressing force and size reduction tends to decrease.

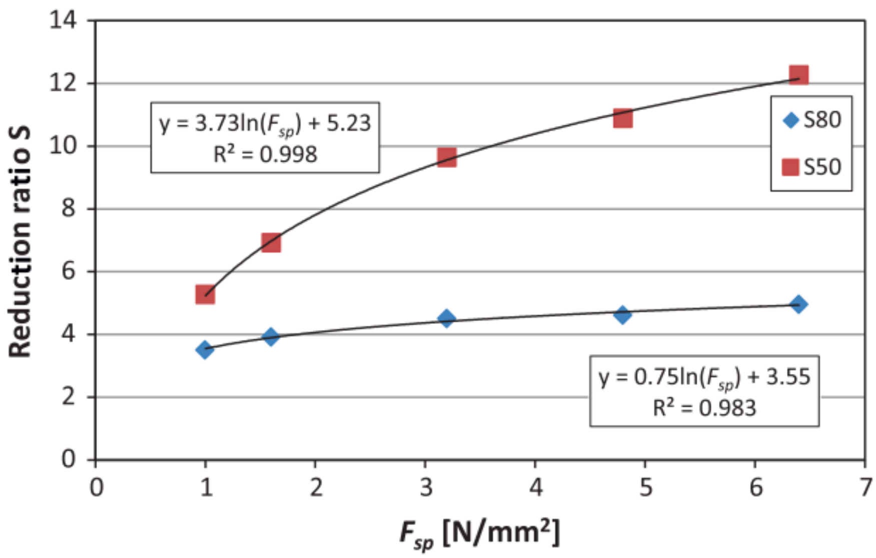

Figure 2-12: Interaction between the specific pressing force and reduction ratio

(Source: Saramak and Kleiv, 2013)

2.3.2 Specific Pressing Force and Net Specific Energy Consumption

The relationship is between the net specific energy consumption and the specific pressing force is typically linear. As an example, Figure 2-13 shows graphical plots (E_{SP} versus F_{SP}) of pilot-scale HPGR test results that were conducted by Wang (2013) for three different samples. According to Davaanyam (2015), the linear relationship between F_{SP} and the E_{SP} is typical for specific pressing forces values that range from 2 to 5 N/mm^2.

In line with the previous findings, Makni et al. (2019) conducted pilot-scale HPGR tests on samples from the Côté Gold Project, and the results also confirmed the linearity between the E_{SP} and F_{SP}. Their test work results revealed that lower operating gaps were recorded at higher pressing forces, and lower m-dot values were observed at low (2-3 N/mm^2) and high (6-7 N/mm^2) pressing forces, as shown in Figure 2-14.

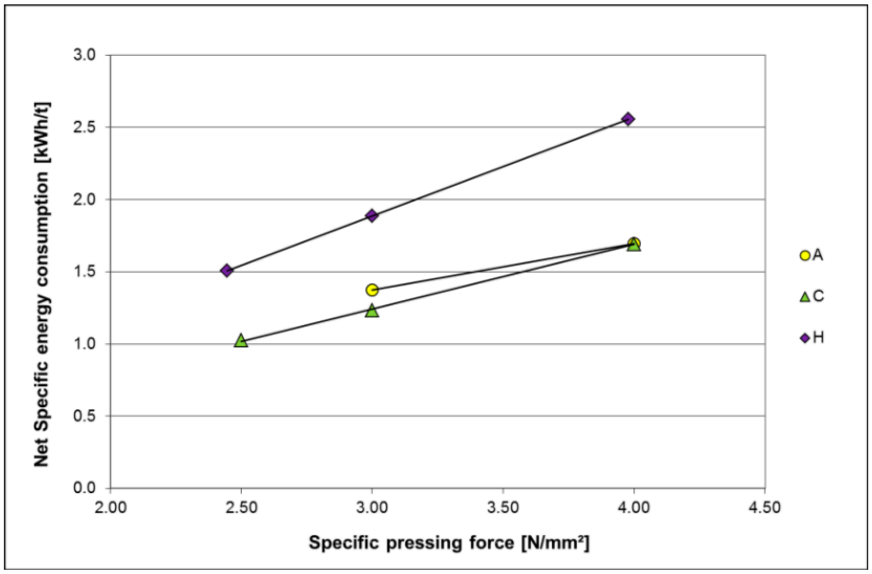

Figure 2-13: Interaction between F_{SP} and net specific energy consumption

(Source: Wang, 2013)

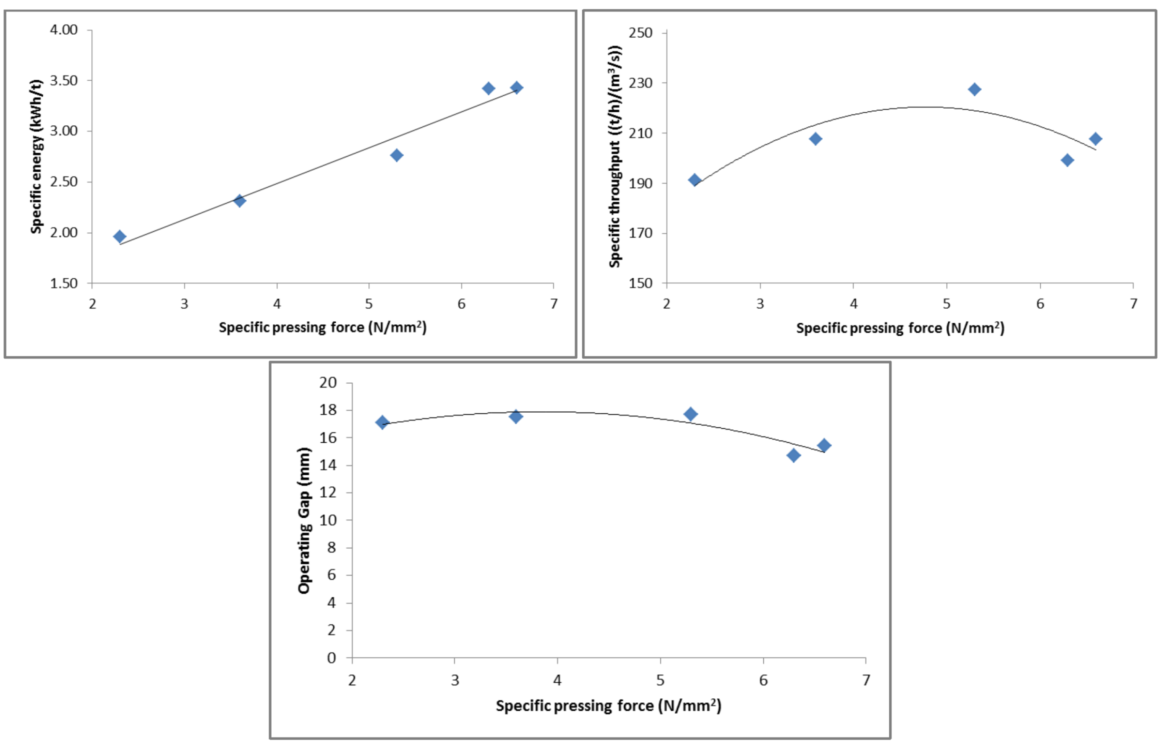

Figure 2-14: Comparison between HPGR operating parameters

(Source: Makni et al., 2019)

2.3.3 Specific Pressing Force and Operating Gap

After completing his first grinding survey with the HPGR, Schönert (1988) observed that the machine operating gap decreased as the specific pressing force and the feed moisture increased. Schönert reported that a finer product (material below 40 μm) and higher specific energy consumption was obtained for experiments at higher moisture levels. Concerning the machine throughput, Klymowsky (2002) found that for most ore types, the specific pressing force has a low impact on the HPGR throughput, and Wang (2013) reinforced this observation by showing, via pilot-scale HPGR tests, that a smaller operating gap is expected at higher pressing forces.

2.4 Effects of Ore Moisture Content on the HPGR Performance

Although the feed material properties play an important role in the HPGR performance, there is still limited literature on the subject, especially concerning the ore moisture content. As previously cited in section 2.1, for certain ores and depending on the application, the HPGR can process ores with up to 12% moisture by weight, which improved significantly compared to other crushing machines. However, the interaction between moisture and HPGR performance is not well researched for several ore types and circuit applications. For iron ore applications, which was the focus of this research, publications that investigate the effects of moisture on the HPGR's net specific energy consumption and throughput for fine crushing applications could not be found.

Saramak (2011) performed a series of pilot-scale HPGR tests on a kimberlite sample to investigate the influence of chosen ore properties on the efficiency of HPGR-based grinding circuits. The results showed that the feed particle size distribution significantly influenced the process throughput and size reduction. For example, screening to remove fines decreased the circuit throughput by up to 30% and also resulted in higher energy consumptions. Also, variations in the feed moisture content decreased the m-dot by up the 15% when low specific pressing forces were applied, and fewer impacts were observed at higher F_{SP} values. Regarding the process size reduction ratio and moisture level, the best-case scenario was found at moistures between 2.5-3%, as shown in Figure 2-15.

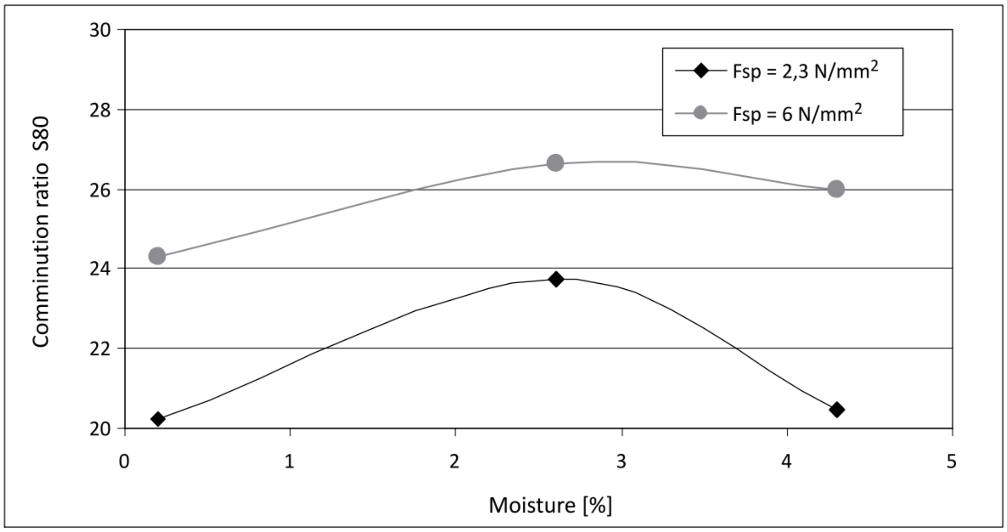

Figure 2-15: Feed moisture content versus reduction ratio of pilot-scale HPGR tests

(Source: Saramak, 2011)

According to Fuerstenau and Abouzeid (2007), excessive moisture in the HPGR feed can trigger the following impacts on the HPGR performance:

i. Removal of the material layer from the rolls.
ii. Increased wear of linings.
iii. Slippage of the feed material, which in turn decreases the circuit throughput.

2.5 HPGR Modelling

In mining applications, modelling and simulation of process equipment are essential tools for developing or optimizing circuit flowsheets. Whether implemented in the early stages of a project or during ongoing operations, models of process equipment can be applied for a variety of purposes, including equipment sizing and equipment trade-offs. According to Bearman (2006), when it comes to HPGR modelling, the critical process variables that need to be estimated or predicted during the design phase of a process plant include the following:

I. Machine specific throughput constant (m-dot),
II. Achieved size reduction (product and oversize),
III. Net specific energy consumption (E_{SP}),
IV. Operating gap and optimum specific pressing force (F_{SP}).

With these parameters, it is possible to conduct preliminary sizing of HPGRs for a given application, which in turn allows for HPGR-based circuit evaluations.

2.5.1 Piston-press Testing

The main ore characterization tests for HPGR modelling are the piston-press and drop-weight procedures. The drop-weight test was developed at University of Queensland's Julius Kruttschnitt Mineral Research Centre (JKMRC) in 1992. The test is a single-particle test and, therefore, when it comes to HPGR applications, it is mainly applied to analyze areas in the HPGR rolls where the breakage is of a single-particle nature. In contrast, the piston-press test is applied in the characterization of the packed-bed breakage zone in the HPGR, which represent the most significant breakage mechanism that takes place in the HPGR.

The piston-press test, also referred to as the piston-die test, was first introduced by Schönert (1988) during his fundamental studies on interparticle breakage. Since then, researches have applied the piston-press test to predict sizing information for HPGRs and also to determine the amenability of different ores to HPGR treatment. In addition to having the same breakage mechanism as the HPGR machine, the piston-die apparatus also requires far less sample than lab-scale HPGRs and allows control over the compression rate. These characteristics are reasons that the piston-die testing has become an appropriate tool for measuring the breakage rates and the breakage distribution functions for modelling that have been published to date (Rashidi et al., 2017).

Table 2-7 summarizes relevant studies performed with the piston-die apparatus that contributed to its acceptance as a suitable tool for predicting the HPGR performance.

According to Davaanyam (2015), the lack of an industry-accepted small-scale test for sizing and selection of an HPGR is one of the main reasons for its slow implementation in the industry. Davaanyam conducted a detailed analysis of various small-scale procedures for sizing HPGRs that were published up to 2015, which were the SPT test and the SAG Mill Comminution (SMC) test, and concluded that they had several shortcomings, including the fact that both are proprietary.

Table 2-7: Researches that utilized the piston-press test for predicting the HPGR performance

Reference	Research Description	Main Findings
Daniel (2003)	Piston-press tests were conducted to correlate its operating parameters such as working gap, critical gap and grinding force with lab-scale HPGR test results.	The results revealed that under a specific energy input range of 2.5-3.5 kWh/t, the product size distribution of the machines that had the same feed size distribution was comparable.
Kalala et al. (2006)	Piston-press tests were performed with different piston-die setups to simulate the breakage in an HPGR. The effect of thickness of the particle bed and pressure were also analyzed.	The author recommended that during piston-press tests, the ratio of initial bed thickness to feed top size should be set at 1.5 and that it is possible to incorporate the edge effect with the piston-die setup.
Hawkins (2007)	Piston-press results were compared to lab-scale HPGR results by applying force and displacement methods.	The results showed that the piston-press test could be applied individually or in combination with lab-scale HPGR tests to predict the performance of an industrial scale HPGR unit.
Bulled and Husain (2008)	The author developed a piston-press procedure called Static Pressure Test (SPT) that can determine a work index for HPGRs.	The SPT test was able to identify a high-pressure grindability index for an HPGR and predict its specific energy consumption.
Davaanyam (2015)	The author proposed three piston-press methodologies that calibrate the piston-press results against results from pilot-scale HPGR tests to predict the machine specific energy consumption and size reduction.	The results reinforced, for many ore types, the similarity in piston and HPGR product size distributions. The energy and size reduction predictions were reasonably accurate and ranged from 10-25% depending on the applied methodology.

With the increasing popularity of the HPGR amongst comminution process designers, the HPGR manufacturers are developing proprietary lab-scale characterization tests which are based on piston-press tests to predict the performance of their machines. For example, Qiu (2019) presented a semi-mechanistic model that makes use of data obtained through piston-press tests to estimate the power, throughput and product size distribution for Metso's HRC^{TM} HPGRs. In this case, the proposed model is only applicable to flanged roll HPGRs and impacts of feed characteristics such as moisture level were not considered in the investigation.

For ore reliable characterization tests, it is important to ensure that their output results are consistent and that the test is reproducible independently. There have been several studies (Nadolski, 2012; Davaanyam, 2015; McClintock, 2018) that showed through extensive test work that piston-press tests can be consistently conducted in different compression machines and that the test responses in terms of product size distribution and specific energy consumption are reliable.

2.5.2 Assessing the Energy Consumption of Piston-Press Tests

Since there are still no specific machines for conducting piston-press tests in the market, test works typically make use of uniaxial compression machines from the cement industry. The problem is that conventional compression machines were not designed to measure parameters such as the total energy consumption of a given test, which is one of the key output parameters from a piston-press test. Nevertheless, if the device can record the force and displacement throughout the test, which can be done by equipping displacement transducers in the compression machine, the total energy consumption can be assessed through numerical integration of the force versus displacement curve (Daniel, 2003; Hawkins, 2007; Nadolski, 2012; Davaanyam, 2015).

According to Davaanyam (2015), during the piston-press test, the loading rate and reading frequency can be controlled (e.g. 200 kN/min and one reading/second), the trapezoidal method to determining the area can be used to accurately estimate the area under the force versus displacement curve, as illustrated by Figure 2-16.

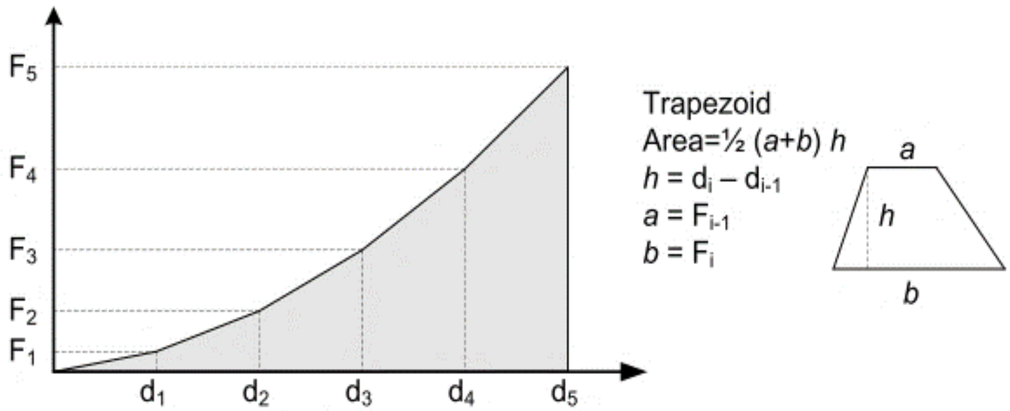

Figure 2-16: Calculating the energy consumption through the trapezoid area approach

(Source: Davaanyam, 2015)

Each piston-press test generates a force-displacement curve. However, the obtained curve also includes the force-displacement of the machine setup due to strain under load of the piston and the metal spacers that are inserted underneath the piston-die arrangement as well as the removable base plate. The force-displacement curve that corresponds to the machine setup is referenced as a strain curve. Therefore, before conducting tests with the samples, an "empty" test is performed to obtain the strain curve of the entire piston-die setup. For an accurate measure of the total energy input to the sample, the strain curve must be subtracted from the curve obtained through the actual test.

2.5.3 Self-similar Product Particle Size Distribution

An important finding for applying methodologies that make use of piston-press tests to predict pilot or large-scale HPGR performance is regarding the self-similar grinding particle size distributions curves of the HPGR products. Fuerstenau et al. (1991) conducted several pilot-scale HPGR tests in which the specific energy consumption was wide-ranging and concluded that the HPGR product size distribution could be normalized, thus leading to self-similar grinding particle size distributions. The self-similarity was verified and validated regardless of variations in moisture, feed size distribution and rolls speed. Normalization of HPGR product particle size distributions can be obtained with the following equation:

$$F(x) = Z\left(\frac{x}{X_{50}}\right) \tag{2.4}$$

where:

$F(x)$ = Product size distribution function,

Z = Self-similar distribution function,

X_{50} = Product median size.

Lim et al. (1996) validated the self-similarity concept for various minerals and ores types and proposed the following empirical equation (Equation 2.5) to describe the entire product size distribution of a given HPGR product:

$$F\left(\frac{x}{X_{50}}\right) = 100\left(1 - \exp\left(-A\left(\frac{x}{X_{50}}\right)^{\left(m\left(\frac{x}{X_{50}}\right)+n\right)}\right)\right) \tag{2.5}$$

where:

x = Particle size,

x / X_{50} = Normalized size,

A, m and n = Fitted parameters.

During his analysis, Lim et al. (1996) fitted Equation 2.5 using least square regression to each set of self-similar curves and noted that the initial feed top size limits the maximum normalized product size.

Davaanyam (2015) verified that the self-similarity concept is also applicable to piston-press tests. In other words, the product size distribution from piston-press tests can also be normalized and, therefore, can be used to predict the actual HPGR product particle size distribution, as exemplified by Figure 2-17. The samples used in the piston-press and pilot-scale HPGR tests must be prepared similarly and present a comparable amount of coarse and fine particles to ensure a proper fit between the normalized PSD curves.

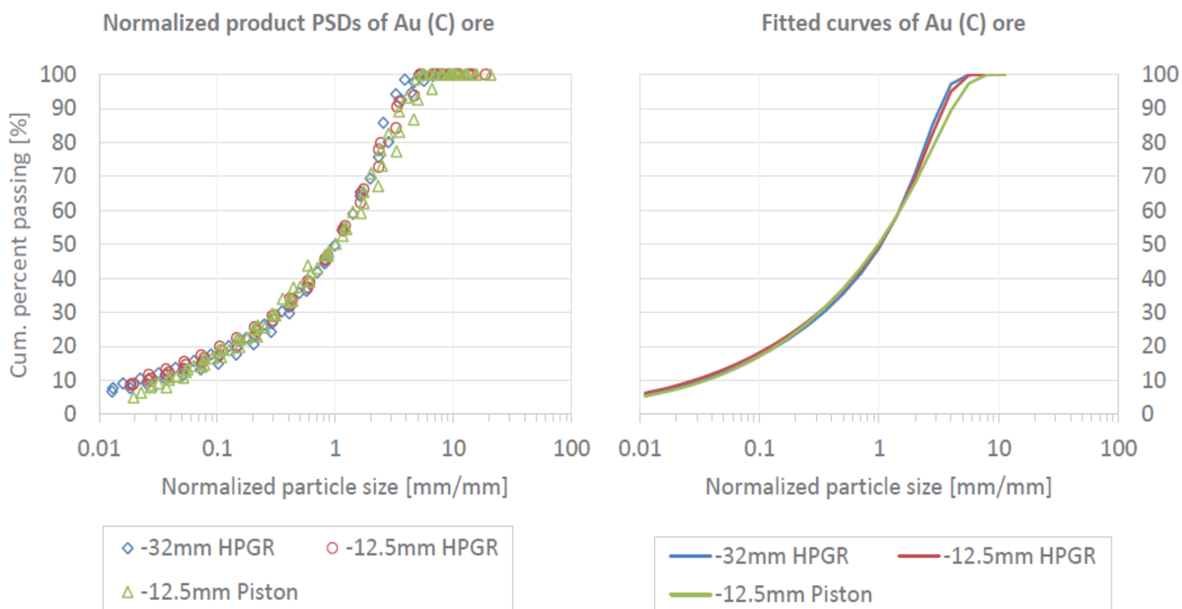

Figure 2-17: Comparison between the normalized product PSDs of piston and HPGR tests

(Source: Davaanyam, 2015)

2.5.4 Predicting the HPGR Performance with Low Sample Requirements

Apart from evaluating the HPGR performance for fine crushing applications, this research also aimed to support its implementation to hard rock applications by validating and extending Davaanyam's (2015) bench-scale Direct Calibration and Database-Calibrated methodologies for predicting HPGRs energy and size reduction through piston-press tests.

Three methodologies were proposed by Davaanyam (2015), as follow:

I. Direct Calibration Methodology.

II. Database-Calibrated Methodology.

III. Simulation-Based Methodology.

The methodologies were validated against an extensive database of pilot-scale HPGR and piston-press tests that were conducted on different ore types at the University of British Columbia. However, iron ore was not included in the analysis, and as such, its responses to the methodologies are still unknown. For reference, UBC's database consists of more than 200 pilot-scale HPGR tests and comprises several ore types from mines around the world.

Also, although all three methodologies target low sample requirements for predicting the HPGR energy consumption and size reduction through piston-press tests, each has a specific procedure with a series of steps to be followed, as well as different applicability, accuracy and limitations that were described in this section.

It is important to note that for evaluating the methodology's accuracy, Davaanyam (2015) compared the actual net specific energy consumption (E_{SP}) of pilot-scale HPGR tests against the predicted E_{SP} of piston-press tests at calibrated piston pressures (P_{piston}). The accuracy of the E_{SP} predictions was established based on a ±10% envelope of the actual value obtained in the pilot-scale test.

2.5.5 Direct Calibration Methodology

The Direct Calibration methodology involves conducting a limited number of pilot-scale HPGR and piston-press tests on the same composite sample. The results are used to calibrate a regression model that allows the prediction of HPGR performance in terms of net specific energy consumption and size reduction. Once the calibrated models are acquired, pilot-scale tests are no longer necessary since piston-press tests can be conducted over different test conditions such as pressing force. In addition, the models can be used to assess HPGR performance for variability testing by conducting the tests on other lithologies from the deposit in order to evaluate a range of HPGR energy-size reduction responses.

2.5.5.1 Application

The Direct Calibration methodology is the most accurate of all three methodologies and is suitable for Preliminary Economic Assessment (PEA), pre-feasibility and feasibility studies, including process design, geo-metallurgical programs, and process performance evaluation. The net specific energy and size reduction predictions are estimated to be in the range of ±10%. As the name suggests, the procedure is an ore-specific methodology, meaning that the resulting regression models should not be applied to predict the HPGR performance of different ore-types or ores from similar deposits.

2.5.5.2 Steps for applying the Direct-Calibration Methodology

The following diagram (Figure 2-18) summarizes the six steps that are required to apply the Direct Calibration Methodology proposed by Davaanyam (2015).

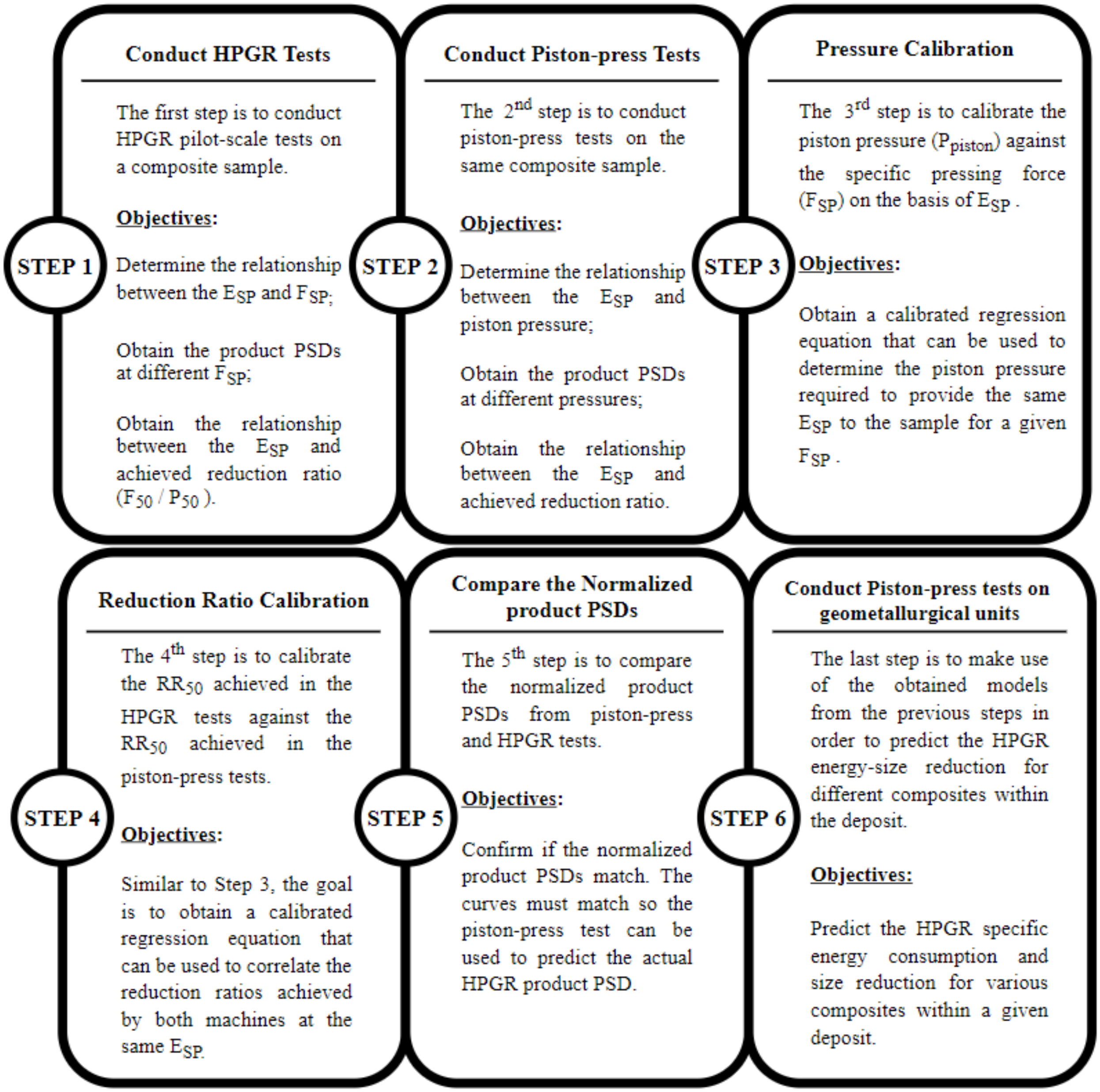

Figure 2-18: Summary of steps for applying the Direct Calibration methodology

Equations 2.6 to 2.9 presents the formulation used in Step 3 to correlate the piston pressure (P_{piston}) to the HPGR specific pressing force (F_{SP}).

$$E_{sp}(kWh/t) = m_1 \cdot P_{piston}(MPa) + b_1 \tag{2.6}$$

$$E_{sp}(kWh/t) = m_2 \cdot F_{SP}(N/mm^2) + b_2 \tag{2.7}$$

$$m_1 \cdot P_{piston}(MPa) + b_1 = m_2 \cdot F_{SP}(N/mm^2) + b_2 \tag{2.8}$$

$$P_{piston} = \frac{m_2}{m_1} \cdot F_{SP} + \frac{b_2 - b_1}{m_1} \tag{2.9}$$

Concerning the reduction ratio calibration, Fuerstenau et al. (1991) stated that a simple linear relationship between the reduction ratio (F_{50}/P_{50}) and specific energy consumption (E) can be established, as shown by Equation. 2.10.

$$\frac{\mathrm{F}_{50}}{\mathrm{P}_{50}} = j(\mathrm{F}_{50}) \times \mathrm{E} + c \tag{2.10}$$

Where $j(F_{50})$ is the slope of the reduction ratio versus specific energy consumption curve, and c is the intercept of the line with the F_{50}/P_{50} axis. Also, in case the reduction ratio (F_{50}/P_{50}) versus E_{SP} shows a curvature, a power equation (Equation 2.11) can be used instead of a linear equation.

$$\frac{\mathrm{F}_{50}}{\mathrm{P}_{50}} = k \cdot E^b + 1 \tag{2.11}$$

2.5.5.3 Sample Requirements

The minimum amount of sample required for applying the Direct Calibration methodology depends on the material specific gravity, but approximately one tonne is recommended. Pilot-scale HPGRs such as the one located in UBC (refer to Table 3-1), requires around 300 Kg of sample per test. A minimum of three pilot-scale tests is necessary for calibrating the results against the piston-press test results. Since the piston-press tests must be performed on the same sample batch as the HPGR tests and require less than 10 Kg of material, additional samples are not required for obtaining the calibrated regression models. It is important to note that the last step of this methodology involves performing piston-press tests on composite samples representing ore variability; for ore variability testing, 10 kilograms composite samples are needed to assess the energy-size reduction predictions across a given ore deposit.

2.5.6 Database-Calibrated Methodology

Davaanyam (2015) made use of over 150 pilot-scale HPGR test results to acquire multilinear regression models that rely exclusively on piston-press testing to predict the energy-size reduction of HPGRs. Unlike the Direct-Calibration methodology, the Database-Calibrated does not require pilot-scale HPGR tests in order to be applied and is not ore-specific. These two characteristics reflect Davaanyam's objective with the methodology, which was to be able to quickly and easily predict an HPGR response in terms of energy consumption and size reduction, regardless of the ore type, with only a few piston-press tests that cost considerably less than standard pilot-scale HPGR tests and has low sample requirements.

2.5.6.1 Application

The Database-Calibrated methodology has an estimated accuracy of ±25% and is considered the least accurate of the three methods developed by Davaanyam. On the other hand, it has the lowest cost and is the most accessible. Its small sample requirements make it suitable for early-stage scoping level studies that need simple and affordable options for assessing the HPGR performance for a specific application.

2.5.6.2 Steps for applying the Database-Calibrated Methodology

The Database-Calibrated methodology can be applied by following similar steps to the Direct Calibration methodology. In this case, since the multi-linear regression models for predicting the equivalent piston pressure (P_{piston}) and equivalent size reduction were already provided by Davaanyam (2015), the procedure for applying the Database-Calibrated methodology is reduced to only four steps, as illustrated in Figure 2-19.

The proposed multi-linear regression models are presented below:

I. Empirical model for estimating the required P_{piston} for a given F_{SP}:

$$\mathbf{P_{piston}} = 5.53 + 53.3\mathbf{F_{SP}} + 24.3\boldsymbol{w} - 86.2\boldsymbol{\rho_{bulk}} + 13.1\boldsymbol{F_{50}^{HPGR}} - 44.4\,\mathbf{F_{50}^{HPGR}}/\mathbf{F_{50}^{Piston}} + 2.98\mathbf{P_{1mm}^{Piston}} \tag{2.12}$$

where:

P_{piston} is the estimated piston pressure in MPa to result in equivalent net specific energy consumption of a given HPGR specific pressing force,

- F_{SP} is the given specific pressing force in N/mm^2,
- w is the feed moisture content in %,
- ρ_{bulk} is the feed bulk density from the piston sample in g/cc,
- F_{50} is the 50% passing size of the feed sample in mm,
- P_{1mm}^{Piston} is the percentage passing 1mm in the piston-press feed.

II. Empirical model for estimating the HPGR reduction ratio:

$$\mathbf{RR_{HPGR}} = 1.86 + 1.41\mathbf{RR_{piston}} + 2.31\,\mathbf{F_{50}^{HPGR}}/\mathbf{F_{50}^{Piston}} - 0.41\mathbf{F_{50}^{HPGR}} - 1.02\boldsymbol{w} \tag{2.13}$$

where:

- RR_{HPGR} is the estimated reduction ratio in the HPGR,
- RR_{piston} is the reduction ratio achieved in the piston-press test,
- F_{50} is the passing sizes of feeds in mm,
- *w* is the feed moisture content in %.

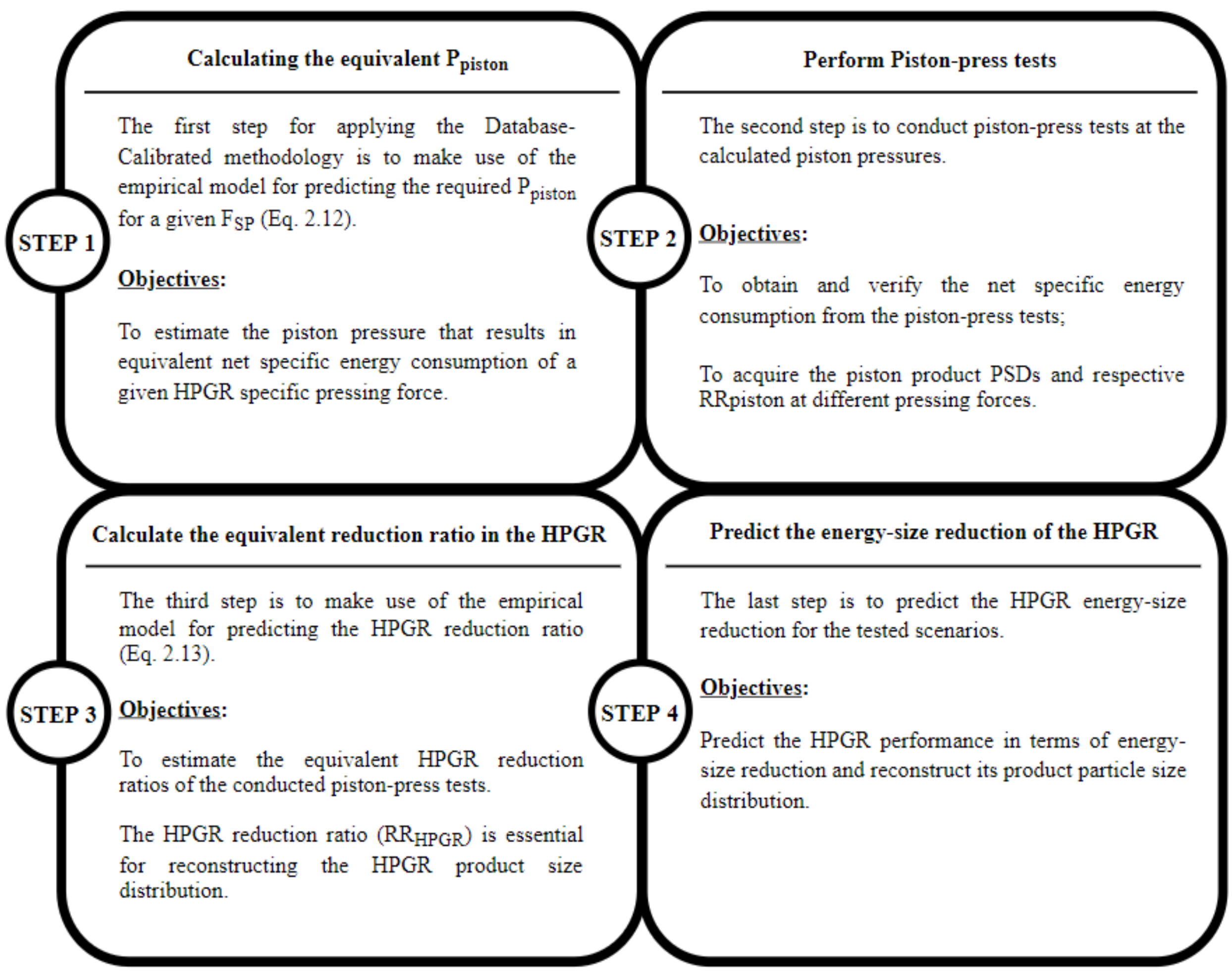

Figure 2-19: Steps for applying the Database-Calibrated methodology

The effect of removing the need for pilot HPGR testing is that the normalized product PSDs from the piston-press and HPGR cannot be compared or validated as it occurs in Step 5 of the Direct Calibration methodology. In this case, the normalized product PSDs are assumed to match.

Davaanyam (2015) established the following conditions for assuming that the normalized product PSDs from the piston-press and HPGR match with each other.

i. The HPGR and piston-press feed must be a product from a cone crusher.
ii. The feed used in both tests cannot be manipulated (e.g., scalped or truncated).
iii. The normalized product PSDs are a result of equivalent net specific energy consumption.

2.5.6.3 Sample Requirements:

As previously described, the most important advantage of the Database-Calibrated methodology is that it does not require pilot testing. Considering this, the sample requirements drop from 5 tons to less than 10 Kg in comparison to the Direct-Calibration approach. For reference, each piston-press test requires approximately 500 g, where the material bulk density defines the exact amount of sample per test.

2.5.6.4 Limitations of Database-Calibrated Methodology

The main objective of the Database-Calibrated Methodology is to create empirical models that allows, without the need for pilot HPGR testing, the correlation between the HPGR specific pressing force to piston pressure, and the correlation between the reduction ratio achieved in the HPGR to the reduction ratio achieved in the piston-press tests. Although removing the need for pilot testing is a significant advantage over the Direct-Calibration methodology it also means that the calibrated models will result in less accurate predictions, and the application of empirical models is constrained to the variable levels such that extrapolation of the model beyond these variable levels may not be applicable.

Table 2-8 summarizes the HPGR test variables used in the development of the current database-calibrated models. The database included over 150 pilot tests conducted for 15 different ore types.

Table 2-8: Summary table of HPGR test variables used in Davaanyam (2015) empirical models

Variables:	Unit:	Mean:	Std. Dev.	Min:	Max:
F_{SP}	[N/mm^2]	3.47	1.02	1.47	5.00
E_{SP}	[kWh/t]	1.82	0.48	0.73	2.61
Moisture	[%]	2.38	0.55	1.48	3.30
ρ_{bulk}	[g/cc]	1.84	0.22	1.55	2.20
F_{80}	[mm]	21.95	2.93	16.68	27.44
F_{50}	[mm]	13.87	3.81	5.20	20.21

The database used for creating the empirical models covered ranges of pressing forces from 1.47 N/mm^2 to 5 N/mm^2, and moisture levels of 1.48% to 3.30 %. For this research, the key variables of the HPGR pilot test work were the specific pressing force and moisture content, which varied from 2.5 N/mm^2 to 4.5 N/mm^2 and 3% to 9%, respectively. It can be noted that the database used to create the empirical models covers a fairly low range of moisture levels, which can affect its applicability if extrapolated to scenarios with high moisture.

Moreover, most of the data points used for creating the empirical models were based on pilot tests conducted for tertiary open circuit applications. As a result, variables related to feed and product particle sizes (e.g., F_{80} and F_{50}) are ideal for predicting the energy-size reduction for similar HPGR circuit applications but may not be adequate for quaternary or quinary applications that process finer feed sizes and generate finer product sizes.

2.6 Summary

Studies have proven that the HPGR is an excellent energy-efficient comminution technology alternative for replacing conventional crushers and grinding tumbling mills. One the major drawbacks for the low implementation of the HPGR technology in the mining industry, especially for hard-rock applications, is the limited access to industry and academic studies about the HPGR performance and the lack of industry-accepted bench-scale tests for sizing and modelling HPGRs.

The key HPGR sizing and operating parameters are the specific throughput constant (m-dot), the net specific energy consumption (E_{SP}), the operating gap and the specific pressing force (F_{SP}). Studies have shown that the specific pressing force normally presents a linear relationship with the net specific energy consumption and size reduction. The HPGR operating gap is also expected to decrease at higher pressing forces.

HPGR manufacturers claim that the technology can process ores with up to 12% moisture depending on the application, but there is very limited literature regarding the effects of moisture on the HPGR performance. Recent studies have shown that moisture can have a negative impact on the machine m-dot at high concentrations. Also, excessive moisture in the HPGR feed can increase the wear of linings and cause slippage of the feed material.

The Direct Calibration methodology is suitable for Preliminary Economic Assessment (PEA), pre-feasibility and feasibility studies. The E_{SP} and size reduction predictions are estimated to be in the range of ±10%. The methodology is ore-specific should not be applied to predict the HPGR performance of different ore-types. The methodology has not been validated for iron ore and neither for quaternary applications.

The Database-Calibrated methodology is suitable for early-stage scoping level studies and has an estimated accuracy of ±25%. This methodology does not require pilot-scale HPGR tests and is not ore-specific. However, the application of the proposed empirical models is constrained to the variable levels (e.g., F_{SP}, F_{80}, F_{50} and moisture level) from the existing HPGR pilot testing database, thus extrapolating the model beyond these variable levels may result in poor energy and size reduction predictions. The database used to develop the current regression models proposed by Davaanyam (2015) did not include iron ore, and most of the database consists of pilot testing for tertiary crushing applications.

Chapter 3

EXPERIMENTAL PROGRAM

The experimental program was developed by taking into consideration ArcelorMittal's case study, which was used to generate the necessary data for evaluating the HPGR amenability to comminute iron ore when implemented in a two-stage HPGR circuit (quaternary crushing and grinding stages), as well as for obtaining a database that was suitable for applying Davaanyam's (2015) Direct Calibration and Database-calibrated methodologies. The experimental program was divided into two sections, the first section focused on open circuit HPGR applications, while the second section involved closed circuit tests.

3.1 ArcelorMittal's Case Study

At the time of writing, ArcelorMittal was developing a new processing facility for their Serra Azul iron ore mine, located in Brazil. Their operation sites are mainly composed of itabirite, also known as banded-quartz hematite, or hematite schist. Their current operation consists of mining and processing friable itabirites, which are known to be relatively easy to crush and grind. Figure 3-1 shows Serra Azul's current mineral processing plant.

The friable itabirites resources were expected to be exhausted in the next years, therefore there is a need for a new and more complex processing facility to process their so-called "Compact" and "Semi-compact" itabirites. The new processing facility will comprise two HPGRs. The first unit will operate in open circuit as a quaternary crusher, while the second unit will replace conventional Ball Milling circuits and operate in closed circuit configuration, as illustrated in Figure 3-2.

Figure 3-1: Serra Azul's mineral processing plant

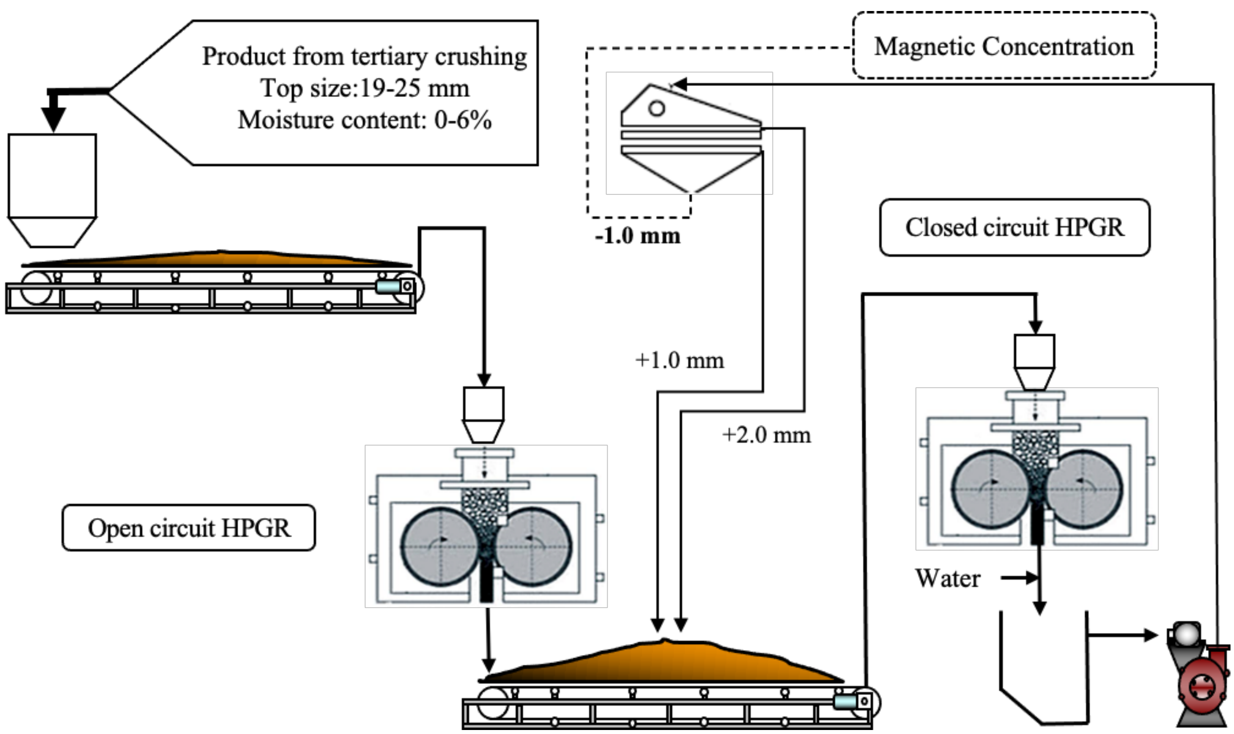

Figure 3-2: Two-stage HPGR circuit at Serra Azul iron ore mine

ArcelorMittal is currently sizing their HPGRs, and pilot-scale tests are now being conducted to assess their performance for crushing/grinding the compact and semi-compact itabirites. As shown in Figure 3-2, the two-stage HGPR circuit targets a product size of -1mm and includes a wet screening stage for classification. The ore moisture level in the first HPGR (open circuit) is expected to vary from 0 to 6%, while the second HPGR (closed circuit) will need to treat ores at moistures that can be as high as 9% due to a wet screening stage.

3.2 Sample Description

The samples used in this research were shipped directly from Serra Azul mine, located in Brazil to UBC in Vancouver. A total of six tons of run-of-mine (ROM) material was acquired, half of it belonging to the Compact Itabirite lithotype, and the other half to the Semi-compact Itabirite lithotype. The received samples were already pre-crushed and had a top size of 19 mm.

3.3 HPGR Pilot-scale Testing

A total of 21 pilot-scale HPGR tests were conducted. The pilot-scale HPGR test work (number of tests and test conditions) was defined by taking into consideration the amount of sample available and the most relevant variables for the study, which were the specific pressing force (F_{SP}) and moisture content. Despite the particularities of each test, the standard test procedure specified by Köppern was followed throughout the entire test program.

3.3.1 HPGR Pilot-scale Unit

The pilot-scale HPGR test program was carried out using a Köppern pilot-scale HPGR unit, as described/shown in Table 3-1 and Figure 3-3, respectively. The machine has 750 mm diameter by 220 mm wide rolls with a Hexadur® liner. The tests with this liner are appropriate for pilot-scale testing since an autogenous layer is not required, and as such, less sample is needed per test. The unit was specially designed for pilot-scale testing and is equipped with a data-logging system that can measure the testing time, roller gap (left and right), pressing force (left and right), and power consumption, which is recorded every 100 ms.

Table 3-1: Technical specifications of UBC's pilot-scale HPGR unit

Description:	Unit:	Value:
Roller diameter	[mm]	750
Roller width	[mm]	220
Roller wear surface	[-]	Hexadur® WTII
Roller edge design	[-]	Cheek plate
Installed power	[kW]	200
Maximum pressing force	[kN]	1,600
Maximum F_{SP}	[N/mm^2]	8.5
Variable speed drive	[rpm]	up to 40 rpm [1.55 m/s]

Figure 3-3: Köppern pilot-scale HPGR at UBC

The pilot-scale HPGR is equipped with a product conveyor belt that has a splitter box that can divide the product into edge and centre fractions, as shown in Figure 3-4. For the given unit, previous studies (e.g. Nadolski (2012)) have shown that the edge material (left and right combined) accounts for about to 30% of the total product.

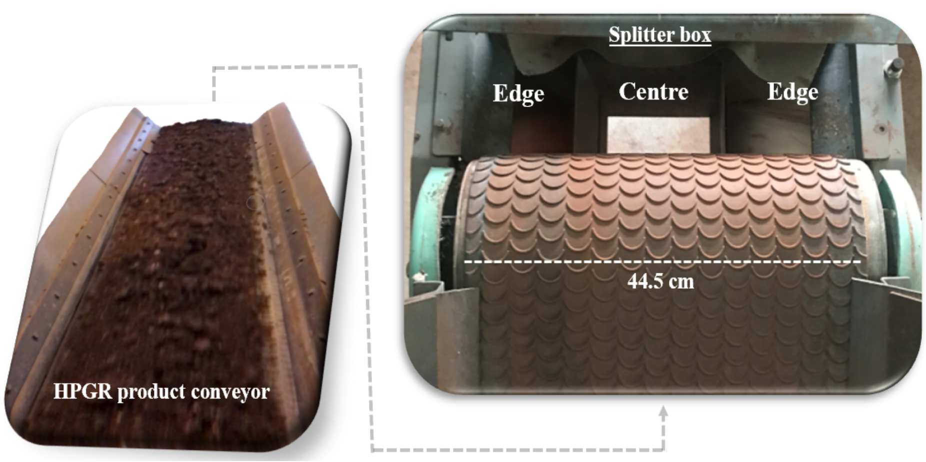

Figure 3-4: HPGR product conveyor and splitter box

3.3.2 Particularities of the HPGR Pilot-test Procedure

3.3.2.1 Pre-test Procedure

Each pilot-scale HPGR test required approximately 250-300 kg of material. The standard top size of Köppern's testing procedure is 32 mm. Since the received samples were pre-crushed to 19 mm top size, further crushing was not required. Once the test conditions were defined (F_{SP}, roll speed and moisture), sampling stages that involved homogenization, blending, splitting and moisture adjustment were performed. Figure 3-5 shows an example where the blending stage was applied to prepare feed samples with 50% of each lithotype.

Figure 3-5: Sample preparation for pilot-scale HPGR test work

The homogenization and splitting stages were conducted with a rotary sample splitter with eight 30 litres capacity bins. Representative sub-samples of approximately 20 kg were split for each HPGR feed sample throughout the splitting stage for subsequent feed characterization analysis and also for preparing samples for the piston-press test work. The moisture adjustment of each feed sample was performed on the same day as the HPGR test to minimize moisture variations from evaporation. Before starting each test, the machine settings were configured to output the desired specific pressing force and roll speed.

For the closed circuit HPGR tests, one stage of wet screening was included after each cycle to remove the fines (-1 mm). Each closed circuit test comprised a total of four cycles. The oversize material from each screening stage was weighed, recombined and homogenized with the fresh feed from the open circuit HPGR product to keep a consistent feed mass before running the next cycle. A small sub-sample with approximately 5 Kg from the oversize material from the 4th cycle of each test was split to estimate the moisture content and the screening efficiency. The wet screening was done with a 36 inch diameter Sweco screen, illustrated in Figure 3-6.

Figure 3-6: Wet-screening stage during HPGR closed circuit test

3.3.2.2 Post-test procedure:

Each pilot test lasted approximately 40-60 seconds, during which product samples were collected for between 15 and 30s during stable operation (refer to Figure 3-7). The waste material was collected for mass balance purposes. At the end of each test, the edge and centre products were weighed separately, and representative sub-samples of each stream were collected using a rotary splitter. All edge and centre sub-samples were oven-dried and submitted to a particle size distribution analysis using screens. For the closed circuit tests, once sub-samples from the centre and edge were collected, the remaining samples were recombined with the waste stream and sent to a wet-screening stage.

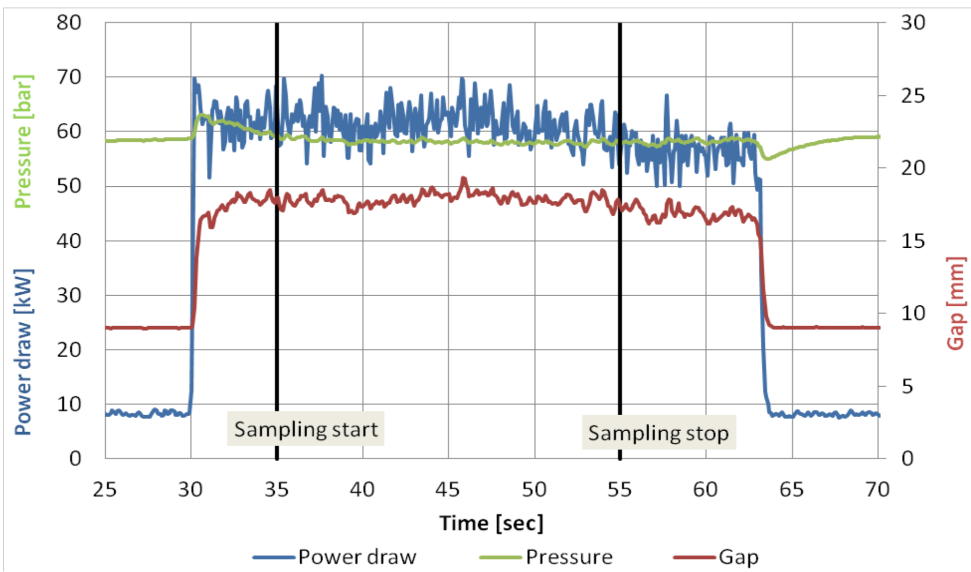

Figure 3-7: Data recording during pilot-scale HPGR test

Once a test was completed, the collected data allowed an in-depth analysis of its product characteristics, including the particle size distribution and reduction ratio, as well as of the operating parameters (F_{SP}, operating gap, m-dot and E_{sp}). Table 3-2 summarizes the main outcomes of each pilot HPGR test.

Table 3-2: Outcome data from pilot-scale HPGR test

Parameters	Unit
Specific Pressing force (F_{SP})	[N/mm^2]
Specific Throughput Constant (m-dot)	[ts/hm^3]
HPGR Throughput	[t/h]
Main Motor Power	[kW]
Specific Energy Consumption	[kWh/t]
Roll Gap	[mm]
Roll Speed	[ms^{-1}]

3.3.3 HPGR Test Conditions

3.3.3.1 Open circuit HPGR tests

A total of 13 tests were performed in open circuit. Table 3-3 shows the selected test conditions for the open circuit HPGR tests. Considering that the compact and semi-compact lithologies are the main lithotypes that compose Serra Azul's deposit, the performance tests were conducted with blended samples with a 1:1 mass ratio of each to provide sample for testing.

The following correlations between the test conditions were analyzed to assess the HPGR performance:

i. Assessment of specific pressing force.
ii. Assessment of moisture content effect.

- Response to specific energy consumption.
- Response to specific throughput constant (m-dot).
- Response to product particle size and size reduction.

iii. Specific energy consumption and product size relationship.

Table 3-3: Open circuit pilot-scale HPGR test conditions

Sample Description	Test Id.	Top Size	Target Moisture	Specific Pressing Force [F_{SP}]	Roll Speed
		mm	%	N/mm^2	rpm [m/s]
50% Compact / 50% Semi-compact Itabirites	SA001	19	3.0	3.5	14 [0.55]
	SA002		6.0		
	SA003		9.0		
	SA004	19	3.0	2.5	14 [0.55]
	SA005		6.0		
	SA006		9.0		
	SA007	19	3.0	4.5	14 [0.55]
	SA008		6.0		
	SA009		9.0		
100% Compact	SA010	19	3.0	4.0	14 [0.55]
	SA011				
100% Semi-compact	SA012	19	3.0	4.0	14 [0.55]
	SA013				

3.3.3.2 Closed circuit HPGR tests

A total of two closed circuit tests were conducted and each consisted of four cycles. The test conditions were defined once the results from the open circuit tests were analyzed. Table 3-4 summarizes the defined test conditions for the closed circuit pilot tests.

Table 3-4: Closed circuit pilot-scale HPGR test conditions

Sample Description	Test No.	Top Size	Target Moisture	Specific Pressing Force [F_{SP}]	Roll Speed
		mm	%	N/mm^2	rpm [m/s]
50% Compact / 50% Semi-compact	SA014 Cycle 1	19	6	4	14 [0.55]
	SA015 Cycle 2				
	SA016 Cycle 3				
	SA017 Cycle 4				
50% Compact / 50% Semi-compact	SA018 Cycle 1	19	8	5	14 [0.55]
	SA019 Cycle 2				
	SA020 Cycle 3				
	SA021 Cycle 4				

Ideally, the results from a closed circuit test should be analyzed under steady-state conditions. However, in the case of pilot-scale HPGR testing, where a considerable amount of sample was required for conducting open circuit tests, the number of cycles required for conducting closed circuit was kept to a minimum. In this study, based on the given circuit configuration, the available sample allowed tests with a maximum of four cycles each. Comparisons between variations in the circulating load, feed and product size properties of each cycle of the closed circuit tests were done to evaluate if four cycles were enough to achieve steady-state conditions.

The screening efficiency of each test was calculated based on the amount of fines (-1 mm material) present in the screen oversize. Sub-samples from the screen oversize of the last cycle (4^{th}) of each test were taken to analyze their particle size distribution and to estimate the screening efficiency.

3.4 Piston-press Testing

3.4.1 Piston-die Arrangement

The piston-press tests were conducted on an instrumented MTS hydraulic press located at the University of British Columbia and on a hydraulic compression machine (Automax Multitest) manufactured by Controls Group. The MTS and Controls Group compression machines can apply pressing forces of up to 1400 kN and 3000 kN, respectively. Both devices were also equipped with force-displacement transducers, which is needed for measuring the specific energy consumption from the piston-press tests. For compressing the samples, one hardened steel-die with 86 mm diameter was used in combination with the hydraulic compression machines. The piston-die arrangement and the MTS unit are illustrated in Figure 3-8. The compression machine from Controls Group is presented in Figure 3-9.

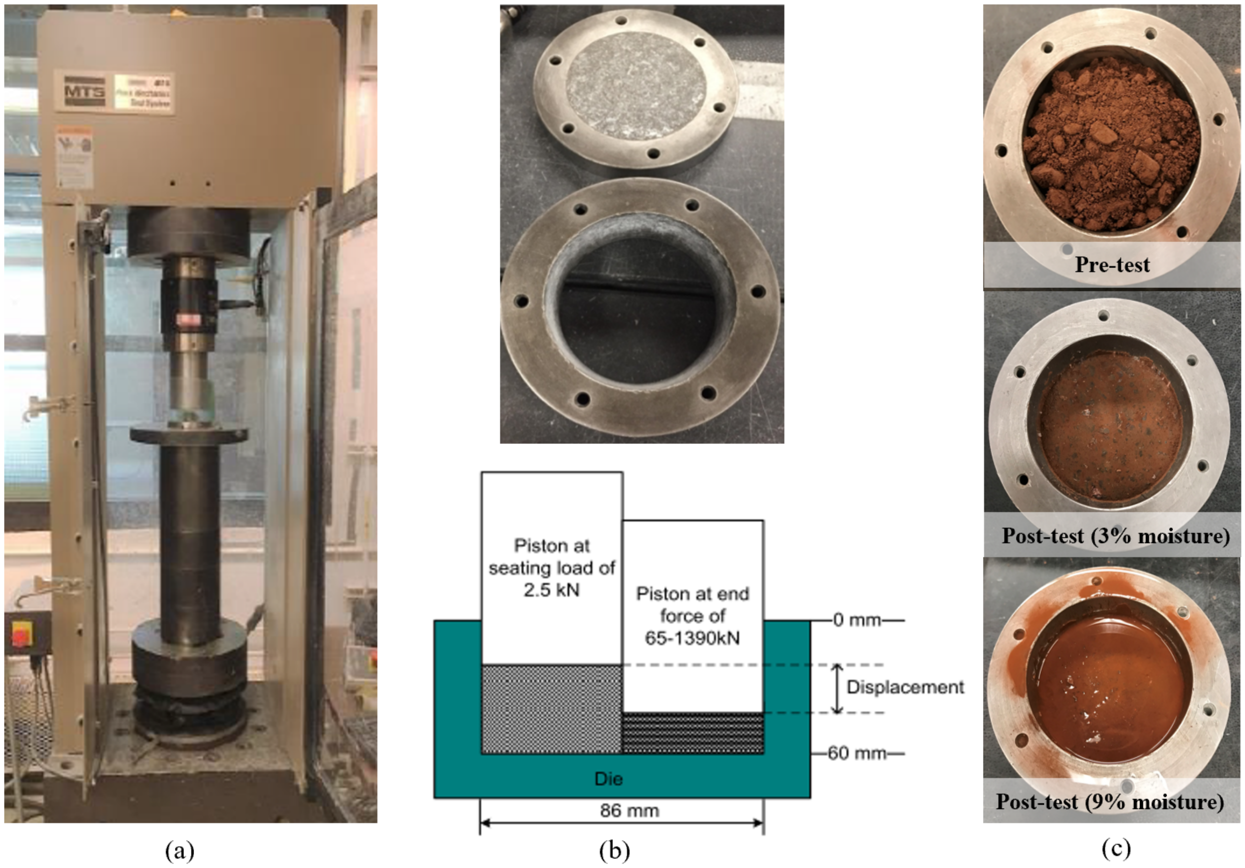

Figure 3-8: (a) MTS hydraulic press at UBC, (b) Piston-die device, (c) Piston-die sample arrangement prior and after tests

The piston-die dimensions were established by Davaanyam (2015). He noted that the maximum pressure observed at the roll centre during the pilot-scale HPGR testing ranges from 200 to 250 MPa. Considering that UBC's MTS machine has a maximum pressing force of 1400 kN, for a piston-press test that is able to achieve pressures as high as 250 MPa, required a die with a 86 mm diameter. The feed particle top size for piston ores testing of 12.5 mm was defined based on the piston-die specifications to minimize errors due to wall effects.

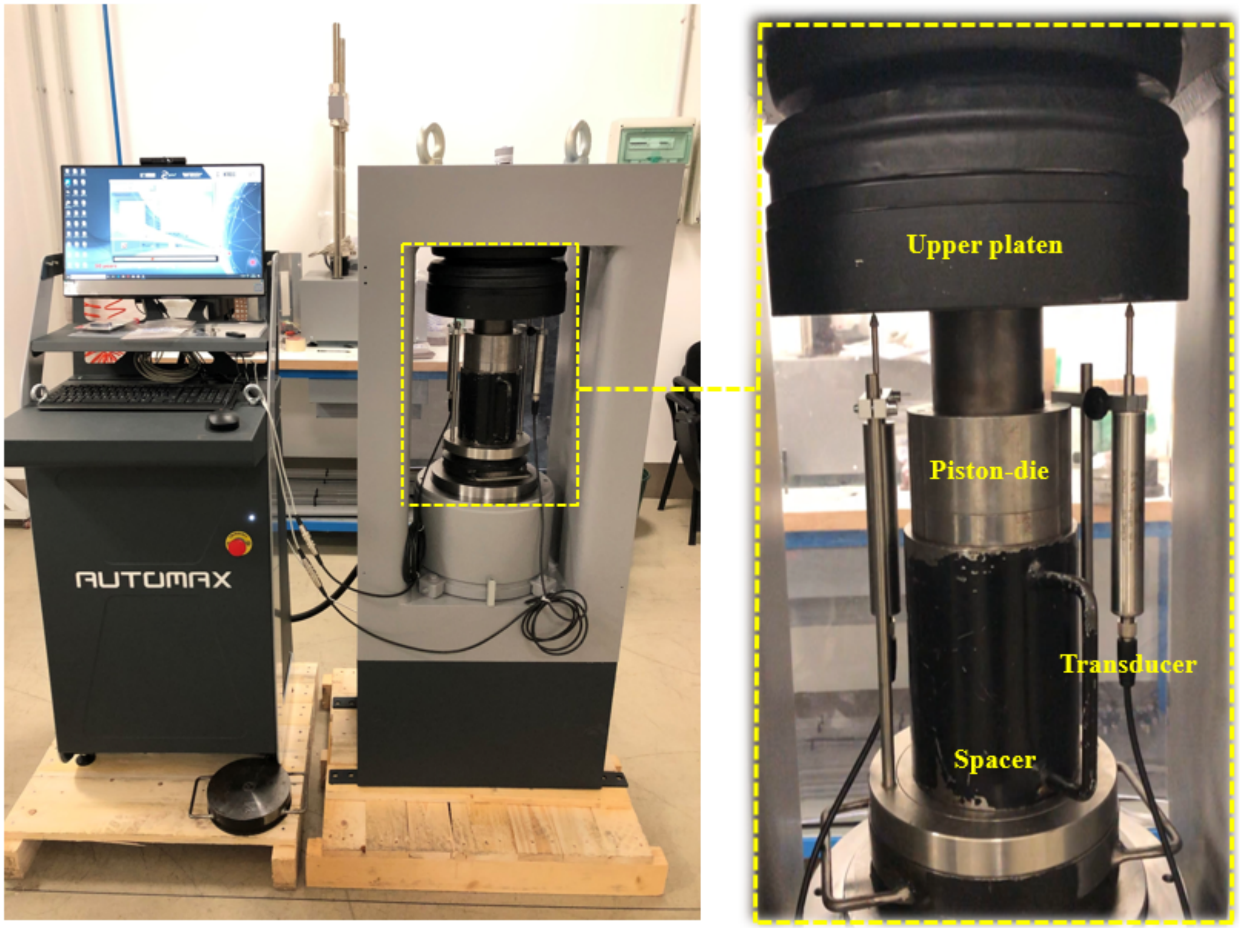

Figure 3-9: Controls Group hydraulic compression machine

3.4.2 Piston-press Test Procedure

The samples which were used to conduct the piston-press tests were collected during the pilot scale HPGR test program. Sub-samples of 240 mL were prepared for each test. Davaanyam (2015) reported that the variation in sub-sample split after the moisture adjustment was considerably lower than dry sub-samples. Considering this, the sub-samples were split after adjusting the moisture and the mass was determined based on the material bulk density the die volume of 240 mL. For each moisture content, one sub-sample of approximately 1 Kg was split for particle size analysis. Figure 3-10 summarizes the steps involved in each piston-press test.

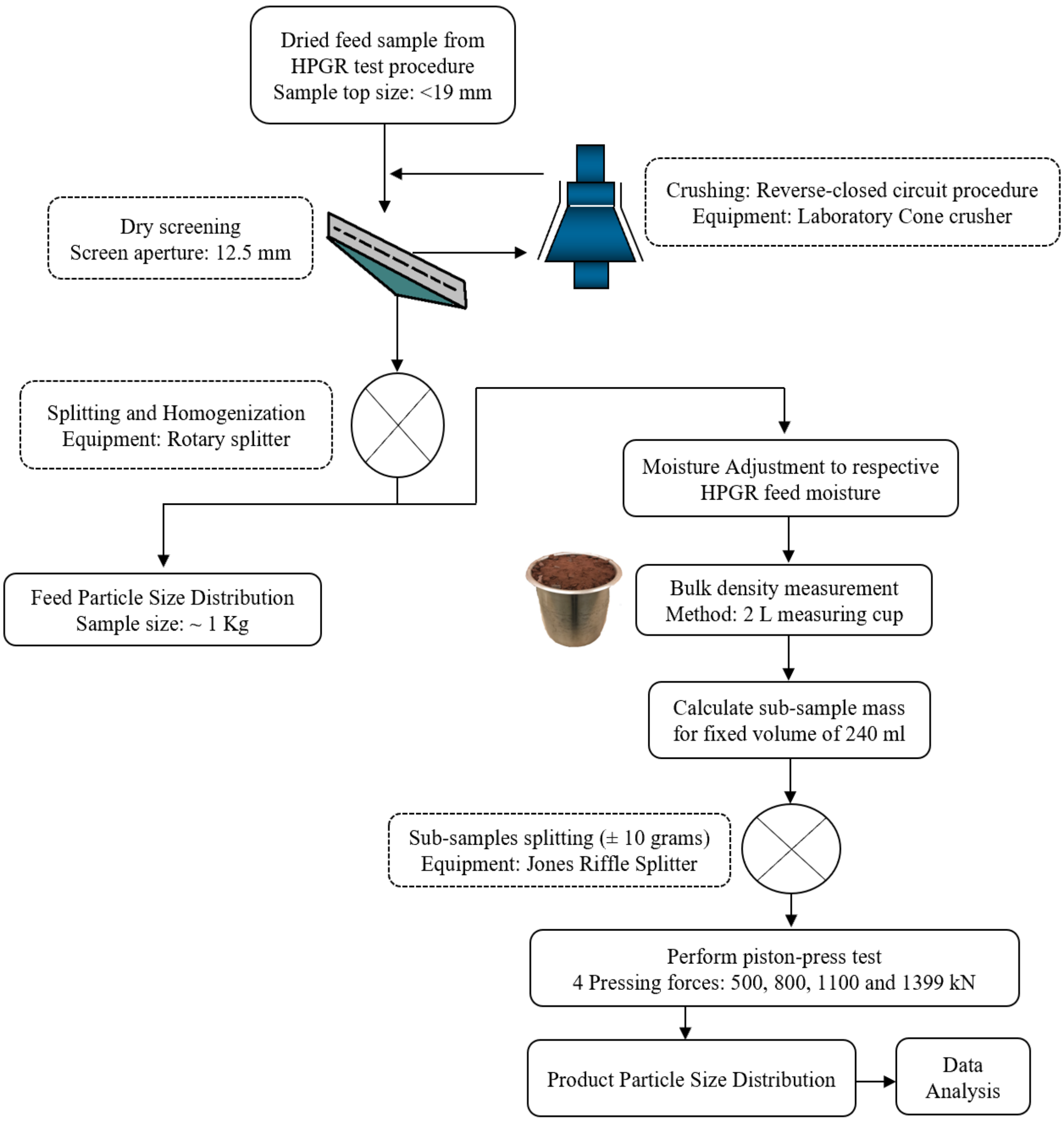

Figure 3-10: Standard piston-press testing procedure

3.4.2.1 Force-Displacement Correction and Specific Energy calculation

After each piston-press test, a corrected force-displacement curve was obtained by subtracting the strain curve from the machine setup, as exemplified in Figure 3-11.

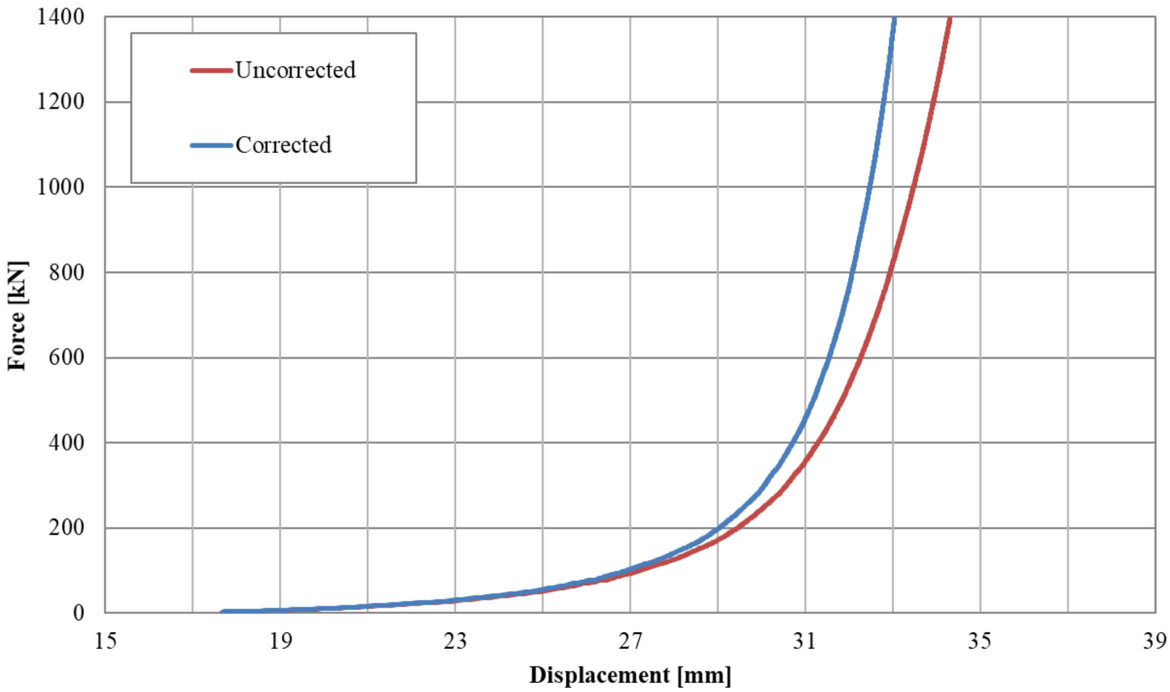

Figure 3-11: Corrected and uncorrected force-displacement curves

Through the trapezoid area approach (refer to Figure 2-16), numerical integration of the corrected force-displacement curves was applied to calculate the total energy input to the samples. The specific energy input of each test was then determined by dividing its total energy input by its respective sample mass.

Chapter 4

HPGR Pilot Testing Results and Discussions

This chapter presents the results of the pilot-scale HPGR tests that were conducted within the scope of this research and assess the HPGR amenability to comminute Serra Azul's iron ore in a two-stage HPGR circuit. Table 4-1 summarizes the test results obtained from the open circuit and closed circuit pilot tests. Detailed data concerning feed and product particle size distributions (PSDs), as well as input and output operating parameters of each test can be found in Appendix A.

Table 4-1: Summary of HPGR test results

Test Id.		Moisture [%]	Specific Pressing Force	Specific Throughput Constant	Net Specific Energy Consumption	Experimental Product PSD (Edge + Centre)	
			F_{SP} [N/mm^2]	m-dot [ts/hm^3]	E_{SP} [kWh/t]	P_{80} [mm]	P_{50} [mm]
Open Circuit	SA001	2.70	3.23	345	1.57	4.98	0.66
	SA002	5.50	3.60	347	1.72	4.69	0.60
	SA003	7.40	3.62	301	1.78	4.72	0.70
	SA004	2.60	2.26	352	1.08	5.49	1.01
	SA005	5.60	2.62	361	1.20	5.28	0.89
	SA006	7.50	2.61	365	1.20	5.50	1.04
	SA007	3.40	4.56	337	2.02	4.50	0.48
	SA008	5.90	4.64	344	2.17	4.25	0.42
	SA009	8.90	4.55	288	1.92	4.54	0.53
	SA010	2.90	4.04	336	1.67	4.31	0.49
	SA011	2.83	4.03	332	1.68	3.78	0.45
	SA012	2.91	4.05	344	1.89	4.43	0.46
	SA013	3.01	4.04	347	1.89	5.37	0.64
Closed Circuit	SA014-Cycle 1	4.73	3.92	286	1.70	2.35	0.17
	SA015-Cycle 2	5.99	4.07	337	1.72	2.48	0.37
	SA016-Cycle 3	5.01	4.02	342	1.71	2.83	0.57
	SA017-Cycle 4	5.14	4.07	343	1.72	2.60	0.60
	SA018-Cycle 1	6.31	5.03	266	2.56	1.92	0.14
	SA019-Cycle 2	8.10	5.00	248	2.45	2.43	0.39
	SA020-Cycle 3	6.80	5.08	224	2.87	2.41	0.42
	SA021-Cycle 4	6.58	5.00	229	2.60	2.35	0.49

4.1 Quaternary HPGR Open Circuit Data Analysis

4.1.1 Assessment of Feed Representability

Feed samples from the open circuit tests were compared in order to evaluate the sampling procedure consistency. Table 4-2 summarizes the statistics of all nine data points relating the feed F_{80} and F_{50} of each test.

Table 4-2: Feed statistics of the open circuit HPGR pilot tests

Statistics	Linear F_{80}	Linear F_{50}
Number of Data Points	9	9
Mean	11.72	4.56
Standard Deviation	0.33	0.12
Standard Error	0.11	0.04
Relative Standard Error	0.9%	0.9%
Coefficient of Variation	2.8%	2.7%
95% Confidence interval	0.25	0.09

The sampling procedure proved to be consistent since no major discrepancies were noted between the sample's PSDs. For comparison, Figure 4-1 presents the feed PSDs of one of the blended samples (1:1 ratio) that were prepared for the open circuit tests and of two samples of the non-blended compact and semi-compact samples that were used in the duplicate tests.

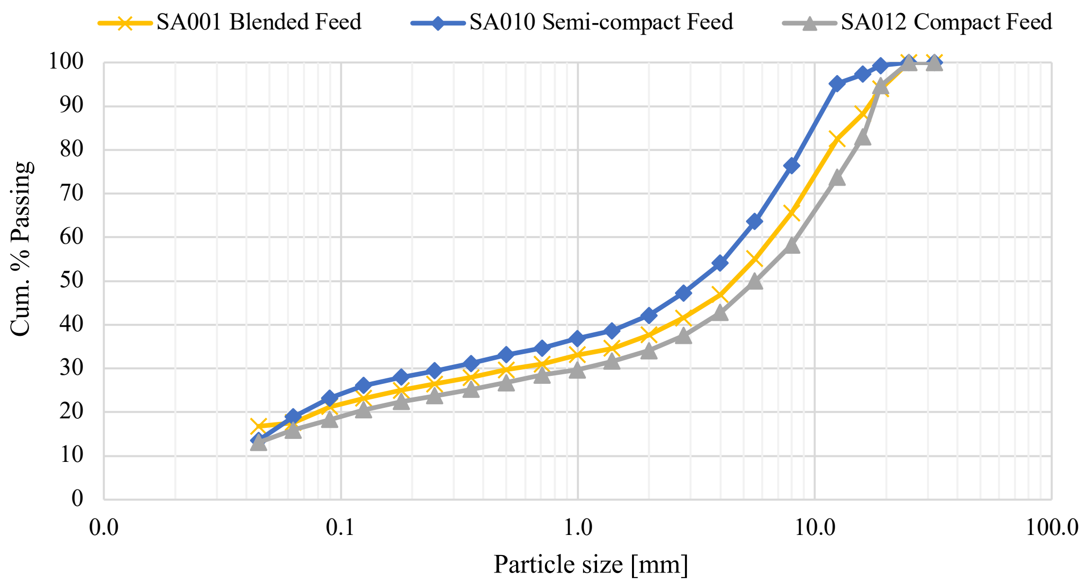

Figure 4-1: Feed PSDs comparison between the compact and semi-compact lithotypes

It can be observed that the compact lithotype is coarser than the semi-compact, and as expected, the PSD curve of the blended feed sits in between the curves of the isolated lithotypes. Comparisons between the linear P_{80}'s and P_{50}'s of each sample can be verified in Table 4-1.

4.1.2 Repeatability of the HPGR Pilot-scale Testing

Duplicate tests were conducted for the compact and semi-compact lithotypes, as shown in Figure 4-2. Although the duplicate tests did not provide enough data points for conducting a detailed statistical analysis, the results proved to be consistent for all the relevant parameters that were used for assessing the HPGR performance.

The results revealed higher net specific energy consumption when crushing the compact material. For reference, operating the HPGR at a pressing force of 4 N/mm^2 resulted in average E_{SP}'s of 1.67 kWh/t and 1.89 kWh/t for crushing the semi-compact and compact lithotypes, respectively, which represents an increase of 13.2% in the machine's energy consumption.

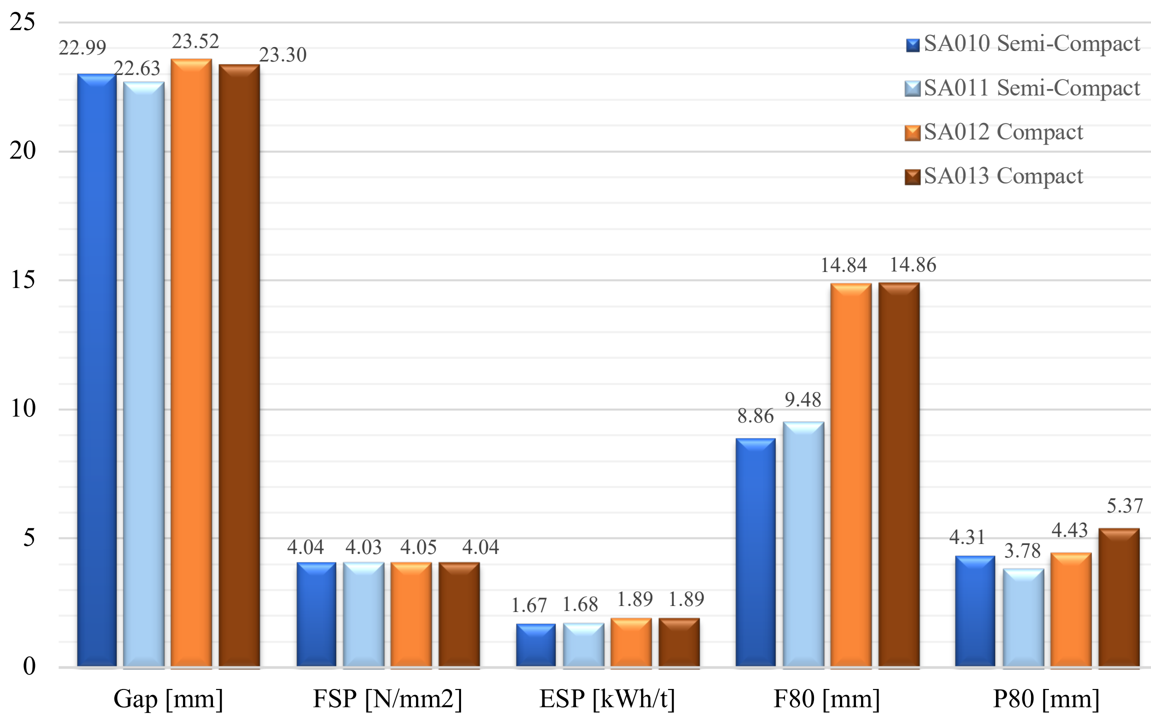

Figure 4-2: Comparison of duplicate pilot-scale HPGR tests

4.1.3 Assessment of Specific Pressing Force

To evaluate how the specific pressing force affected the HPGR performance, a sensitivity analysis was conducted based on the following output parameters from the open circuit pilot test work:

i. Net Specific Energy Consumption (E_{SP})

ii. Specific Throughput Constant (m-dot)

iii. Operating Gap

iv. Product Particle Size and Reduction Ratio

4.1.3.1 Relationship with the Net Specific Energy Consumption

The net specific energy consumption (E_{SP}) of each test was calculated from the recorded process data using Equation 2.2 and represents the actual energy input during stable operation.

Figure 4-3 shows the correlation between the E_{SP} and the applied F_{SP} of the open circuit tests. The E_{SP} showed to increase linearly with the increase of F_{SP} over the range of pressing forces tested, and an exceptionally good data fitting was obtained with a R^2 of 0.96. The linear relationship between the F_{SP} and E_{SP} is in agreement with the reviewed literature.

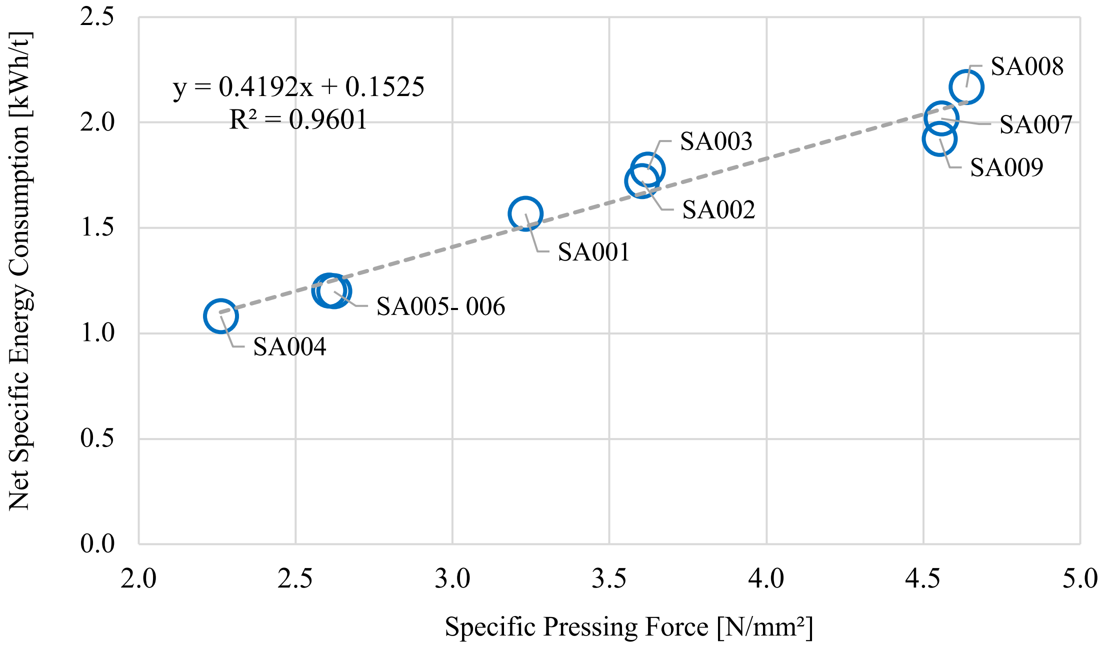

Figure 4-3: Relationship between E_{SP} and F_{SP}

4.1.3.2 Relationship with the Specific Throughput Constant

Figure 4-4 presents the relationship between the specific throughput constant and the applied specific pressing force. The results showed that the F_{SP} negatively affected the m-dot, but the correlation was considered weak since the samples also had different moisture contents. The highest m-dot values ranged from 350 to 365 ts/hm^3 when an F_{SP} of 2.5 N/mm^2 was targeted, and the lowest value of 288 ts/hm^3 corresponded to the highest F_{SP} of 4.5 N/mm^2.

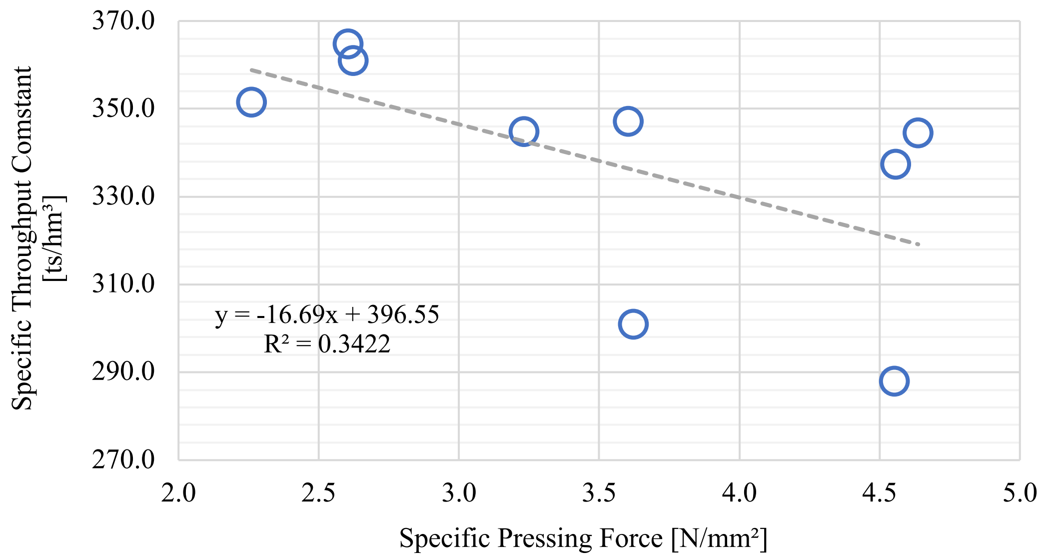

Figure 4-4: Relationship between m-dot and F_{SP}

4.1.3.3 Relationship with the Operating Gap

As illustrated by Figure 4-5, the operating gap decreased as the F_{SP} increased, reaching a maximum and minimum value of 24.33 mm and 17.38 mm at the pressing forces of 2.26 N/mm^2 and 4.5 N/mm^2 respectively. The average operating gap from all tests was 22.2 mm, which turned up to be bigger than the 18.75 mm value predicted by the Knapp et al. (2019) estimation and the 18.69 mm average operating gap from UBC's database.

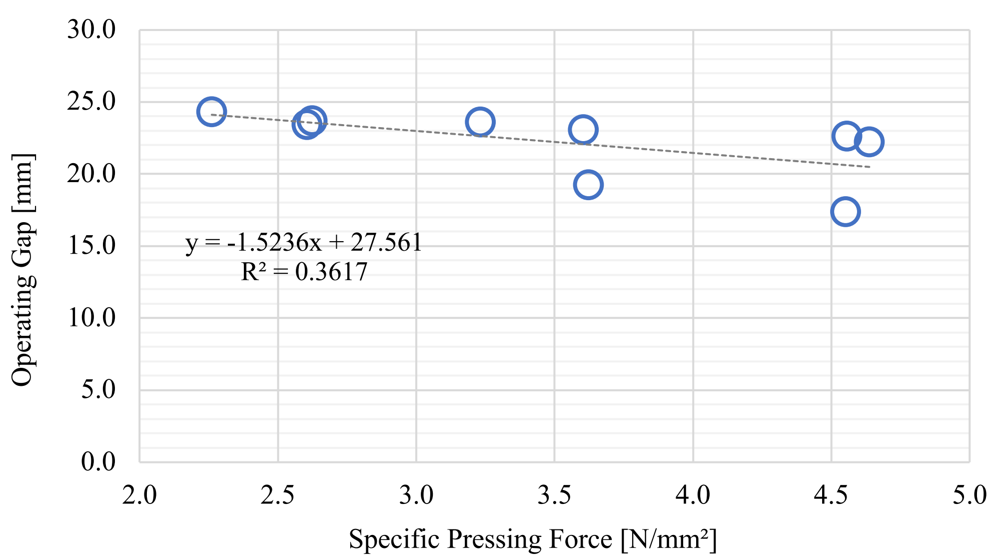

Figure 4-5: Operating gap versus F_{SP}

4.1.3.4 Relationship with the Product Particle Size and Reduction Ratio

The effect of the applied F_{SP} on product size and reduction ratio is illustrated in Figure 4-6 and Figure 4-7. The data analysis accounted for the combined product size distributions of the edges and centre streams. Despite the differences in moisture content between the tests, the product particle size, as well as the reduction ratio, presented a linear relationship with the specific pressing force.

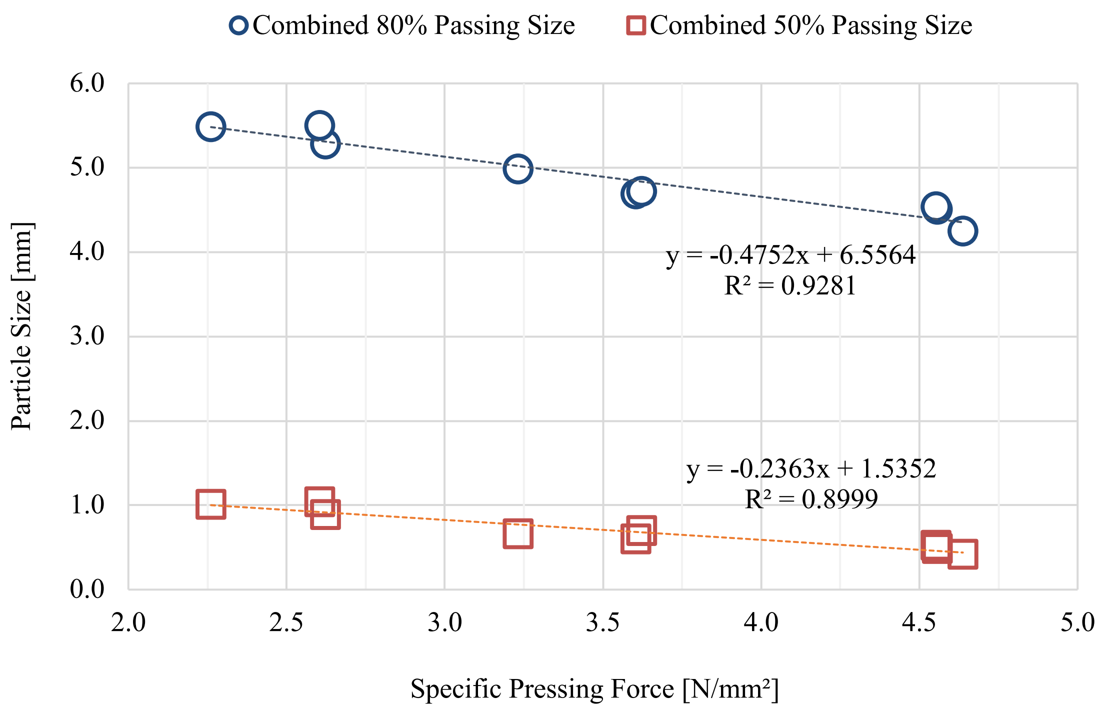

Figure 4-6: Relationship between F_{SP} and product particle size

Given that the target cut size of the two-stage HPGR circuit was 1mm, the effects of the pressing force on the generation of fines (material below 1 mm) was verified. Figure 4-8 shows that the amount of fines increased linearly with the increase of the applied F_{SP}. For example, the tests that were conducted at 4.5 N/mm^2 generated up to 10% more fines than the ones conducted at 2.5 N/mm^2.

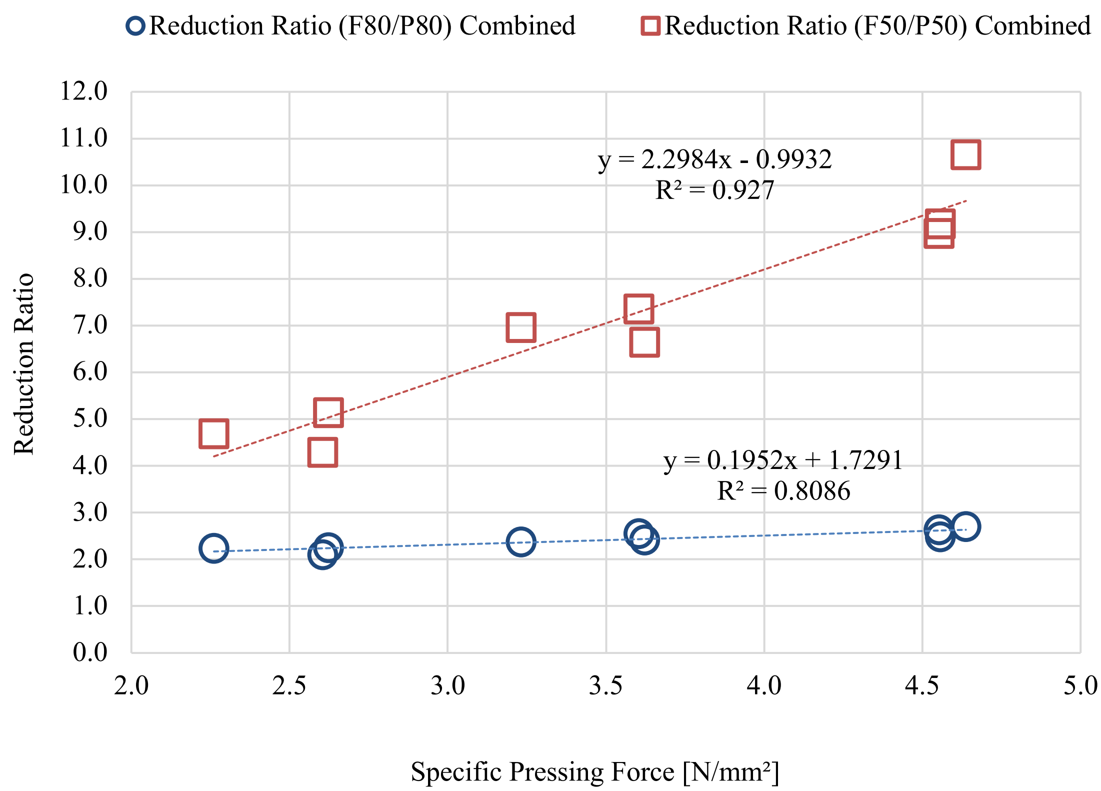

Figure 4-7: Relationship between F_{SP} and reduction ratio

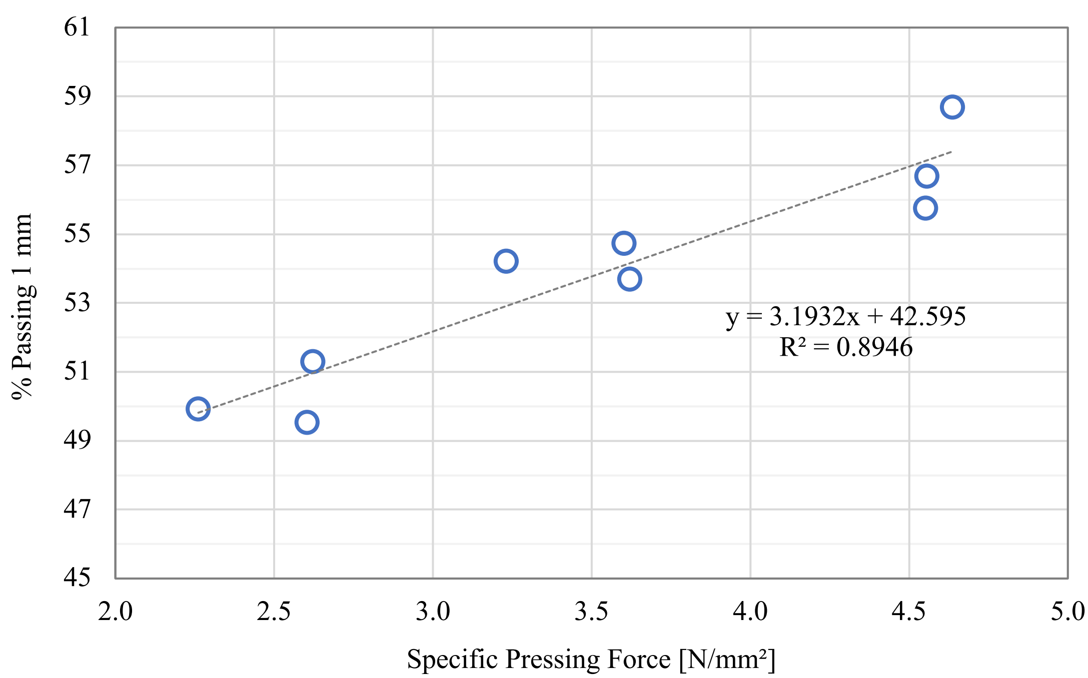

Figure 4-8: % Passing 1 mm of combined product

4.1.4 Assessment of the Ore Moisture Content

To evaluate how the ore moisture level affected the HPGR performance, a sensitivity analysis was conducted based on the following output parameters from the open circuit pilot test work:

i. Net Specific Energy Consumption (E_{SP})

ii. Specific Throughput Constant (m-dot)

iii. Product Particle Size and Reduction Ratio

4.1.4.1 Relationship with the Net Specific Energy Consumption

The relationship between the ore moisture content and the net specific energy consumption for each test are presented in Figure 4-9.

It can be observed that at 2.5 N/mm^2 and 3.5 N/mm^2, marginally higher E_{SP}'s were reported by the tests that aimed for 9% moisture when compared to 6% moisture. For this analysis, the data points from the tests that targeted 2.5 N/mm^2 and 3.5 N/mm^2 with 3% moisture (highlighted by the circles in Figure 4-9) were disregarded since the target F_{SP} was not achieved and as such, their E_{SP} was also lower. Thus, the lower E_{SP}'s from these tests could not be attributed to the ore moisture content.

In contrast, the tests that applied a F_{SP} of 4.5 N/mm^2 revealed to be more sensitive to variations in the ore moisture content. The results showed higher E_{SP} (2.17 kWh/t) at an intermediate moisture level of 6% while the lowest E_{SP} (1.92 kWh/t) was observed at 9% moisture.

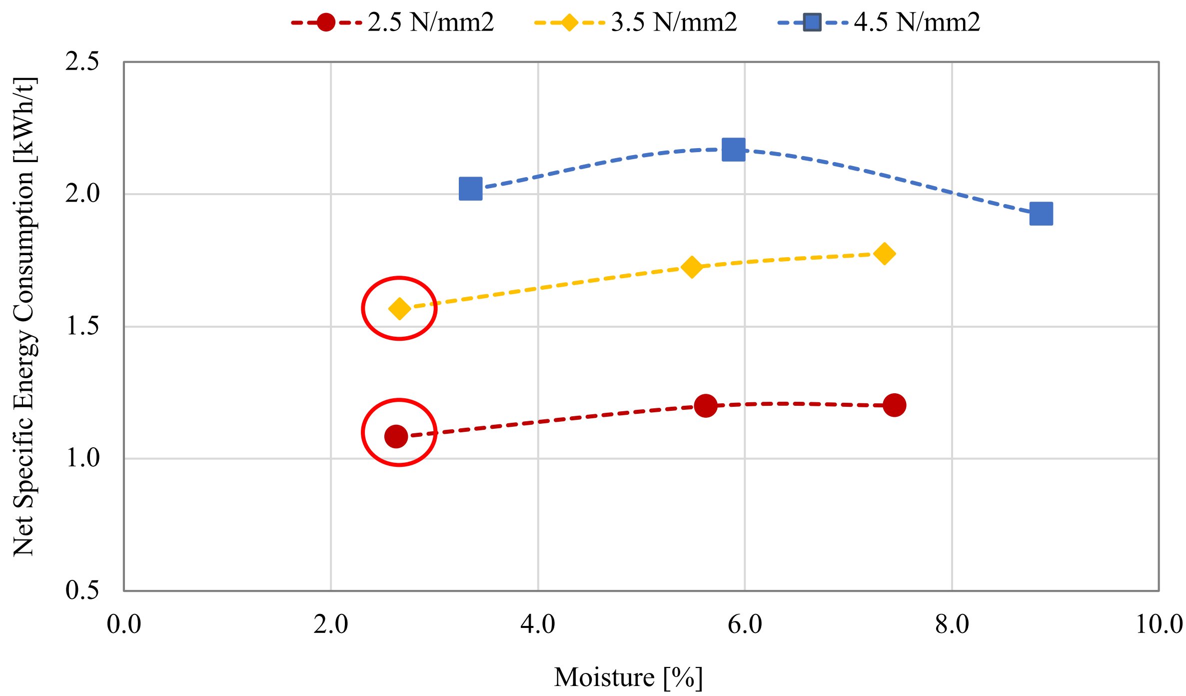

Figure 4-9: Relationship between ore moisture content and E_{SP}

4.1.4.2 Relationship with the Specific Throughput Constant

Except for the tests conducted at low pressing forces (2.5 N/mm^2), substantial impacts on the specific throughput constant were observed once the ore moisture level exceeded 6%. The effect of moisture on the m-dot of each test is shown in Figure 4-10.

The HPGR tests conducted at 2.5 N/mm^2 showed slightly higher m-dot as the moisture content increased, with a minimum value of 352 ts/hm³ and a maximum of 365 ts/hm³ at 3% and 9% moisture level, respectively. In contrast, the tests that aimed for higher pressing forces suffered a major impact on their m-dot at 6% and 9% moisture content. In these scenarios, reductions of up to 15% were observed in the machine m-dot when increasing the moisture from 3% to 9%.

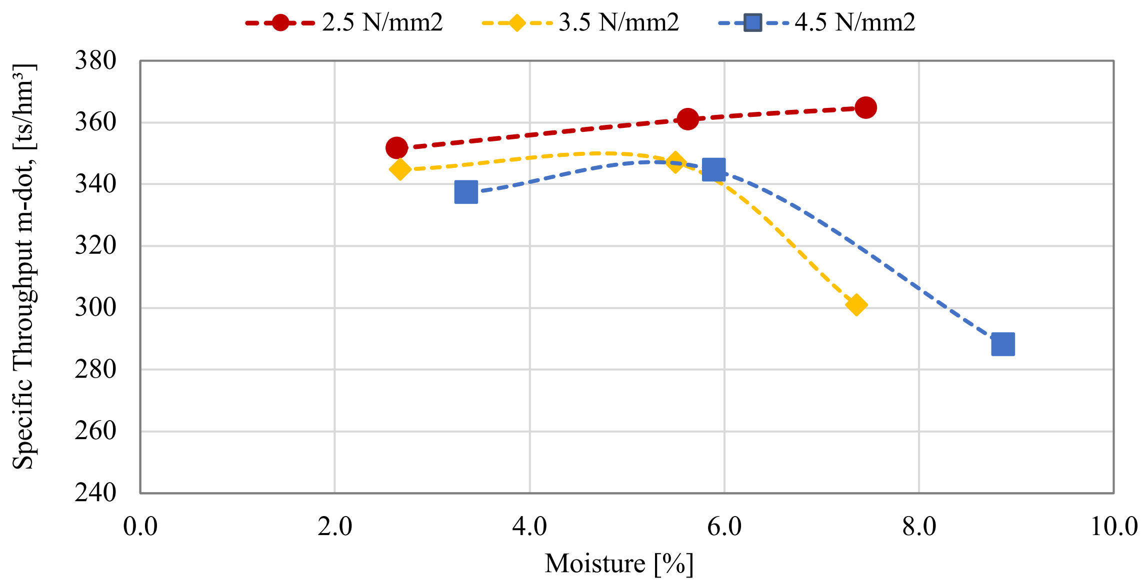

Figure 4-10: Relationship between ore moisture and m-dot

4.1.4.3 Relationship with the Operating Gap

The relationship between moisture content and operating gap supports the previous observations regarding the effect of moisture in the m-dot. Figure 4-11 shows that the operating gap decreased as the moisture level increased from 3% to 9%. For reference, the average operating gap of the tests conducted at 2.5 N/mm^2 and 3% moisture is 23.5 mm, which is approximately 15% higher than the average value reported by the tests that targeted 4.5 N/mm^2 F_{SP} and 9% moisture.

While performing the HPGR tests at the same test conditions and different moisture, there was a clear difference between how the product was discharged onto the product conveyor. As shown in Figure 4-12, it can be seen that there is more edge material and fewer flakes at 3% moisture compared to the scenarios with 6% and 9% moisture.

It is worth remembering that for running the pilot tests, the HPGR is fed through a feed chute where the sample is placed prior to the test. At high moisture content, which in this study translates to 9%, the moist material may not flow as well at the edge of the feed chute as it does at its center. In this case, most of the feed will flow towards the center of the HPGR rolls, and the machine will not be completely choke fed as required, thus leading to performance issues such as reduced throughput.

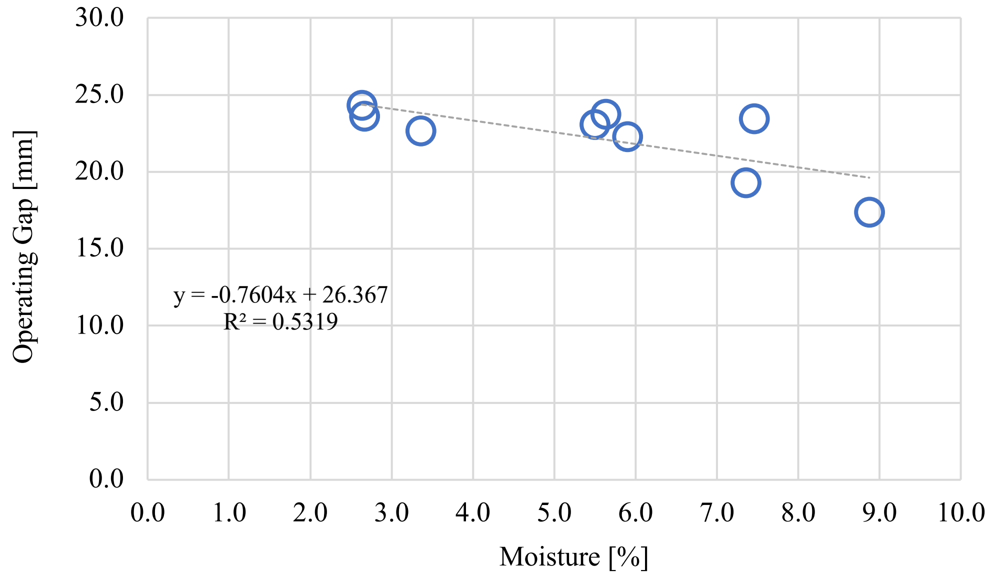

Figure 4-11: Relationship between ore moisture and operating gap

(a) 4.5 N/mm^2 and 3% Moisture

(b) 4.5 N/mm^2 and 6% Moisture

(c) 4.5 N/mm^2 and 9% Moisture

Figure 4-12: HPGR product at different moisture content

4.1.4.4 Relationship with the Reduction Ratio

The effect of moisture on the size reduction ratio (F_{50}/P_{50}) is presented in Figure 4-13. Regardless of the applied specific pressing force, the results showed that the ore moisture level did not significantly impact the reduction ratio, yet a trend was noted. For all nine tests, the RR_{50} showed to be optimum at intermediate moisture levels of 6%, reaching 10.65 at 4.5 N/mm^2, and lower values were reported as the moisture increased to 9% or decreased to 3%.

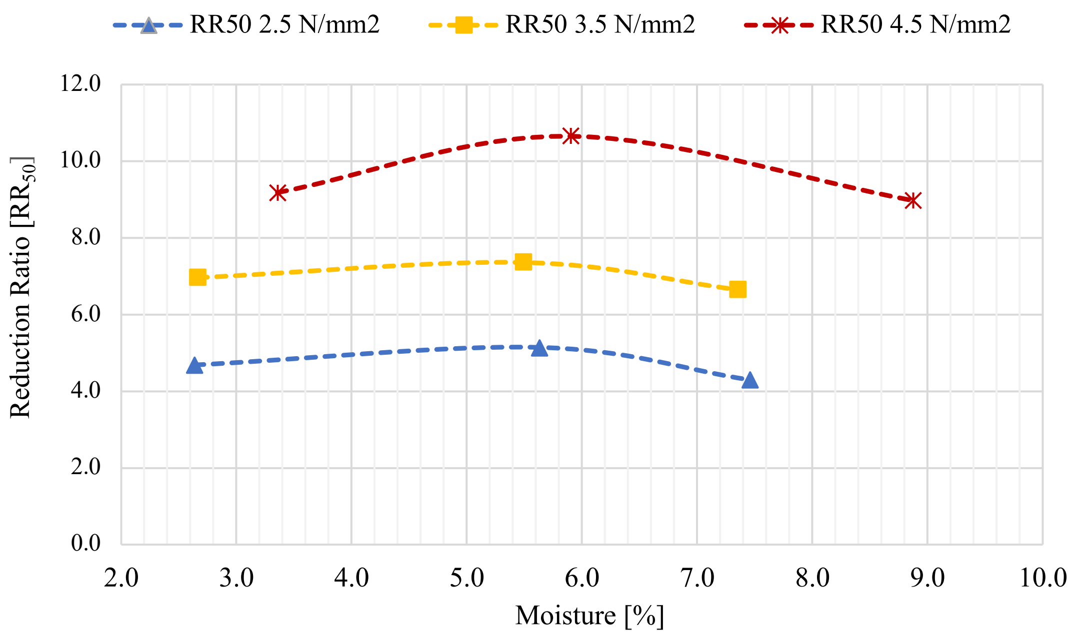

Figure 4-13: Relationship between the ore moisture and reduction ratio

Although Figure 4-12 shows that most of the HPGR product from the test at 9% moisture was discharged at the center of the conveyor belt, the product PSD's analysis showed that higher moisture did not result in higher amounts of fines or higher reduction ratios.

4.1.5 Relationship between the E_{SP} and Product Particle Size

The relationship between the net specific energy consumption and product particle size from the open circuit tests is presented in Figure 4-14. The data analysis was done for both P_{80} and P_{50} sizes. In both cases, the PSD curves revealed a strong linear relationship between the E_{SP} and product particle size.

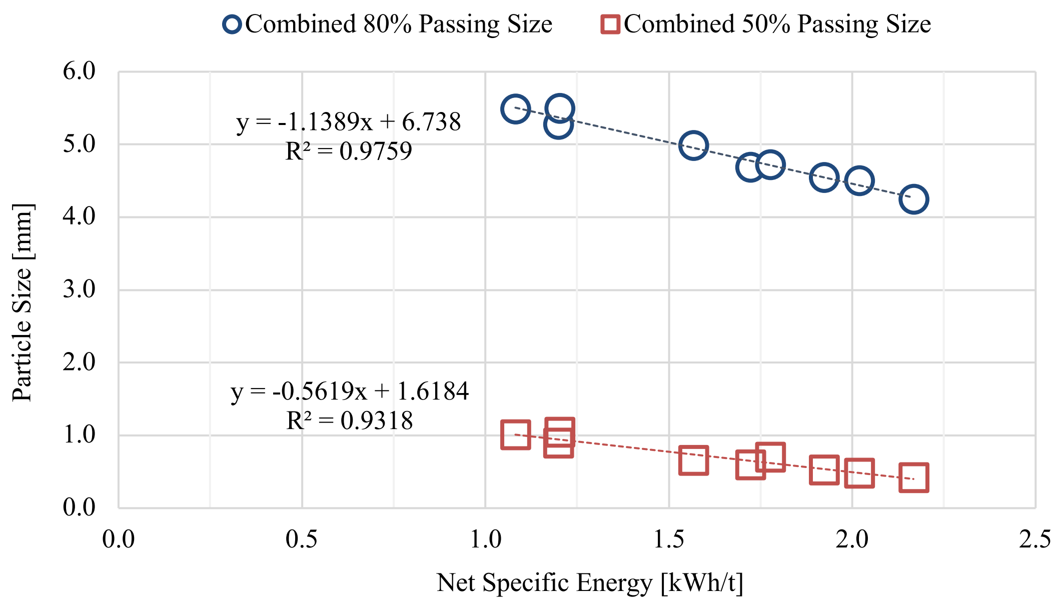

Figure 4-14: Relationship between E_{SP} and product particle size

Figure 4-15 presents the relationship between the net specific energy consumption and fines generated from each test. The results indicated a linear relationship between the E_{SP} and product particle size. An increase of almost 10% in the percentage passing 1 mm was noted when the applied specific pressing force increased from 2.5 N/mm^2 to 4.5 N/mm^2. The tests that targeted a pressing force of 2.5 N/mm^2 showed an average E_{SP} of 1.2 kWh/t and 50% of material below 1 mm, whilst an average E_{SP} of 2 kWh/t and 57% of material below 1 mm was noted when targeting 4.5 N/mm^2.

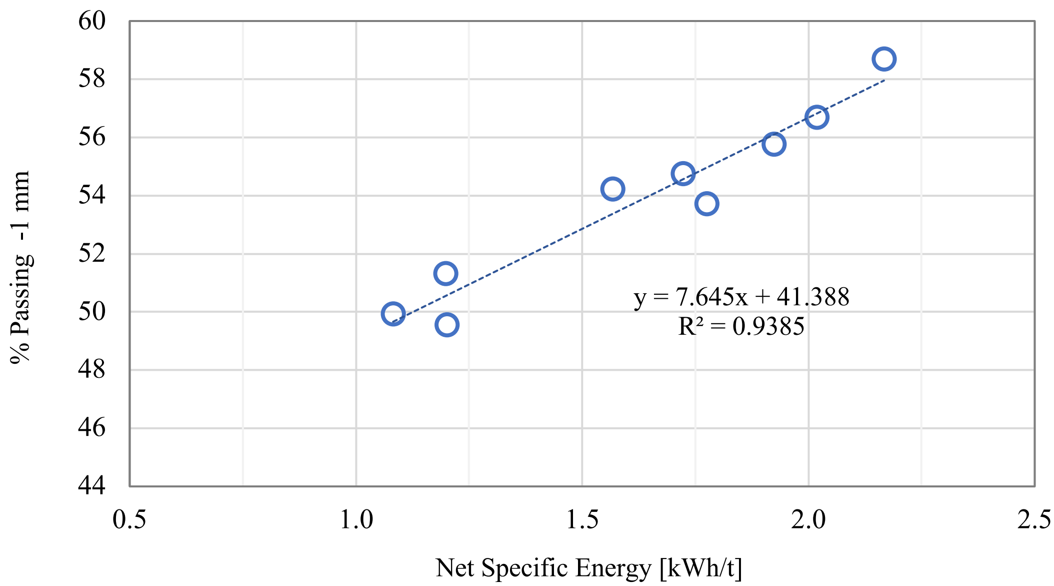

Figure 4-15: Effect of F_{SP} in the % passing – 1 mm

4.2 Quinary HPGR Closed Circuit Data Analysis

For the data analysis of the closed circuit HPGR tests, the first objective was to assess the representability of the testing procedure. Sizing of HPGRs for closed circuit applications often rely on results from open circuit testing due to the large sample requirements of closed circuit tests. As a result, output parameters such as the m-dot and E_{SP}, which are critical for sizing the HPGR, may not accurately represent the true scenario and the machine sizing is likely to be in either undersized or oversized. Similarly to the analysis conducted with the results from the open circuit tests, an additional objective was to evaluate how the applied pressing force and ore moisture content affected the HPGR performance.

4.2.1 Assessing the Representability of the HPGR Closed Circuit Tests

The approach used to analyze if the selected number of cycles was sufficient to achieve a steady-state condition was to compare the output operating variables (m-dot and circulating load) and the product size properties (P80 and RR_{80}) for each cycle. Figure 4-16 shows a comparison between the circulating load and m-dot of the closed circuit tests. For both closed circuit tests, it was be observed that the circulating load and the m-dot approached steady-state conditions by the 4th cycle.

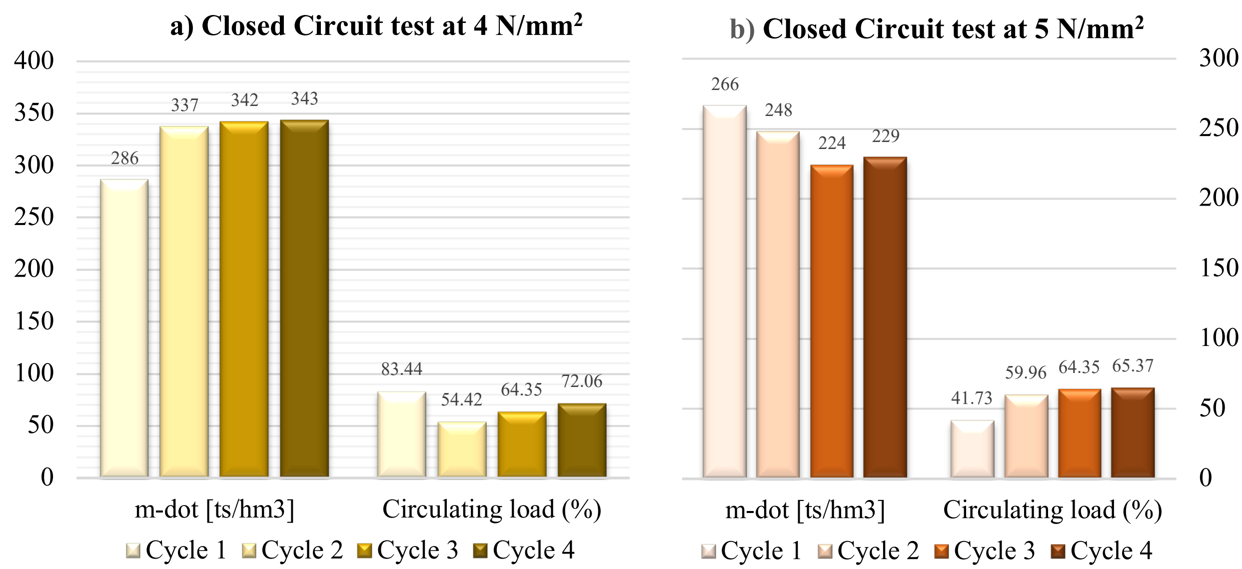

Figure 4-16: Comparison between the circulating load and m-dot of closed circuit tests

Figure 4-17, Figure 4-18 and Figure 4-19 present a comparison between the feed and product size properties of each cycle. In both tests, the reported P_{80} was finer in the first cycle and coarser values were observed in the 2nd and 3rd cycles until it stabilized by the 4th cycle. As expected, an inverse trend was noted in the reduction ratio (RR_{80}) for each cycle, with higher size reduction in the first cycle, followed by decreases in the 2nd and 3rd cycles.

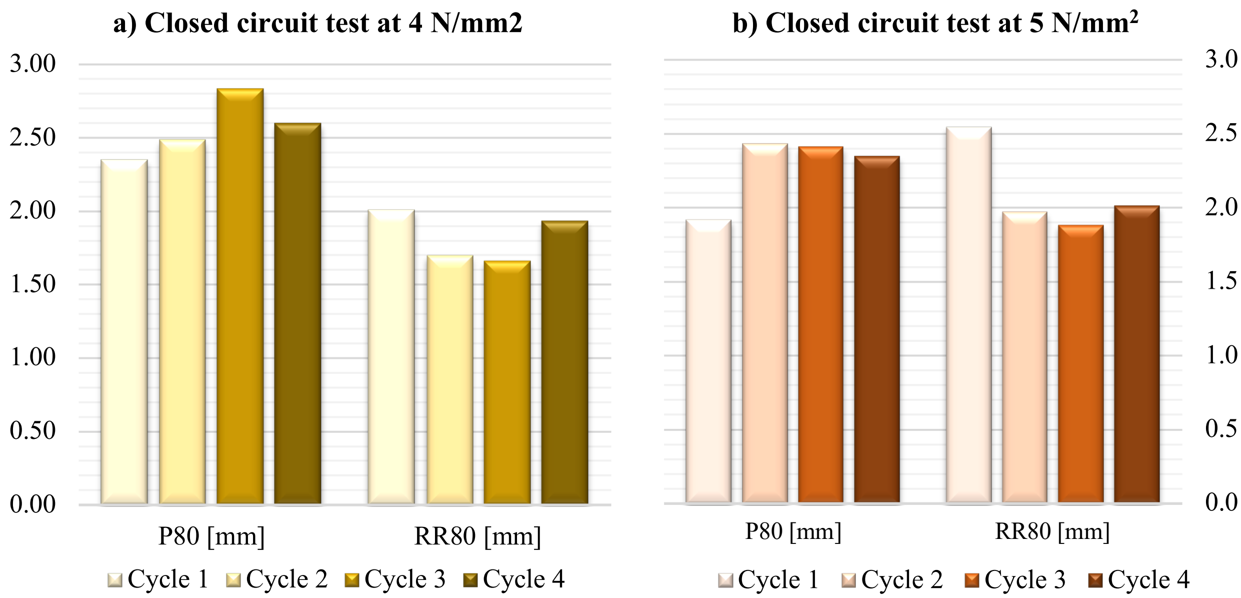

Figure 4-17: Product size properties of closed circuit tests

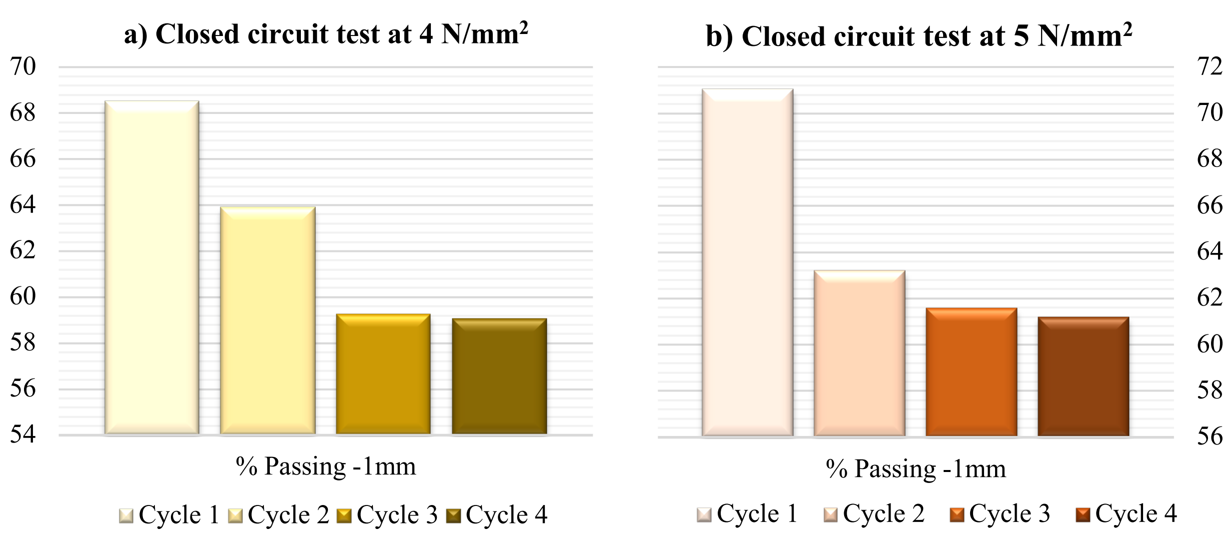

Figure 4-18: Comparison between the % passing 1 mm after each cycle

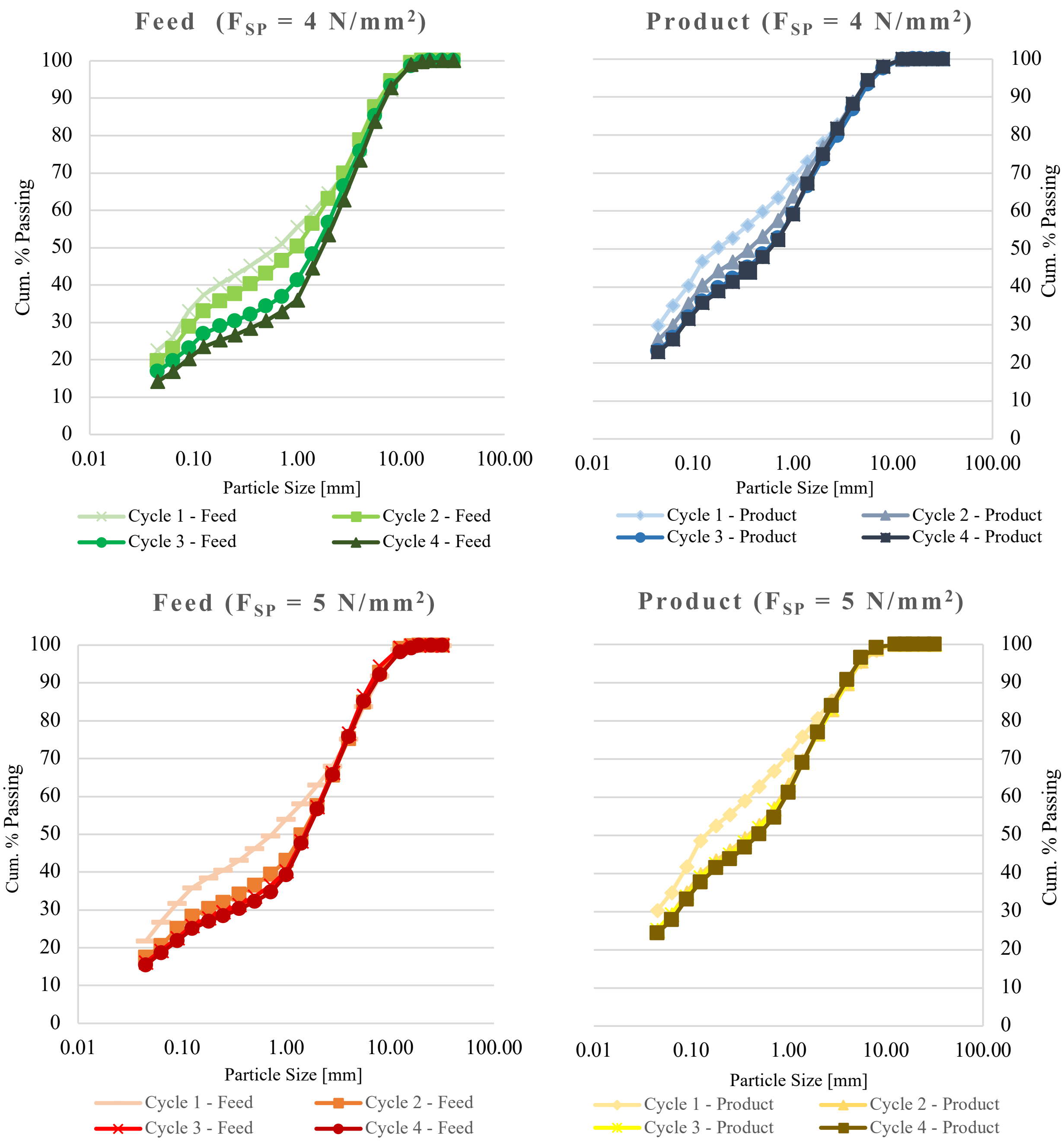

Figure 4-19: Comparison between the feed and product PSDs of each cycle

It was noted that the 4th cycle generated considerably fewer fines than the 1st and 2nd cycles. For comparison, at 4 N/mm^2, the 1st and 2nd passes showed 68.5 % and 64% of material below 1 mm respectively, while both the 3rd and 4th cycle generated 59% fines.

The results from the 1st and 2nd cycles did not accurately represent the product properties of the closed circuit HPGR tests. A total of four cycles proved to generate consistent results that resemble steady-state conditions. This analysis reiterates the importance of conducting locking cycle tests to obtain results for machine sizing and process circuit design.

4.2.2 Assessment of Specific Pressing Force and Moisture content

The analysis of the applied specific pressing forces and moisture levels were based on the results from the last cycle (Cycle 4) of each closed circuit test. Considering that the closed circuit test work was not able to cover a wide range of ore moisture content and pressing forces, the results were compared against the outcomes from the open circuit tests. Figure 4-20 illustrates the correlation between the E_{SP} and F_{SP} of both closed circuit tests. The datapoints from the open circuit tests were also illustrated to support the observations. Figure 4-21 shows the correlation between the E_{SP} and m-dot of both closed circuit tests.

The results from the closed circuit test followed the linear trends that were observed in the open circuit tests. Increasing the F_{SP} from 4.0 N/mm^2 to 5.0 N/mm^2 resulted in a 51% increase in the E_{SP}. For comparison, the open circuit tests showed a difference of only 10-25% in the E_{SP} when the F_{SP} was increased from 3.5 N/mm^2 to 4.5 N/mm^2.

The sharp increase between the E_{SP} of both closed circuit tests calls attention to the *energy saturation point* mentioned by Saramak and Kleiv (2013). Further test work at higher pressing forces would be required to establish the *energy saturation point* of Serra Azul's iron ore. Nonetheless, the results indicate that running the HPGR at 5 N/mm^2 and high moisture levels may lead to inefficient performance in terms of energy consumption.

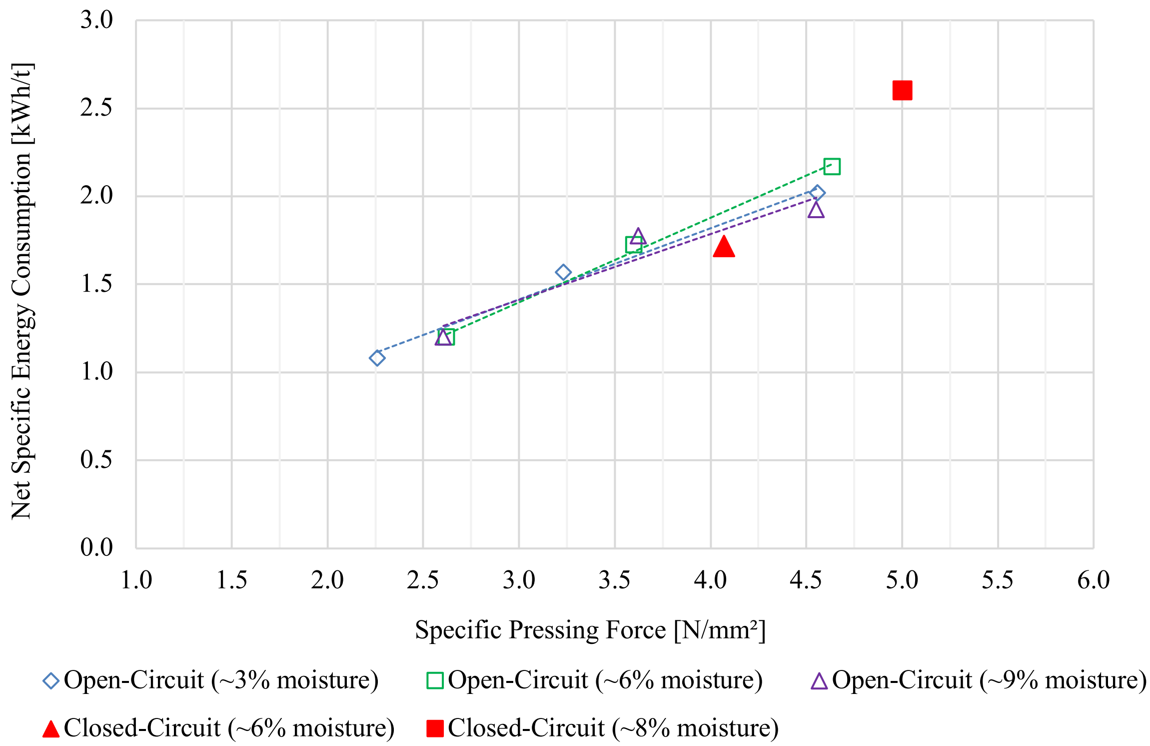

Figure 4-20: Closed circuit tests: correlation between E_{SP} and F_{SP}

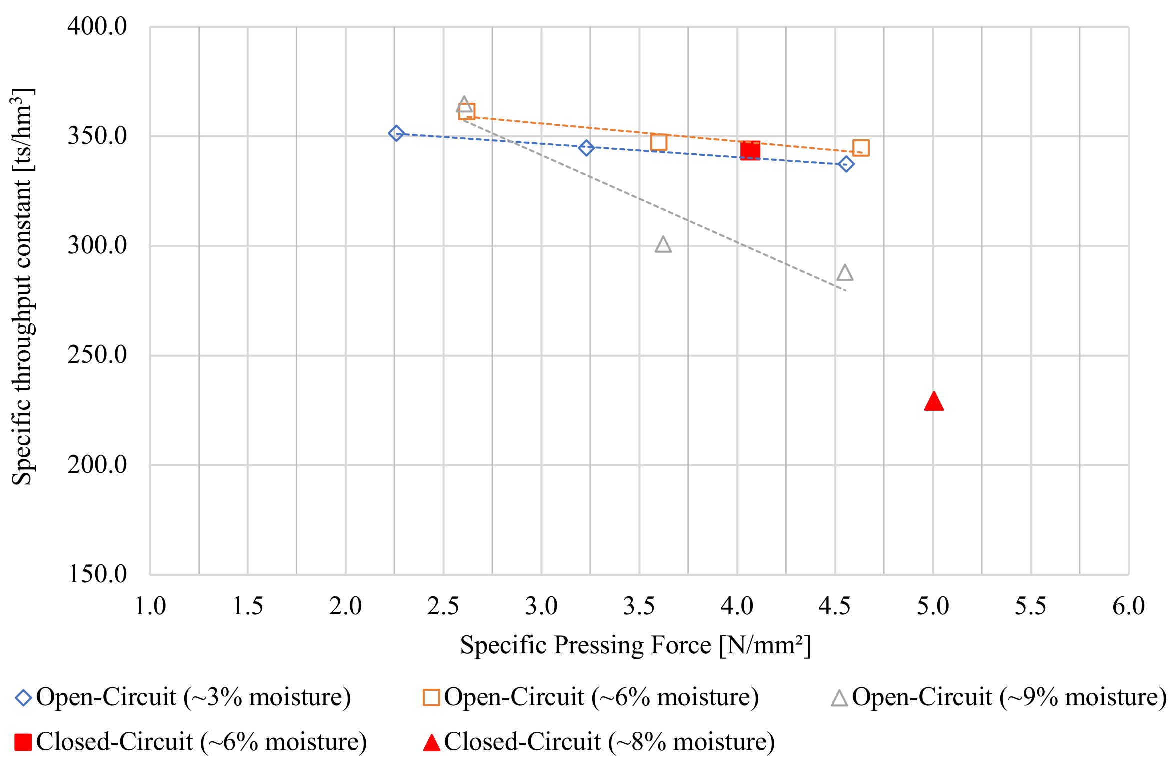

Figure 4-21: Closed circuit tests: correlation between m-dot and F_{SP}

The m-dot of the closed circuit test performed at 4.0 N/mm^2 was approximately 350 ts/m^3h. This result was comparable to the throughputs observed in the open circuit tests with ore moisture levels of 3% and 6%. In contrast, the closed circuit test conducted at 5.0 N/mm^2 resulted in a noticeably lower m-dot (229 ts/m^3h) and was equivalent to the results from the open circuit tests conducted at 9 % moisture.

The closed circuit test conducted at 5 N/mm^2 revealed the lowest m-dot of all HPGR pilot-scale tests performed in the pilot testing program, and the difference between the m-dot of both closed circuit tests was 33%. The justification for such low performance lies in the combination of applying high pressing forces at high moisture levels. Combining high pressures with high moisture levels proved detrimental to the HPGR performance for both quaternary and quinary applications.

As shown in Figure 4-19, in the 4^{th} cycle, the closed circuit tests that were conducted at 4 N/mm^2 and 5 N/mm^2 produced product with P_{80}'s of 5.02 mm and 4.72 mm, respectively. Regarding the generation of fines (material below 1 mm), Figure 4-22 shows that both tests achieved similar results to the open circuit tests conducted at 4.5 N/mm^2. The test conducted at 5.0 N/mm^2 resulted in a product with a slightly higher amount of fines. Applying 4 N/mm^2 F_{SP} resulted in a product with approximately 59% of its total mass below 1 mm, whereas 61% was achieved at 5 N/mm^2.

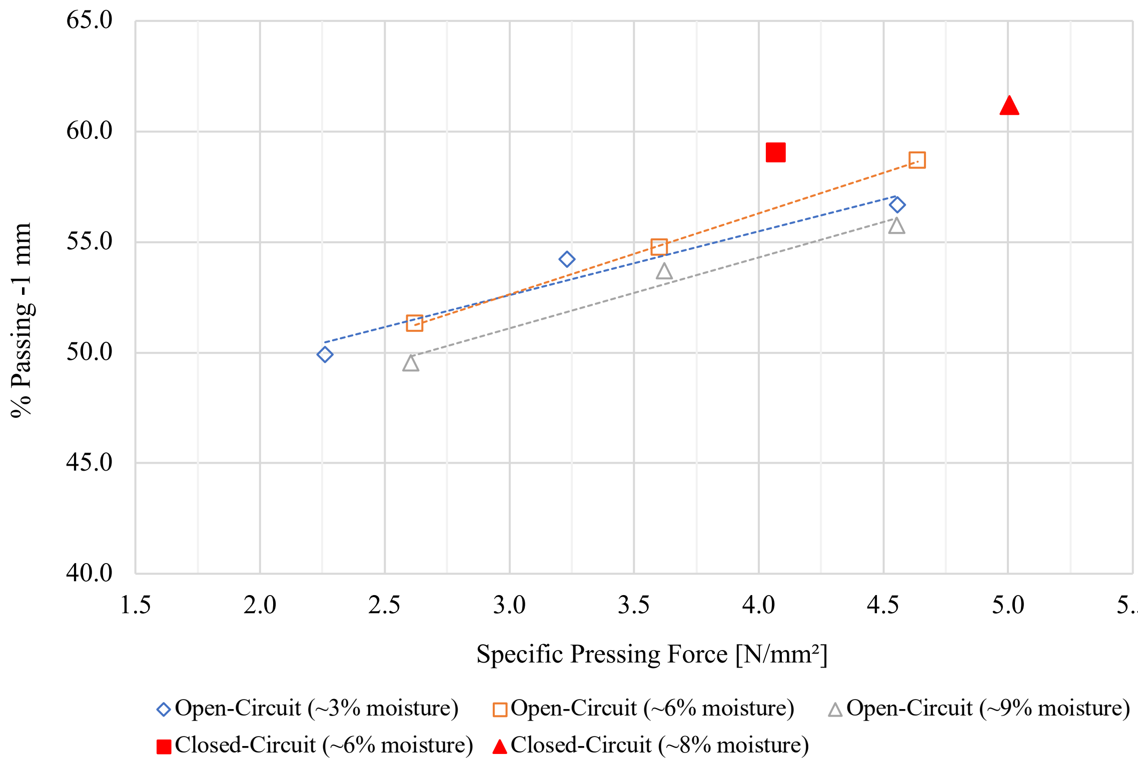

Figure 4-22: Closed circuit tests: comparison of fines generation (% -1mm)

4.3 Two-stage HPGR Circuit Analysis

An overall assessment of the results from the open and closed circuit tests was done to analyze the overall circuit performance. Table 4-3 summarizes the key input and output parameters of the test work. The results from the open circuit test work correspond to the average values obtained from the duplicate tests (SA010-SA013), which were the ones selected since their blended product was used to conduct the closed circuit tests. For the closed circuit tests, the circuit E_{SP} was estimated based on the E_{SP} reported in the last cycle (4th cycle) and the achieved circulating load.

For the closed circuit tests, the circulating load was taken into consideration for calculating the circuit E_{SP}. For example, the closed circuit test conducted at 4 N/mm^2 resulted in a net specific energy consumption of 1.72 kWh/t, but given that the corresponding circulating load was 78%, the circuit E_{SP} was 78% higher than the E_{SP} reported in the test work.

Table 4-3: Two-stage HPGR circuit analysis

Operating Parameters	Open Circuit Test work (Average)	Closed Circuit Test work (4th Cycle)	
F_{SP} [N/mm^2]	4.04	4.07	5.00
Achieved Moisture [%]	2.91	5.14	6.58
m-dot [ts/hm^3]	339.74	343.27	229.37
Circulating Load [%]	-	78.67	76.45
Circuit E_{SP} [kWh/t]	1.78	3.07	4.59
Linear Feed F_{80} [mm]	12.01	5.02	4.72
Feed % Passing 1mm	32.16	35.96	39.23
Linear Product P_{80} [mm]	4.47	2.60	2.35
Product % Passing 1 mm	56.50	59.04	61.19
Screen Undersize P_{80} [mm]	-	0.38	0.31
Screening Efficiency [%]	-	94.80	92.62

The analysis revealed that the two-stage HPGR circuit was able to nearly double the percentage of material passing 1 mm. As shown in Figure 4-23, the amount of material passing 1mm increased from 33% to approximately 60% depending on the applied pressing force. Despite having a finer feed compared to the open circuit stage, the product from the closed circuit tests presented a similar amount of fines, with 59% of material below -1mm and screen undersize P_{80} of 380 µm. Although this study did not focus on comparing different circuit options for Serra Azul's processing plant, the two-stage HPGR circuit was able to meet ArcelorMittal's requirements for the screen undersize product size (P_{80}) and the target percentage of material passing 1mm.

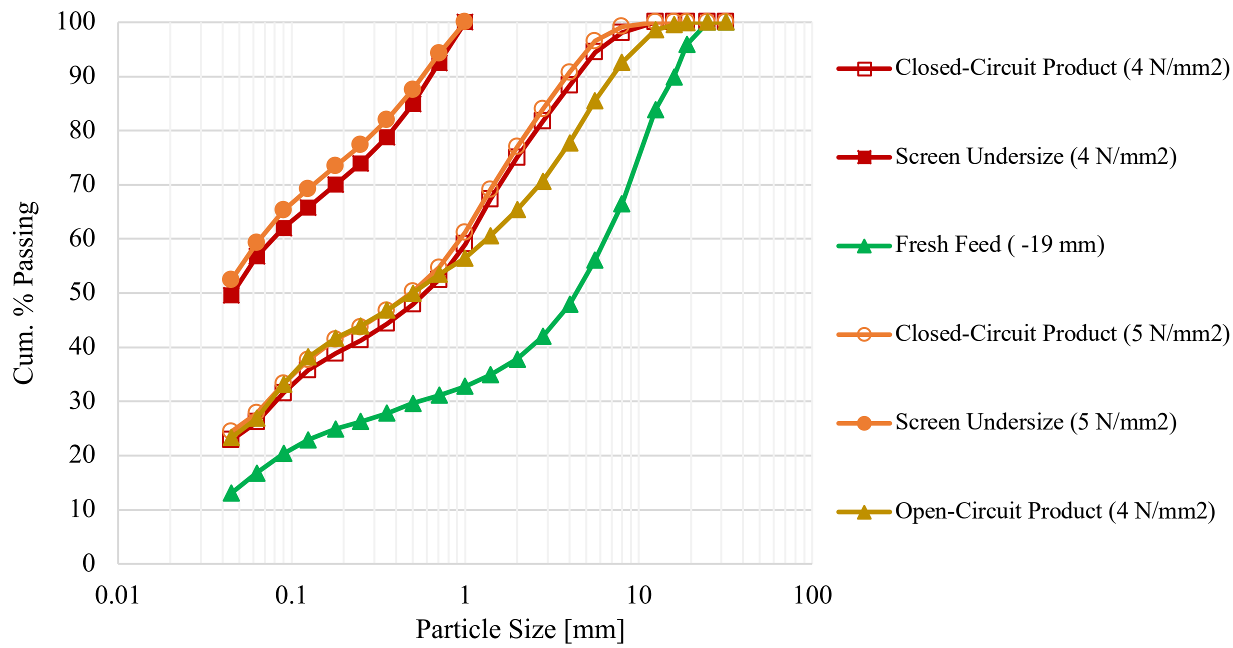

Figure 4-23: Two-stage HPGR circuit analysis

Selecting the optimum specific pressing force depends on ArcelorMittal's transfer size requirements for the quinary HPGR circuit and the final target grind size. If size reduction and fines generation is the main priority, F_{SP}'s values ranging from 3.5 N/mm^2 to 4.5 N/mm^2 revealed products with 55% to 60% of particles below 1 mm. If operated at 2.5 N/mm^2, the percentage of material below 1 mm dropped to approximately 50%. For the open circuit quaternary stage, considering that the expected ore moisture content is lower than 6%, m-dot values ranging 320 ts/m^{3}h to 345 ts/m^{3}h are expected. In contrast, the results showed that if moisture exceeds 6% in the closed circuit stage, the m-dot will drop and may reach low levels such as 230 ts/m^{3}h if the moisture content reaches approximately 8% by weight.

4.4 Summary

Results obtained from the open circuit pilot test work indicated that the two-stage HPGR circuit may perform exceptionally well as a quaternary crusher for Serra Azul's iron ore. For this application, the expected ore moisture content is approximately 3% for most of the year and should not exceed 6%. Under these conditions, quaternary HPGR circuit pilot tests achieved an average specific throughput constant of 340 ts/m^{3}h.

The net specific energy consumption increased linearly with increasing specific pressing force and E_{SP}'s ranging 1.1 to 2.2 kWh/t were recorded in the pilot test work. Both the specific throughput constant and operating gap were negatively affected by the applied specific pressing force, and a maximum m-dot of 365 ts/m^{3}h was recorded at a specific pressing force of 2.65 N/mm^2. In addition, the size reduction improved as the specific pressing force increased. An increase of 10% in the percentage of material below 1 mm was observed when the applied specific pressing force increased from 2.5 N/mm^2 to 4.5 N/mm^2.

The effect of moisture on the HPGR performance was also evaluated, and the analysis focused on assessing its impacts on the E_{SP}, m-dot, operating gap and reduction ratio. For the effects on the E_{SP}, the ore moisture content did not affect the machine performance by a significant amount, thus minor deviations were observed across the test work results. The results indicated that feeding a material with moisture content of up to 6% resulted in marginally lower E_{SP}'s when the HPGR was operated at 2.5 N/mm^2 and 3.5 N/mm^2.

The data analysis also indicated that operating the HPGR at high moisture contents can lead to significantly lower throughput and smaller operating gap. For example, while crushing Serra Azul's iron ore at 6% moisture and 4.5 N/mm^2, the HPGR achieved an m-dot of 344 ts/m^{3}h compared to 288 ts/m^{3}h at the same pressing force but at 9% moisture. In addition, it was also noted that the HPGR was able to comminute high moist ores without significant reductions on its throughput if operated at low pressing forces. Contrasting the previous example, a pilot test conducted at 2.5 N/mm^2 and 9% moisture resulted in a m-dot of 337 ts/m^3h, which was close to 352 ts/m^3h from another test at same pressing force, but at 3 % moisture.

A distinct relationship between the product fineness and the feed moisture content was not identified. Visual observations of the HPGR discharge showed that the material flow was not uniform across the conveyor width for the scenarios that targeted moisture levels higher than 6%. For these scenarios, most of the discharged product concentrated at the center of the conveyor, which suggests that most of the material breakage occurred at the center of the rolls, where the pressure is optimum, and higher size reduction is normally observed. However, the results showed that the reduction ratio was in fact, lower than scenarios with equivalent pressing force and lower moisture.

The closed circuit test results followed the linear trends between the specific pressing force and net specific energy consumption observed in the open circuit tests. It was found that increasing the F_{SP} from 4.0 N/mm^2 to 5.0 N/mm^2 increased the E_{SP} by 51%, which indicates that running the HPGR at 5 N/mm^2 and high moisture levels is detrimental to the HPGR performance. The m-dot of the closed circuit test performed at 4.0 N/mm^2 was approximately 350 ts/m^3h, which is comparable with the throughputs observed in the open circuit tests with less than 6% moisture.

The analysis of the two-stage HPGR circuit performance indicated that the HPGR is suitable for both the open circuit quaternary and closed circuit quinary applications. At a target pressing force of 4 N/mm^2 in both stages, the circuit achieved a product P_{80} of 0.38 mm and nearly doubled the amount of material below the target grind size of 1 mm, which increased from approximately 30% to 60%.

Chapter 5

Direct Calibration Methodology: Applications to Iron Ore

This chapter focused on demonstrating, validating and extending the direct calibration methodology to iron ore, with emphasis on quaternary open circuit application. Combined with the database from the piston-press test work, the pilot-scale HPGR database from Serra Azul's tests provided enough data points to apply the methodology and conduct detailed comparisons for various settings.

The following contributions were targeted:

- Extend and validate the methodology applications to iron ore, with focus on quaternary stage open circuit crushing.
- Provide calibrated regression models for Serra Azul's iron ore that allows the prediction of HPGR performance in terms of energy consumption and size reduction through piston-press-tests.
- Evaluate how moisture affects the accuracy of the energy-size reduction predictions.
- Evaluate if there are limitations associated with applying the calibrated regression models to composite samples for predicting the HPGR's product size distribution.

5.1 Direct Calibration Methodology: A Step-by-Step Analysis

5.1.1 HPGR Pilot Testing

The open circuit experimental program generated a matrix with nine pilot-scale HPGR tests that had the F_{SP} and moisture content as the main variables (refer to Table 4-1). This resulted in three settings where the Direct Calibration method could be applied and allowed a detailed analysis over its applicability to iron ore. Table 5-1 shows how the HPGR experimental program was planned in order to apply the methodology in three settings:

Table 5-1: Settings used to apply the Direct Calibration methodology

Sample description	Setting	Test Id.	Top size	Moisture (target)	Specific pressing force (target)
			mm	%	N/mm^2
50% Compact / 50% Semi-compact	1	SA001	19	3.0	3.5
		SA004			2.5
		SA007			4.5
	2	SA002	19	6.0	3.5
		SA005			2.5
		SA008			4.5
	3	SA003	19	9.0	3.5
		SA007			2.5
		SA009			4.5

5.1.2 Piston-Press Testing

Table 5-2 shows how the piston-press experimental program was planned and correlated to the HPGR tests. In total, 12 piston-press tests were performed to generate the necessary data for applying the Direct Calibration methodology and the Database Calibrated methodology. The test results can be found in Appendix B.

Table 5-2: Piston-press test conditions

Sample Description	Setting	Test Id.	Top Size	Moisture (target)	Pressing Force (target)
			mm	%	kN
50% Compact / 50% Semi-compact	1	PP3 -01	12.5	3	1399
		PP3-02			1100
		PP3-03			800
		PP3-04			500
	2	PP6 -01	12.5	6	1399
		PP6-02			1100
		PP6-03			800
		PP6-04			500
	3	PP6 -01	12.5	9	1399
		PP6-02			1100
		PP6-03			800
		PP6-04			500

5.1.3 Correlating the Piston-Pressure with the Specific Pressing Force

For all three settings, the piston-press pressures were calibrated against the specific pressing force. Figure 5-1 exemplifies the fitted regression lines for the E_{SP} versus P_{piston} and E_{SP} versus F_{SP} for Setting 1.

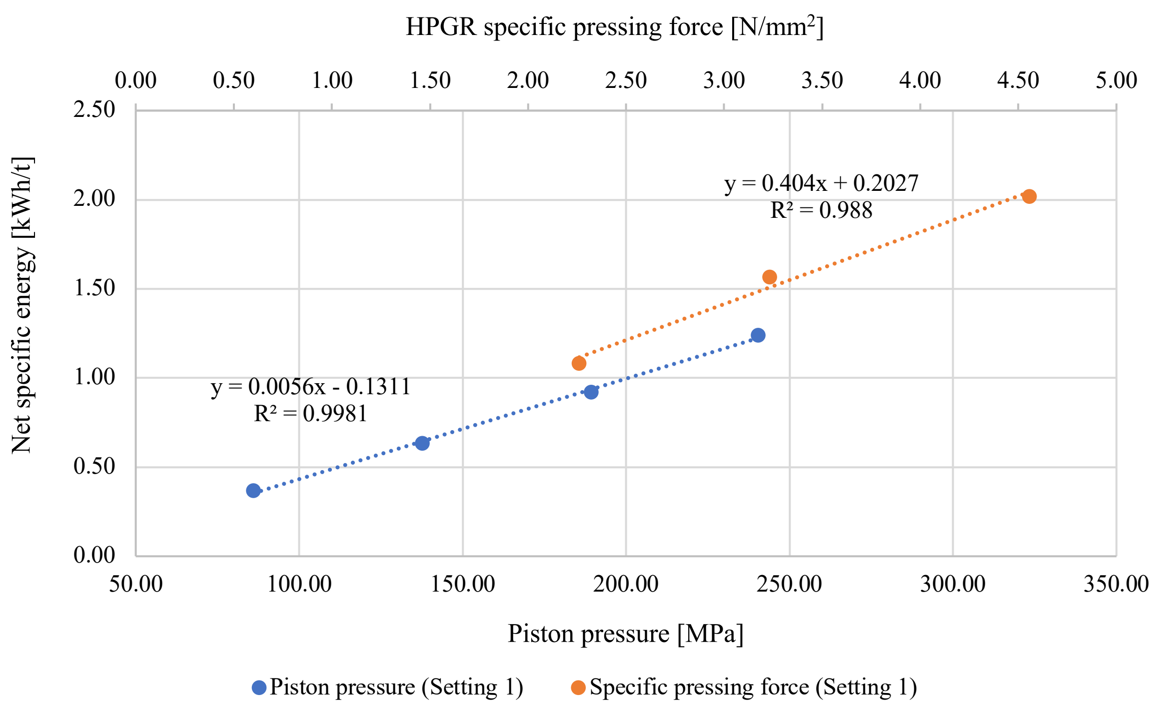

Figure 5-1: Step 3 - Pressure calibration

To obtain the generic formula that provides the equivalent piston pressure for a given F_{SP}, Eq. 2.9 was applied. Table 5-3 summarizes the calibration slopes and intercepts of each setting:

$$P_{piston} = \frac{m_2}{m_1} \cdot F_{SP} + \frac{b_2 - b_1}{m_1} \tag{2.9 revisited}$$

Table 5-3: Slopes and intercepts for determining equivalent P_{piston} for a given F_{SP}

Setting	Slope $\left(\frac{m_2}{m_1}\right)$	Intercept $\left(\frac{b_2-b_1}{m_1}\right)$
1	72.14	59.61
2	81.37	18.54
3	73.31	71.10

The calibrated equation from each set was used to calculate the equivalent piston pressure to provide the same E_{SP} as the pilot HPGR tests. Next, the equivalent piston pressures were applied in their respective piston-press equations to predict the net specific energy consumption. Figure 5-2 compares the E_{SP} from the HPGR tests to those predicted from piston-press tests using the calibration equations.

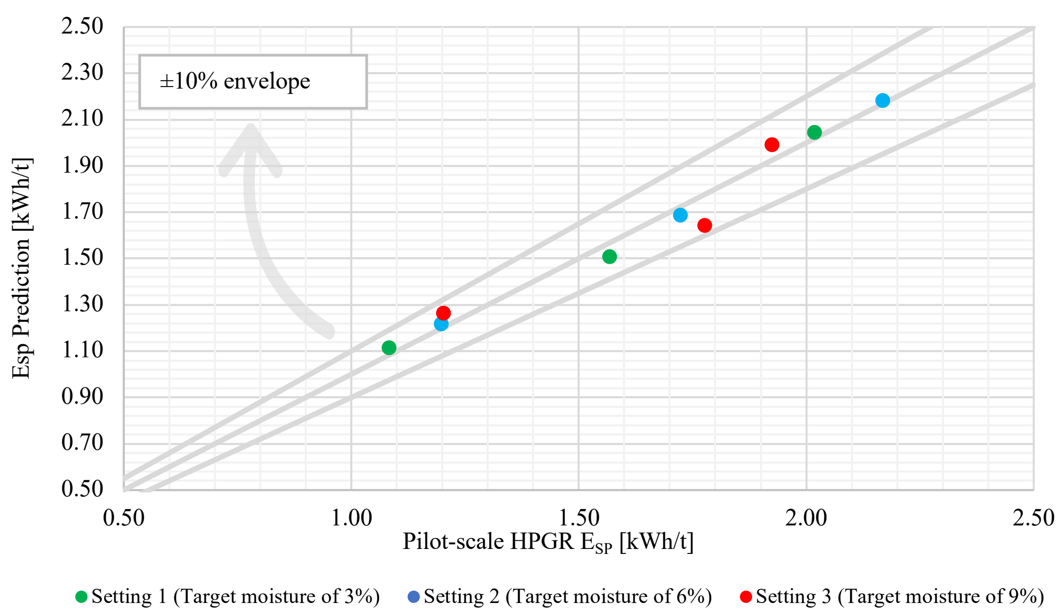

Figure 5-2: Comparison of the predicted net specific energy consumption

For all settings, the predicted E_{SP}'s lies within the ±10% envelope, which is the expected accuracy of the direct calibration methodology.

5.1.4 Relating HPGR to Piston-press Reduction Ratio

To obtain the calibrated regression model, it was first necessary to determine the reduction ratios from the piston-press tests at the same net specific energy as from the pilot HPGR tests. Eq. 2.10 was used to model the reduction ratios achieved in the piston-press tests, as exemplified in Figure 5-3A. The predicted piston-press RR_{50}'s at the same E_{SP}'s as the HPGR tests were plotted against the pilot HPGR RR_{50}'s in order to obtain the reduction ratio calibrated equation (Figure 5-3B).

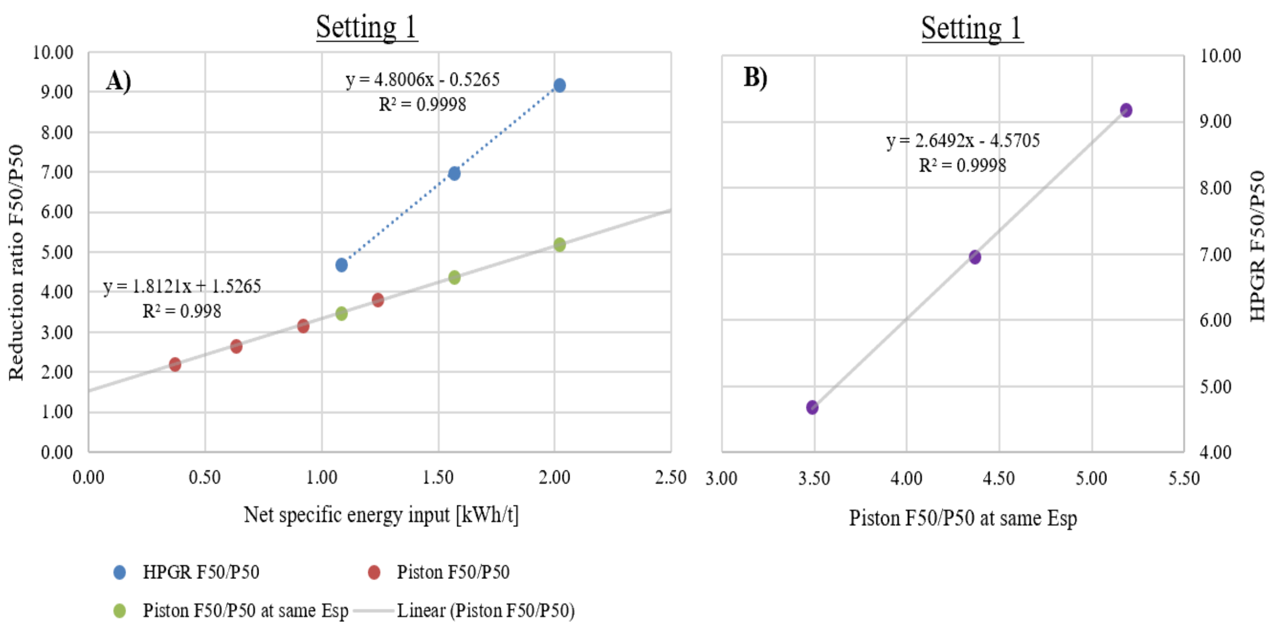

Figure 5-3: A) Determining the piston RR_{50} at same E_{SP} as the HPGR tests; B) Calibrating the predicted piston-press RR_{50}'s against the pilot HPGR RR_{50}'s

Table 5-3 summarizes the slopes and intercepts from the reduction ratio calibrated equations:

Table 5-4: Slopes and intercepts for the reduction ratio calibrated equations

Setting	Slope	Intercept	R^2
1	2.65	- 4.57	1.00
2	2.95	- 6.81	0.97
3	3.70	- 8.93	0.90

The predicted scaled-up reduction ratios of the piston-press tests were compared to the reduction ratios achieved in the pilot HPGR tests, as shown by Figure 5-4 below:

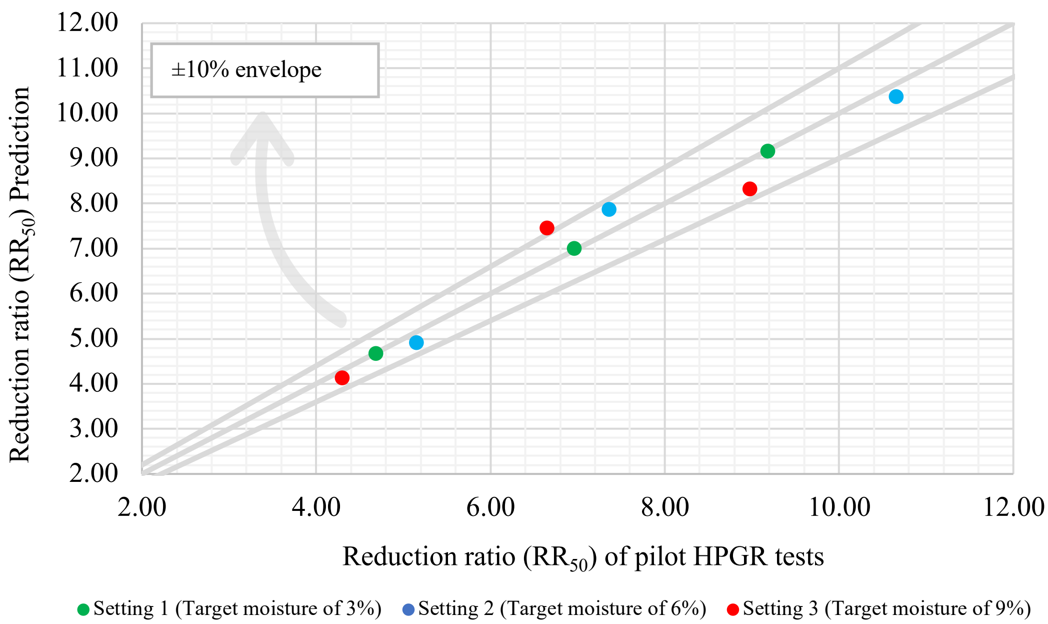

Figure 5-4: Comparison of the predicted RR_{50}'s against the pilot HPGR RR_{50}'s

It was found that except for one data point where the target moisture content was high at 9%, the predicted reduction ratios were within the ±10% envelope.

5.1.5 Assessing the Moisture Effect on the Energy and Size Reduction Predictions

Table 5-5 and Figure 5-5 compare the relative percentage errors associated with the net specific energy consumption and size reduction (RR_{50}) predictions. In both cases, the comparisons revealed that applying the direct calibration methodology at high moisture levels can be detrimental to the overall accuracy of the predictions. For the E_{SP} prediction, lower moisture levels (< 3%) were more consistent and accurate. As for the RR_{50} predictions, the lowest relative errors were noted at Setting 2 (target moisture of 6%). Despite the targeted specific pressing force, the least accurate size reduction predictions were observed at Setting 3.

The pilot test results from the open circuit tests (refer to Section 4.1.4) showed that moisture impacted not only the specific throughput constant but also the specific pressing force and reduction ratio, especially at levels higher than 6%. Considering that Davaanyam's methodologies assume that the piston-press test results can be calibrated against the pilot test results due to its similar breakage behaviour, it is expected that variables such as moisture should have the same effect on the operating parameters despite the test conditions. However, as observed from the piston-press test results (refer to Appendix B), even at 9%, the moisture content did not impact the energy consumption and size reduction as much as it did in the pilot-scale tests. Consequently, since the energy and size reduction calibrations between the piston-press and pilot-scale HPGR results were based on linear relationships, applying the methodology to scenarios with high moisture resulted in less accurate predictions.

It is important to note that the calibrated models are still applicable in scenarios with higher moisture content, but as described by Davaanyam (2015), the effects such as higher energy consumptions at higher moisture levels must be taken into account during the scale-up process.

Table 5-5: Comparison of the relative errors associated with the E_{SP} and RR_{50} predictions

Target Moisture (%)	Measured RR_{50}	Predicted RR_{50}	Error %
3	9.18	9.16	0.20
	6.96	7.00	0.51
	4.69	4.67	0.36
6	10.65	10.37	2.61
	7.36	7.87	6.97
	5.14	4.91	4.57
9	8.97	8.32	7.25
	6.65	7.46	12.31
	4.30	4.13	3.89

Target Moisture (%)	Measured E_{sp} kWh/t	Predicted E_{sp} kWh/t	Error %
3	2.02	2.04	1.25
	1.57	1.51	3.77
	1.08	1.12	3.16
6	2.17	2.18	0.80
	1.72	1.69	2.06
	1.20	1.22	1.53
9	1.92	1.99	3.57
	1.78	1.64	7.39
	1.20	1.26	5.24

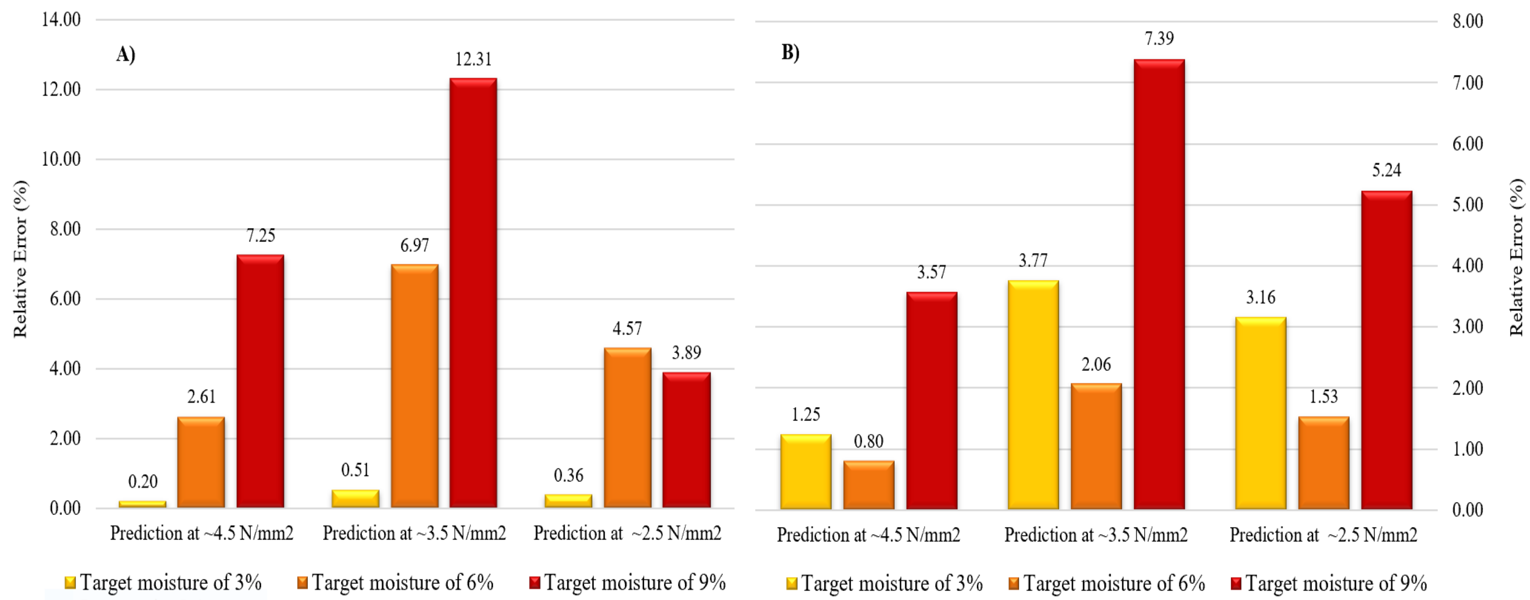

Figure 5-5: A) Comparison of the relative errors associated with the RR_{50} predictions; B) Comparison of the relative errors associated with the E_{SP} predictions

5.1.6 Comparing the Normalized Product PSDs

The assessment of the HPGR performance for the quaternary stage open circuit crushing confirmed some of the requirements for applying the direct calibration methodology and database calibrated methodology, such as the linear relationship between the specific pressing force (F_{SP}) and the net specific energy consumption (E_{SP}). However, another critical requirement is the self-similar characteristic between the HPGR and piston-press products. To demonstrate this step, Setting 1 (target 3% moisture) was selected since it presented the highest accuracy of all three settings during the energy and size reduction predictions.

Figure 5-6 shows the normalized PSDs and fitted curves of products from the pilot-scale HPGR and piston-press tests for Setting 1.

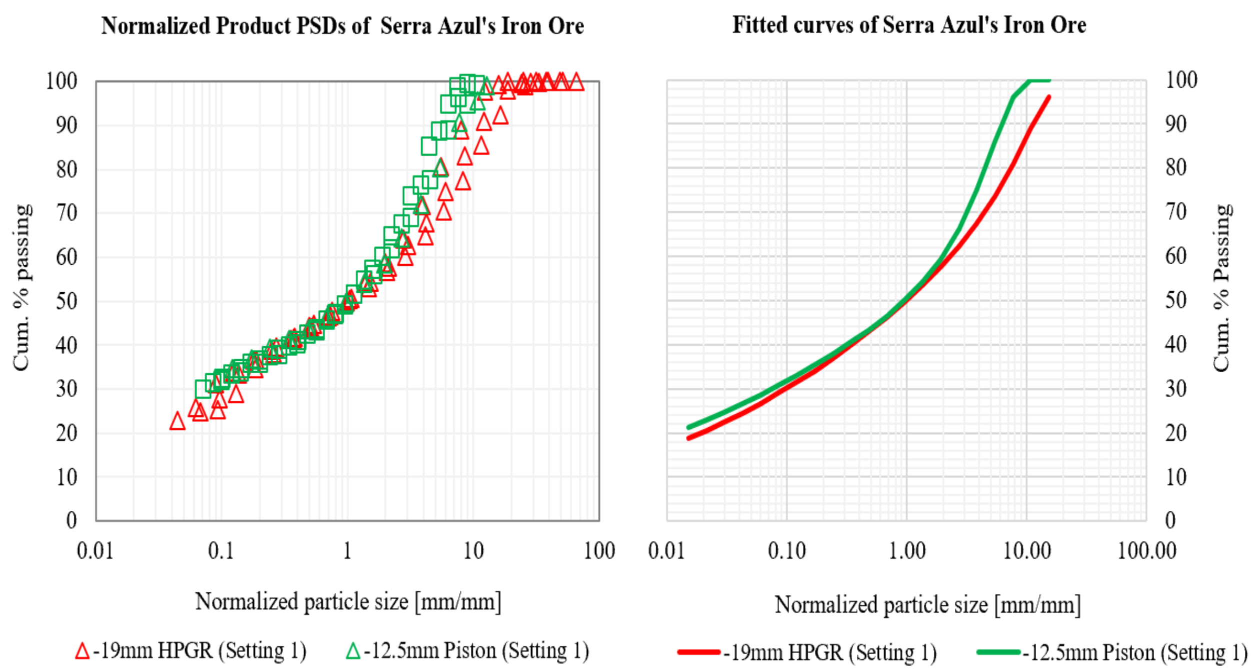

Figure 5-6: Analysis of normalized PSDs of products from piston-press and HPGR tests

The normalized PSDs and the fitted curves matched well for size fractions below 1mm, whereas discrepancies were observed in the higher percentage passing sizes (coarser particles).

As exemplified in Figure 5-7, some of Davaanyam's analysis also presented discrepancies in the coarse and fine passing sizes. He reported that the minor differences in the fines might occur since the piston-press product is wet-screened while the HPGR product is dry-screened. Concerning the variances in the coarse fractions, his justification was that the HPGR assures that particles larger than the operating gap will not report to the product, whereas the same cannot be assumed from the piston-press tests.

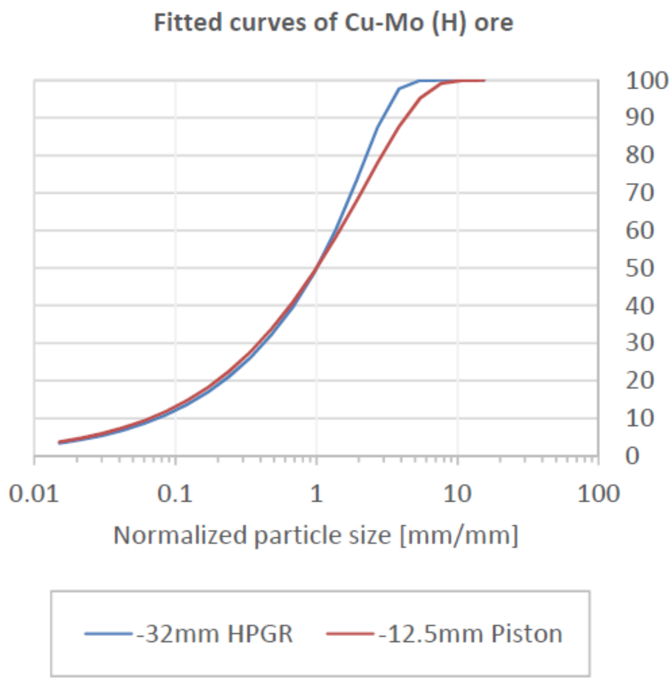

Figure 5-7: Comparison of fitted curves of a Cu-Mo ore

(Source: Davaanyam, 2015)

The discrepancies in the iron ore fitted curves can be related to the following hypothesis:

i. **Specific characteristics of the ore**: Some hematites from Brazilian iron ore deposits (e.g., Serra Azul) are known to be friable and therefore susceptible to generating high amounts of fines during crushing and grinding stages. The samples used in the piston-press tests went through extra stages of crushing and screening in order to achieve the top size requirements, which in turn might have increased the proportion of fines in the sample compared to the HPGR's sample. This hypothesis was verified based on the percentage of material below 1mm in the feed samples used in the HPGR and piston-press tests. The feed samples used in the HPGR tests had approximately 32 % of material below 1mm compared to 35 % in the piston-press tests.

ii. **Correlation between the HPGR feed top size and achieved roller gap:** The top size of an HPGR product is dictated by the actual gap between the rolls during the test, meaning that if the actual roller gap is larger than the feed top size, coarse particles as big as the feed top size can still be present in the product. The results from the open circuit tests (feed top size of -19 mm) show that the actual roller gap during the tests ranged from 24.33 mm to 19.28 mm. Graphically speaking, this scenario results in a product PSD curve that is less steep than a typical product PSD curve of a piston-press test, as exemplified in Figure 5-8.

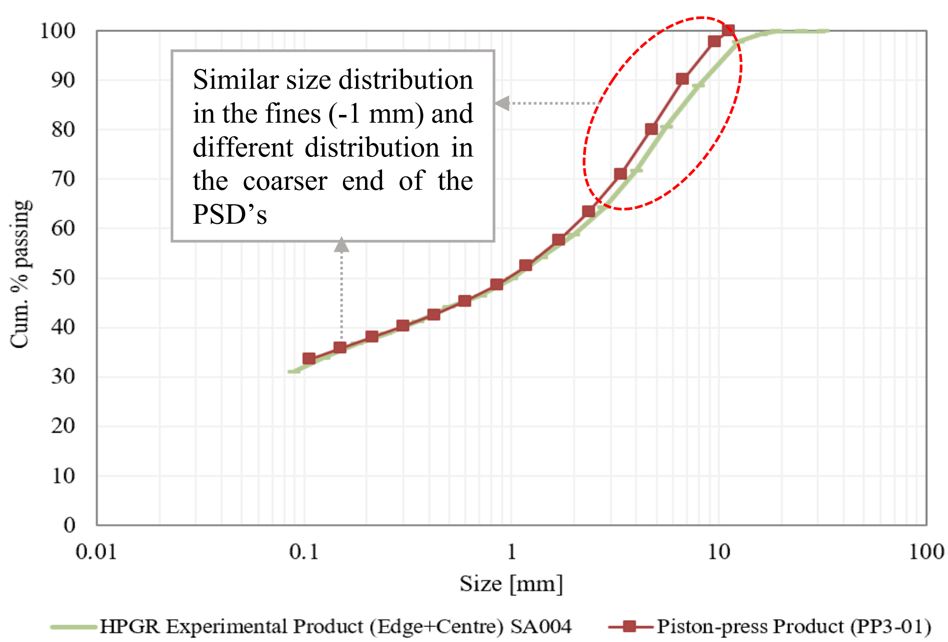

Figure 5-8: Comparison between HPGR and piston-press product PSDs

5.1.7 Applying the Calibrated Models on Geometallurgical Units

The last step focused on demonstrating how the direct calibrated regression models obtained through steps 3 and 4 can be applied to geometallurgical samples. The first objective was to use the calibrated regression models for assessing the HPGR performance varies across the ore deposit in terms of energy consumption. The second objective was to investigate if there are limitations regarding the application of the calibrated models to composite samples for predicting the HPGR's product size distribution.

A total of four geometallurgical drill hole core samples from Serra Azul's deposit were available for performing the piston-press tests. Table 5-6 presents the chemical composition of each sample in terms of iron (Fe) and silica (SiO_2). Figure 5-9 illustrate the feed PSD of each sample. Although all of them were classified as compact itabirites, their chemical analysis and feed PSD indicated a high degree of variability within the deposit.

Table 5-6: Geometallurgical units from Serra Azul deposit

Geo Unit:	Geological Classification:	Chemical Analysis:		Feed Characteristics:	
		Fe [%]	SiO_2 [%]	F_{50} [mm]	% Passing 1mm
1	Compact Itabirite	27.08	60.64	7.41	6.51
2		32.58	52.49	7.27	8.44
3		34.21	51.08	5.98	15.81
4		51.41	25.48	4.63	31.86

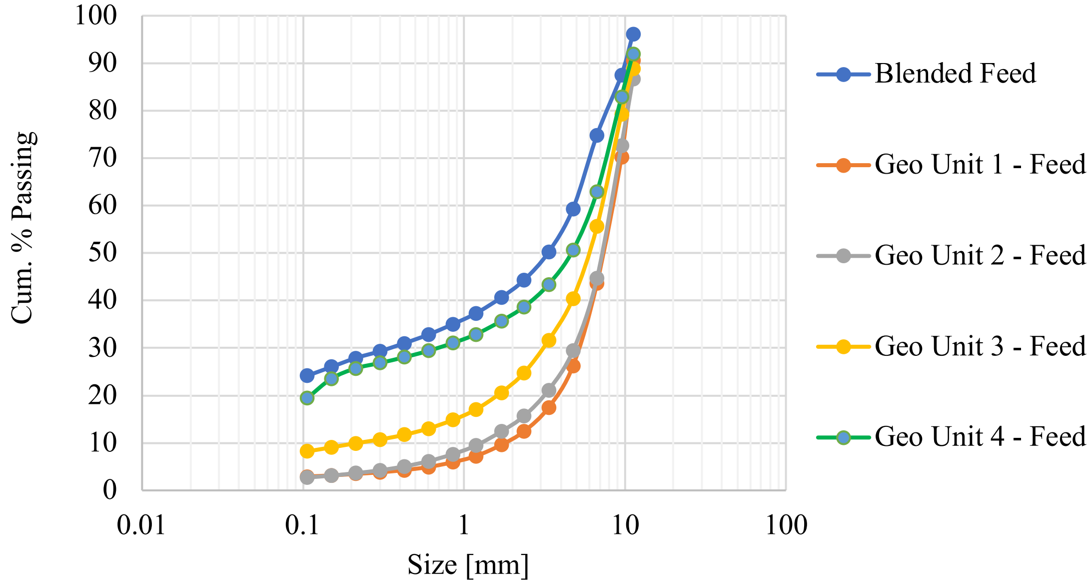

Figure 5-9: Feed PSD of each geometallurgical unit

Given that all geometallurgical samples were classified as compact itabirites, the best-case scenario for conducting the validation analysis was to make use of the results from the open circuit HPGR tests (SA012-013) conducted on the compact itabirites. However, the pilot test conducted on the compact itabirite had a target pressing force of 4 N/mm^2, and to match the F_{SP} from those tests, a piston pressure of approximately 2,000 kN was required. As shown in Figure 5-1, at its maximum pressing force of 1399 kN, the UBC's MTS compression machine was only able to match the net specific energy of HPGR tests conducted at pressing forces below 3.0 N/mm^2.

Considering this, two approaches were proposed for validating and demonstrating the methodology's applicability:

I. The first approach selected the calibrated regression models from Setting 1 and made use of the MTS machine to conduct a single piston-press test for each of the geometallurgical units at the equivalent piston pressure of the open circuit HPGR tests that were performed at a pressing force of 2.6 N/mm^2. In this case, the results from the piston-press test were validated against the results from the pilot tests conducted on blended samples with a 1:1 ratio of compact and semi-compact itabirite at target moisture content of 6% and 9%.

II. The second approach involved making use of the calibrated regression models from Setting 1 (3% moisture) and conducting one piston-press test for each of the geometallurgical units at the equivalent piston pressure from the open circuit HPGR tests that were conducted on the compact itabirites at 4 N/mm^2 and 3% moisture. This approach was also used as an opportunity to assess if the piston press tests can be performed by different compression machines and at independent laboratories. The tests were conducted on a compression machine manufactured by Controls Group.

The test work conditions of both approaches and the individual test results for the specific energy consumption and reduction ratio (RR_{50}) are presented in Table 5-7. Duplicate tests were performed at 4 N/mm^2 to ensure the results from the Controls Group compression machine were reliable.

As illustrated in Figure 5-10 and Figure 5-11, in most cases the MTS and Controls Group compression machines produced similar specific energy consumption and reduction ratios. It is important to note that minor deviations between the test results were expected since the errors can be explained by variations in sampling and the precision of the machine readings. In addition, even at the same test conditions, the particles may break differently from one test to another due to different particle arrangement in the piston die. Considering these factors, the compression machine from Controls Group generated results that are similar to those obtained from tests with the MTS equipment.

For the first approach, the test results obtained from the MTS machine showed that the specific energy consumption at 2.6 N/mm^2 ranged from 1.25 kWh/t (Geo unit 4) to 2.01 kWh/t (Geo unit 2), which means the energy consumption can vary by up to 60.8% between geometallurgical units. For comparison, at 4 N/mm^2, the energy consumption ranged from 2.2 kWh/t (Geo unit 4) to 3.25 kWh/t (Geo unit 1), which represents a variation of up to 47.7%.

Table 5-7: Summary of piston-press tests results on 4 geometallurgical units

Target F_{SP}	Equivalent P_{piston}		Compression Machine	Geo Unit	Specific Energy	Reduction Ratio
[N/mm^2]	[MPa]	[kN]			[kWh/t]	F_{50}/P_{50}
2.6	247.0	1436.0	MTS	1	1.94	3.85
			Controls Group		1.85	3.90
			MTS	2	2.01	4.53
			Controls Group		1.84	4.42
			MTS	3	1.65	4.36
			Controls Group		1.88	4.03
			MTS	4	1.25	3.23
			Controls Group		1.14	3.99
4	348	2022	Controls Group	1	3.25	4.83
				1 Duplicate	3.18	5.00
				2	3.17	4.80
				2 Duplicate	3.18	4.79
				3	2.63	4.58
				3 Duplicate	2.59	5.01
				4	2.20	4.67
				4 Duplicate	2.18	4.52

Figure 5-12 and Figure 5-13 present the predicted E_{SP} of the piston-press tests performed for each geometallurgical unit and compare the results against the E_{SP} from pilot HPGR tests conducted at equivalent pressing forces. In both approaches, geometallurgical units 1, 2 and 3 were identified as having high circuit specific energy requirements compared to the results from the pilot test. Although Geo unit 4 resulted in similar E_{SP}'s compared to the E_{SP}'s from the pilot tests, the values were also slightly higher. It is important to note that since all composite samples were classified as compact itabirites, which as discussed in Section 4.1, are generally harder than the semi-compact itabirite that composed the feed material of the pilot HPGR tests in a 1:1 ratio, it was expected that the piston-press tests on Geo units 1-4 would also result in higher E_{SP}'s.

In addition, Figure 5-12 and Figure 5-13 also compares the amount of fines that were present in the feed for the pilot tests and for the piston-press tests using the geometallurgical samples. The graphics shows that Geo unit 4 has similar amount of material below 1 mm compared to both pilot tests conducted on the blended samples and individual samples of compact itabirite. This analysis is critical for understanding the reason why the E_{SP} reported from the geometallurgical units varied by up to 60.8% if they are all classified as compact itabirite. In sum, the PSD analysis revealed that there is a high degree of variability within Serra Azul's composites, which in turn affects the HPGR performance.

The ability to assess how the specific energy consumption varies across geometallurgical units is important to the mine planning as it can significantly impact process operations. This exercise supports one of the applicability's of the Direct Calibration methodology, which based on a quick assessment through piston-press tests can provide information on how the energy consumption of the HPGR may vary when crushing different composites of a given ore deposit.

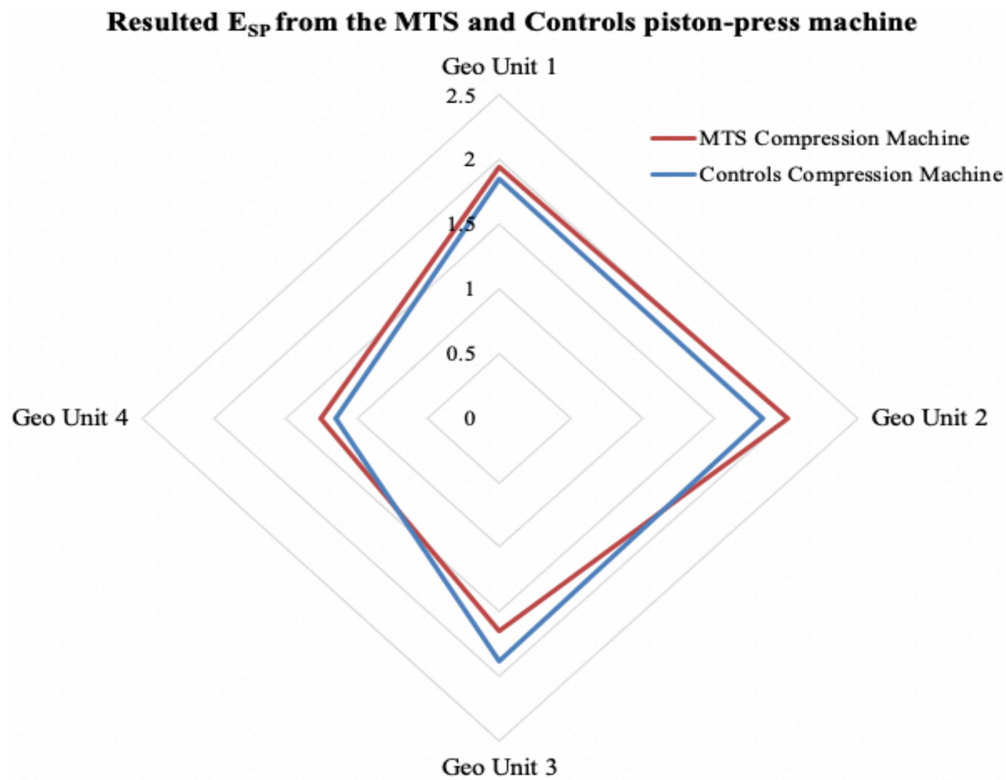

Figure 5-10: Resulted E_{SP} from the MTS and Controls Group compression machines

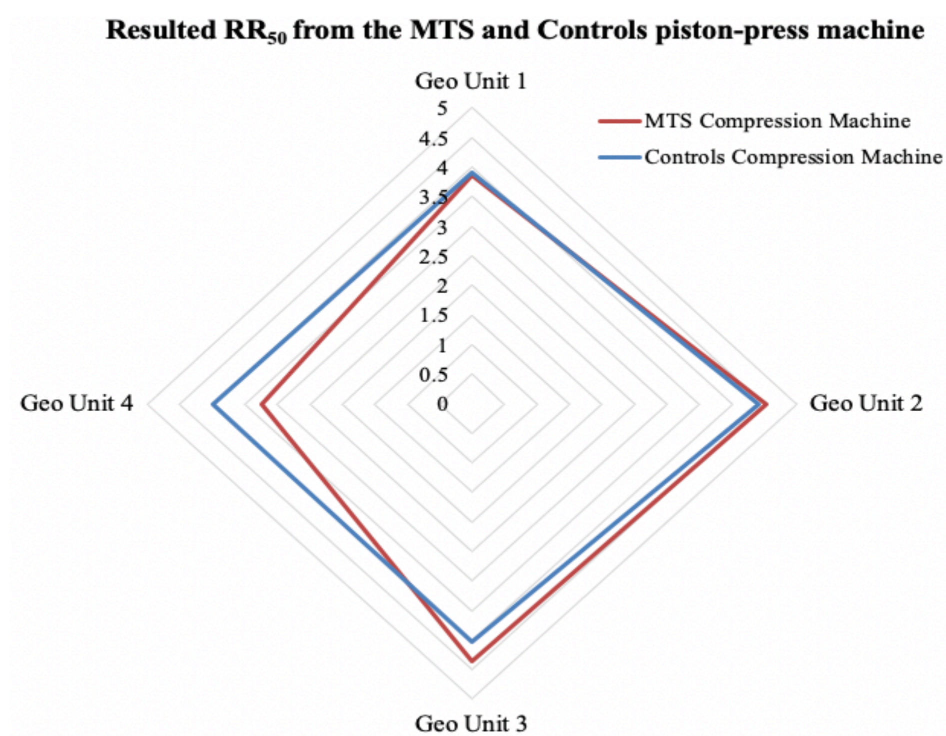

Figure 5-11: Resulted RR_{50} from the MTS and Controls Group compression machines

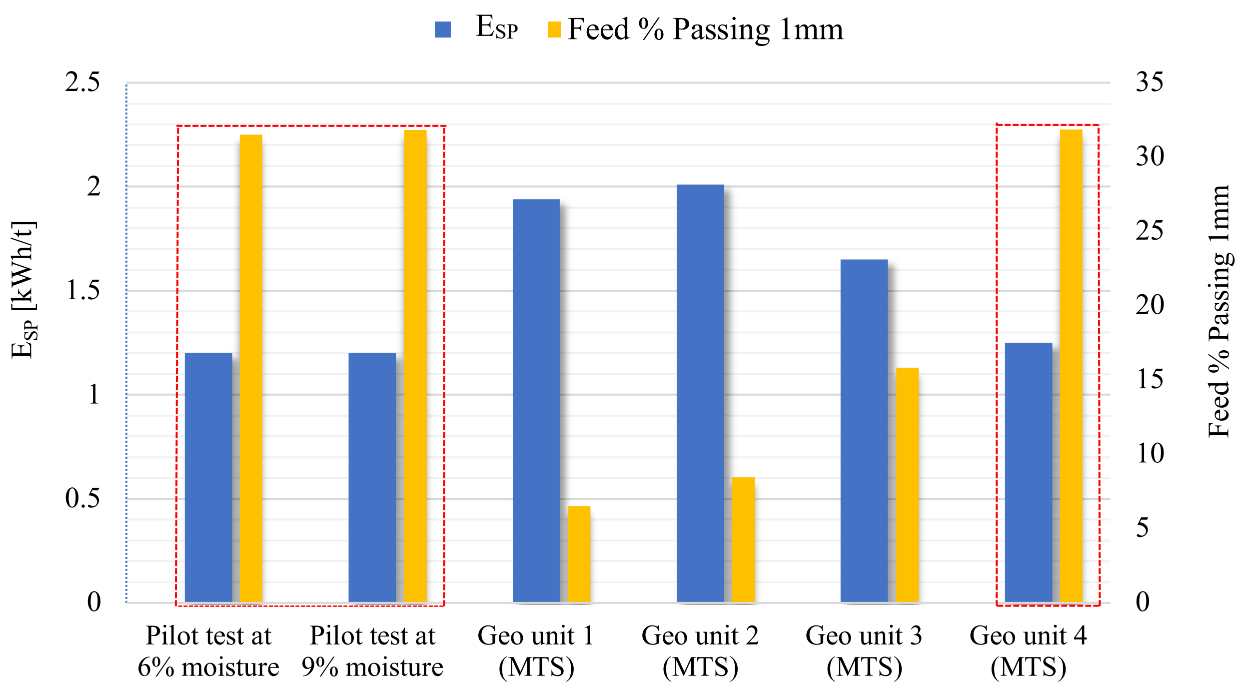

Figure 5-12: Prediction of E_{SP} for each geometallurgical unit at 2.6 N/mm^2

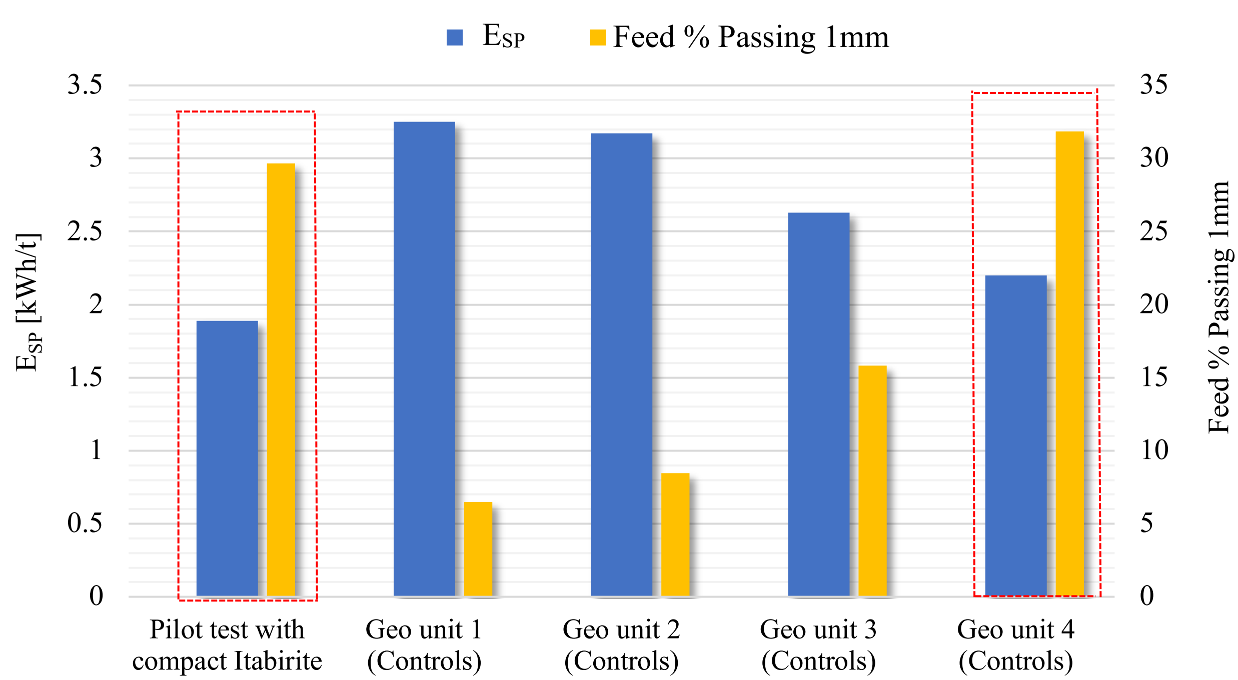

Figure 5-13:Prediction of E_{SP} for each geometallurgical unit at 4.0 N/mm^2

The last objective was to evaluate if there are limitations associated with applying the models to composite samples for predicting the HPGR's product size distribution. The slope and intercept of the reduction ratio calibrated equation from Setting 1 (refer to Table 5-4) were used for calculating the scaled HPGR reduction ratio (RR_{50}) from the piston-press tests that targeted a specific pressing force of $4 N/mm^2$. Table 5-8 summarizes the scaled-up RR_{50}'s from the piston-press tests.

Table 5-8: Summary of the scale-up results of the piston-press tests

Target F_{SP}	Equivalent P_{piston}	Compression Machine	Geo Unit	Reduction Ratio	Scaled-up Reduction Ratio
[N/mm^2]	[kN]			RR_{50}	RR_{50}
4	2022	Controls Group	1	3.25	8.23
			2	3.17	8.15
			3	2.63	7.56
			4	2.20	7.80

The scaled-up reduction ratio from all tests were slightly lower than the RR_{50} of 9.02 observed in the pilot test that used the compact itabirite sample (SA013). It is important to note that even though all composites resulted in similar size reduction, the previous analysis showed that they were highly variable in terms of feed characteristics. In addition, the methodology can only be applied to predict the product size distribution of HPGRs if the product from the piston-press test and HPGR are self-similar. Considering this, the reduction ratio could not be used as a parameter for assessing the machine performance in terms of product size, but it was useful to back-calculate the scaled P_{50} of the HPGR given that the F_{80} from the pilot test was known. The piston-press normalized curves combined with the scaled P_{50} of each composite were used to predict the HPGR product PSDs. The predicted PSDs are presented in Figure 5-14.

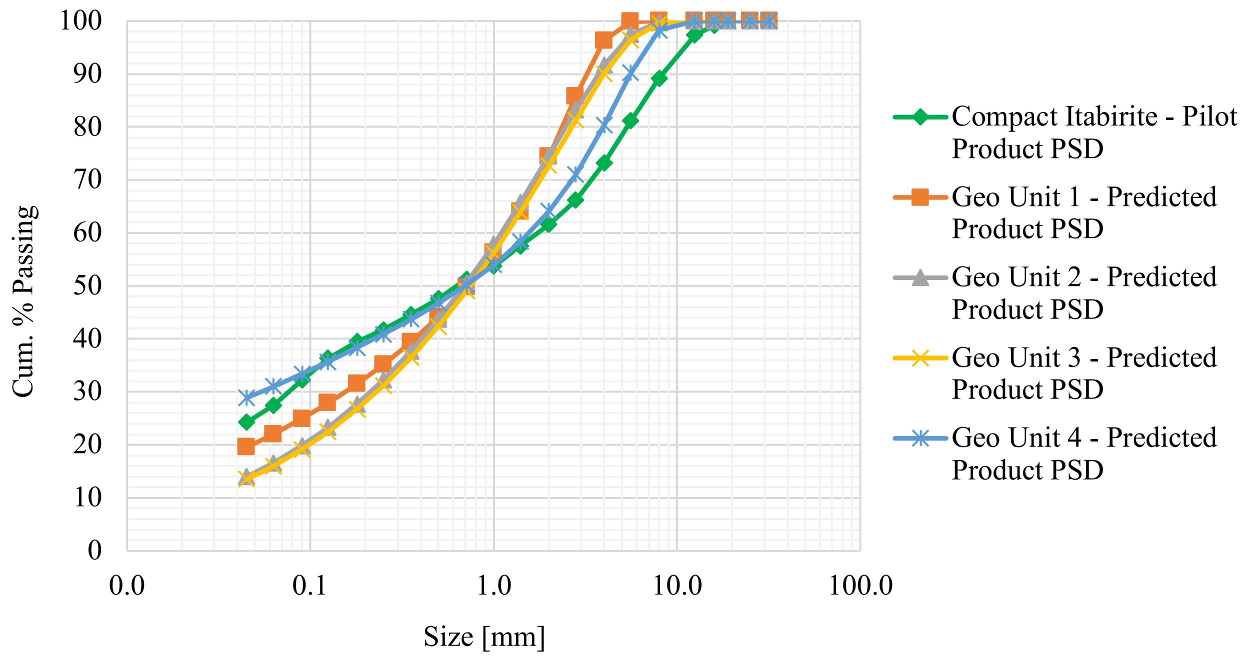

Figure 5-14: Predicted HPGR product PSDs

It was found that the data from Geo units 1-3 did not result in accurate predictions of the HPGR product PSD, which means that the normalized product PSDs from the piston-press tests did not match the normalized product PSD from the pilot HPGR test. In contrast, the predicted product PSD from Geo unit 4 showed reasonable similarities to the HPGR's product PSD, as summarized in Table 5-9. The predicted PSD from Geo Unit 4 matched well for size fractions below 1mm, whereas discrepancies were observed in the coarser end of the size distribution.

The results obtained from this analysis indicate that the Direct Calibration methodology may not be suitable for predicting the product PSD of HPGRs through geometallurgical units that have feed size characteristics considerably different than the samples used to calibrate the energy and size reduction regression models.

Table 5-9: Geo Unit 4 predicted product PSD

Cumulative % Passing	Predicted PSD (Geo Unit 4)	Pilot HPGR Product PSD (SA013)
	Size [mm]	Size [mm]
P90	5.56	8.45
P80	3.96	5.37
P70	2.68	3.45
P60	1.57	1.77
P50	0.70	0.64
P40	0.23	0.20
P30	0.05	0.08
1 mm	53.96	53.71

5.2 Summary

The Direct Calibration methodology was successfully applied to Serra Azul's iron ore. The methodology was applied for three different settings that had moisture as the main variable. The slopes and intercepts for the regression models of each setting were summarized in Table 5-3 and Table 5-4. For all scenarios, the predicted net specific energy consumption and size reduction lies within a ±10% envelope, which is the expected accuracy of the methodology.

The effect of moisture on the accuracy of the energy consumption and size reduction predictions was also evaluated. The results showed that applying the direct calibration methodology at high moisture levels can be detrimental to the overall accuracy of the predictions.

Despite the targeted specific pressing force, the least accurate size reduction predictions were observed in scenarios with 9% moisture.

Regarding the normalization of the piston-press and pilot HPGR product PSDs, it was found that the curves did not match well in the coarser end of the size distribution. The accuracy of the Direct-Calibration methodology can be greatly impacted by errors associated with sampling since the samples used for conducting the piston-press need further crushing and screening to reduce the top size to 12.5 mm. For friable ores such as Serra Azul's iron ore, extra stages of crushing will generate high amounts of fines, which can affect the normalized piston-press product PSD.

Results obtained from the regression models' application on four different geometallurgical units from Serra Azul's deposit showed that the HPGR energy consumption varied by up to 60.8% between composites, which indicates a high degree of variability within the deposit. It was also found that the Direct Calibration methodology is not adequate for predicting the product PSD of HPGRs through geometallurgical samples that have different feed size characteristics than the samples used to calibrate the energy and size reduction regression models.

Chapter 6

Database-Calibrated Methodology: Applications to Iron Ore

The database calibrated models proposed by Davaanyam (2015) did not include pilot HPGR or piston-press test work on iron ore, and at the time of writing, comparisons or validations were not yet investigated. This chapter focused on analyzing the applicability of the energy and size reduction Database-Calibrated models for iron ore applications through Serra Azul's case study.

6.1 Preliminary Observations

As shown in Table 6-1**,** some of the HPGR test variables used by Davaanyam (2015) in the development of the Database-Calibrated models were considerably different from the ones from Serra Azul's open circuit case study (*). Although the pressing force and net specific energy were in similar ranges, the feed samples from the Serra Azul database were significantly finer. Moreover, Serra Azul's database covered tests with moisture levels up to 9%, while the maximum moisture level in Davaanyam's database was 3.3%.

The second observation was regarding the product size distribution from both databases and their respective normalized PSD curves. Since the database methodology assumes that the normalized product size distribution from the HPGR and piston-press tests match, before making use of the size reduction regression model (Equation 2.13), it is critical to make sure the feed particle size characteristics from a given ore are similar to the ones used to obtain the regression model. Wang et al. (2019) compared the normalized PSDs of the products from Serra Azul database to a master normalized curve which was generated after fitting Lim's model (Equation 2.5) to the entire product PSD database from UBC's tests (Figure 6-1) and noted the evident difference between both. The normalized iron ore curve showed a broader size distribution in the coarse fraction and higher content of fines in comparison with the entire database, which includes the results from more than 200 pilot tests.

Table 6-1: Summary of HPGR test variables applied in the Database-Calibrated models

Variables:	Unit:	Mean:		Std. Dev.		Min:		Max:	
F_{SP}	[N/mm^2]	3.47	**3.52***	1.02	**0.86***	1.47	**2.26***	5.00	**4.64***
E_{SP}	[kWh/t]	1.82	**1.63***	0.48	**0.37***	0.73	**1.0***	2.61	**2.17***
Moisture	[%]	2.38	**5.49***	0.55	**2.10***	1.48	**2.64***	3.30	**8.87***
ρ_{bulk}	[g/cc]	1.84	**2.19***	0.22	**0.14***	1.55	**2.04***	2.20	**2.51***
F_{80}	[mm]	21.95	**11.72***	2.93	**0.31***	16.68	**11.21***	27.44	**12.25***
F_{50}	[mm]	13.87	**4.56***	3.81	**0.12***	5.20	**4.40***	20.21	**4.73***

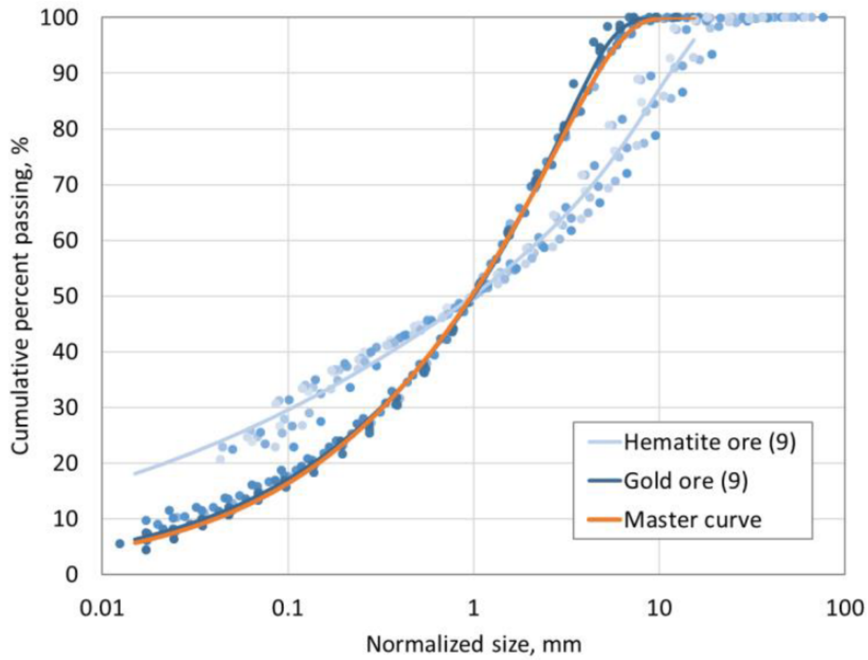

Figure 6-1: Normalized product PSD's from Serra Azul's database and UBC 's database

(Source: Wang et al., 2019)

6.2 Multi-linear Regression Models Applicability to Iron Ore

The analysis was divided into two, the first one concerning the accuracy of the specific energy consumption prediction and the second one regarding the size reduction prediction and product PSD scale-up.

6.2.1 Predicting the Net Specific Energy Consumption

To evaluate the E_{SP} prediction accuracy, piston-press tests were conducted at the same test conditions as the open circuit pilot HPGR tests that targeted 2.5 N/mm^2 F_{SP} (refer to tests SA004-006 in Table 3-3).

Equation 2.12 was used to calculate the equivalent P_{piston} that should result in the same net specific energy consumption as the HPGR tests:

$$\mathbf{P_{piston}} = 5.53 + 53.3\mathbf{F_{SP}} + 24.3\boldsymbol{w} - 86.2\boldsymbol{\rho_{bulk}} + 13.1\boldsymbol{F_{50}^{HPGR}} - 44.4\,\mathbf{F_{50}^{HPGR}}/\mathbf{F_{50}^{Piston}} + 2.98\mathbf{P_{1mm}^{Piston}} \quad \text{(2.12 revisited)}$$

Table 6-2 presents the feed parameters and test results at the calculated P_{piston}.

Table 6-2: Piston-press tests input variables and test results

F_{SP}	Measured E_{SP}	Target w	F_{50} HPGR	F_{50} Piston	P_{1mm}^{Piston}	Measured P_{piston}	Predicted E_{SP}	Error
[N/mm^2]	[kWh/t]	[%]	[mm]	[mm]	[%]	[MPa]	[kWh/t]	[%]
2.26	1.08	3	4.72	2.89	38.38	727	0.57	47.22
2.6	1.20	6	4.58	2.95	37.80	1197	1.05	12.32
2.6	1.20	9	4.48	3.32	36.63	1384	1.23	2.45

Despite the previously mentioned particularities in the iron feed characteristics, except for the test conducted at 3% moisture, the energy predictions were satisfactory and within the ±25% accuracy. At 6% and 9% moisture, the piston-press predicted energies were 12.32% lower and 2.45% higher than the HPGR test results, respectively. Since moisture content was the main difference in all tests, it is evident that its value greatly influenced the calculated P_{piston} and, consequently, the predicted E_{SP}.

Davaanyam's regression model for predicting the equivalent P_{piston} and assessing the required net specific energy consumption for a given F_{SP} through piston-press tests proved to be suitable for Serra Azul's iron ore when intermediate to high (6-9%) moisture levels were considered in the test conditions.

6.2.2 Predicting the Size Reduction and Product PSD

Equation 2.13 was applied to predict the reduction ratio achieved in the HPGR based on the piston-press test results. Next, the normalized product PSD curves from the piston tests were used to predict the HPGR product PSD.

$$\mathbf{RR_{HPGR}} = 1.86 + 1.41\mathbf{RR_{piston}} + 2.31\,\mathbf{F_{50}^{HPGR}}/\mathbf{F_{50}^{Piston}} - 0.41\mathbf{F_{50}^{HPGR}} - 1.02\boldsymbol{w} \qquad \text{(2.13 revisited)}$$

Table 6-3 summarizes the predicted reduction ratio and the measured RR_{50} from the pilot tests and Figure 6-2 compares the predicted and measured HPGR product PSDs of the pilot tests conducted at 3% and 6% moisture.

Table 6-3: Comparison between measured and predicted RR_{HPGR}

F_{SP}	Target w	Measured HPGR P_{50}	Measured RR_{50}	Predicted HPGR P_{50}	Predicted Reduction Ratio	Error
[N/mm^2]	[%]	[mm]	[mm]	[mm]	[mm]	[%]
2.26	3	1.01	4.69	1.07	4.40	6.18
2.6	6	0.89	5.14	1.98	2.32	54.86
2.6	9	1.04	4.30	-3.09	-1.45	N/A

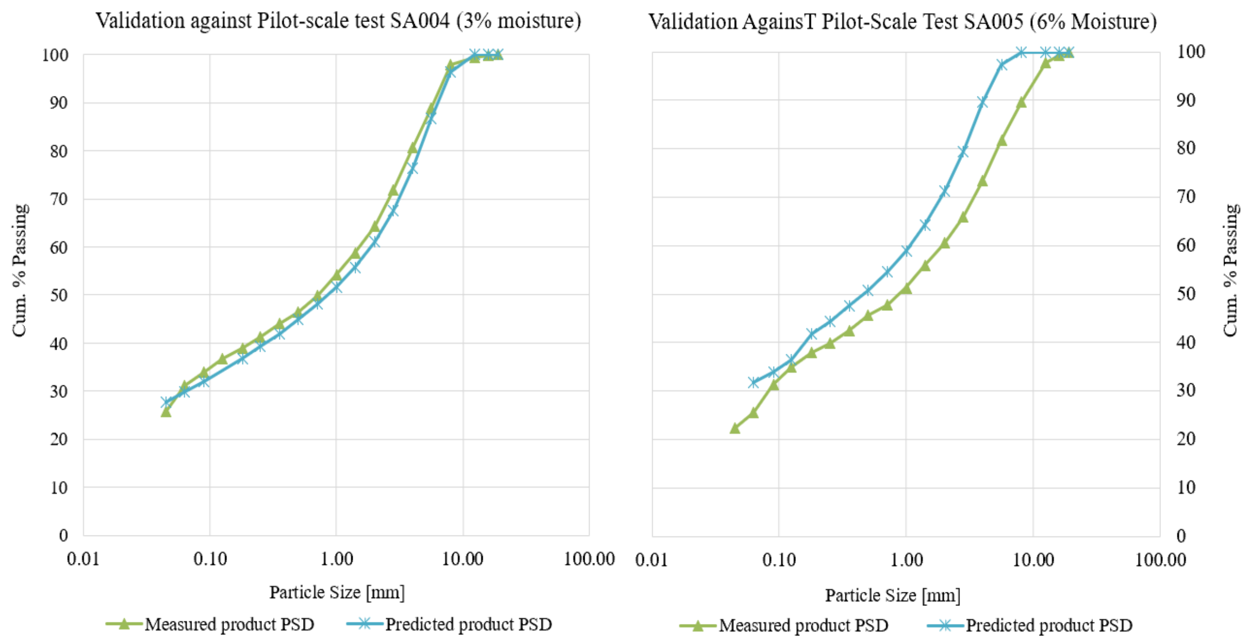

Figure 6-2: Comparison between the measured and predicted HPGR product PSDs

The only comparison that showed positive results was the one at 3% moisture, where the predicted reduction ratio was similar to the one achieved in the pilot test.

The comparisons against the pilot tests conducted at 6% and 9% moisture were not within the ±25% envelope. For these scenarios, it was not possible to predict the HPGR product PSD since the empirical model for estimating the HPGR reduction ratio resulted in negative values.

6.3 Summary

Comparisons between UBC's HPGR pilot testing database and Serra Azul's database revealed that although the pressing force and net specific energy were in similar ranges, the feed samples from Serra Azul's database were significantly finer. In addition, Serra Azul's database included tests with moisture levels up to 9%, while the maximum moisture level in Davaanyam's database was 3.3%.

Results obtained from the analysis showed that Davaanyam's regression model for predicting the equivalent P_{piston} and assessing the required net specific energy consumption for a given F_{SP} through piston-press tests proved to be suitable for Serra Azul's iron ore when intermediate to high (6-9%) moisture levels were considered in the test conditions. Except for the test conducted at 3% moisture, the E_{SP} predictions were within the proposed ±25% envelope.

Overall, the analysis showed that the multi-linear regression models proposed by Davaanyam (2015) resulted in reasonable predictions regarding the net specific energy and poor predictions in terms of the HPGR product PSD. It was also found that the normalized product PSD of Serra Azul's iron ore was considerably different from UBC's database used for calibrating the models. The current database-calibrated regression models were not adequate because the variable levels such as high moisture levels and high pressing forces extend beyond the ones used by Davaanyam (2015) for developing the current database-calibrated models. The results indicate that the database needs to be extended to cover wider ranges of feed sizes, moisture level and ore types.

Chapter 7

Conclusions and Recommendations

7.1 Main Research Findings

This thesis focused on the study of fine crushing of iron ores with the HPGR and the ability to predict its performance in terms of energy consumption and size reduction through piston-press tests. The primary objectives were to evaluate the HPGR performance for comminuting iron ore in a two-stage HPGR circuit, and to extend and validate the applicability of Davaanyam's Direct Calibration and Database-Calibrated methodologies for predicting the energy consumption and size reduction of HPGRs with low sample requirements. To achieve these objectives, literature was reviewed to identify the key operating variables of the HPGR and investigate how the specific pressing force and moisture affect the machine performance. It was also important to fully understand Davaanyam's (2015) methodologies to evaluate its application to iron ore. The assessment of the HPGR performance and modelling evaluation for quaternary and quinary applications was supported by a combination of laboratory-scale testing, pilot-scale testing and modelling work. The conclusions of this research can be summarized as follows:

- Results obtained from the open circuit pilot test work showed that the HPGR performed exceptionally well as a quaternary crusher for Serra Azul's iron ore case study. For this application, the HPGR achieved an average specific throughput constant of 340 ts/hm^3.
- The pilot test work showed that the net specific energy consumption and size reduction increased linearly with the specific pressing force. An increase of up to 10% in the amount

of particles below the target cut size of 1 mm was observed between the pilot tests that targeted F_{SP}'s of 2.5 N/mm^2 and 4.5 N/mm^2.

- The work has also evaluated the effect of moisture on the HPGR performance, and the results revealed that it did not significantly impact the HPGR energy consumption. In contrast, results indicated that operating the HPGR at high moisture can lead to significantly lower throughput and smaller operating gap. For Serra Azul's case study, at 6% moisture and 4.5 N/mm^2, the HPGR achieved an m-dot of 344 ts/hm^3 compared to 288 ts/hm^3 at the same pressing force and 9% moisture.
- For the quinary closed circuit application, the pilot test results followed the linear relationship between the specific pressing force and net specific energy consumption observed in the quaternary open circuit tests. It was found that increasing the F_{SP} from 4.0 N/mm^2 to 5.0 N/mm^2 increased the E_{SP} by 51%, which indicates that running the HPGR at 5 N/mm^2 and high moisture is detrimental to the HPGR performance.
- The analysis of the two-stage HPGR circuit performance indicated that the HPGR is suitable for both the open circuit quaternary and closed circuit quinary applications. At target pressing force of 4 N/mm^2 in both stages, the circuit achieved a product P_{80} of 0.38 mm and nearly doubled the amount of material below the target grind size of 1 mm, which increased from approximately 30% to 60%.
- The work has proven that the Direct Calibration methodology can be applied to iron ore. The methodology was validated for three scenarios through Serra Azul's case study. For all scenarios, the predicted net specific energy consumption and size reduction lies within a ±10% envelope, which is the expected accuracy of the methodology. The proposed

models can be applied to further evaluate the machine performance at different test conditions.

- The work has demonstrated that the Direct Calibration methodology may not be adequate for predicting the product PSD of HPGRs through geometallurgical samples that have different feed size characteristics than the samples used to calibrate the energy and size reduction regression models.
- The work has demonstrated that the multi-linear regression models proposed by Davaanyam (2015) are not applicable to Serra Azul's iron ore. Comparisons against the UBC's HPGR pilot testing database revealed that the normalized product PSD from the iron ore database is different than other ore types used to develop the Database-Calibrated regression models. The results indicate that the database needs to be extended to cover wider ranges of feed sizes, moisture level and ore types.

7.2 Future Research Opportunities

Some future opportunities are proposed as follows:

- Comparison between the two-stage HPGR circuit performance against conventional AG-SAG mill circuits. Although this research showed promising results for Serra Azul's circuit, it would be of great value to conduct trade-offs against other circuit options to compare their performance in terms of energy consumption and size reduction.
- Further pilot testing is recommended to evaluate if truncating the feed to the open circuit quaternary stage would benefit the circuit's energy consumption and size reduction. It was noted that the feed to the quaternary stage has nearly 30% of material below the target cut size of 1mm.

- Developing ore-specific Database-Calibrated models would result in more accurate energy-size predictions. The UBC's HPGR pilot testing database now has more than 220 pilot tests conducted over several ore types. The Database-Calibrated models could be constantly updated to optimize its models, and ore-specific models could be developed for ores that have sufficient data available.
- Investigating if using a larger diameter for the piston-die apparatus can reduce the errors associated with the difference in the normalized product PSD's of piston and HPGRs.

REFERENCES

Abazarpoor, A., & Halali, M. (2017). Investigation on the particle size and shape of iron ore pellet feed using ball mill and HPGR grinding methods. *Physicochem Probl Miner Process*, *53*(2), 908–919.

Abazarpoor, A., Halali, M., Hejazi, R., & Saghaeian, M. (2018). HPGR effect on the particle size and shape of iron ore pellet feed using response surface methodology. *Mineral Processing and Extractive Metallurgy*, *127*(1), 40–48.

Adams, M. D. (2016). *Gold Ore Processing: Project Development and Operations*. Elsevier Science.

Anguelov, R., Ghaffari, H., & Alexander, J. (2008). High pressure grinding rolls (HPGR) an alternative technology versus SAG milling. *Comminution 2008 Conference*.

Aydoğan, N. A., Ergün, L., & Benzer, H. (2006). High pressure grinding rolls (HPGR) applications in the cement industry. *Minerals Engineering*, *19*(2), 130–139.

Barani, K., & Balochi, H. (2016). Comparative study on the effect of using conventional and high pressure grinding rolls crushing on the ball mill grinding kinetics of an iron ore. *Physicochemical Problems of Mineral Processing*, *52*.

Barrios, G. K. P., & Tavares, L. M. (2016). A preliminary model of high pressure roll grinding using the discrete element method and multi-body dynamics coupling. *International Journal of Mineral Processing*, *156*, 32–42.

Bearman, R. (2006). High-pressure grinding rolls: characterizing and defining process performance for engineers. *Advances in Comminution*, *1*, 3–14.

Bulled, D., & Husain, K. (2008). The development of a small-scale test to determine work index for high pressure grinding rolls. *Proceedings 40th Annual Meeting of the Canadian Mineral*

Processors, 145–164.

Burchardt, E., & Kessler, M. (2015). High pressure grinding rolls —A promising and cost-effective technology of ore pretreatment in mineral processing. *Technology and Technics of Ore Preparation Processes, ThyssenKrupp Resource Technology*, 131–16.

Burchardt, E., Patzelt, N., Knecht, J., & Klymowsky, R. (2011). HPGR's in Minerals: What do Existing Operations Tell us for the Future. *Autogenous and Semi-Autogenous Grinding Technology Conference, Vancouver*.

Casteel, K. (2005). High-pressure grinding - playing a wider role. *Mining & Quarry World*, *3*(09), 12–17.

Casteel, K. (2006). HPGR: Making its case for commercialization. *Engineering and Mining Journal*, *207*(1), 60.

Daniel, M., & Bailey, C. . (2009). Uses and benefits of laboratory-scale HPGR tests. *Procemin 2009*, 147–156.

Daniel, M. J. (2003). Particle Bed Compression Comminution using a Piston-die to Predict the Performance of a HPGR. *JKMRC Conference, Brisbane*, 67–83.

Davaanyam, Z. (2015). *Piston press test procedures for predicting energy-size reduction of high pressure grinding rolls*. University of British Columbia.

DOE, U. S. (2007). Mining industry energy bandwidth study. *Washington: US Department of Energy*.

Drozdiak, J. A. (2011). *A pilot-scale examination of a novel high pressure grinding roll/stirred mill comminution circuit for hard-rock mining applications*. University of British Columbia.

Dunne, R., Maxton, D., Morrell, S., & Lane, G. (2004). HPGR—The Australian Experience. *Improving and Optimizing Operations: Things That Actually Work! Plant Operators' Forum*

2004.

Fuerstenau, D. W., & Abouzeid, A. (2007). Role of feed moisture in high-pressure roll mill comminution. *International Journal of Mineral Processing*, *82*(4), 203–210.

Fuerstenau, D. W., Shukla, A., & Kapur, P. C. (1991). Energy consumption and product size distributions in choke-fed, high-compression roll mills. *International Journal of Mineral Processing*, *32*(1–2), 59–79.

Gunter, H., Muller, M., & Sonntag, P. (1996). The Application of Roller Presses for High Pressure Comminution. *Symposium on Grinding Processes*, 14–15.

Hawkins, R. A. (2007). *A piston and die test to predict laboratory-scale HPGR performance*.

Jankovic, A. (2015). Developments in iron ore comminution and classification technologies. In L. Lu (Ed.), *Iron Ore – Mineralogy, Processing and Environmental Sustainability* (pp. 251–282). Elsevier.

Jankovic, A., & Valery, W. (2010). Reducing Grinding Energy and Cost-Magnetite Iron Ore Design Case Study. *Proceedings, XIIth International Mineral Processing Symposium 6-8 October 2010, Cappadocia, Turkey*, *78*.

Kalala, J. T., Dong, H., & Hinde, A. L. (2006). *Using piston-die press to predict the breakage behavior of HPGR"*.

KHD. (2018). *High Pressure Grinding Rolls. Providing KHD High Pressure Grinding Rolls technology and Weir Minerals Service to the mining mill circuit worldwide*.

Klymowsky, R., Patzelt, N., Knecht, J., & Burchardt, E. (2002). Selection and sizing of high pressure grinding rolls. *Mineral Processing Plant Design, Practice and Control Proceedings*, *1*, 636–668.

Knapp, H., Hannot, S., & van der Meer, F. (2019). HPGR : Why skewing is a requirement for operational applications. *International Semi-Autogenous Grinding and High Pressure Grinding Roll Technology 2019*.

Knecht, J. (2004). High pressure grinding rolls – Adding value to the platinum industry. *October 3-7*.

Köppern. (2018). *High Pressure-Grinding brochure Ore Grinding*.

Kumar, A. (2014). *Predicting HPGR performance and understanding rock particle behavior through DEM modelling*. University of British Columbia.

Lim, I. L., Voigt, W., & Weller, K. R. (1996). Product size distribution and energy expenditure in grinding minerals and ores in high pressure rolls. *International Journal of Mineral Processing*, *44*, 539–559.

Lim, W. I. L., & Weller, K. R. (1997). *Modelling of throughput in high pressure grinding rolls*.

Lynch, A. J., & Rowland, C. A. (2005). The History of Grinding, Society of Mining, Metallurgy and Exploration. *Inc.(SME), Littleton*.

Makni, S., Lapointe, R., Croteau, C., & Sato, D. (2019). Selection of HPGR Technology for the Côté Gold Project: Evaluation of the Impact on Cost and Metallurgy. *SAG Conference, 2019*.

McClintock, M. (2018). *Validation of methodologies for sizing a high pressure grinding roll*. University of British Columbia.

Morley, C. (2003). HPGR in hard rock applications. *Mining Magazine*, *189*(3), 118–127.

Morley, C. (2006). High pressure grinding rolls: a technology review. *3rd International Symposium Advances in Comminution, Society for Mining, Metallurgy and Exploration (SME)*.

Morley, C. (2010). Hpgr-Faq. *Journal of the Southern African Institute of Mining and Metallurgy*, *110*(3), 107–115.

Morley, C., & Staples, P. (2010). SAG or HPGR?—The current dilemma. *Proceedings of the 42nd Annual Meeting of the Canadian Mineral Processors*, *1101*, 491–508.

Nadolski, S. (2012). *Development of a laboratory scale procedure for predicting throughput of high pressure grinding rolls*. University of British Columbia.

Neumann, E. W. (2006). Some Basics in High Pressure Grinding Rolls. *Advances in Comminution. Society of Mining and Petroleum Engineers (SME), Littelton, Colorado*, 41.

Qiu, X., Vien, A., Mular, M., Alkac, D., & Pate, B. (2019). LINKING THE PACKED BED TEST TO FULL SIZE HRC™ PERFORMANCE. *SAG Conference, 2019*.

Rashidi, S., Rajamani, R. K., & Fuerstenau, D. W. (2017). A Review of the Modeling of High Pressure Grinding Rolls. *KONA Powder and Particle Journal*, *34*, 125–140.

Rosario, P., Hall, R., Grundy, M., & Klein, B. (2011). A preliminary investigation into the feasibility of a novel HPGR-based circuit for hard, weathered ores containing clayish material. *Minerals Engineering*, *24*(3–4), 290–302.

Rosario, P. P. (2010). *Comminution circuit design and simulation for the development of a novel high pressure grinding roll circuit*. University of British Columbia.

Saramak, D. (2011). The influence of chosen ore properties on efficiency of HPGR-based grinding circuits. *Gospodarka Surowcami Mineralnymi*, *27*, 33–44.

Saramak, D., & Kleiv, R. A. (2013). The effect of feed moisture on the comminution efficiency of HPGR circuits. *Minerals Engineering*, *43*, 105–111.

Schneider, C. L., Alves, V. K., & Austin, L. G. (2009). Modeling the contribution of specific grinding pressure for the calculation of HPGR product size distribution. *Minerals Engineering*, *22*(7–8), 642–649.

Schönert, K. (1988). A first survey of grinding with high-compression roller mills. *International*

Journal of Mineral Processing, *22*(1–4), 401–412.

Schönert, K. (1995). *Comminution from theory to practice*.

Schönert, K., & Lubjhun, U. (1990). Throughput of high compression roller mills with plane and corrugated rollers. *Proceedings of 7th European Symposium on Comminution*, 213–217.

Senchenko, A., & Kulikov, Y. V. (2016). Special aspects of circuits design with the use of HPGR technology based on pilot testing data and industrial operating experience. *IMPC 2016: XXVIII International Mineral Processing Congress Proceedings*.

Shu, L., & Yongqing, W. (2008). Application of RP 3.6-120/50 Roll Press in Chengchao's Pelletizing Production. *Metal Mine*, 263–268.

van der Ende, R., Knapp, H., & van der Meer, F. (2019). Reducing edge effect and material bypass using spring-loaded cheek plates in HPGR grinding. *International Semi-Autogenous Grinding and High Pressure Grinding Roll Technology 2019*.

van der Meer, F. P. (2015). Pellet feed grinding by HPGR. *Minerals Engineering*, *73*, 21–30.

van der Meer, F. P., & Gruendken, A. (2010). Flowsheet considerations for optimal use of high pressure grinding rolls. *Minerals Engineering*, *23*(9), 663–669.

van der Meer, F. P., Lessing, E., & Matthies, E. (2015). Iron Ore Final Grinding by HPGR and Air Classification. *Iron Ore Conference*, *July*, 197–203.

van der Meer, F. P., & Maphosa, W. (2012). High pressure grinding moving ahead in copper, iron, and gold processing. *Journal of the Southern African Institute of Mining and Metallurgy*, *112*(7), 637–647.

Vanderbeek, J. L., Linde, T. B., Brack, W. S., & Marsden, J. O. (2006). HPGR implementation at Cerro Verde. *Proceedings of the SAG Conference*, 45–61.

von Michaelis, H. (2009). How energy efficient is HPGR? *World Gold Conference. Cape Town,* *South African: Southern African Institute of Mining and Metallurgy (SAIMM) in Conjunction with the Canadian Institute of Mining, Metallurgy and Petroleum (CIM), and the Australasian Institute of Mining and Metallurgy (Aus*, 7–15.

Wang, C. (2013). *Comparison of HPGR-ball mill and HPGR-stirred mill circuits to the existing AG/SAG mill-ball mill circuits*. University of British Columbia.

Wang, C., Nadolski, S., Mejia, O., Drozdiak, J., & Klein, B. (2013). Energy and Cost Comparisons of HPGR-based Circuits. *Engineering and Mining Journal*, *214*(12), 102.

Wang, F., & Klein, B. (2019). A review of 10 years of HPGR pilot tests at the UBC. *International Semi-Autogenous Grinding and High Pressure Grinding Roll Technology 2019*.

Wüstner, H. (1986). Energy saving with the roller press comminution process. *World Cement*, *17*(3), 94–96.

Appendices

Appendix A: HPGR Test Work Data

Table A.7-1: Summary of Open Circuit pilot-scale HPGR tests at different moisture levels

Data	Description	Symbol	Unit	SA001	SA002	SA003	SA004	SA005	SA006	SA007	SA008	SA009
Press Constants	Roller Diameter (D)	[m]	0.750									
	Roller Width (W)	[m]	0.220									
Data	Description	Test Number:		SA001	SA002	SA003	SA004	SA005	SA006	SA007	SA008	SA009
		Symbol	Unit	Moisture Tests			Moisture Test			Moisture Test		
Process Set Points	Speed	n	[m/s]	0.55	0.55	0.55	0.55	0.55	0.55	0.55	0.55	0.55
		n	[rpm]	14.04	14.04	14.04	14.04	14.04	14.04	14.04	14.04	14.04
	Static Gap	X_0	[mm]	9.0	9.0	9.0	9.0	9.0	9.0	9.0	9.0	9.0
	Hydraulic Pressure	P	[bar]	71.8	71.8	71.8	51.3	51.3	51.3	92.3	92.3	92.3
	Pressing Force	F	[kN]	577.5	577.5	577.5	412.5	412.5	412.5	742.5	742.5	742.5
	Specific Pressing Force	F_{SP}	[N/mm^2]	**3.5**	**3.5**	**3.5**	**2.5**	**2.5**	**2.5**	**4.5**	**4.5**	**4.5**
Process Data	**Test Time**	t	[s]	16.24	18.97	15.45	18.08	15.91	16.95	15.46	15.77	14.84
	Average Actual Speed:	w_{AV}	[m/s]	0.56	0.56	0.56	0.56	0.56	0.56	0.56	0.56	0.56
	Standard Deviation	s_w		0.19	0.25	0.19	0.21	0.15	0.18	0.17	0.22	0.21
	Actual Roller gap (average)	X_{gAV}	[mm]	**23.62**	**23.09**	**19.28**	**24.33**	**23.72**	**23.43**	**22.66**	**22.26**	**17.38**
	Standard Deviation	s_X		0.26	0.29	0.93	0.35	0.51	1.08	0.43	0.34	0.68
	Actual Hydraulic Pressure (average)	P_{AV}	[bar]	**66.1**	**73.7**	**74.1**	**46.3**	**53.7**	**53.3**	**93.2**	**94.9**	**93.1**
	Standard Deviation			2.61	0.78	1.71	1.03	2.12	1.49	3.01	2.68	0.57
	Actual Pressing Force (average)	F_{AV}	[kN]	532	593	596	372	432	429	750	763	749
	Actual Specific Pressure (average)	F_{SPAV}	[N/mm^2]	**3.23**	**3.60**	**3.62**	**2.26**	**2.62**	**2.61**	**4.56**	**4.64**	**4.55**
	Idle Power Draw	Pi	[kW]	5.69	5.75	5.83	5.68	5.79	5.72	5.64	5.83	6.50
	Power Draw	P	[kW]	55.16	60.78	55.13	40.73	45.62	45.82	68.27	74.14	57.57
	Total Specific Energy Consumption	E_{SP}	[kWh/t]	1.75	1.90	1.99	1.26	1.37	1.37	2.20	2.35	2.17
	Net Specific Energy Consumption	$E_{SP\ net}$	[kWh/t]	**1.57**	**1.72**	**1.78**	**1.08**	**1.20**	**1.20**	**2.02**	**2.17**	**1.92**
	Press throughput	W	[t/h]	31.56	31.93	27.76	32.39	33.24	33.37	31.03	31.53	26.55
	Specific Throughput Constant	m dot	[ts/hm^3]	**345**	**347**	**301**	**352**	**361**	**365**	**337**	**344**	**288**
Material Data	**Average Flake Density**	r_F	[t/m^3]	**2.68**	**2.66**	**2.66**	**2.62**	**2.59**	**2.67**	**2.69**	**2.65**	**2.62**
	Standard Deviation			0.07	0.05	0.10	0.06	0.06	0.06	0.09	0.07	0.06
	Flake Thickness Average	X_F	[mm]	**24.5**	**26.8**	**22.6**	**25.5**	**27.9**	**26.9**	**25.1**	**26.0**	**21.1**
	Standard Deviation			2.3	2.1	2.0	1.4	1.9	1.5	1.6	1.2	1.5
	Feed Moisture (target)		[%]	**3.00**	**6.00**	**9.00**	**3.00**	**6.00**	**9.00**	**3.00**	**6.00**	**9.00**
	Feed Moisture (actual)		[%]	**2.67**	**5.49**	**7.36**	**2.64**	**5.63**	**7.45**	**3.36**	**5.90**	**8.87**
	Feed Bulk Density (loose)		[t/m^3]	2.19	2.21	2.33	2.04	2.10	2.14	2.06	2.17	2.51
	Feed Bulk Density (packed)		[t/m^3]									
	Particle Size Distribution			PSD001	PSD002	PSD003	PSD004	PSD005	PSD006	PSD007	PSD008	PSD009
	Feed: 100% Passing Size		[mm]	25.00	25.00	25.00	25.00	25.00	25.00	25.00	25.00	25.00
	Feed: 80% Passing Size	F_{80}	[mm]	11.81	11.99	11.43	12.25	11.87	11.54	11.21	11.48	11.94
	Feed: 50% Passing Size	F_{50}	[mm]	**4.60**	**4.40**	**4.65**	**4.72**	**4.58**	**4.48**	**4.44**	**4.45**	**4.73**
	Centre: 80% Passing Size	P_{80}	[mm]	4.06	3.70	4.46	4.85	4.72	5.09	3.70	3.63	4.20
	Centre: 50% Passing Size	P_{50}	[mm]	**0.43**	**0.39**	**0.62**	**0.79**	**0.69**	**0.91**	**0.35**	**0.33**	**0.46**
	Edge: 80% Passing Size	P_{80}	[mm]	7.87	7.43	5.64	8.22	7.54	7.49	7.08	6.50	6.65
	Edge: 50% Passing Size	P_{50}	[mm]	2.21	1.95	0.94	2.50	1.99	1.89	1.81	1.32	1.55
	Full 80% Passing Size	P_{80}	[mm]	4.98	4.69	4.72	5.49	5.28	5.50	4.50	4.25	4.54
	Full 50% Passing Size	P_{50}	[mm]	**0.66**	**0.60**	**0.70**	**1.01**	**0.89**	**1.04**	**0.48**	**0.42**	**0.53**
	Combined 90% Center & 10% Edge: 80% Passing Size	P_{80}	[mm]	4.44	4.04	4.58	5.14	4.98	5.28	4.01	3.90	4.44
	Combined 90% Center & 10% Edge: 50% Passing Size	P_{50}	[mm]	**0.50**	**0.45**	**0.66**	**0.89**	**0.78**	**0.97**	**0.40**	**0.37**	**0.50**
	Reduction Ratio F80/P80 full			2.37	2.56	2.42	2.23	2.25	2.10	2.49	2.70	2.63
	Reduction Ratio F50/P50 full			**6.96**	**7.36**	**6.65**	**4.69**	**5.14**	**4.30**	**9.18**	**10.65**	**8.97**
	Reduction Ratio F80/P80 (90% C & 10% E Product)			2.66	2.97	2.50	2.39	2.38	2.19	2.80	2.94	2.69
	Reduction Ratio F50/P50 (90% C & 10% E Product)			**9.26**	**9.79**	**7.07**	**5.33**	**5.88**	**4.61**	**11.06**	**12.14**	**9.54**
	Percentage Passing 1 mm (Combined)			**54.22**	**54.74**	**53.70**	**49.92**	**51.30**	**49.54**	**56.69**	**58.68**	**55.76**
	Percentage Passing 1 mm (90% C & 10% E)		[%]	**56.88**	**57.36**	**54.16**	**51.40**	**52.72**	**50.31**	**59.18**	**60.28**	**56.26**
	Percentage Passing 0.045 mm (Combined)		[%]	**24.75**	**23.40**	**23.81**	**22.83**	**22.41**	**20.73**	**25.44**	**22.82**	**22.89**
	Mass Balance											
	Total Feed Material	M_F	[kg]	234	234	234	220	256	252	251	245	249
	Total Centre Product	M_C	[kg]	99.6	91.5	82.3	98.9	104.2	101.1	87.8	95.2	71.1
	Centre Product % of Centre & Edge Material	MCE%	[%]	74.9%	73.3%	77.9%	77.8%	78.0%	78.6%	75.9%	78.2%	85.9%
	Total Edge Product	M_E	[kg]	33.4	33.3	23.3	28.3	29.4	27.5	27.9	26.6	11.7
	Edge Product % of Centre & Edge Material	$M_{EF\%}$	[%]	25.1%	26.7%	22.1%	22.2%	22.0%	21.4%	24.1%	21.8%	14.1%
	Edge Product % of Centre Product	$M_{EC\%}$	[%]	33.5%	36.4%	28.3%	28.6%	28.2%	27.2%	31.8%	27.9%	16.5%
	Total Waste Product	M_W	[kg]	93.5	103.3	119.8	85.2	117.7	119.9	128.3	119.5	140.0
	Waste Product % of Total Feed	$M_{WF\%}$	[%]	40.0%	44.2%	51.2%	38.8%	46.1%	47.6%	51.2%	48.8%	56.2%
	Total Recovered Product	M_P	[kg]	226.5	228	225	212	251	249	244	241	223
	Mass Reconciliation (+ "gain; - "loss")	$M_{PF\%}$	[%]	-3.2%	-2.3%	-3.7%	-3.2%	-1.6%	-1.4%	-2.6%	-1.6%	-10.5%

Test No.		Feed		Centre Product		Edge Product		Experimental Full PSD	Scaled HPGR Product
SA001									90% Center + 10% Edge
Screen Size	Particle Size, mm	Retained (g)	Cum % Pass	Retained (g)	Cum % Pass	Retained (g)	Cum % Pass	Cum % Pass	Cum % Pass
-35.5 to +32	32.000	**0.00**	100.00	**0.00**	100.00	**0.00**	100.00	100.00	100.00
-32 to +25	25.000	**0.00**	100.00	**0.00**	100.00	**0.00**	100.00	100.00	100.00
-25 to +19	19.000	**441.20**	93.97	**0.00**	100.00	**29.30**	99.63	99.91	99.96
-19 to 16	16.000	**412.90**	88.32	**24.10**	99.81	**101.80**	98.36	99.45	99.67
-16 to +12.5	12.500	**417.60**	82.61	**84.00**	99.15	**261.40**	95.08	98.13	98.74
-12.5 to +8	8.000	**1242.80**	65.61	**583.70**	94.56	**1156.20**	80.57	91.05	93.16
-8 to +5.6	5.600	**765.50**	55.14	**878.10**	87.66	**858.80**	69.80	83.18	85.88
-5.6 to +4	4.000	**600.00**	46.93	**1015.90**	79.68	**718.10**	60.79	74.94	77.79
-4 to +2.8	2.800	**391.60**	41.58	**926.80**	72.40	**550.40**	53.89	67.75	70.55
-2.8 to +2	2.000	**285.20**	37.68	**638.60**	67.38	**419.60**	48.62	62.67	65.50
-2 to +1.4	1.400	**226.60**	34.58	**684.90**	62.00	**303.60**	44.82	57.68	60.28
-1.4 to +1	1.000	**105.70**	33.13	**427.20**	58.64	**300.80**	41.04	54.22	56.88
-1 to +.71	0.710	**154.60**	31.02	**494.60**	54.75	**196.10**	38.58	50.69	53.13
-.71 to +.5	0.500	**97.30**	29.69	**400.90**	51.60	**178.90**	36.34	47.77	50.07
-.5 to +.355	0.355	**127.90**	27.94	**439.80**	48.15	**157.50**	34.36	44.68	46.77
-.355 to +.25	0.250	**108.30**	26.45	**398.60**	45.01	**146.20**	32.53	41.88	43.76
-.25 to +.18	0.180	**103.80**	25.03	**299.40**	42.66	**135.80**	30.83	39.69	41.48
-.18 to +.125	0.125	**133.50**	23.21	**404.30**	39.48	**189.40**	28.45	36.71	38.38
-.125 to +.09	0.090	**140.70**	21.28	**446.20**	35.98	**173.50**	26.27	33.54	35.01
-.09 to +.063	0.063	**268.60**	17.61	**734.50**	30.20	**434.00**	20.83	27.85	29.27
-.063 to +.045	0.045	**60.10**	16.79	**390.00**	27.14	**255.70**	17.62	24.75	26.19
-0.045	Pan	**1227.50**		**3453.50**		**1404.80**			
Total mass		7311.40		12725.10		7971.90			
Initial wt.		**7388.20**		**12926.70**		**8000.00**			
Delta wt.		-76.80		-201.60		-28.10			
Delta %		-1.04%		-1.56%		-0.35%			
Size Distribution Interpolations									
%passing 1 mm			**33.13**		**58.64**		**41.04**	**54.22**	**56.88**
Linear P50	[mm]		**4.60**		**0.43**		**2.21**	**0.66**	**0.50**
Linear P80	[mm]		**11.81**		**4.06**		**7.87**	**4.98**	**4.44**

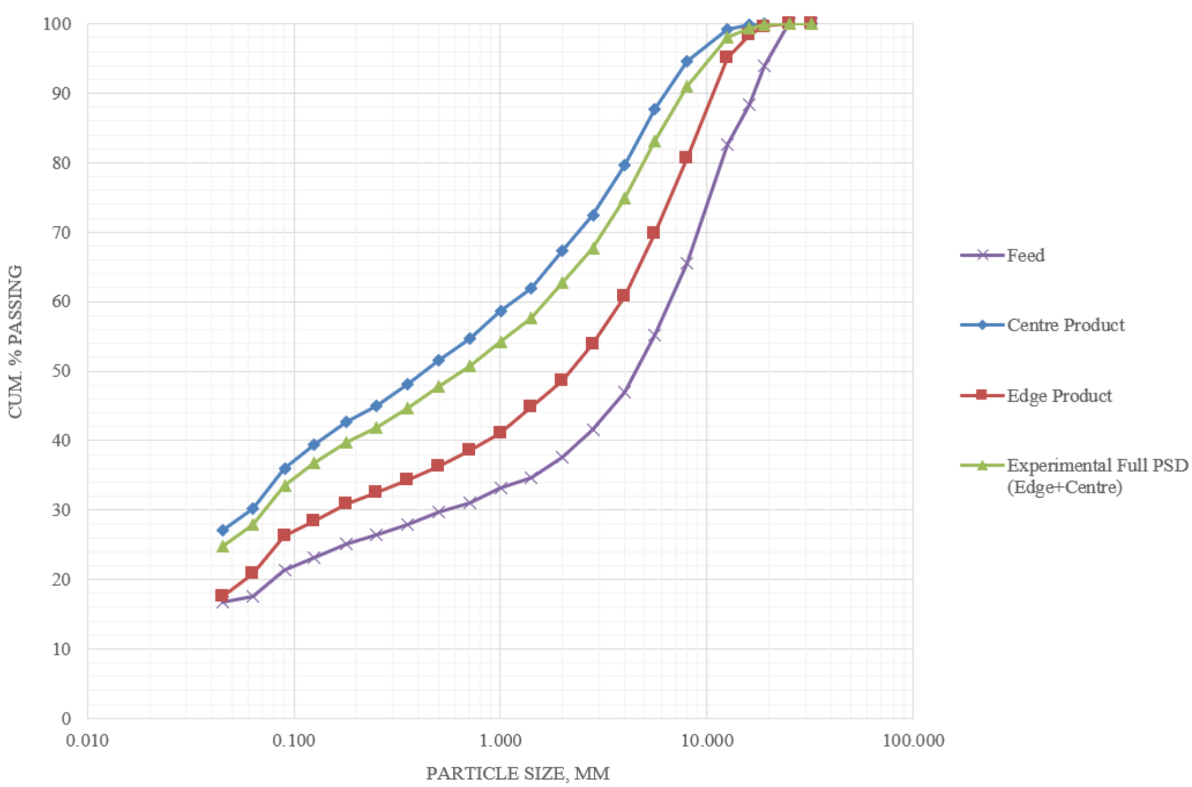

Figure A. 7-1: Feed and product PSDs of test No. SA001

Test No.		Feed		Centre Product		Edge Product		Experimental Full PSD	Scaled HPGR Product
SA002									90% Center + 10% Edge
Screen Size	Particle Size, mm	Retained (g)	Cum % Pass	Retained (g)	Cum % Pass	Retained (g)	Cum % Pass	Cum % Pass	Cum % Pass
-35.5 to +32	32.00	**0.00**	100.00	**0.00**	100.00	**0.00**	100.00	100.00	100.00
-32 to +25	25.00	**0.00**	100.00	**0.00**	100.00	**0.00**	100.00	100.00	100.00
-25 to +19	19.00	**297.70**	95.93	**0.00**	100.00	**16.20**	99.79	99.94	99.98
-19 to 16	16.00	**539.80**	88.54	**5.90**	99.95	**59.80**	99.02	99.70	99.86
-16 to +12.5	12.50	**495.40**	81.76	**99.90**	99.12	**192.30**	96.52	98.43	98.86
-12.5 to +8	8.00	**1135.80**	66.22	**545.60**	94.60	**1085.20**	82.46	91.36	93.39
-8 to +5.6	5.60	**741.90**	56.07	**657.40**	89.16	**807.40**	72.00	84.58	87.44
-5.6 to +4	4.00	**593.50**	47.95	**895.90**	81.73	**744.00**	62.36	76.56	79.79
-4 to +2.8	2.80	**430.40**	42.06	**836.30**	74.80	**528.20**	55.52	69.66	72.87
-2.8 to +2	2.00	**325.10**	37.61	**711.80**	68.90	**395.20**	50.40	63.97	67.05
-2 to +1.4	1.40	**226.40**	34.52	**615.00**	63.81	**342.30**	45.96	59.05	62.02
-1.4 to +1	1.00	**187.00**	31.96	**589.20**	58.93	**209.80**	43.24	54.74	57.36
-1 to +.71	0.71	**131.50**	30.16	**430.30**	55.36	**203.30**	40.61	51.42	53.89
-.71 to +.5	0.50	**108.80**	28.67	**342.60**	52.52	**173.70**	38.36	48.74	51.11
-.5 to +.355	0.36	**106.80**	27.21	**397.50**	49.23	**186.40**	35.94	45.68	47.90
-.355 to +.25	0.25	**104.70**	25.78	**368.50**	46.17	**160.50**	33.86	42.89	44.94
-.25 to +.18	0.18	**99.40**	24.42	**276.20**	43.89	**135.50**	32.11	40.74	42.71
-.18 to +.125	0.13	**165.80**	22.15	**441.10**	40.23	**206.80**	29.43	37.35	39.15
-.125 to +.09	0.09	**126.20**	20.42	**668.50**	34.69	**250.50**	26.18	32.42	33.84
-.09 to +.063	0.06	**314.10**	16.12	**698.20**	28.91	**457.90**	20.25	26.60	28.04
-.063 to +.045	0.05	**152.00**	14.04	**390.60**	25.67	**239.50**	17.15	23.40	24.82
-0.045	Pan	**1026.30**		**3097.90**		**1323.40**			
Total mass		7308.60		12068.40		7717.90			
Initial wt.		**7331.70**		**12212.60**		**7772.50**			
Delta wt.		-23.10		-144.20		-54.60			
Delta %		-0.32%		-1.18%		-0.70%			
Size Distribution Interpolations									
%passing 1 mm			**31.96**		**58.93**		**43.24**	**54.74**	**57.36**
Linear P50	[mm]		**4.40**		**0.39**		**1.95**	**0.60**	**0.45**
Linear P80	[mm]		**11.99**		**3.70**		**7.43**	**4.69**	**4.04**

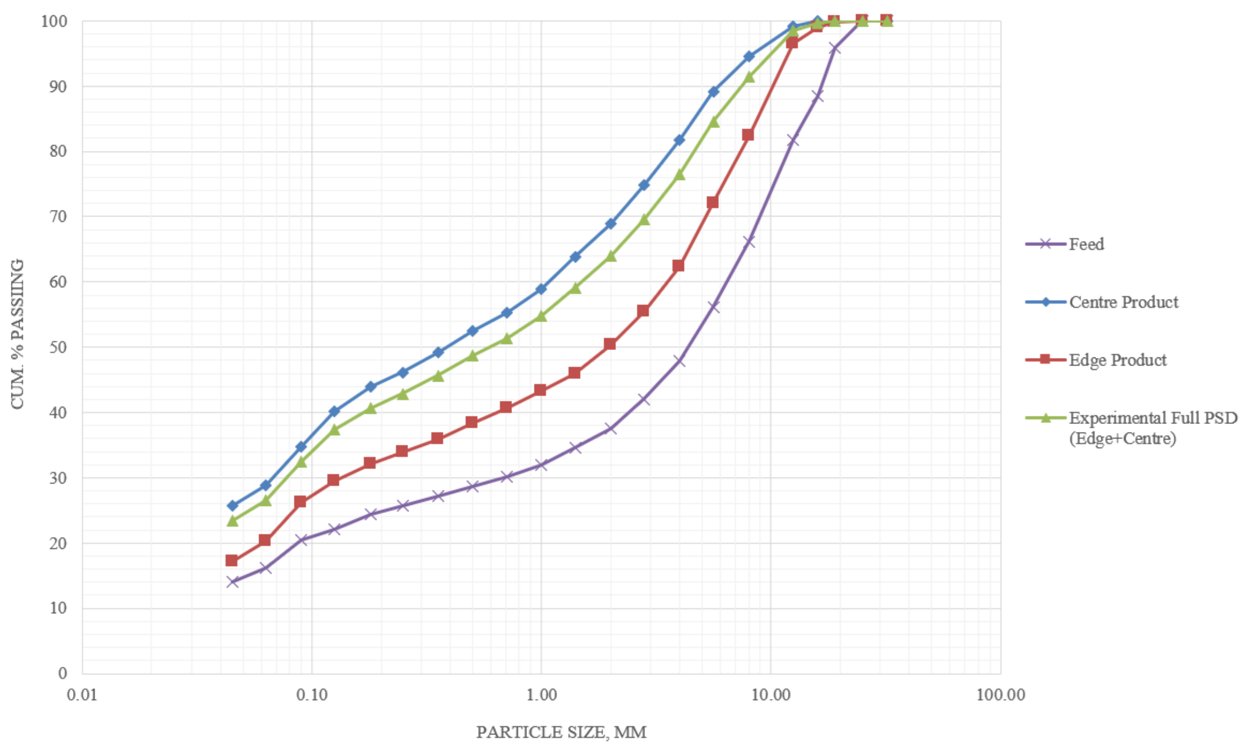

Figure A. 7-2: Feed and product PSDs of test No. SA002

Test No.		Feed		Centre Product		Edge Product		Experimental Full PSD	Scaled HPGR Product
SA003									90% Center + 10% Edge
Screen Size	Particle Size, mm	Retained (g)	Cum % Pass	Retained (g)	Cum % Pass	Retained (g)	Cum % Pass	Cum % Pass	Cum % Pass
-35.5 to +32	32.00	**0.00**	100.00	**0.00**	100.00	**0.00**	100.00	100.00	100.00
-32 to +25	25.00	**0.00**	100.00	**0.00**	100.00	**0.00**	100.00	100.00	100.00
-25 to +19	19.00	**595.30**	96.10	**0.00**	100.00	**0.00**	100.00	100.00	100.00
-19 to 16	16.00	**937.40**	89.95	**4.90**	99.95	**19.00**	99.62	99.88	99.92
-16 to +12.5	12.50	**844.70**	84.41	**26.70**	99.66	**47.00**	98.69	99.45	99.57
-12.5 to +8	8.00	**2822.10**	65.91	**557.40**	93.73	**497.40**	88.81	92.64	93.23
-8 to +5.6	5.60	**1659.80**	55.03	**711.20**	86.15	**451.20**	79.85	84.76	85.52
-5.6 to +4	4.00	**1297.20**	46.52	**809.50**	77.52	**444.80**	71.01	76.09	76.87
-4 to +2.8	2.80	**875.20**	40.79	**691.30**	70.16	**355.90**	63.94	68.79	69.54
-2.8 to +2	2.00	**630.90**	36.65	**524.70**	64.57	**273.40**	58.51	63.23	63.96
-2 to +1.4	1.40	**451.60**	33.69	**476.30**	59.50	**248.40**	53.58	58.19	58.90
-1.4 to +1	1.00	**261.80**	31.97	**465.90**	54.53	**141.30**	50.77	53.70	54.16
-1 to +.71	0.71	**292.20**	30.06	**339.50**	50.92	**178.30**	47.23	50.10	50.55
-.71 to +.5	0.50	**252.80**	28.40	**212.10**	48.66	**95.80**	45.33	47.92	48.32
-.5 to +.355	0.36	**228.10**	26.91	**287.50**	45.59	**167.10**	42.01	44.80	45.23
-.355 to +.25	0.25	**216.30**	25.49	**261.30**	42.81	**123.90**	39.54	42.09	42.48
-.25 to +.18	0.18	**209.80**	24.11	**197.60**	40.70	**104.40**	37.47	39.99	40.38
-.18 to +.125	0.13	**334.50**	21.92	**374.00**	36.72	**167.30**	34.15	36.15	36.46
-.125 to +.09	0.09	**320.80**	19.82	**297.70**	33.55	**182.00**	30.53	32.88	33.25
-.09 to +.063	0.06	**642.70**	15.60	**571.20**	27.46	**333.10**	23.92	26.68	27.11
-.063 to +.045	0.05	**413.30**	12.89	**278.20**	24.50	**128.20**	21.37	23.81	24.19
-0.045	Pan	**1966.40**		**2299.70**		**1075.80**			
Total mass		15252.90		9386.70		5034.30			
Initial wt.		**15345.80**		**9468.80**		**5078.00**			
Delta wt.		-92.90		-82.10		-43.70			
Delta %		-0.61%		-0.87%		-0.86%			
Size Distribution Interpolations									
%passing 1 mm			**31.97**		**54.53**		**50.77**	**53.70**	**54.16**
Linear P50	[mm]		**4.65**		**0.62**		**0.94**	**0.70**	**0.66**
Linear P80	[mm]		**11.43**		**4.46**		**5.64**	**4.72**	**4.58**

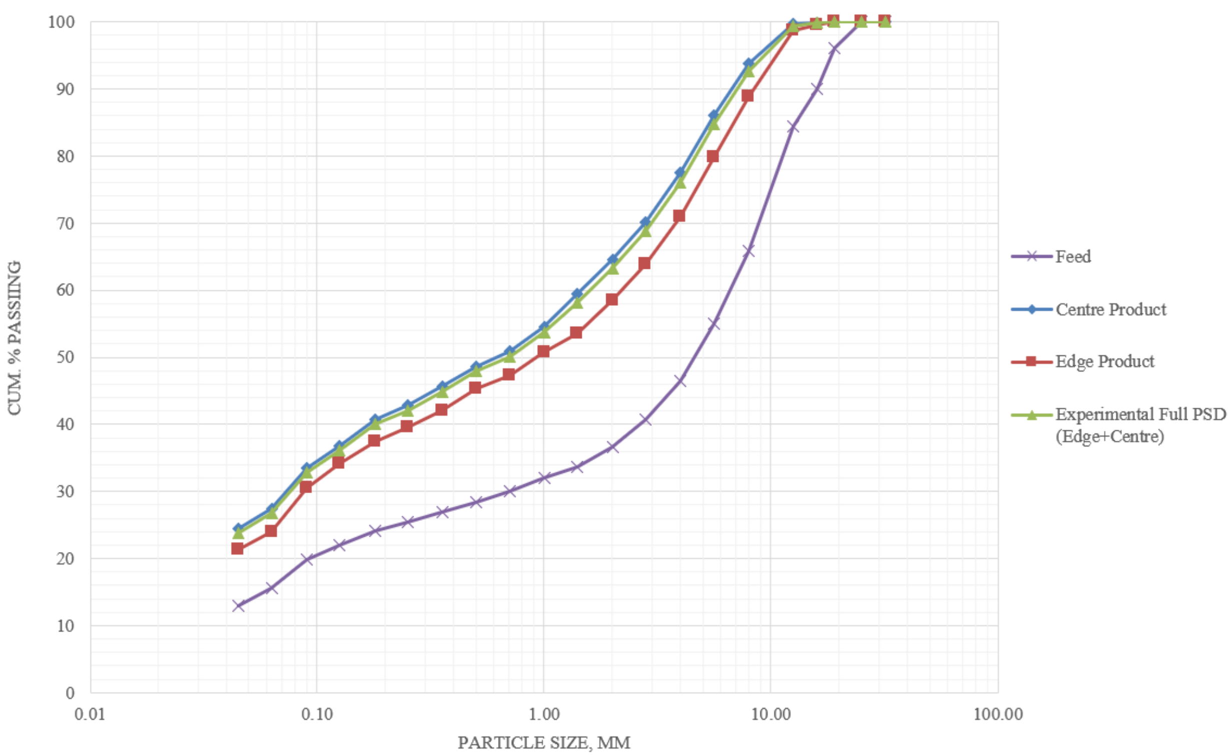

Figure A. 7-3: Feed and product PSDs of test No. SA003

Test No.		Feed		Centre Product		Edge Product		Experimental Full PSD	Scaled HPGR Product
SA004									90% Center + 10% Edge
Screen Size	Particle Size, mm	Retained (g)	Cum % Pass	Retained (g)	Cum % Pass	Retained (g)	Cum % Pass	Cum % Pass	Cum % Pass
-35.5 to +32	32.00	**0.00**	100.00	**0.00**	100.00	**0.00**	100.00	100.00	100.00
-32 to +25	25.00	**0.00**	100.00	**0.00**	100.00	**0.00**	100.00	100.00	100.00
-25 to +19	19.00	**886.50**	93.99	**0.00**	100.00	**24.20**	99.64	99.92	99.96
-19 to 16	16.00	**976.00**	87.38	**35.10**	99.71	**118.00**	97.90	99.31	99.53
-16 to +12.5	12.50	**956.90**	80.90	**127.80**	98.67	**212.70**	94.76	97.80	98.28
-12.5 to +8	8.00	**2413.00**	64.55	**859.60**	91.64	**1051.40**	79.25	88.88	90.40
-8 to +5.6	5.60	**1514.40**	54.29	**920.50**	84.11	**732.00**	68.45	80.62	82.54
-5.6 to +4	4.00	**1151.60**	46.48	**1069.50**	75.36	**619.20**	59.31	71.79	73.75
-4 to +2.8	2.80	**865.50**	40.62	**932.60**	67.73	**485.30**	52.15	64.26	66.17
-2.8 to +2	2.00	**600.80**	36.55	**668.50**	62.26	**389.00**	46.41	58.74	60.68
-2 to +1.4	1.40	**435.40**	33.60	**575.00**	57.56	**263.80**	42.52	54.21	56.06
-1.4 to +1	1.00	**228.60**	32.05	**605.50**	52.61	**135.50**	40.52	49.92	51.40
-1 to +.71	0.71	**286.00**	30.11	**441.60**	49.00	**192.70**	37.67	46.48	47.86
-.71 to +.5	0.50	**219.70**	28.62	**301.70**	46.53	**122.80**	35.86	44.15	45.46
-.5 to +.355	0.36	**241.40**	26.99	**365.80**	43.54	**165.20**	33.42	41.29	42.52
-.355 to +.25	0.25	**220.00**	25.50	**325.20**	40.88	**131.70**	31.48	38.79	39.94
-.25 to +.18	0.18	**212.60**	24.06	**262.30**	38.73	**119.60**	29.72	36.72	37.83
-.18 to +.125	0.13	**281.80**	22.15	**364.10**	35.75	**146.50**	27.55	33.93	34.93
-.125 to +.09	0.09	**297.60**	20.13	**353.40**	32.86	**159.50**	25.20	31.16	32.10
-.09 to +.063	0.06	**620.50**	15.93	**683.10**	27.27	**319.00**	20.49	25.77	26.60
-.063 to +.045	0.05	**346.00**	13.58	**338.30**	24.51	**239.50**	16.96	22.83	23.75
-0.045	Pan	**2004.40**		**2996.20**		**1149.30**			
Total mass		14758.70		12225.80		6776.90			
Initial wt.		**14877.40**		**12347.00**		**6842.30**			
Delta wt.		-118.70		-121.20		-65.40			
Delta %		-0.80%		-0.98%		-0.96%			
Size Distribution Interpolations									
%passing 1 mm			**32.05**		**52.61**		**40.52**	**49.92**	**51.40**
Linear P50	[mm]		**4.72**		**0.79**		**2.50**	**1.01**	**0.89**
Linear P80	[mm]		**12.25**		**4.85**		**8.22**	**5.49**	**5.14**

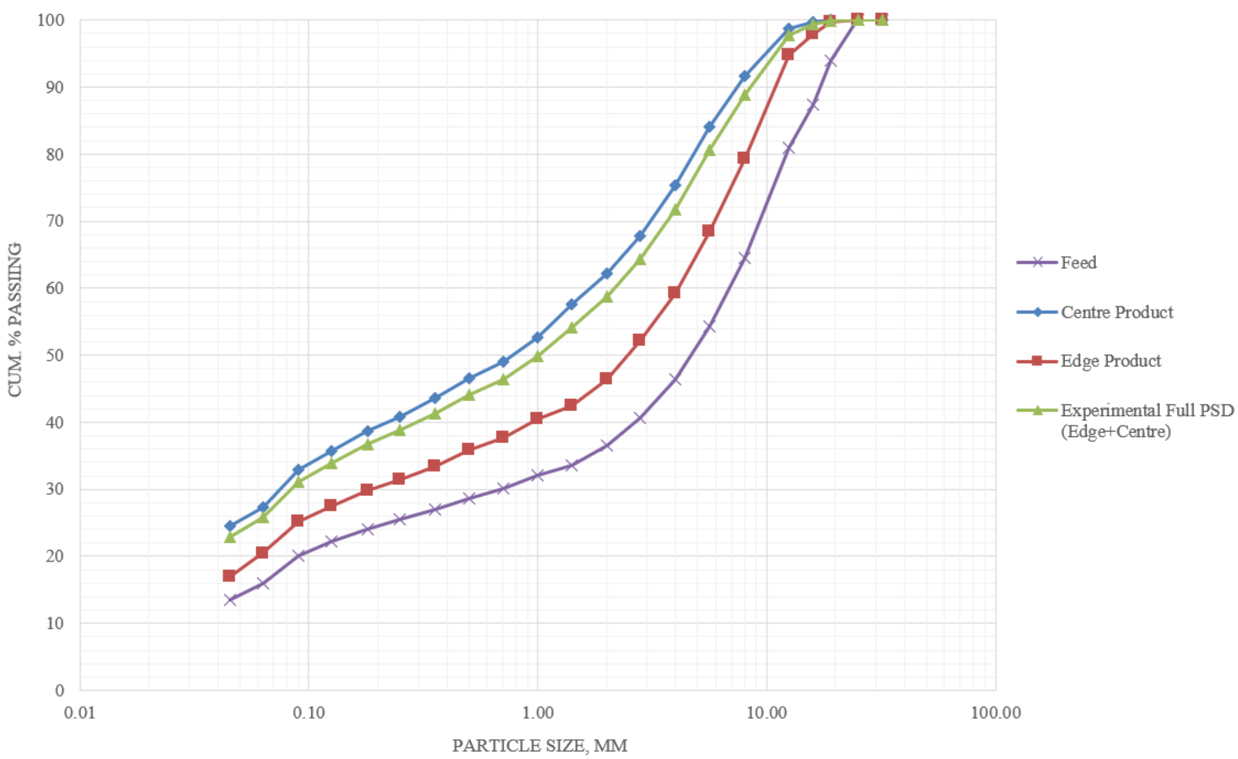

Figure A. 7-4: Feed and product PSDs of test No. SA004

Test No.		Feed		Centre Product		Edge Product		Experimental Full PSD	Scaled HPGR Product
SA005									90% Center + 10% Edge
Screen Size	Particle Size, mm	Retained (g)	Cum % Pass	Retained (g)	Cum % Pass	Retained (g)	Cum % Pass	Cum % Pass	Cum % Pass
-35.5 to +32	32.00	**0.00**	100.00	**0.00**	100.00	**0.00**	100.00	100.00	100.00
-32 to +25	25.00	**0.00**	100.00	**0.00**	100.00	**0.00**	100.00	100.00	100.00
-25 to +19	19.00	**378.20**	94.79	**14.20**	99.88	**0.00**	100.00	99.91	99.89
-19 to 16	16.00	**389.00**	89.44	**45.70**	99.50	**100.80**	98.58	99.30	99.41
-16 to +12.5	12.50	**510.20**	82.42	**129.50**	98.42	**195.00**	95.83	97.85	98.16
-12.5 to +8	8.00	**1245.00**	65.28	**800.00**	91.74	**988.80**	81.87	89.57	90.75
-8 to +5.6	5.60	**706.50**	55.55	**879.90**	84.39	**697.10**	72.03	81.67	83.15
-5.6 to +4	4.00	**632.20**	46.85	**958.90**	76.38	**656.40**	62.77	73.39	75.02
-4 to +2.8	2.80	**429.00**	40.95	**898.00**	68.88	**518.80**	55.45	65.92	67.54
-2.8 to +2	2.00	**299.00**	36.83	**646.90**	63.48	**382.00**	50.06	60.52	62.14
-2 to +1.4	1.40	**198.80**	34.09	**576.40**	58.66	**299.00**	45.84	55.84	57.38
-1.4 to +1	1.00	**188.70**	31.50	**570.10**	53.90	**266.20**	42.08	51.30	52.72
-1 to +.71	0.71	**130.30**	29.70	**442.20**	50.21	**178.70**	39.56	47.87	49.14
-.71 to +.5	0.50	**102.90**	28.29	**288.30**	47.80	**103.90**	38.09	45.67	46.83
-.5 to +.355	0.36	**115.00**	26.70	**387.60**	44.56	**210.80**	35.12	42.49	43.62
-.355 to +.25	0.25	**97.40**	25.36	**322.60**	41.87	**146.20**	33.06	39.93	40.99
-.25 to +.18	0.18	**107.70**	23.88	**259.00**	39.71	**127.40**	31.26	37.85	38.86
-.18 to +.125	0.13	**138.90**	21.97	**364.50**	36.66	**175.20**	28.78	34.93	35.88
-.125 to +.09	0.09	**124.00**	20.26	**471.10**	32.73	**170.90**	26.37	31.33	32.09
-.09 to +.063	0.06	**299.80**	16.13	**700.60**	26.88	**401.10**	20.71	25.52	26.26
-.063 to +.045	0.05	**212.80**	13.20	**365.40**	23.83	**233.80**	17.41	22.41	23.18
-0.045	Pan	**959.20**		**2852.90**		**1233.90**			
Total mass		7264.60		11973.80		7086.00			
Initial wt.		**7303.00**		**12121.80**		**7200.40**			
Delta wt.		-38.40		-148.00		-114.40			
Delta %		-0.53%		-1.22%		-1.59%			
Size Distribution Interpolations									
%passing 1 mm			**31.50**		**53.90**		**42.08**	**51.30**	**52.72**
Linear P50	[mm]		**4.58**		**0.69**		**1.99**	**0.89**	**0.78**
Linear P80	[mm]		**11.87**		**4.72**		**7.54**	**5.28**	**4.98**

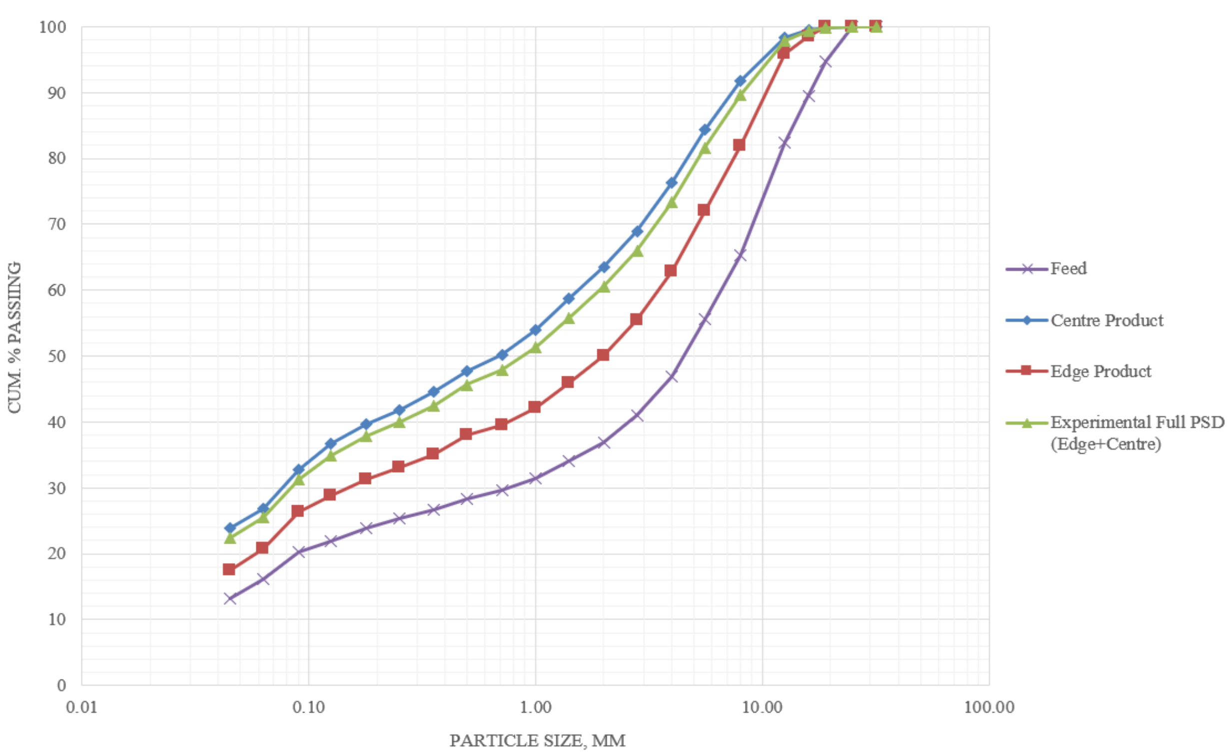

Figure A. 7-5: Feed and product PSDs of test No. SA005

Test No.		Feed		Centre Product		Edge Product		Experimental Full PSD	Scaled HPGR Product
SA006									90% Center + 10% Edge
Screen Size	Particle Size, mm	Retained (g)	Cum % Pass	Retained (g)	Cum % Pass	Retained (g)	Cum % Pass	Cum % Pass	Cum % Pass
-35.5 to +32	32.00	**0.00**	100.00	**0.00**	100.00	**0.00**	100.00	100.00	100.00
-32 to +25	25.00	**0.00**	100.00	**0.00**	100.00	**0.00**	100.00	100.00	100.00
-25 to +19	19.00	**342.00**	95.43	**0.00**	100.00	**0.00**	100.00	100.00	100.00
-19 to 16	16.00	**495.20**	88.81	**33.10**	99.69	**38.00**	99.25	99.59	99.64
-16 to +12.5	12.50	**381.50**	83.71	**113.60**	98.62	**157.40**	96.15	98.09	98.37
-12.5 to +8	8.00	**1298.40**	66.35	**836.70**	90.74	**714.00**	82.07	88.89	89.88
-8 to +5.6	5.60	**777.20**	55.96	**841.20**	82.82	**497.70**	72.26	80.57	81.77
-5.6 to +4	4.00	**638.50**	47.42	**934.80**	74.02	**453.90**	63.32	71.73	72.95
-4 to +2.8	2.80	**439.50**	41.55	**769.50**	66.78	**358.70**	56.25	64.53	65.73
-2.8 to +2	2.00	**305.70**	37.46	**652.30**	60.64	**279.20**	50.74	58.52	59.65
-2 to +1.4	1.40	**221.80**	34.49	**517.30**	55.77	**213.90**	46.53	53.79	54.85
-1.4 to +1	1.00	**199.30**	31.83	**507.90**	50.99	**117.40**	44.21	49.54	50.31
-1 to +.71	0.71	**133.50**	30.05	**356.20**	47.63	**144.90**	41.36	46.29	47.01
-.71 to +.5	0.50	**90.50**	28.84	**199.40**	45.76	**80.50**	39.77	44.48	45.16
-.5 to +.355	0.36	**122.10**	27.20	**358.70**	42.38	**160.70**	36.60	41.15	41.80
-.355 to +.25	0.25	**110.80**	25.72	**277.60**	39.77	**106.80**	34.50	38.64	39.24
-.25 to +.18	0.18	**100.70**	24.38	**223.80**	37.66	**97.50**	32.58	36.57	37.15
-.18 to +.125	0.13	**192.50**	21.80	**341.90**	34.44	**140.20**	29.81	33.45	33.98
-.125 to +.09	0.09	**135.70**	19.99	**327.80**	31.36	**99.90**	27.84	30.61	31.01
-.09 to +.063	0.06	**329.90**	15.58	**634.60**	25.38	**280.50**	22.31	24.73	25.08
-.063 to +.045	0.05	**193.20**	12.99	**448.10**	21.16	**161.70**	19.13	20.73	20.96
-0.045	Pan	**972.00**		**2248.20**		**970.40**			
Total mass		7480.00		10622.70		5073.30			
Initial wt.		**7498.20**		**10844.90**		**5125.50**			
Delta wt.		-18.20		-222.20		-52.20			
Delta %		-0.24%		-2.05%		-1.02%			
Size Distribution Interpolations									
%passing 1 mm			**31.83**		**50.99**		**44.21**	**49.54**	**50.31**
Linear P50	[mm]		**4.48**		**0.91**		**1.89**	**1.04**	**0.97**
Linear P80	[mm]		**11.54**		**5.09**		**7.49**	**5.50**	**5.28**

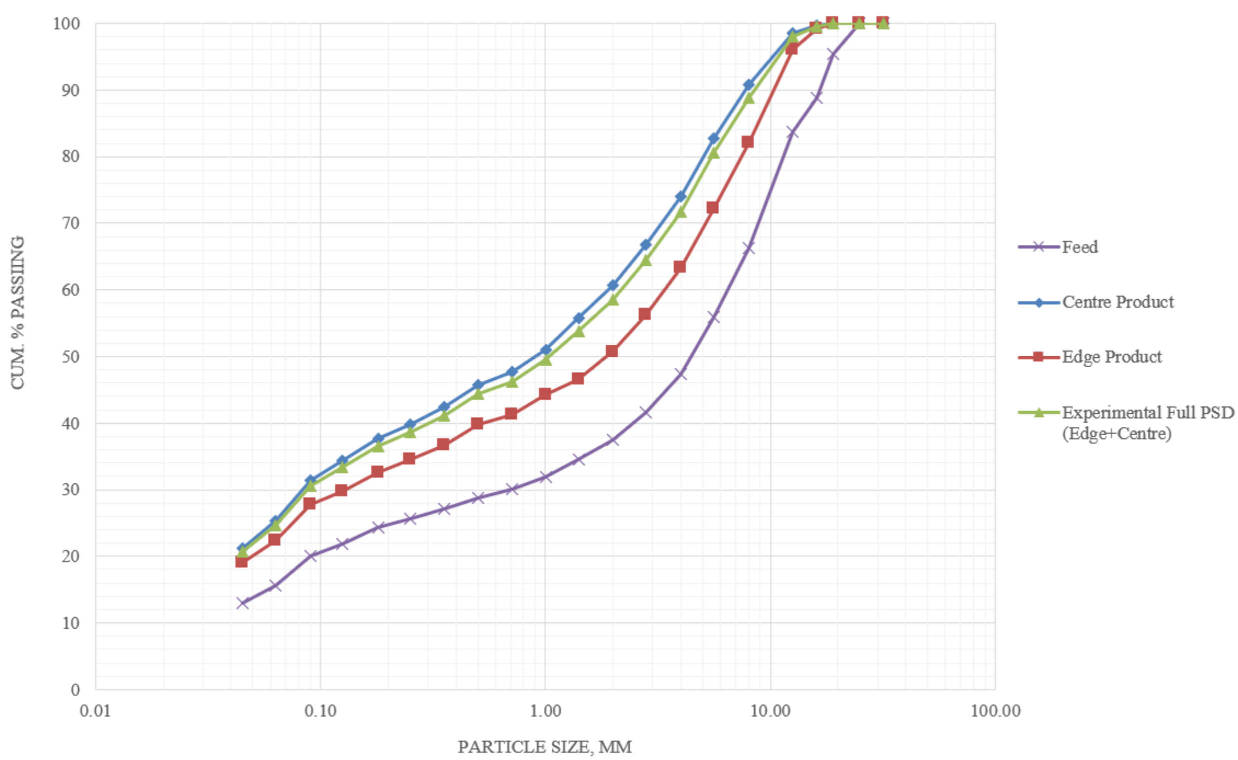

Figure A. 7-6: Feed and product PSDs of test No. SA006

Test No. SA007		Feed		Centre Product		Edge Product		Experimental Full PSD	Scaled HPGR Product 90% Center + 10% Edge
Screen Size	Particle Size, mm	Retained (g)	Cum % Pass	Retained (g)	Cum % Pass	Retained (g)	Cum % Pass	Cum % Pass	Cum % Pass
-35.5 to +32	32.00	**0.00**	100.00	**0.00**	100.00	**0.00**	100.00	100.00	100.00
-32 to +25	25.00	**0.00**	100.00	**0.00**	100.00	**0.00**	100.00	100.00	100.00
-25 to +19	19.00	**320.70**	96.19	**0.00**	100.00	**0.00**	100.00	100.00	100.00
-19 to 16	16.00	**438.00**	90.98	**0.00**	100.00	**65.90**	99.01	99.76	99.90
-16 to +12.5	12.50	**477.90**	85.29	**50.70**	99.48	**91.80**	97.63	99.03	99.30
-12.5 to +8	8.00	**1556.60**	66.78	**431.50**	95.06	**903.10**	84.07	92.41	93.96
-8 to +5.6	5.60	**908.80**	55.97	**565.50**	89.27	**707.70**	73.45	85.45	87.68
-5.6 to +4	4.00	**695.00**	47.70	**739.20**	81.69	**608.30**	64.31	77.50	79.95
-4 to +2.8	2.80	**503.70**	41.71	**660.60**	74.92	**492.30**	56.92	70.58	73.12
-2.8 to +2	2.00	**350.10**	37.55	**553.10**	69.26	**371.20**	51.35	64.93	67.46
-2 to +1.4	1.40	**249.30**	34.58	**477.50**	64.36	**277.60**	47.18	60.21	62.64
-1.4 to +1	1.00	**137.50**	32.95	**334.30**	60.94	**255.50**	43.34	56.69	59.18
-1 to +.71	0.71	**158.10**	31.07	**393.60**	56.90	**174.30**	40.73	53.00	55.29
-.71 to +.5	0.50	**112.60**	29.73	**280.20**	54.03	**117.70**	38.96	50.39	52.53
-.5 to +.355	0.36	**166.60**	27.75	**375.30**	50.19	**183.80**	36.20	46.81	48.79
-.355 to +.25	0.25	**125.80**	26.25	**309.50**	47.02	**140.00**	34.10	43.90	45.73
-.25 to +.18	0.18	**116.20**	24.87	**233.70**	44.62	**117.90**	32.33	41.65	43.39
-.18 to +.125	0.13	**168.10**	22.87	**363.20**	40.90	**171.60**	29.75	38.21	39.79
-.125 to +.09	0.09	**173.60**	20.81	**359.40**	37.22	**178.80**	27.06	34.77	36.20
-.09 to +.063	0.06	**364.50**	16.47	**570.60**	31.37	**363.80**	21.60	29.01	30.40
-.063 to +.045	0.05	**184.80**	14.27	**356.40**	27.72	**221.20**	18.28	25.44	26.78
-0.045	Pan	**1200.10**		**2705.50**		**1217.50**			
Total mass		8408.00		9759.80		6660.00			
Initial wt.		**8469.40**		**9853.60**		**6686.40**			
Delta wt.		-61.40		-93.80		-26.40			
Delta %		-0.72%		-0.95%		-0.39%			
Size Distribution Interpolations									
%passing 1 mm			**32.95**		**60.94**		**43.34**	**56.69**	**59.18**
Linear P50	[mm]		**4.44**		**0.35**		**1.81**	**0.48**	**0.40**
Linear P80	[mm]		**11.21**		**3.70**		**7.08**	**4.50**	**4.01**

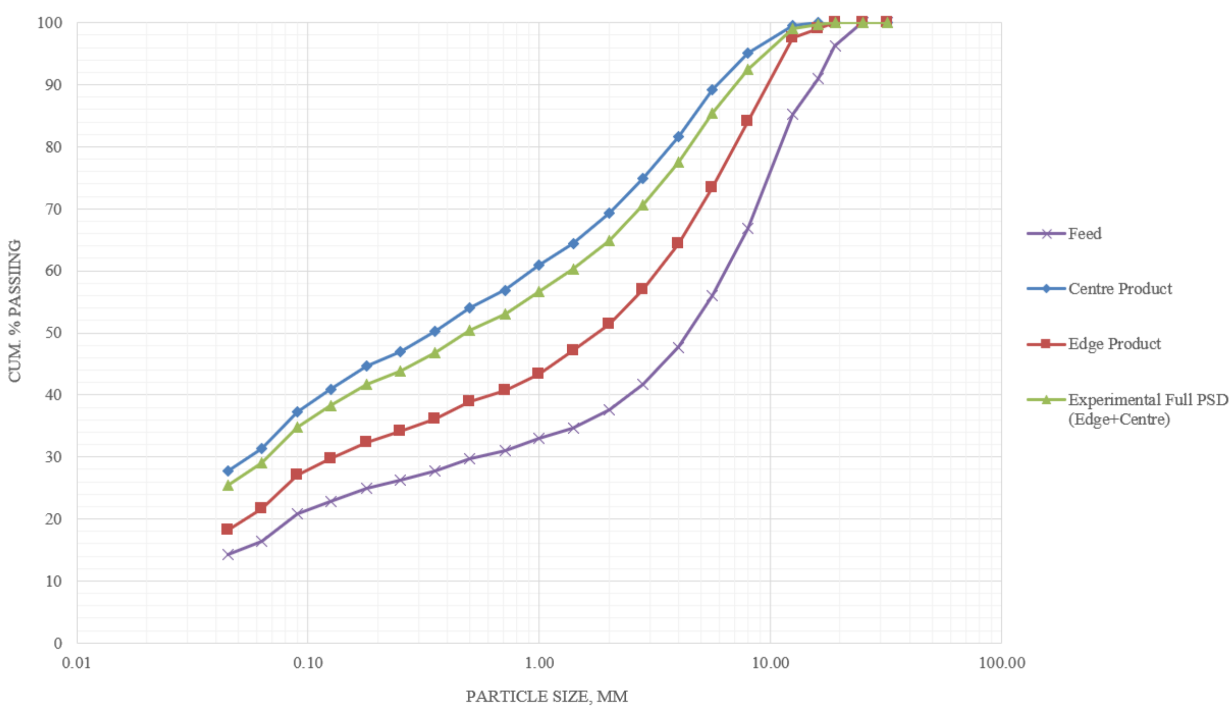

Figure A. 7-7: Feed and product PSDs of test No. SA007

Test No.		Feed		Centre Product		Edge Product		Experimental Full PSD	Scaled HPGR Product
SA008									90% Center + 10% Edge
Screen Size	Particle Size, mm	Retained (g)	Cum % Pass	Retained (g)	Cum % Pass	Retained (g)	Cum % Pass	Cum % Pass	Cum % Pass
-35.5 to +32	32.00	**0.00**	100.00	**0.00**	100.00	**0.00**	100.00	100.00	100.00
-32 to +25	25.00	**0.00**	100.00	**0.00**	100.00	**0.00**	100.00	100.00	100.00
-25 to +19	19.00	**287.80**	95.84	**0.00**	100.00	**0.00**	100.00	100.00	100.00
-19 to 16	16.00	**402.60**	90.01	**0.00**	100.00	**27.00**	99.59	99.91	99.96
-16 to +12.5	12.50	**420.50**	83.93	**41.80**	99.63	**86.70**	98.27	99.34	99.50
-12.5 to +8	8.00	**1194.10**	66.65	**483.60**	95.41	**803.70**	86.08	93.37	94.48
-8 to +5.6	5.60	**715.50**	56.29	**680.30**	89.46	**641.60**	76.34	86.60	88.15
-5.6 to +4	4.00	**607.30**	47.51	**845.40**	82.08	**618.00**	66.96	78.77	80.56
-4 to +2.8	2.80	**398.90**	41.73	**768.20**	75.36	**447.50**	60.17	72.04	73.84
-2.8 to +2	2.00	**297.40**	37.43	**613.20**	70.01	**349.30**	54.87	66.70	68.49
-2 to +1.4	1.40	**207.30**	34.43	**593.80**	64.82	**288.10**	50.49	61.69	63.38
-1.4 to +1	1.00	**104.10**	32.93	**364.40**	61.63	**155.90**	48.13	58.68	60.28
-1 to +.71	0.71	**138.60**	30.92	**460.00**	57.61	**194.40**	45.18	54.90	56.37
-.71 to +.5	0.50	**79.90**	29.76	**356.10**	54.50	**123.80**	43.30	52.05	53.38
-.5 to +.355	0.36	**139.40**	27.75	**424.90**	50.79	**221.80**	39.93	48.42	49.70
-.355 to +.25	0.25	**102.00**	26.27	**379.40**	47.47	**152.70**	37.61	45.32	46.49
-.25 to +.18	0.18	**95.50**	24.89	**280.90**	45.02	**132.80**	35.60	42.96	44.08
-.18 to +.125	0.13	**142.50**	22.83	**703.50**	38.87	**197.40**	32.60	37.50	38.24
-.125 to +.09	0.09	**127.20**	20.99	**471.70**	34.75	**221.20**	29.25	33.55	34.20
-.09 to +.063	0.06	**304.20**	16.59	**684.40**	28.77	**438.80**	22.59	27.42	28.15
-.063 to +.045	0.05	**192.70**	13.80	**557.00**	23.90	**239.60**	18.95	22.82	23.40
-0.045	Pan	**953.50**		**2735.00**		**1248.50**			
Total mass		6911.00		11443.60		6588.80			
Initial wt.		**6937.10**		**11703.90**		**6604.40**			
Delta wt.		-26.10		-260.30		-15.60			
Delta %		-0.38%		-2.22%		-0.24%			
Size Distribution Interpolations									
%passing 1 mm			**32.93**		**61.63**		**48.13**	**58.68**	**60.28**
Linear P50	[mm]		**4.45**		**0.33**		**1.32**	**0.42**	**0.37**
Linear P80	[mm]		**11.48**		**3.63**		**6.50**	**4.25**	**3.90**

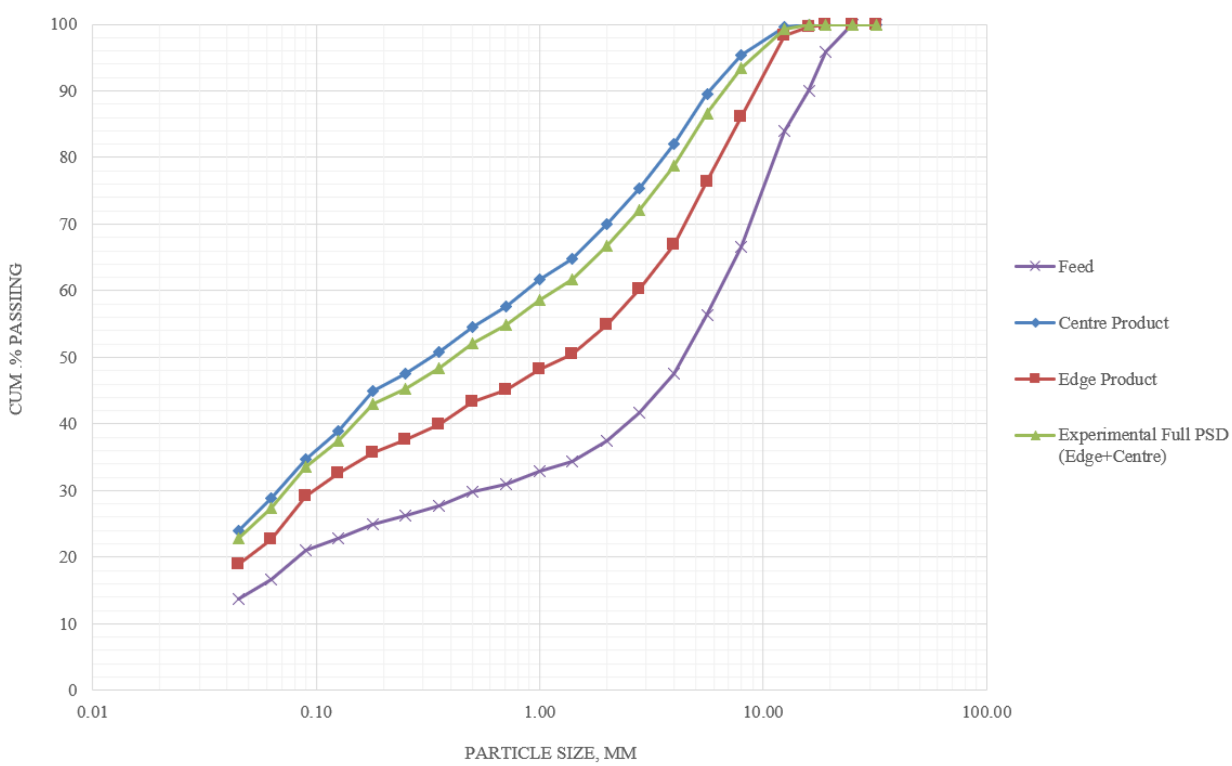

Figure A. 7-8: Feed and product PSDs of test No. SA008

Test No.		Feed		Centre Product		Edge Product		Experimental Full PSD	Scaled HPGR Product
SA009									90% Center + 10% Edge
Screen Size	Particle Size, mm	Retained (g)	Cum % Pass	Retained (g)	Cum % Pass	Retained (g)	Cum % Pass	Cum % Pass	Cum % Pass
-35.5 to +32	32.00	**0.00**	100.00	**0.00**	100.00	**0.00**	100.00	100.00	100.00
-32 to +25	25.00	**0.00**	100.00	**0.00**	100.00	**0.00**	100.00	100.00	100.00
-25 to +19	19.00	**335.70**	95.24	**0.00**	100.00	**0.00**	100.00	100.00	100.00
-19 to 16	16.00	**388.10**	89.75	**19.90**	99.77	**16.40**	99.83	99.78	99.77
-16 to +12.5	12.50	**535.60**	82.16	**43.20**	99.26	**100.00**	98.76	99.19	99.21
-12.5 to +8	8.00	**1228.70**	64.75	**454.00**	93.94	**1155.60**	86.49	92.89	93.20
-8 to +5.6	5.60	**717.40**	54.59	**528.50**	87.75	**1083.50**	74.98	85.94	86.47
-5.6 to +4	4.00	**594.60**	46.17	**753.80**	78.91	**929.70**	65.11	76.96	77.53
-4 to +2.8	2.80	**403.50**	40.45	**659.00**	71.19	**647.10**	58.24	69.36	69.90
-2.8 to +2	2.00	**279.80**	36.49	**482.90**	65.53	**480.20**	53.14	63.78	64.29
-2 to +1.4	1.40	**197.30**	33.69	**435.50**	60.43	**390.80**	48.99	58.81	59.29
-1.4 to +1	1.00	**186.00**	31.06	**251.90**	57.48	**348.60**	45.29	55.76	56.26
-1 to +.71	0.71	**113.40**	29.45	**317.30**	53.76	**247.30**	42.66	52.19	52.65
-.71 to +.5	0.50	**59.40**	28.61	**223.20**	51.14	**177.90**	40.77	49.68	50.11
-.5 to +.355	0.36	**139.30**	26.64	**319.50**	47.40	**228.10**	38.35	46.12	46.50
-.355 to +.25	0.25	**101.40**	25.20	**262.20**	44.33	**199.90**	36.23	43.18	43.52
-.25 to +.18	0.18	**95.30**	23.85	**194.60**	42.05	**149.00**	34.64	41.00	41.31
-.18 to +.125	0.13	**131.80**	21.98	**369.80**	37.71	**267.50**	31.80	36.88	37.12
-.125 to +.09	0.09	**137.20**	20.04	**311.90**	34.06	**340.80**	28.18	33.23	33.47
-.09 to +.063	0.06	**304.00**	15.73	**567.90**	27.40	**524.60**	22.61	26.73	26.93
-.063 to +.045	0.05	**168.50**	13.35	**319.40**	23.66	**417.50**	18.18	22.89	23.11
-0.045	Pan	**942.20**		**2019.20**		**1711.80**			
Total mass		7059.20		8533.70		9416.30			
Initial wt.		**7083.70**		**8565.00**		**9491.80**			
Delta wt.		-24.50		-31.30		-75.50			
Delta %		-0.35%		-0.37%		-0.80%			
Size Distribution Interpolations									
%passing 1 mm			**31.06**		**57.48**		**45.29**	**55.76**	**56.26**
Linear P50	[mm]		**4.73**		**0.46**		**1.55**	**0.53**	**0.50**
Linear P80	[mm]		**11.94**		**4.20**		**6.65**	**4.54**	**4.44**

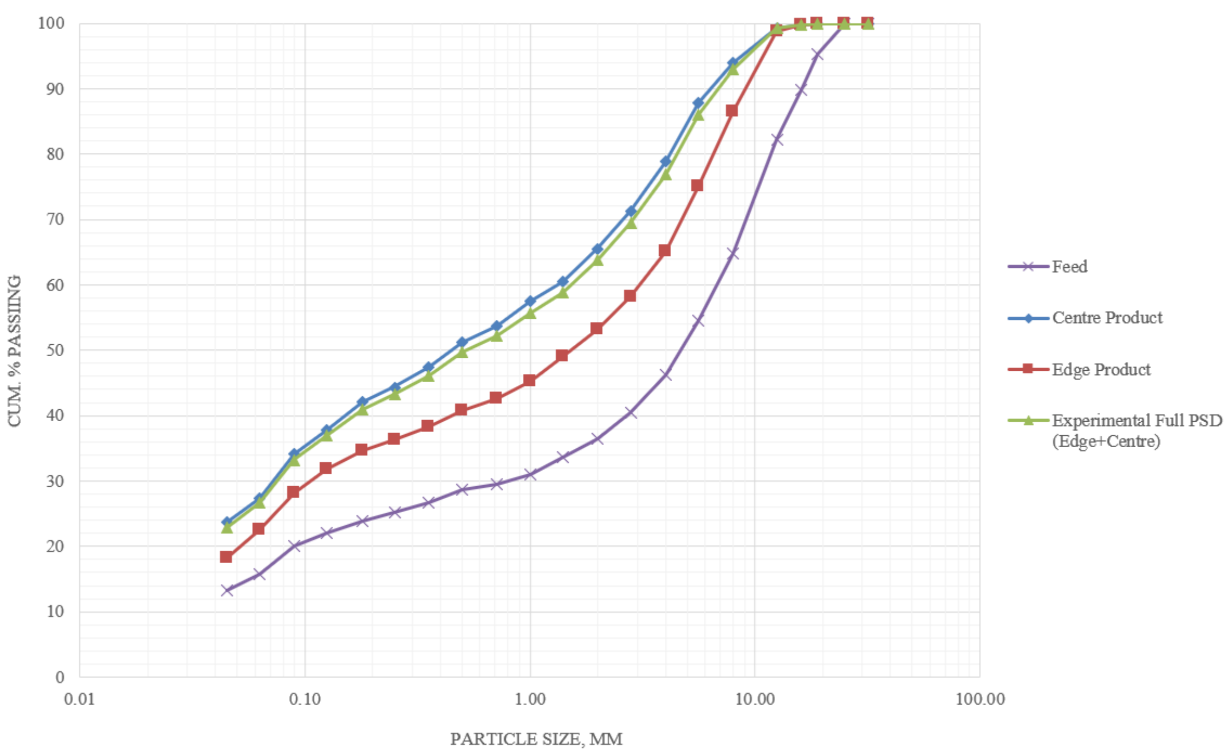

Figure A. 7-9: Feed and product PSDs of test No. SA009

Table A. 7-2: Summary of duplicate open circuit pilot-scale HPGR tests

Press Constants	Roller Diameter (D)	[m]	0.750				
	Roller Width (W)	[m]	0.220				
Data	**Description**	**Test Number:**		**SA010**	**SA011**	**SA012**	**SA013**
		Symbol	**Unit**	**Duplicate Test**		**Duplicate Test**	
Process Set Points	Speed	n	[m/s]	0.55	0.55	0.55	0.55
		n	[rpm]	14.04	14.04	14.04	14.04
	Static Gap	X_0	[mm]	9.0	9.0	9.0	9.0
	Hydraulic Pressure	P	[bar]	82.1	82.1	82.1	82.1
	Pressing Force	F	[kN]	660.0	660.0	660.0	660.0
	Specific Pressing Force	F_{SP}	[N/mm^2]	**4.0**	**4.0**	**4.0**	**4.0**
Process Data	**Test Time**	t	[s]	15.36	13.58	18.65	20.51
	Average Actual Speed:	w_{AV}	[m/s]	0.56	0.56	0.56	0.56
	Standard Deviation	s_w		0.25	0.23	0.30	0.32
	Actual Roller gap (average)	X_{gAV}	**[mm]**	**22.99**	**22.63**	**23.52**	**23.30**
	Standard Deviation	s_X		0.24	0.30	0.29	0.33
	Actual Hydraulic Pressure (average)	P_{AV}	[bar]	**82.7**	**82.5**	**82.9**	**82.6**
	Standard Deviation			0.27	0.42	0.58	0.78
	Actual Pressing Force (average)	F_{AV}	[kN]	665	664	666	664
	Actual Specific Pressure (average)	F_{SPAV}	[N/mm^2]	**4.04**	**4.03**	**4.05**	**4.04**
	Idle Power Draw	Pi	[kW]	5.24	5.18	4.37	4.90
	Power Draw	P	[kW]	57.35	56.30	64.32	65.38
	Total Specific Energy Consumption	E_{SP}	[kWh/t]	1.84	1.85	2.03	2.04
	Net Specific Energy Consumption	$E_{SP\ net}$	**[kWh/t]**	**1.67**	**1.68**	**1.89**	**1.89**
	Press throughput	W	[t/h]	31.12	30.42	31.72	32.04
	Specific Throughput Constant	**m dot**	[ts/hm^3]	**336**	**332**	**344**	**347**
Material Data	**Particle Size Distribution**			PSD010	PSD011	PSD012	PSD013
	Feed: 100% Passing Size		[mm]	25.00	25.00	25.00	25.00
	Feed: 80% Passing Size	F_{80}	[mm]	8.86	9.48	14.84	14.86
	Feed: 50% Passing Size	F_{50}	[mm]	**3.28**	**3.64**	**5.61**	**5.75**
	Centre: 80% Passing Size	P_{80}	[mm]	3.89	3.40	3.77	4.52
	Centre: 50% Passing Size	P_{50}	[mm]	**0.41**	**0.36**	**0.34**	**0.44**
	Edge: 80% Passing Size	P_{80}	[mm]	6.34	5.46	8.16	8.25
	Edge: 50% Passing Size	P_{50}	[mm]	1.50	1.10	2.21	2.16
	Full 80% Passing Size	P_{80}	[mm]	4.31	3.78	4.43	5.37
	Full 50% Passing Size	P_{50}	[mm]	**0.49**	**0.45**	**0.46**	**0.64**
	Combined 90% Center & 10% Edge: 80% Passing Size	P_{80}	[mm]	4.12	3.61	4.16	4.85
	Combined 90% Center & 10% Edge: 50% Passing Size	P_{50}	[mm]	**0.45**	**0.41**	**0.41**	**0.51**
	Reduction Ratio F80/P80 full			2.06	2.51	3.35	2.77
	Reduction Ratio F50/P50 full			**6.69**	**8.16**	**12.18**	**9.02**
	Reduction Ratio F80/P80 (90% C & 10% E Product)			2.15	2.63	3.57	3.06
	Reduction Ratio F50/P50 (90% C & 10% E Product)			**7.21**	**8.96**	**13.56**	**11.29**
	Percentage Passing 1 mm (Combined)			**56.91**	**57.82**	**57.55**	**53.71**
	Percentage Passing 1 mm (90% C & 10% E)		[%]	**57.84**	**58.76**	**58.72**	**56.23**
	Percentage Passing 0.045 mm (Combined)		[%]	**23.69**	**19.24**	**26.08**	**24.25**
	Mass Balance						
	Total Feed Material	M_F	[kg]	589	626	637	632
	Total Centre Product	M_C	[kg]	228.7	199.6	185.0	190.4
	Centre Product % of Centre & Edge Material	MCE%	[%]	82.5%	81.3%	83.9%	74.1%
	Total Edge Product	M_E	[kg]	48.4	45.8	35.5	66.5
	Edge Product % of Centre & Edge Material	$M_{EF\%}$	[%]	17.5%	18.7%	16.1%	25.9%
	Edge Product % of Centre Product	$M_{EC\%}$	[%]	21.2%	22.9%	19.2%	34.9%
	Total Waste Product	M_W	[kg]	290.9	358.5	371.0	363.5
	Waste Product % of Total Feed	$M_{WF\%}$	[%]	49.4%	57.3%	58.2%	57.5%
	Total Recovered Product	M_P	[kg]	568	604	592	620
	Mass Reconciliation (+ "gain; - "loss")	$M_{PF\%}$	[%]	-3.6%	-3.5%	-7.1%	-1.8%

Test No.		Feed		Centre Product		Edge Product		Experimental Full PSD	Scaled HPGR Product
SA010									90% Center + 10% Edge
Screen Size	Particle Size, mm	Retained (g)	Cum % Pass	Retained (g)	Cum % Pass	Retained (g)	Cum % Pass	Cum % Pass	Cum % Pass
-35.5 to +32	32.000	**0.00**	100.00	**0.00**	100.00	**0.00**	100.00	100.00	100.00
-32 to +25	25.000	**0.00**	100.00	**0.00**	100.00	**0.00**	100.00	100.00	100.00
-25 to +19	19.000	**67.10**	99.29	**0.00**	100.00	**0.00**	100.00	100.00	100.00
-19 to 16	16.000	**187.90**	97.31	**9.00**	99.91	**7.80**	99.93	99.91	99.91
-16 to +12.5	12.500	**200.60**	95.20	**23.20**	99.68	**79.00**	99.22	99.60	99.63
-12.5 to +8	8.000	**1785.90**	76.39	**439.00**	95.32	**1364.40**	86.95	93.86	94.48
-8 to +5.6	5.600	**1211.30**	63.63	**669.90**	88.67	**1115.60**	76.91	86.62	87.49
-5.6 to +4	4.000	**904.30**	54.11	**806.70**	80.66	**999.50**	67.92	78.43	79.39
-4 to +2.8	2.800	**646.80**	47.30	**704.60**	73.66	**857.80**	60.20	71.31	72.32
-2.8 to +2	2.000	**486.10**	42.18	**611.60**	67.59	**699.50**	53.91	65.20	66.22
-2 to +1.4	1.400	**334.90**	38.65	**529.20**	62.34	**526.30**	49.17	60.04	61.02
-1.4 to +1	1.000	**168.80**	36.87	**326.80**	59.09	**286.90**	46.59	56.91	57.84
-1 to +.71	0.710	**205.20**	34.71	**335.20**	55.76	**349.00**	43.45	53.61	54.53
-.71 to +.5	0.500	**150.90**	33.12	**363.60**	52.15	**250.40**	41.20	50.24	51.06
-.5 to +.355	0.355	**185.70**	31.17	**350.00**	48.68	**279.80**	38.68	46.93	47.68
-.355 to +.25	0.250	**162.30**	29.46	**302.00**	45.68	**249.00**	36.44	44.07	44.76
-.25 to +.18	0.180	**135.30**	28.03	**226.60**	43.43	**205.60**	34.59	41.89	42.55
-.18 to +.125	0.125	**184.40**	26.09	**324.40**	40.21	**289.70**	31.99	38.77	39.39
-.125 to +.09	0.090	**269.20**	23.25	**500.00**	35.25	**400.70**	28.38	34.05	34.56
-.09 to +.063	0.063	**412.90**	18.90	**550.70**	29.78	**741.40**	21.71	28.37	28.97
-.063 to +.045	0.045	**504.90**	13.59	**470.70**	25.10	**523.10**	17.01	23.69	24.29
-0.045	Pan	**1290.00**		**2528.40**		**1890.70**			
Total mass		9494.50		10071.60		11116.20			
Initial wt.		**9546.60**		**10170.70**		**11185.30**			
Delta wt.		-52.10		-99.10		-69.10			
Delta %		-0.55%		-0.97%		-0.62%			
Size Distribution Interpolations									
%passing 1 mm			**36.87**		**59.09**		**46.59**	**56.91**	**57.84**
Linear P50	[mm]		**3.28**		**0.41**		**1.50**	**0.49**	**0.45**
Linear P80	[mm]		**8.86**		**3.89**		**6.34**	**4.31**	**4.12**

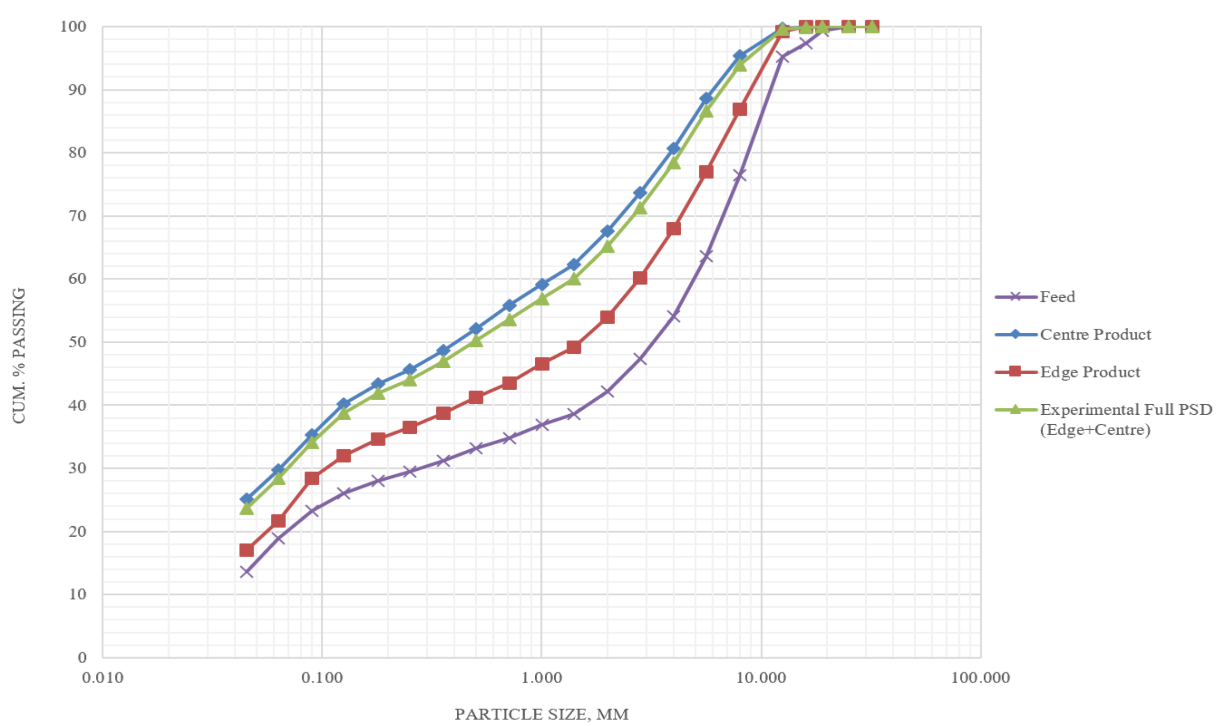

Figure A. 7-10: Feed and product PSDs of test No. SA010

Test No.		Feed		Centre Product		Edge Product		Experimental Full PSD	Scaled HPGR Product
SA011									90% Center + 10% Edge
Screen Size	Particle Size, mm	Retained (g)	Cum % Pass	Retained (g)	Cum % Pass	Retained (g)	Cum % Pass	Cum % Pass	Cum % Pass
-35.5 to +32	32.000	**0.00**	100.00	**0.00**	100.00	**0.00**	100.00	100.00	100.00
-32 to +25	25.000	**0.00**	100.00	**0.00**	100.00	**0.00**	100.00	100.00	100.00
-25 to +19	19.000	**226.00**	97.70	**0.00**	100.00	**0.00**	100.00	100.00	100.00
-19 to 16	16.000	**163.10**	96.04	**0.00**	100.00	**17.50**	99.83	99.97	99.98
-16 to +12.5	12.500	**293.00**	93.05	**15.60**	99.87	**45.20**	99.38	99.78	99.82
-12.5 to +8	8.000	**1910.20**	73.60	**390.80**	96.73	**901.60**	90.45	95.56	96.10
-8 to +5.6	5.600	**1197.00**	61.41	**723.80**	90.91	**973.50**	80.81	89.02	89.90
-5.6 to +4	4.000	**928.60**	51.95	**907.90**	83.61	**956.40**	71.34	81.32	82.38
-4 to +2.8	2.800	**633.40**	45.50	**897.30**	76.39	**766.40**	63.75	74.03	75.13
-2.8 to +2	2.000	**486.40**	40.55	**685.30**	70.88	**612.50**	57.68	68.42	69.56
-2 to +1.4	1.400	**315.60**	37.33	**676.80**	65.44	**455.00**	53.17	63.15	64.21
-1.4 to +1	1.000	**275.60**	34.52	**694.40**	59.85	**422.70**	48.99	57.82	58.76
-1 to +.71	0.710	**193.40**	32.55	**455.60**	56.19	**291.00**	46.10	54.30	55.18
-.71 to +.5	0.500	**102.90**	31.51	**416.00**	52.84	**272.20**	43.41	51.08	51.90
-.5 to +.355	0.355	**209.30**	29.38	**369.60**	49.87	**254.00**	40.89	48.19	48.97
-.355 to +.25	0.250	**158.30**	27.76	**391.70**	46.72	**243.40**	38.48	45.18	45.89
-.25 to +.18	0.180	**138.30**	26.35	**304.70**	44.27	**195.30**	36.55	42.83	43.50
-.18 to +.125	0.125	**201.90**	24.30	**529.70**	40.01	**319.10**	33.39	38.77	39.34
-.125 to +.09	0.090	**305.10**	21.19	**945.10**	32.41	**425.90**	29.17	31.80	32.08
-.09 to +.063	0.063	**495.90**	16.14	**1316.40**	21.82	**947.40**	19.79	21.44	21.61
-.063 to +.045	0.045	**371.30**	12.36	**215.70**	20.08	**427.40**	15.55	19.24	19.63
-0.045	Pan	**1213.50**		**2497.00**		**1570.50**			
Total mass		9818.80		12433.40		10097.00			
Initial wt.		**9976.00**		**12610.90**		**10180.60**			
Delta wt.		-157.20		-177.50		-83.60			
Delta %		-1.58%		-1.41%		-0.82%			
Size Distribution Interpolations									
%passing 1 mm			**34.52**		**59.85**		**48.99**	**57.82**	**58.76**
Linear P50	[mm]		**3.64**		**0.36**		**1.10**	**0.45**	**0.41**
Linear P80	[mm]		**9.48**		**3.40**		**5.46**	**3.78**	**3.61**

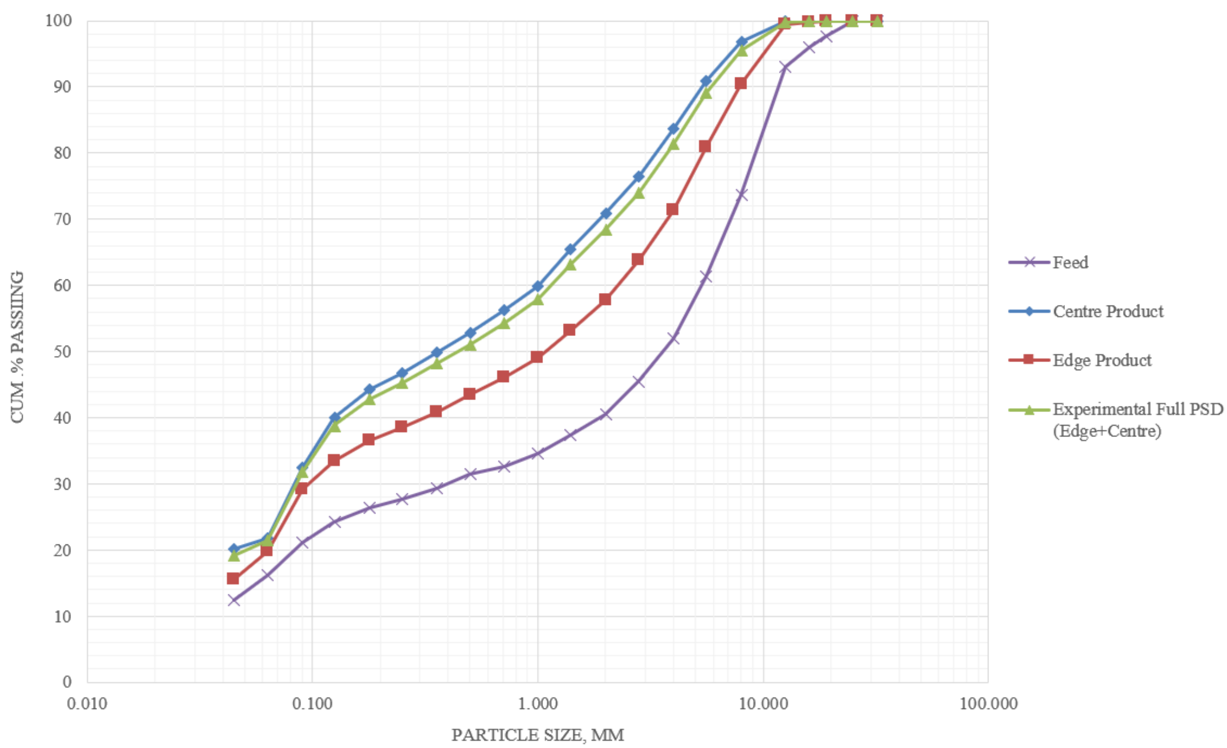

Figure A. 7-11: Feed and product PSDs of test No. SA011

Test No.		Feed		Centre Product		Edge Product		Experimental Full PSD	Scaled HPGR Product
SA012									90% Center + 10% Edge
Screen Size	Particle Size, mm	Retained (g)	Cum % Pass	Retained (g)	Cum % Pass	Retained (g)	Cum % Pass	Cum % Pass	Cum % Pass
-35.5 to +32	32.000	**0.00**	100.00	**0.00**	100.00	**0.00**	100.00	100.00	100.00
-32 to +25	25.000	**0.00**	100.00	**0.00**	100.00	**0.00**	100.00	100.00	100.00
-25 to +19	19.000	**556.40**	94.66	**0.00**	100.00	**38.50**	99.52	99.92	99.95
-19 to 16	16.000	**1209.90**	83.06	**79.20**	99.28	**150.30**	97.63	99.01	99.11
-16 to +12.5	12.500	**962.60**	73.83	**82.70**	98.52	**331.10**	93.49	97.71	98.02
-12.5 to +8	8.000	**1620.60**	58.29	**500.60**	93.94	**1117.00**	79.49	91.62	92.50
-8 to +5.6	5.600	**867.50**	49.97	**622.40**	88.25	**745.10**	70.16	85.34	86.44
-5.6 to +4	4.000	**742.80**	42.85	**756.60**	81.34	**735.10**	60.95	78.05	79.30
-4 to +2.8	2.800	**557.30**	37.50	**754.00**	74.44	**559.70**	53.94	71.14	72.39
-2.8 to +2	2.000	**352.60**	34.12	**508.30**	69.80	**424.20**	48.62	66.39	67.68
-2 to +1.4	1.400	**256.60**	31.66	**554.40**	64.73	**298.00**	44.89	61.53	62.74
-1.4 to +1	1.000	**207.30**	29.67	**448.00**	60.63	**269.30**	41.51	57.55	58.72
-1 to +.71	0.710	**123.00**	28.49	**320.60**	57.70	**259.30**	38.26	54.57	55.76
-.71 to +.5	0.500	**178.40**	26.78	**432.60**	53.74	**186.90**	35.92	50.88	51.96
-.5 to +.355	0.355	**160.60**	25.24	**375.90**	50.31	**163.80**	33.87	47.66	48.66
-.355 to +.25	0.250	**152.20**	23.78	**341.00**	47.19	**160.10**	31.86	44.72	45.66
-.25 to +.18	0.180	**142.50**	22.42	**252.20**	44.88	**147.30**	30.02	42.49	43.40
-.18 to +.125	0.125	**199.00**	20.51	**396.60**	41.26	**187.10**	27.68	39.07	39.90
-.125 to +.09	0.090	**223.10**	18.37	**521.70**	36.49	**210.30**	25.04	34.65	35.34
-.09 to +.063	0.063	**251.40**	15.96	**519.90**	31.74	**286.20**	21.46	30.08	30.71
-.063 to +.045	0.045	**299.70**	13.08	**449.80**	27.62	**273.20**	18.03	26.08	26.66
-0.045	Pan	**1364.30**		**3021.50**		**1439.30**			
Total mass		10427.80		10938.00		7981.80			
Initial wt.		**10464.30**		**11135.50**		**8001.10**			
Delta wt.		-36.50		-197.50		-19.30			
Delta %		-0.35%		-1.77%		-0.24%			
Size Distribution Interpolations									
%passing 1 mm			**29.67**		**60.63**		**41.51**	**57.55**	**58.72**
Linear P50	[mm]		**5.61**		**0.34**		**2.21**	**0.46**	**0.41**
Linear P80	[mm]		**14.84**		**3.77**		**8.16**	**4.43**	**4.16**

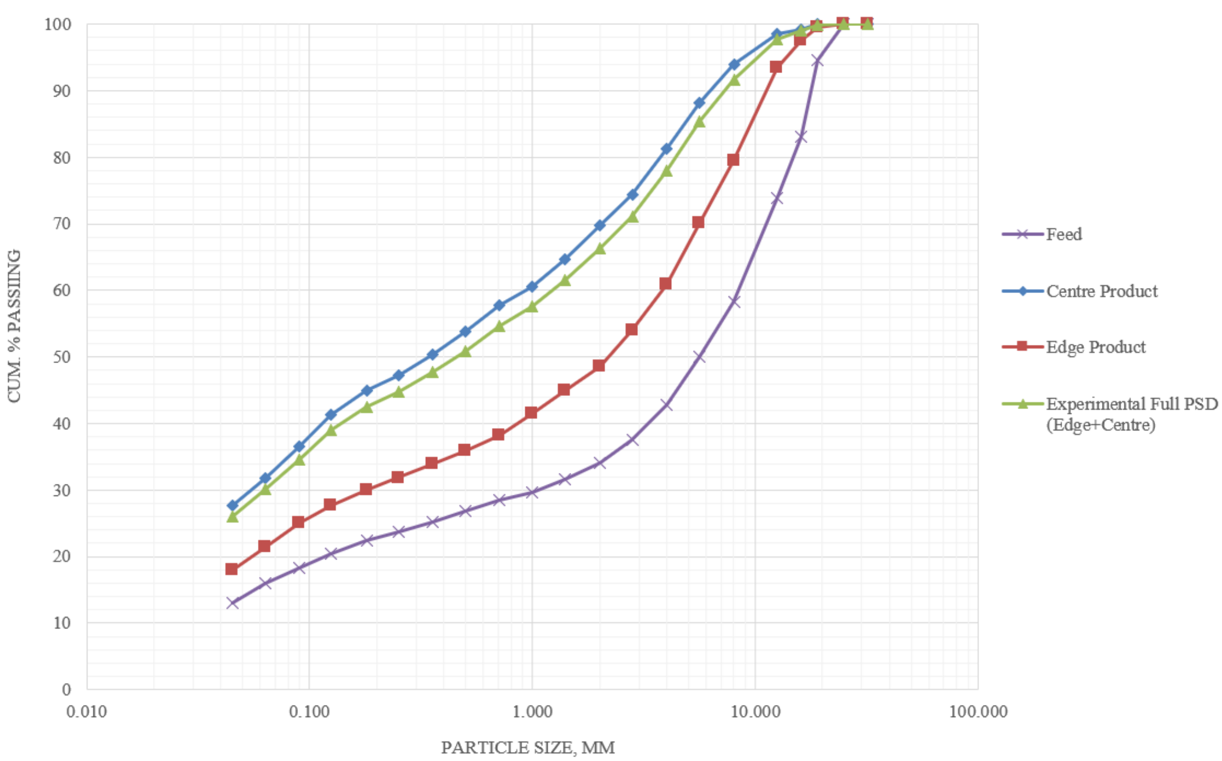

Figure A. 7-12: Feed and product PSDs of test No. SA012

Test No.		Feed		Centre Product		Edge Product		Experimental Full PSD	Scaled HPGR Product
SA013									90% Center + 10% Edge
Screen Size	Particle Size, mm	Retained (g)	Cum % Pass	Retained (g)	Cum % Pass	Retained (g)	Cum % Pass	Cum % Pass	Cum % Pass
-35.5 to +32	32.000	**0.00**	100.00	**0.00**	100.00	**0.00**	100.00	100.00	100.00
-32 to +25	25.000	**0.00**	100.00	**0.00**	100.00	**0.00**	100.00	100.00	100.00
-25 to +19	19.000	**887.30**	91.81	**0.00**	100.00	**0.00**	100.00	100.00	100.00
-19 to 16	16.000	**923.90**	83.28	**34.60**	99.71	**171.20**	97.83	99.22	99.52
-16 to +12.5	12.500	**1089.90**	73.22	**122.30**	98.68	**343.40**	93.48	97.33	98.16
-12.5 to +8	8.000	**1687.80**	57.64	**712.80**	92.66	**1126.00**	79.22	89.18	91.32
-8 to +5.6	5.600	**880.60**	49.51	**878.10**	85.25	**767.70**	69.50	81.17	83.68
-5.6 to +4	4.000	**736.00**	42.71	**925.90**	77.44	**672.10**	60.99	73.18	75.79
-4 to +2.8	2.800	**550.50**	37.63	**819.50**	70.52	**564.90**	53.83	66.20	68.85
-2.8 to +2	2.000	**358.60**	34.32	**542.60**	65.94	**378.20**	49.04	61.57	64.25
-2 to +1.4	1.400	**255.60**	31.96	**488.60**	61.82	**302.00**	45.22	57.52	60.16
-1.4 to +1	1.000	**218.90**	29.94	**475.40**	57.81	**255.40**	41.98	53.71	56.23
-1 to +.71	0.710	**129.60**	28.74	**307.30**	55.21	**154.10**	40.03	51.28	53.70
-.71 to +.5	0.500	**177.30**	27.11	**469.30**	51.25	**230.90**	37.11	47.59	49.84
-.5 to +.355	0.355	**171.30**	25.53	**381.30**	48.04	**186.70**	34.74	44.60	46.71
-.355 to +.25	0.250	**156.30**	24.08	**373.00**	44.89	**162.00**	32.69	41.73	43.67
-.25 to +.18	0.180	**135.10**	22.84	**279.50**	42.53	**147.10**	30.83	39.50	41.36
-.18 to +.125	0.125	**220.90**	20.80	**408.70**	39.08	**190.10**	28.42	36.32	38.02
-.125 to +.09	0.090	**222.70**	18.74	**550.20**	34.44	**200.50**	25.88	32.22	33.58
-.09 to +.063	0.063	**278.40**	16.17	**630.10**	29.12	**245.50**	22.77	27.48	28.49
-.063 to +.045	0.045	**318.90**	13.23	**360.50**	26.08	**296.40**	19.02	24.25	25.37
-0.045	Pan	**1432.70**		**3090.30**		**1501.80**			
Total mass		10832.30		11850.00		7896.00			
Initial wt.		**10860.50**		**11905.30**		**7952.40**			
Delta wt.		-28.20		-55.30		-56.40			
Delta %		-0.26%		-0.46%		-0.71%			
Size Distribution Interpolations									
%passing 1 mm			**29.94**		**57.81**		**41.98**	**53.71**	**56.23**
Linear P50	[mm]		**5.75**		**0.44**		**2.16**	**0.64**	**0.51**
Linear P80	[mm]		**14.86**		**4.52**		**8.25**	**5.37**	**4.85**

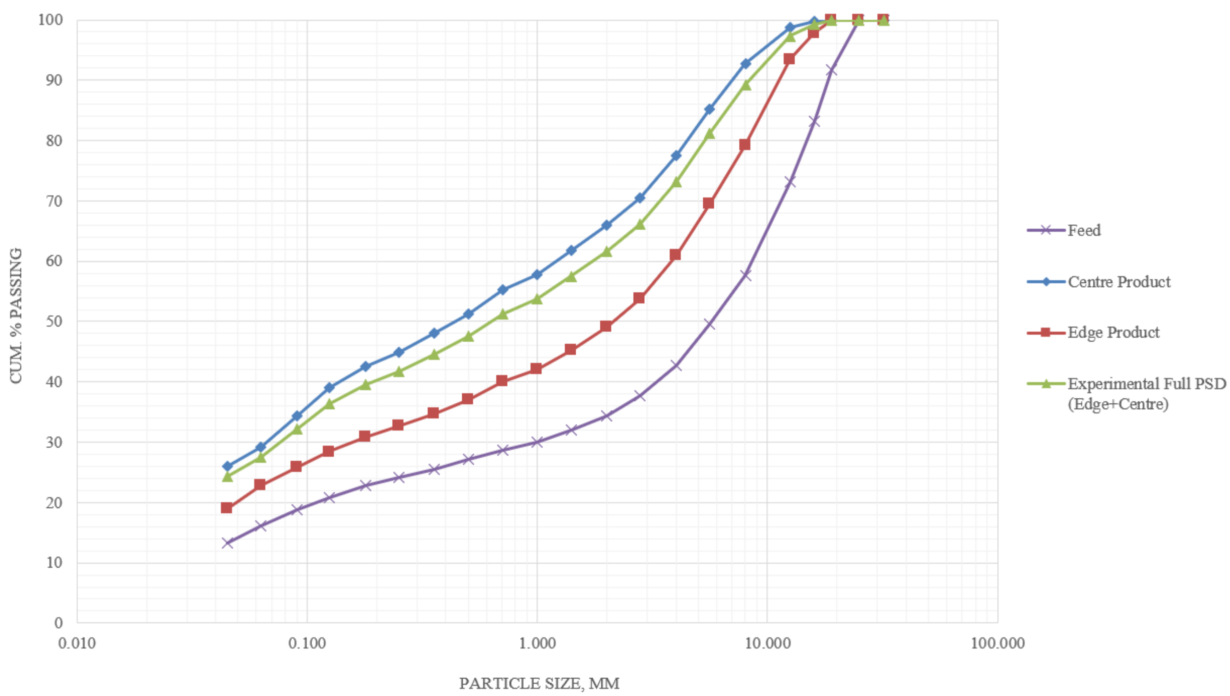

Figure A. 7-13: Feed and product PSDs of test No. SA013

Table A.7-3: Summary of the closed circuit pilot-scale HPGR tests

Data	Description	Symbol	Unit	SA014	SA015	SA016	SA017	SA018	SA019	SA020	SA021
Press Constants	Roller Diameter (**D**)	[m]	0.750								
	Roller Width (**W**)	[m]	0.220								
Data	**Description**	**Test Number:**		**SA014**	**SA015**	**SA016**	**SA017**	**SA018**	**SA019**	**SA020**	**SA021**
		Symbol	**Unit**	**Closed-circuit Test**				**Closed-circuit Test**			
Process Set Points	Speed	**n**	[m/s]	0.55	0.55	0.55	0.55	0.55	0.55	0.55	0.55
		n	[rpm]	14.04	14.04	14.04	14.04	14.04	14.04	14.04	14.04
	Static Gap	X_0	[mm]	9.0	9.0	9.0	9.0	9.00	9.00	9.00	9.00
	Hydraulic Pressure	**P**	[bar]	82.1	82.1	82.1	82.1	102.58	102.58	102.58	102.58
	Pressing Force	**F**	[kN]	660.0	660.0	660.0	660.0	825.00	825.00	825.00	825.00
	Specific Pressing Force	F_{SP}	[N/mm^2]	**4.0**	**4.0**	**4.0**	**4.0**	**5.00**	**5.00**	**5.00**	**5.00**
Process Data	**Test Time**	t	[s]	16.89	17.11	17.25	15.65	13.52	13.50	13.58	13.54
	Average Actual Speed:	w_{AV}	[m/s]	0.56	0.55	0.56	0.56	0.56	0.56	0.56	0.56
	Standard Deviation	s_w		0.29	0.26	0.26	0.18	0.22	0.15	0.20	0.19
	Actual Roller gap (average)	X_{gAV}	[mm]	**19.06**	**21.32**	**21.55**	**21.56**	**17.05**	**14.94**	**13.91**	**13.93**
	Standard Deviation	s_X		0.40	0.20	0.22	0.21	0.34	0.42	0.38	0.29
	Actual Hydraulic Pressure (average)	P_{AV}	[bar]	**80.1**	**83.2**	**82.2**	**83.3**	**102.85**	**102.22**	**103.94**	**102.41**
	Standard Deviation			0.95	0.71	0.23	1.31	0.37	0.40	1.19	0.45
	Actual Pressing Force (average)	F_{AV}	[kN]	644	669	661	670	827.15	822.14	835.97	823.62
	Actual Specific Pressure (average)	F_{SPAV}	[N/mm^2]	**3.92**	**4.07**	**4.02**	**4.07**	**5.03**	**5.00**	**5.08**	**5.00**
	Idle Power Draw	Pi	[kW]	4.78	5.39	3.25	4.14	4.60	7.58	4.04	4.15
	Power Draw	P	[kW]	49.45	58.23	56.82	58.57	67.49	63.28	62.91	58.81
	Total Specific Energy Consumption	E_{SP}	[kWh/t]	1.88	1.89	1.82	1.85	2.75	2.78	3.06	2.79
	Net Specific Energy Consumption	$E_{SP\ net}$	[kWh/t]	**1.70**	**1.72**	**1.71**	**1.72**	**2.56**	**2.45**	**2.87**	**2.60**
	Press throughput	W	[t/h]	26.29	30.76	31.25	31.66	24.54	22.78	20.54	21.04
	Specific Throughput Constant	m dot	[ts/hm^3]	**286**	**337**	**342**	**343**	**266**	**248**	**224**	**229**
Material Data	**Particle Size Distribution**			PSD014	PSD015	PSD016	PSD017	PSD018	PSD019	PSD020	PSD021
	Feed: 100% Passing Size		[mm]	25.00	25.00	25.00	25.00	25.00	25.00	25.00	25.00
	Feed: 80% Passing Size	F_{80}	[mm]	4.71	4.22	4.71	5.02	4.87	4.79	4.54	4.72
	Feed: 50% Passing Size	F_{50}	[mm]	**0.64**	**0.98**	**1.52**	**1.77**	**0.74**	**1.42**	**1.53**	**1.56**
	Centre: 80% Passing Size	P_{80}	[mm]	1.89	2.05	2.53	2.27	1.74	2.29	2.27	2.22
	Centre: 50% Passing Size	P_{50}	[mm]	**0.14**	**0.29**	**0.46**	**0.48**	**0.12**	**0.35**	**0.38**	**0.45**
	Edge: 80% Passing Size	P_{80}	[mm]	3.56	3.65	3.76	3.55	2.51	2.79	2.75	2.74
	Edge: 50% Passing Size	P_{50}	[mm]	0.40	0.74	1.00	1.03	0.21	0.56	0.57	0.65
	Full 80% Passing Size	P_{80}	[mm]	2.35	2.48	2.83	2.60	1.92	2.43	2.41	2.35
	Full 50% Passing Size	P_{50}	[mm]	**0.17**	**0.37**	**0.57**	**0.60**	**0.14**	**0.39**	**0.42**	**0.49**
	Combined 90% Center & 10% Edge: 80% Passing Size	P_{80}	[mm]	2.05	2.24	2.66	2.41	1.81	2.35	2.33	2.27
	Combined 90% Center & 10% Edge: 50% Passing Size	P_{50}	[mm]	**0.15**	**0.32**	**0.50**	**0.53**	**0.13**	**0.36**	**0.40**	**0.47**
	Reduction Ratio F80/P80 full			2.01	1.70	1.66	1.93	2.54	1.97	1.88	2.01
	Reduction Ratio F50/P50 full			**3.65**	**2.66**	**2.69**	**2.96**	**5.09**	**3.61**	**3.59**	**3.20**
	Reduction Ratio F80/P80 (90% C & 10% E Product)			2.30	1.88	1.77	2.08	2.69	2.04	1.95	2.08
	Reduction Ratio F50/P50 (90% C & 10% E Product)			**4.18**	**3.03**	**3.05**	**3.37**	**5.59**	**3.89**	**3.83**	**3.36**
	Percentage Passing 1 mm (Combined)			**68.50**	**63.88**	**59.26**	**59.04**	**71.01**	**63.19**	**61.56**	**61.19**
	Percentage Passing 1 mm (90% C & 10% E)		[%]	**70.37**	**65.72**	**60.93**	**60.93**	**71.88**	**64.04**	**62.45**	**61.95**
	Percentage Passing 0.045 mm (Combined)		[%]	**29.78**	**26.03**	**23.19**	**22.85**	**30.30**	**25.01**	**25.29**	**24.41**
	Mass Balance										
	Total Feed Material	M_F	[kg]	278	278	280	278	289.00	287.80	286.00	287.70
	Total Centre Product	M_C	[kg]	50.2	57.5	61.5	48.1	47.00	41.20	38.10	43.50
	Centre Product % of Centre & Edge Material	MCE%	[%]	74.0%	76.1%	76.1%	75.3%	0.74	0.76	0.74	0.77
	Total Edge Product	M_E	[kg]	17.6	18.1	19.3	15.8	16.70	13.20	13.40	13.10
	Edge Product % of Centre & Edge Material	$M_{EF\%}$	[%]	26.0%	23.9%	23.9%	24.7%	0.26	0.24	0.26	0.23
	Edge Product % of Centre Product	$M_{EC\%}$	[%]	35.1%	31.5%	31.4%	32.8%	0.36	0.32	0.35	0.30
	Total Waste Product	M_W	[kg]	206.8	197.2	195.0	210.2	272.50	267.50	269.00	265.50
	Waste Product % of Total Feed	$M_{WF\%}$	[%]	74.5%	70.9%	69.8%	75.6%	0.94	0.93	0.94	0.92
	Total Recovered Product	M_P	[kg]	275	273	276	274	336.20	321.90	320.50	322.10
	Mass Reconciliation (+ "gain; - "loss")	$M_{PF\%}$	[%]	-1.0%	-1.9%	-1.3%	-1.5%	0.16	0.12	0.12	0.12

Test No.		Feed		Centre Product		Edge Product		Experimental Full PSD	Scaled HPGR Product
SA014									90% Center + 10% Edge
Screen Size	Particle Size, mm	Retained (g)	Cum % Pass	Retained (g)	Cum % Pass	Retained (g)	Cum % Pass	Cum % Pass	Cum % Pass
-35.5 to +32	32.000	**0.00**	100.00	**0.00**	100.00	**0.00**	100.00	100.00	100.00
-32 to +25	25.000	**0.00**	100.00	**0.00**	100.00	**0.00**	100.00	100.00	100.00
-25 to +19	19.000	**0.00**	100.00	**0.00**	100.00	**0.00**	100.00	100.00	100.00
-19 to 16	16.000	**0.00**	100.00	**0.00**	100.00	**0.00**	100.00	100.00	100.00
-16 to +12.5	12.500	**78.60**	99.20	**0.00**	100.00	**21.00**	99.76	99.94	99.98
-12.5 to +8	8.000	**697.80**	92.14	**82.60**	98.35	**378.10**	95.39	97.58	98.06
-8 to +5.6	5.600	**773.70**	84.31	**123.40**	95.89	**494.60**	89.69	94.28	95.27
-5.6 to +4	4.000	**765.10**	76.56	**260.40**	90.69	**623.80**	82.49	88.56	89.87
-4 to +2.8	2.800	**714.90**	69.33	**278.20**	85.14	**593.00**	75.65	82.67	84.19
-2.8 to +2	2.000	**478.80**	64.48	**213.80**	80.87	**523.30**	69.61	77.95	79.74
-2 to +1.4	1.400	**497.90**	59.44	**241.70**	76.05	**461.70**	64.28	72.99	74.87
-1.4 to +1	1.000	**395.90**	55.43	**225.90**	71.54	**386.50**	59.82	68.50	70.37
-1 to +.71	0.710	**434.40**	51.04	**258.50**	66.38	**383.40**	55.40	63.53	65.28
-.71 to +.5	0.500	**298.10**	48.02	**196.60**	62.45	**285.40**	52.11	59.77	61.42
-.5 to +.355	0.355	**279.00**	45.19	**187.70**	58.71	**263.20**	49.07	56.21	57.74
-.355 to +.25	0.250	**267.10**	42.49	**173.20**	55.25	**250.10**	46.18	52.90	54.34
-.25 to +.18	0.180	**215.80**	40.31	**130.70**	52.64	**206.00**	43.81	50.35	51.76
-.18 to +.125	0.125	**288.80**	37.38	**177.90**	49.09	**309.60**	40.23	46.79	48.21
-.125 to +.09	0.090	**430.50**	33.02	**365.10**	41.80	**381.70**	35.83	40.25	41.21
-.09 to +.063	0.063	**710.00**	25.84	**253.90**	36.74	**462.90**	30.49	35.11	36.11
-.063 to +.045	0.045	**326.10**	22.54	**279.30**	31.16	**402.20**	25.85	29.78	30.63
-0.045	Pan	**2226.30**		**1561.20**		**2240.00**			
Total mass		9878.80		5010.10		8666.50			
Initial wt.		**9975.40**		**5039.80**		**8775.50**			
Delta wt.		-96.60		-29.70		-109.00			
Delta %		-0.97%		-0.59%		-1.24%			
Size Distribution Interpolations									
%passing 1 mm			**55.43**		**71.54**		**59.82**	**68.50**	**70.37**
Linear P50	[mm]		**0.64**		**0.14**		**0.40**	**0.17**	**0.15**
Linear P80	[mm]		**4.71**		**1.89**		**3.56**	**2.35**	**2.05**

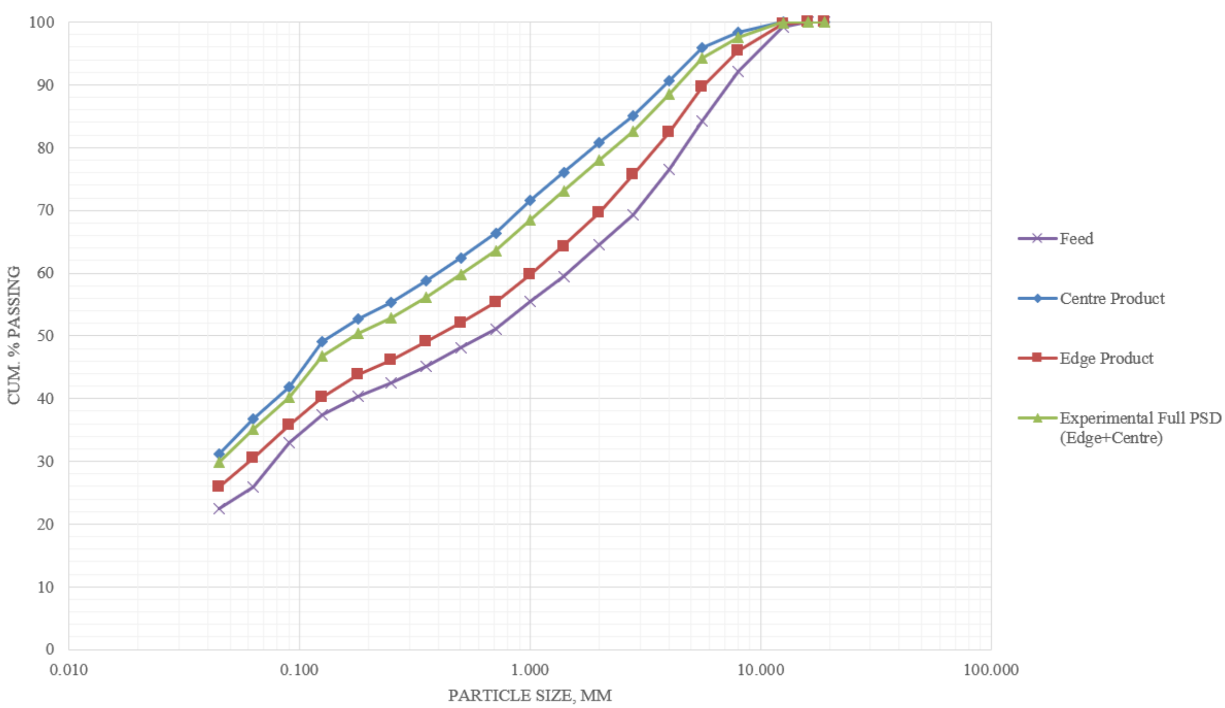

Figure A. 7-14: Feed and product PSDs of test No. SA014

Test No.		Feed		Centre Product		Edge Product		Experimental Full PSD	Scaled HPGR Product
SA015									90% Center + 10% Edge
Screen Size	Particle Size, mm	Retained (g)	Cum % Pass	Retained (g)	Cum % Pass	Retained (g)	Cum % Pass	Cum % Pass	Cum % Pass
-35.5 to +32	32.000	**0.00**	100.00	**0.00**	100.00	**0.00**	100.00	100.00	100.00
-32 to +25	25.000	**0.00**	100.00	**0.00**	100.00	**0.00**	100.00	100.00	100.00
-25 to +19	19.000	**0.00**	100.00	**0.00**	100.00	**0.00**	100.00	100.00	100.00
-19 to 16	16.000	**0.00**	100.00	**0.00**	100.00	**0.00**	100.00	100.00	100.00
-16 to +12.5	12.500	**39.30**	99.40	**0.00**	100.00	**34.60**	99.63	99.91	99.96
-12.5 to +8	8.000	**319.70**	94.54	**81.00**	98.75	**341.90**	96.01	98.09	98.48
-8 to +5.6	5.600	**454.40**	87.64	**195.20**	95.73	**551.80**	90.17	94.40	95.18
-5.6 to +4	4.000	**582.30**	78.79	**329.90**	90.64	**737.60**	82.36	88.65	89.81
-4 to +2.8	2.800	**586.20**	69.88	**386.60**	84.66	**763.10**	74.28	82.18	83.62
-2.8 to +2	2.000	**449.60**	63.05	**324.10**	79.66	**661.60**	67.27	76.69	78.42
-2 to +1.4	1.400	**443.40**	56.31	**399.40**	73.49	**658.50**	60.29	70.33	72.17
-1.4 to +1	1.000	**396.30**	50.29	**417.70**	67.03	**606.10**	53.88	63.88	65.72
-1 to +.71	0.710	**255.10**	46.41	**454.30**	60.01	**407.10**	49.56	57.51	58.97
-.71 to +.5	0.500	**216.70**	43.12	**283.10**	55.64	**349.00**	45.87	53.30	54.66
-.5 to +.355	0.355	**194.00**	40.17	**242.30**	51.90	**301.00**	42.68	49.69	50.98
-.355 to +.25	0.250	**167.10**	37.63	**213.50**	48.60	**247.60**	40.06	46.55	47.75
-.25 to +.18	0.180	**126.90**	35.70	**160.20**	46.12	**186.10**	38.09	44.20	45.32
-.18 to +.125	0.125	**175.80**	33.03	**264.90**	42.03	**263.60**	35.29	40.42	41.36
-.125 to +.09	0.090	**276.70**	28.83	**337.90**	36.81	**373.90**	31.33	35.50	36.26
-.09 to +.063	0.063	**389.40**	22.91	**369.70**	31.10	**512.60**	25.91	29.86	30.58
-.063 to +.045	0.045	**217.70**	19.60	**253.40**	27.19	**335.20**	22.36	26.03	26.70
-0.045	Pan	**1290.00**		**1759.70**		**2110.90**			
Total mass		6580.60		6472.90		9442.20			
Initial wt.		**6661.20**		**6546.40**		**9530.40**			
Delta wt.		-80.60		-73.50		-88.20			
Delta %		-1.21%		-1.12%		-0.93%			
Size Distribution Interpolations									
%passing 1 mm			**50.29**		**67.03**		**53.88**	**63.88**	**65.72**
Linear P50	[mm]		**0.98**		**0.29**		**0.74**	**0.37**	**0.32**
Linear P80	[mm]		**4.22**		**2.05**		**3.65**	**2.48**	**2.24**

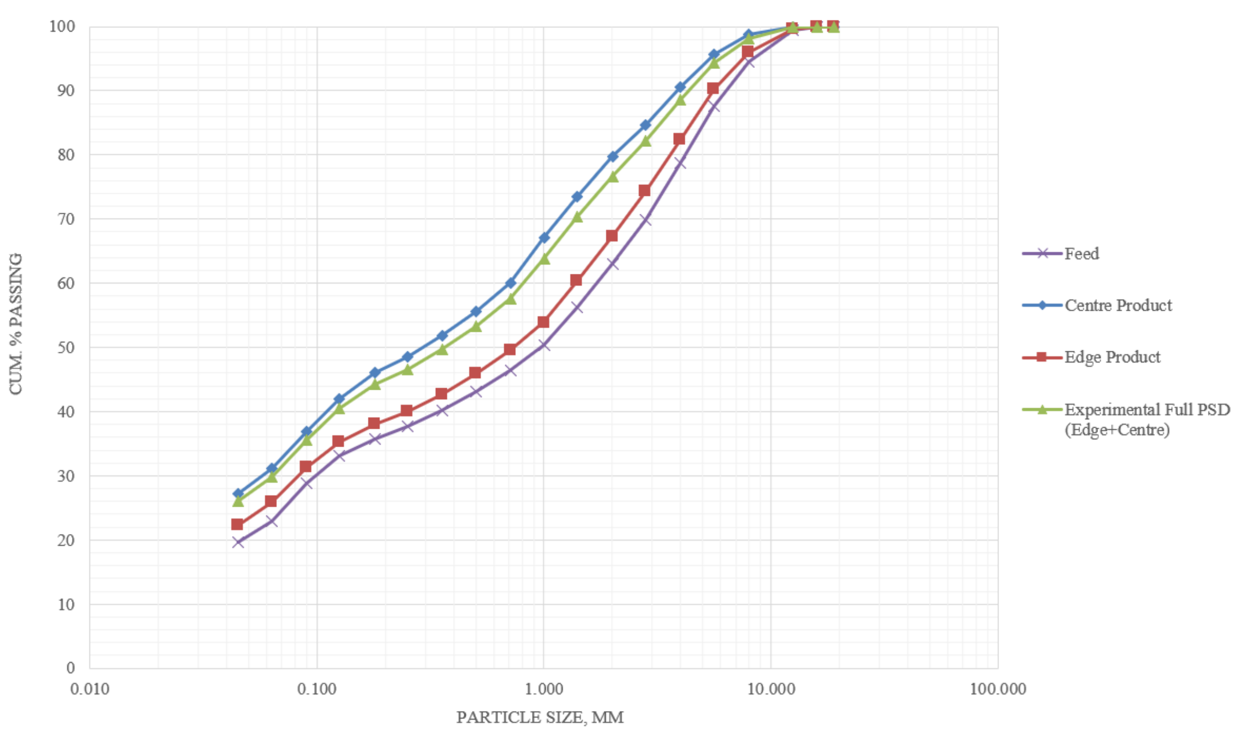

Figure A. 7-15: Feed and product PSDs of test No. SA015

Test No.		Feed		Centre Product		Edge Product		Experimental Full PSD	Scaled HPGR Product
SA016									90% Center + 10% Edge
Screen Size	Particle Size, mm	Retained (g)	Cum % Pass	Retained (g)	Cum % Pass	Retained (g)	Cum % Pass	Cum % Pass	Cum % Pass
-35.5 to +32	32.000	**0.00**	100.00	**0.00**	100.00	**0.00**	100.00	100.00	100.00
-32 to +25	25.000	**0.00**	100.00	**0.00**	100.00	**0.00**	100.00	100.00	100.00
-25 to +19	19.000	**0.00**	100.00	**0.00**	100.00	**0.00**	100.00	100.00	100.00
-19 to 16	16.000	**36.70**	99.63	**0.00**	100.00	**0.00**	100.00	100.00	100.00
-16 to +12.5	12.500	**102.30**	98.60	**0.00**	100.00	**17.50**	99.81	99.96	99.98
-12.5 to +8	8.000	**529.30**	93.29	**169.00**	98.18	**381.30**	95.77	97.61	97.94
-8 to +5.6	5.600	**803.10**	85.23	**345.30**	94.47	**570.10**	89.72	93.34	94.00
-5.6 to +4	4.000	**938.50**	75.80	**571.00**	88.34	**760.80**	81.65	86.74	87.67
-4 to +2.8	2.800	**932.60**	66.44	**602.30**	81.86	**788.40**	73.29	79.81	81.00
-2.8 to +2	2.000	**969.70**	56.70	**517.40**	76.30	**750.00**	65.33	73.68	75.20
-2 to +1.4	1.400	**838.90**	48.28	**641.50**	69.41	**735.40**	57.53	66.57	68.22
-1.4 to +1	1.000	**696.10**	41.29	**676.40**	62.14	**702.80**	50.08	59.26	60.93
-1 to +.71	0.710	**442.50**	36.85	**630.00**	55.36	**499.30**	44.78	52.84	54.31
-.71 to +.5	0.500	**254.80**	34.29	**405.30**	51.01	**327.40**	41.31	48.69	50.04
-.5 to +.355	0.355	**214.90**	32.13	**345.90**	47.29	**269.90**	38.44	45.18	46.41
-.355 to +.25	0.250	**179.10**	30.33	**298.10**	44.09	**214.90**	36.16	42.19	43.29
-.25 to +.18	0.180	**138.90**	28.94	**229.30**	41.62	**201.60**	34.03	39.81	40.86
-.18 to +.125	0.125	**197.90**	26.95	**357.50**	37.78	**244.80**	31.43	36.26	37.15
-.125 to +.09	0.090	**385.40**	23.08	**402.90**	33.45	**373.10**	27.47	32.02	32.85
-.09 to +.063	0.063	**337.50**	19.69	**492.80**	28.15	**532.60**	21.82	26.64	27.52
-.063 to +.045	0.045	**286.50**	16.82	**355.90**	24.33	**214.20**	19.55	23.19	23.85
-0.045	Pan	**1675.00**		**2263.50**		**1843.00**			
Total mass		9959.70		9304.10		9427.10			
Initial wt.		**10071.80**		**9387.60**		**9528.10**			
Delta wt.		-112.10		-83.50		-101.00			
Delta %		-1.11%		-0.89%		-1.06%			
Size Distribution Interpolations									
%passing 1 mm			**41.29**		**62.14**		**50.08**	**59.26**	**60.93**
Linear P50	[mm]		**1.52**		**0.46**		**1.00**	**0.57**	**0.50**
Linear P80	[mm]		**4.71**		**2.53**		**3.76**	**2.83**	**2.66**

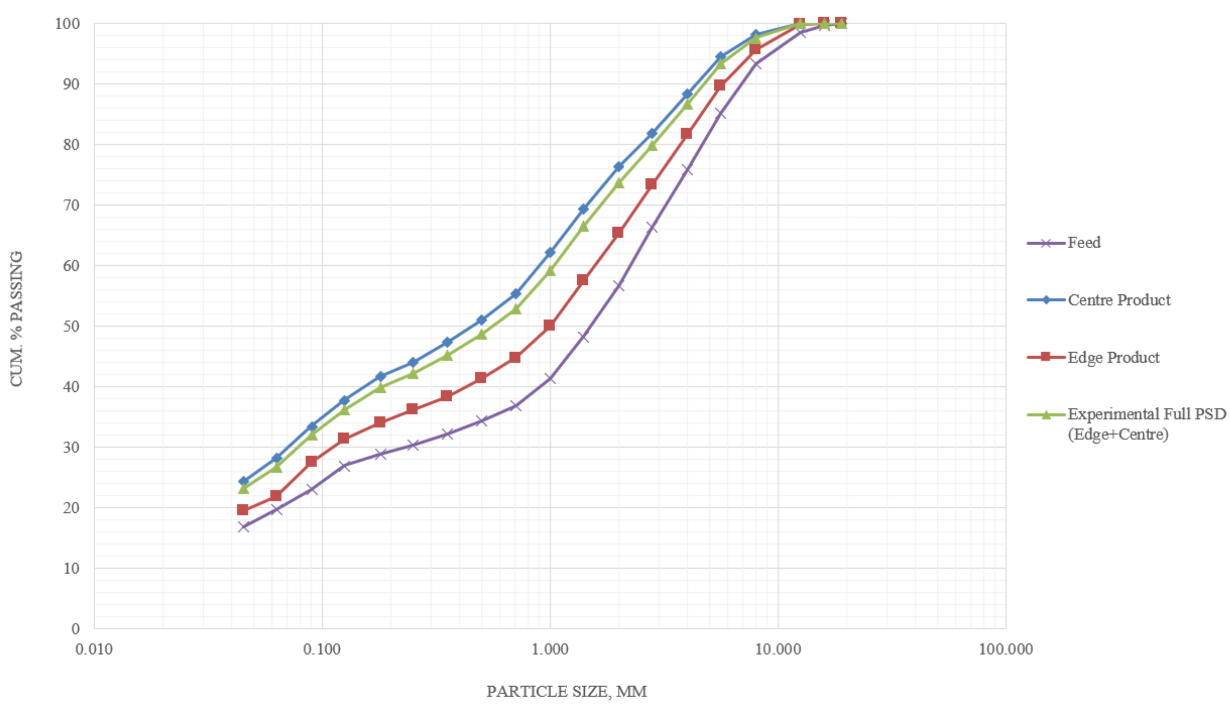

Figure A. 7-16: Feed and product PSDs of test No. SA016

Test No.		Feed		Centre Product		Edge Product		Experimental Full PSD	Scaled HPGR Product	Screen O.S		Screen U.S	
SA017									90% Center + 10% Edge				
Screen Size	Particle Size, mm	Retained (g)	Cum % Pass	Retained (g)	Cum % Pass	Retained (g)	Cum % Pass	Cum % Pass	Cum % Pass	Retained (g)	Cum % Pass	Retained (g)	Cum % Pass
-35.5 to +32	32.000	0.00	100.00	0.00	100.00	0.00	100.00	100.00	100.00	0.00	100.00	0.00	100.00
-32 to +25	25.000	0.00	100.00	0.00	100.00	0.00	100.00	100.00	100.00	0.00	100.00	0.00	100.00
-25 to +19	19.000	0.00	100.00	0.00	100.00	0.00	100.00	100.00	100.00	0.00	100.00	0.00	100.00
-19 to 16	16.000	25.60	99.72	0.00	100.00	0.00	100.00	100.00	100.00	0.00	100.00	0.00	100.00
-16 to +12.5	12.500	68.70	98.96	0.00	100.00	0.00	100.00	100.00	100.00	35.50	99.75	0.00	100.00
-12.5 to +8	8.000	559.20	92.79	129.20	98.47	234.40	96.80	98.06	98.30	588.50	95.53	0.00	100.00
-8 to +5.6	5.600	818.50	83.75	249.20	95.51	404.80	91.27	94.47	95.09	1210.50	86.85	0.00	100.00
-5.6 to +4	4.000	936.00	73.42	465.50	90.00	594.40	83.16	88.31	89.31	1908.70	73.16	0.00	100.00
-4 to +2.8	2.800	960.60	62.81	506.60	83.99	617.40	74.73	81.70	83.07	2170.80	57.60	0.00	100.00
-2.8 to +2	2.000	845.00	53.48	513.00	77.91	628.80	66.14	75.00	76.74	2609.30	38.89	0.00	100.00
-2 to +1.4	1.400	816.30	44.47	619.00	70.58	650.80	57.25	67.28	69.24	2582.40	20.38	0.00	100.00
-1.4 to +1	1.000	770.70	35.96	706.00	62.21	576.20	49.38	59.04	60.93	2117.70	5.20	0.00	100.00
-1 to +.71	0.710	280.90	32.86	572.40	55.42	435.40	43.44	52.46	54.22	0.00	5.20	40.90	92.53
-.71 to +.5	0.500	217.20	30.46	417.20	50.48	253.90	39.97	47.88	49.43	0.00	5.20	41.90	84.87
-.5 to +.355	0.355	184.50	28.43	317.10	46.72	213.80	37.05	44.33	45.75	0.00	5.20	33.10	78.82
-.355 to +.25	0.250	166.30	26.59	276.00	43.45	169.40	34.74	41.30	42.58	0.00	5.20	26.70	73.94
-.25 to +.18	0.180	122.00	25.25	213.40	40.92	155.30	32.62	38.87	40.09	0.00	5.20	21.40	70.03
-.18 to +.125	0.125	163.40	23.44	285.70	37.53	159.40	30.44	35.78	36.82	0.00	5.20	23.10	65.81
-.125 to +.09	0.090	287.60	20.27	379.90	33.03	260.90	26.88	31.51	32.41	0.00	5.20	20.80	62.01
-.09 to +.063	0.063	309.90	16.85	481.80	27.32	313.30	22.60	26.15	26.85	0.00	5.20	28.60	56.79
-.063 to +.045	0.045	246.30	14.13	290.40	23.88	211.90	19.71	22.85	23.46	0.00	5.20	39.30	49.61
-0.045	Pan	1279.60		2014.50		1443.40				724.70		271.49	
Total mass		9058.30		8436.90		7323.50				13948.10		547.29	
Initial wt.		9147.30		8554.20		7446.00				13952.70		549.39	
Delta wt.		-89.00		-117.30		-122.50				-4.60		-2.10	
Delta %		-0.97%		-1.37%		-1.65%				-0.03%		-0.38%	
Size Distribution Interpolations													
%passing 1 mm			35.96		62.21		49.38	59.04	60.93		5.20		100.00
Linear P50	[mm]		1.77		0.48		1.03	0.60	0.53		2.47		0.05
Linear P80	[mm]		5.02		2.27		3.55	2.60	2.41		4.80		0.38

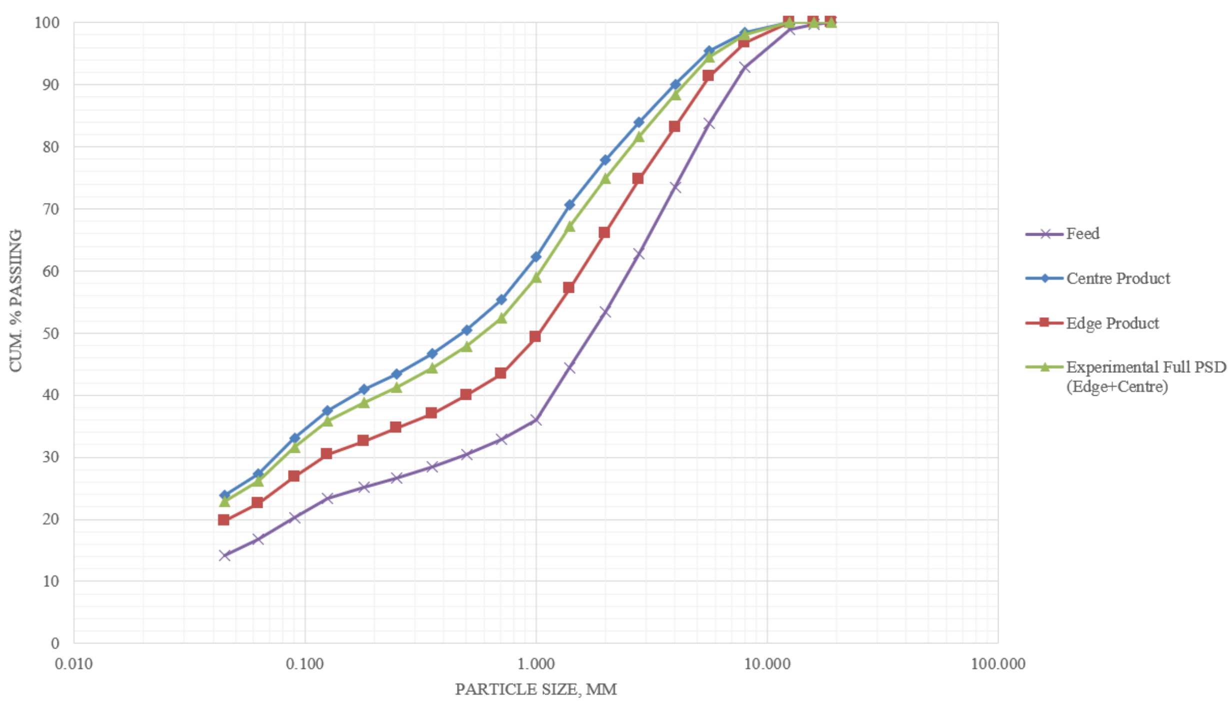

Figure A. 7-17: Feed and product PSDs of test No. SA017

Test No.		Feed		Centre Product		Edge Product		Experimental Full PSD	Scaled HPGR Product
SA018									90% Center + 10% Edge
Screen Size	Particle Size, mm	Retained (g)	Cum % Pass	Retained (g)	Cum % Pass	Retained (g)	Cum % Pass	Cum % Pass	Cum % Pass
-35.5 to +32	32.000	**0.00**	100.00	**0.00**	100.00	**0.00**	100.00	100.00	100.00
-32 to +25	25.000	**0.00**	100.00	**0.00**	100.00	**0.00**	100.00	100.00	100.00
-25 to +19	19.000	**0.00**	100.00	**0.00**	100.00	**0.00**	100.00	100.00	100.00
-19 to 16	16.000	**27.90**	99.56	**0.00**	100.00	**0.00**	100.00	100.00	100.00
-16 to +12.5	12.500	**37.10**	98.98	**0.00**	100.00	**0.00**	100.00	100.00	100.00
-12.5 to +8	8.000	**454.70**	91.83	**83.30**	98.54	**141.00**	98.07	98.42	98.49
-8 to +5.6	5.600	**504.20**	83.91	**150.60**	95.90	**310.70**	93.82	95.36	95.70
-5.6 to +4	4.000	**548.30**	75.29	**252.70**	91.48	**420.10**	88.07	90.58	91.14
-4 to +2.8	2.800	**457.70**	68.09	**281.90**	86.54	**461.30**	81.75	85.29	86.06
-2.8 to +2	2.000	**321.50**	63.04	**261.20**	81.97	**351.90**	76.93	80.65	81.46
-2 to +1.4	1.400	**315.40**	58.08	**263.40**	77.36	**386.60**	71.64	75.86	76.78
-1.4 to +1	1.000	**259.90**	54.00	**281.90**	72.42	**336.00**	67.04	71.01	71.88
-1 to +.71	0.710	**281.10**	49.58	**216.60**	68.63	**369.50**	61.98	66.88	67.96
-.71 to +.5	0.500	**215.30**	46.19	**238.00**	64.46	**274.90**	58.22	62.82	63.83
-.5 to +.355	0.355	**192.20**	43.17	**228.70**	60.45	**245.50**	54.86	58.99	59.89
-.355 to +.25	0.250	**168.10**	40.53	**208.30**	56.81	**234.50**	51.65	55.45	56.29
-.25 to +.18	0.180	**128.80**	38.50	**176.40**	53.72	**189.60**	49.05	52.49	53.25
-.18 to +.125	0.125	**169.90**	35.83	**206.40**	50.10	**343.50**	44.35	48.59	49.53
-.125 to +.09	0.090	**262.90**	31.70	**423.10**	42.69	**381.50**	39.13	41.76	42.34
-.09 to +.063	0.063	**311.50**	26.81	**357.40**	36.43	**594.30**	30.99	35.01	35.89
-.063 to +.045	0.045	**317.30**	21.82	**283.80**	31.46	**289.00**	27.04	30.30	31.02
-0.045	Pan	**1388.00**		**1796.70**		**1975.20**			
Total mass		6361.80		5710.40		7305.10			
Initial wt.		**6654.90**		**5804.60**		**7388.60**			
Delta wt.		-293.10		-94.20		-83.50			
Delta %		-4.40%		-1.62%		-1.13%			
Size Distribution Interpolations									
%passing 1 mm			**54.00**		**72.42**		**67.04**	**71.01**	**71.88**
Linear P50	[mm]		**0.74**		**0.12**		**0.21**	**0.14**	**0.13**
Linear P80	[mm]		**4.87**		**1.74**		**2.51**	**1.92**	**1.81**

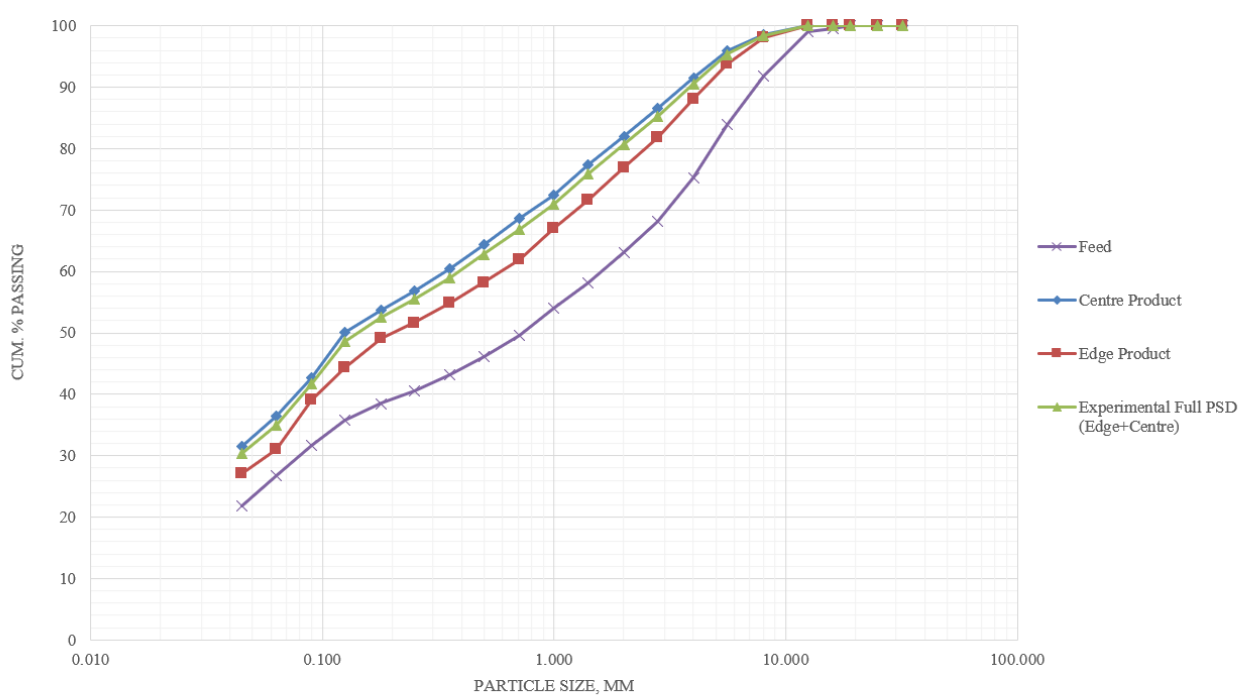

Figure A. 7-18: Feed and product PSDs of test No. SA018

Test No.		Feed		Centre Product		Edge Product		Experimental Full PSD	Scaled HPGR Product
SA019									90% Center + 10% Edge
Screen Size	Particle Size, mm	Retained (g)	Cum % Pass	Retained (g)	Cum % Pass	Retained (g)	Cum % Pass	Cum % Pass	Cum % Pass
-35.5 to +32	32.000	**0.00**	100.00	**0.00**	100.00	**0.00**	100.00	100.00	100.00
-32 to +25	25.000	**0.00**	100.00	**0.00**	100.00	**0.00**	100.00	100.00	100.00
-25 to +19	19.000	**0.00**	100.00	**0.00**	100.00	**0.00**	100.00	100.00	100.00
-19 to 16	16.000	**27.40**	99.72	**0.00**	100.00	**0.00**	100.00	100.00	100.00
-16 to +12.5	12.500	**70.80**	98.99	**0.00**	100.00	**0.00**	100.00	100.00	100.00
-12.5 to +8	8.000	**615.10**	92.69	**104.50**	99.00	**72.40**	98.70	98.92	98.97
-8 to +5.6	5.600	**758.60**	84.93	**310.90**	96.02	**217.60**	94.78	95.72	95.89
-5.6 to +4	4.000	**944.80**	75.25	**590.90**	90.35	**393.00**	87.72	89.71	90.08
-4 to +2.8	2.800	**944.00**	65.58	**668.80**	83.93	**424.20**	80.09	83.00	83.55
-2.8 to +2	2.000	**785.10**	57.54	**641.70**	77.78	**412.40**	72.67	76.54	77.27
-2 to +1.4	1.400	**760.50**	49.75	**710.40**	70.96	**421.70**	65.09	69.54	70.38
-1.4 to +1	1.000	**661.30**	42.98	**658.90**	64.64	**358.20**	58.64	63.19	64.04
-1 to +.71	0.710	**347.50**	39.42	**670.60**	58.21	**313.60**	53.00	56.95	57.69
-.71 to +.5	0.500	**288.10**	36.47	**465.70**	53.74	**226.90**	48.92	52.57	53.26
-.5 to +.355	0.355	**229.30**	34.12	**365.50**	50.24	**190.70**	45.49	49.09	49.76
-.355 to +.25	0.250	**207.90**	31.99	**343.50**	46.94	**158.30**	42.65	45.90	46.51
-.25 to +.18	0.180	**161.80**	30.34	**289.00**	44.17	**116.90**	40.54	43.29	43.81
-.18 to +.125	0.125	**207.70**	28.21	**392.30**	40.41	**147.60**	37.89	39.80	40.16
-.125 to +.09	0.090	**309.00**	25.04	**496.40**	35.65	**296.80**	32.55	34.90	35.34
-.09 to +.063	0.063	**440.20**	20.54	**646.20**	29.45	**239.80**	28.24	29.15	29.33
-.063 to +.045	0.045	**299.10**	17.47	**426.80**	25.35	**239.00**	23.94	25.01	25.21
-0.045	Pan	**1706.00**		**2643.20**		**1331.20**			
Total mass		9764.20		10425.30		5560.30			
Initial wt.		**9870.00**		**10643.90**		**5737.70**			
Delta wt.		-105.80		-218.60		-177.40			
Delta %		-1.07%		-2.05%		-3.09%			
Size Distribution Interpolations									
%passing 1 mm			**42.98**		**64.64**		**58.64**	**63.19**	**64.04**
Linear P50	[mm]		**1.42**		**0.35**		**0.56**	**0.39**	**0.36**
Linear P80	[mm]		**4.79**		**2.29**		**2.79**	**2.43**	**2.35**

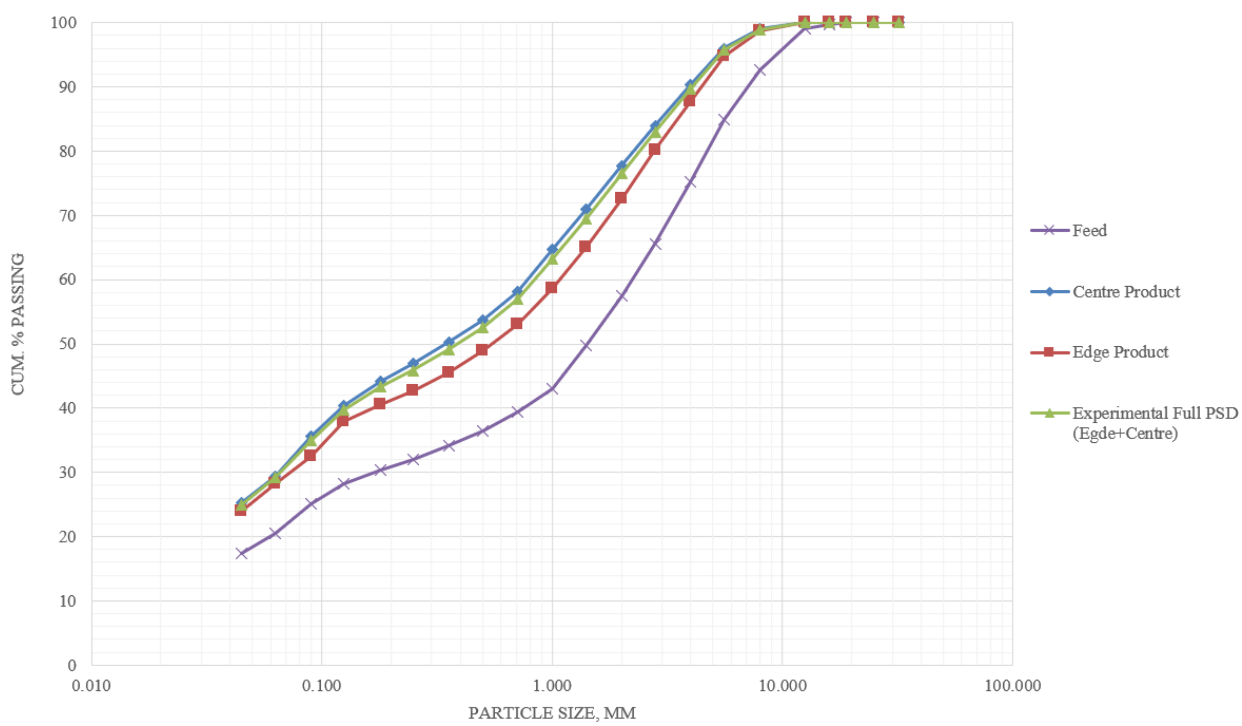

Figure A. 7-19: Feed and product PSDs of test No. SA019

Test No.		Feed		Centre Product		Edge Product		Experimental Full PSD	Scaled HPGR Product
SA020									90% Center + 10% Edge
Screen Size	Particle Size, mm	Retained (g)	Cum % Pass	Retained (g)	Cum % Pass	Retained (g)	Cum % Pass	Cum % Pass	Cum % Pass
-35.5 to +32	32.000	**0.00**	100.00	**0.00**	100.00	**0.00**	100.00	100.00	100.00
-32 to +25	25.000	**0.00**	100.00	**0.00**	100.00	**0.00**	100.00	100.00	100.00
-25 to +19	19.000	**0.00**	100.00	**0.00**	100.00	**0.00**	100.00	100.00	100.00
-19 to 16	16.000	**7.30**	99.92	**0.00**	100.00	**0.00**	100.00	100.00	100.00
-16 to +12.5	12.500	**57.40**	99.33	**0.00**	100.00	**0.00**	100.00	100.00	100.00
-12.5 to +8	8.000	**472.00**	94.41	**55.30**	99.33	**72.10**	98.78	99.18	99.27
-8 to +5.6	5.600	**748.20**	86.62	**215.80**	96.70	**190.60**	95.56	96.40	96.58
-5.6 to +4	4.000	**959.20**	76.63	**476.00**	90.90	**426.30**	88.36	90.24	90.64
-4 to +2.8	2.800	**991.00**	66.31	**552.30**	84.17	**464.90**	80.51	83.22	83.80
-2.8 to +2	2.000	**871.30**	57.23	**516.90**	77.87	**449.00**	72.92	76.58	77.38
-2 to +1.4	1.400	**877.90**	48.09	**605.80**	70.49	**468.50**	65.01	69.06	69.94
-1.4 to +1	1.000	**753.80**	40.24	**614.30**	63.01	**447.90**	57.44	61.56	62.45
-1 to +.71	0.710	**369.00**	36.40	**409.60**	58.02	**273.90**	52.81	56.66	57.50
-.71 to +.5	0.500	**275.60**	33.53	**396.90**	53.18	**253.40**	48.53	51.97	52.71
-.5 to +.355	0.355	**207.00**	31.37	**321.10**	49.27	**207.80**	45.02	48.16	48.84
-.355 to +.25	0.250	**184.90**	29.45	**270.90**	45.97	**176.60**	42.04	44.94	45.57
-.25 to +.18	0.180	**149.10**	27.89	**200.60**	43.52	**132.80**	39.79	42.55	43.15
-.18 to +.125	0.125	**202.10**	25.79	**301.10**	39.85	**176.50**	36.81	39.06	39.55
-.125 to +.09	0.090	**316.30**	22.49	**420.20**	34.74	**321.70**	31.38	33.86	34.40
-.09 to +.063	0.063	**314.30**	19.22	**371.40**	30.21	**274.40**	26.74	29.31	29.86
-.063 to +.045	0.045	**292.00**	16.18	**325.20**	26.25	**247.30**	22.56	25.29	25.88
-0.045	Pan	**1553.60**		**2154.40**		**1335.50**			
Total mass		9602.00		8207.80		5919.20			
Initial wt.		**9657.80**		**8263.60**		**5949.00**			
Delta wt.		-55.80		-55.80		-29.80			
Delta %		-0.58%		-0.68%		-0.50%			
Size Distribution Interpolations									
%passing 1 mm			**40.24**		**63.01**		**57.44**	**61.56**	**62.45**
Linear P50	[mm]		**1.53**		**0.38**		**0.57**	**0.42**	**0.40**
Linear P80	[mm]		**4.54**		**2.27**		**2.75**	**2.41**	**2.33**

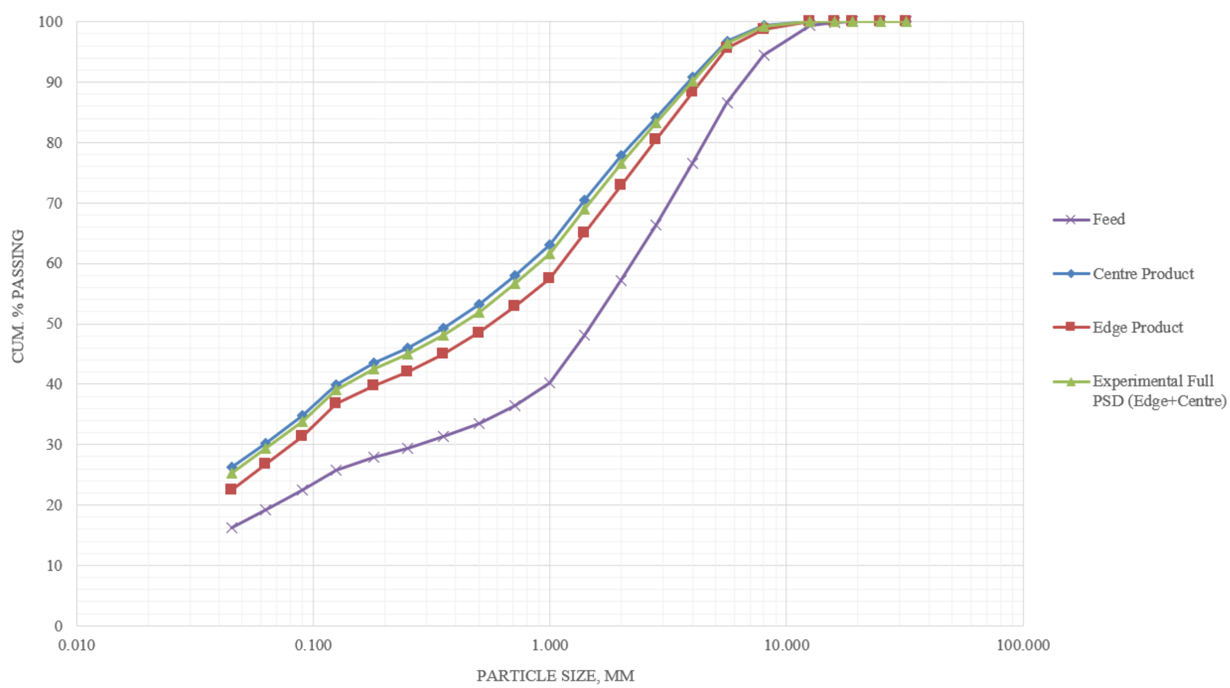

Figure A. 7-20: Feed and product PSDs of test No. SA020

Test No.		Feed		Centre Product		Edge Product		Experimental Full PSD	Scaled HPGR Product	Screen O.S		Screen U.S	
SA021									90% Center + 10% Edge				
Screen Size	Particle Size, mm	Retained (g)	Cum % Pass	Retained (g)	Cum % Pass	Retained (g)	Cum % Pass	Cum % Pass	Cum % Pass	Retained (g)	Cum % Pass	Retained (g)	Cum % Pass
-35.5 to +32	32.000	**0.00**	100.00	**0.00**	100.00	**0.00**	100.00	100.00	100.00	**0.00**	100.00	**0.00**	100.00
-32 to +25	25.000	**0.00**	100.00	**0.00**	100.00	**0.00**	100.00	100.00	100.00	**0.00**	100.00	**0.00**	100.00
-25 to +19	19.000	**0.00**	100.00	**0.00**	100.00	**0.00**	100.00	100.00	100.00	**0.00**	100.00	**0.00**	100.00
-19 to 16	16.000	**65.00**	99.26	**0.00**	100.00	**0.00**	100.00	100.00	100.00	**0.00**	100.00	**0.00**	100.00
-16 to +12.5	12.500	**90.40**	98.23	**0.00**	100.00	**0.00**	100.00	100.00	100.00	**0.00**	100.00	**0.00**	100.00
-12.5 to +8	8.000	**536.40**	92.13	**75.40**	99.31	**66.80**	98.79	99.19	99.26	**170.00**	98.60	**0.00**	100.00
-8 to +5.6	5.600	**613.70**	85.16	**271.60**	96.82	**182.40**	95.50	96.52	96.69	**785.30**	92.14	**0.00**	100.00
-5.6 to +4	4.000	**829.00**	75.73	**585.70**	91.46	**396.00**	88.36	90.74	91.15	**1623.60**	78.78	**0.00**	100.00
-4 to +2.8	2.800	**885.30**	65.66	**708.10**	84.97	**431.80**	80.57	83.95	84.53	**2007.10**	62.27	**0.00**	100.00
-2.8 to +2	2.000	**796.10**	56.61	**746.70**	78.13	**407.30**	73.22	76.99	77.64	**2298.20**	43.36	**0.00**	100.00
-2 to +1.4	1.400	**798.20**	47.53	**850.90**	70.33	**466.90**	64.80	69.05	69.78	**2348.70**	24.03	**0.00**	100.00
-1.4 to +1	1.000	**730.00**	39.23	**851.10**	62.54	**448.50**	56.71	61.19	61.95	**2024.60**	7.38	**0.00**	100.00
-1 to +.71	0.710	**403.60**	34.64	**737.90**	55.78	**306.80**	51.18	54.71	55.32	**0.00**	7.38	**31.43**	94.23
-.71 to +.5	0.500	**219.90**	32.14	**494.60**	51.24	**230.30**	47.02	50.27	50.82	**0.00**	7.38	**36.53**	87.53
-.5 to +.355	0.355	**167.50**	30.24	**382.40**	47.74	**186.50**	43.66	46.80	47.33	**0.00**	7.38	**30.00**	82.02
-.355 to +.25	0.250	**156.90**	28.45	**340.90**	44.62	**160.30**	40.77	43.73	44.23	**0.00**	7.38	**25.61**	77.32
-.25 to +.18	0.180	**132.30**	26.95	**250.00**	42.33	**120.70**	38.59	41.46	41.95	**0.00**	7.38	**20.81**	73.50
-.18 to +.125	0.125	**168.70**	25.03	**420.30**	38.48	**198.30**	35.01	37.68	38.13	**0.00**	7.38	**23.13**	69.26
-.125 to +.09	0.090	**285.70**	21.78	**437.90**	34.47	**320.10**	29.24	33.26	33.94	**0.00**	7.38	**21.71**	65.27
-.09 to +.063	0.063	**277.80**	18.62	**621.20**	28.78	**252.10**	24.69	27.83	28.37	**0.00**	7.38	**32.70**	59.27
-.063 to +.045	0.045	**278.90**	15.45	**381.80**	25.28	**175.70**	21.52	24.41	24.90	**0.00**	7.38	**37.34**	52.42
-0.045	Pan	**1359.00**		**2759.20**		**1192.90**				**896.40**		**285.59**	
Total mass		8794.40		10915.70		5543.40				12153.90		544.85	
Initial wt.		**8835.20**		**11002.00**		**5563.80**				**12156.90**		**549.39**	
Delta wt.		-40.80		-86.30		-20.40				-3.00		-4.54	
Delta %		-0.46%		-0.78%		-0.37%				-0.02%		-0.83%	
Size Distribution Interpolations													
%passing 1 mm			**39.23**		**62.54**		**56.71**	**61.19**	**61.95**		**7.38**		**100.00**
Linear P50	[mm]		**1.56**		**0.45**		**0.65**	**0.49**	**0.47**		**2.28**		-
Linear P80	[mm]		**4.72**		**2.22**		**2.74**	**2.35**	**2.27**		**4.15**		**0.31**

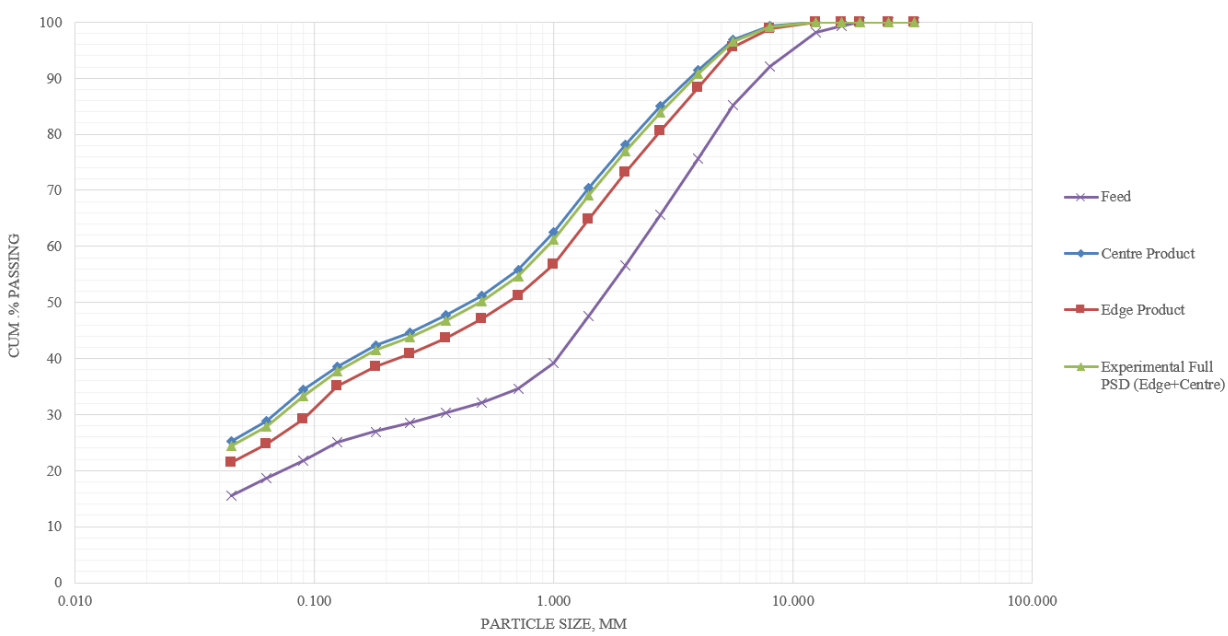

Figure A.7-21: Feed and product PSDs of test No. SA021

Appendix B: MTS Piston-press Test Work Results

Table 7-4: Summary of piston-press tests results (1:1 ratio)

Sample:	Feed	PP3-01	PP3-02	PP3-03	PP3-04	Feed	PP6-01	PP6-02	PP6-03	PP6-04	Feed	PP9-01	PP9-02	PP9-03	PP9-04
Moisture, %	3	3	3	3	3	6	6	6	6	6	9	9	9	9	9
Force, kN	-	1396	1099	799	500	-	1394	1099	799	498	-	1395	1098	799	498
Piston pressure, MPa	-	240.4	189.2	137.6	86.0	-	240.1	189.2	137.5	85.8	-	240.2	189.0	137.5	85.7
Specific Energy, kWh/t	-	**1.24**	**0.92**	**0.63**	**0.37**	-	**1.29**	**0.92**	**0.62**	**0.38**	-	**1.18**	**0.87**	**0.61**	**0.39**
Thickness, mm	-	28.00	27.79	28.80	30.27	-	28.06	28.42	28.37	28.36	-	32.92	32.98	33.52	34.12
Density, g/cc	-	3.47	3.42	3.31	3.19	-	3.56	3.51	3.44	3.34	-	3.69	3.63	3.54	3.41
P50	3.32	0.87	1.05	1.25	1.50	3.49	0.89	0.90	1.26	1.51	3.42	0.99	1.11	1.31	1.54
P80	7.78	4.69	5.13	5.27	5.74	7.73	4.86	4.61	5.33	5.49	7.50	4.74	5.12	5.16	5.53
Reduction ratio F50/P50	-	3.80	3.16	2.66	2.21	-	3.92	3.87	2.77	2.32	-	3.46	3.08	2.61	2.22
Reduction ratio F80/P80	-	1.66	1.52	1.48	1.36	-	1.59	1.68	1.45	1.41	-	1.58	1.47	1.45	1.36

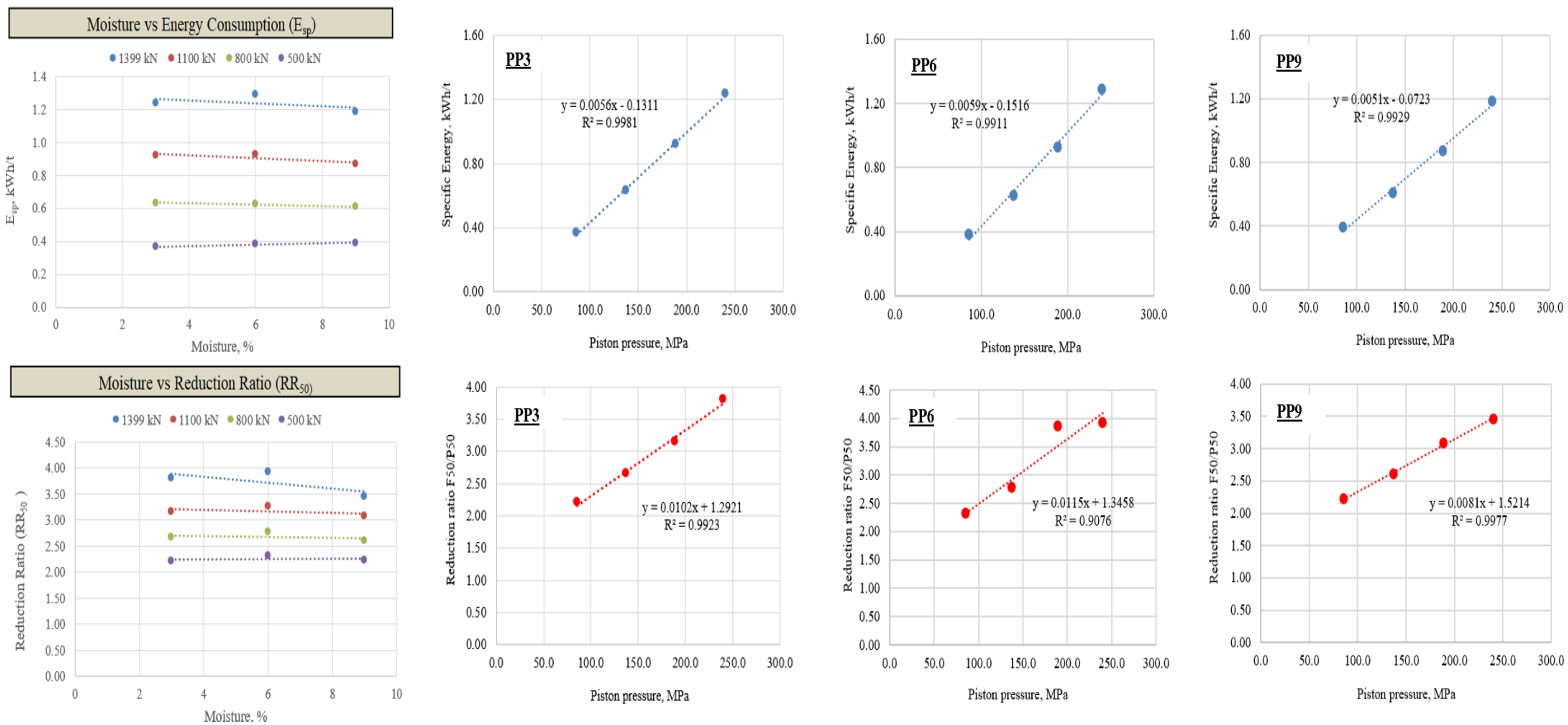

Figure 7-22: Graphical analysis of piston-press tests results (1:1 ratio)